Design and Synthesis of Multifunctional Nanocarriers for Biological Applications

by

Anjali Sharma

August 2013

Department of Chemistry, McGill University

Montréal, Québec, Canada

A thesis submitted to McGill University in partial fulfilment of the requirements of the degree of Doctor of Philosophy

© Anjali Sharma, 2013

This thesis is dedicated to my parents, Amrit Kaur and Sadhu Singh; my husband, Rishi Sharma; and my daughter Manya Sharma

Acknowledgements

I would never have been able to finish my dissertation without the guidance of my supervisor, committee members, help from friends, and support from my husband.

Foremost, I would like to express my most sincere gratitude to my advisor Dr. Ashok Kakkar for his excellent guidance, continuous support, patience, motivation, enthusiasm, and immense knowledge. His guidance helped me throughout my research and writing of this thesis. I could not have imagined having a better advisor and mentor for my Ph.D study. I would like to thank him from the bottom of my heart.

Besides my advisor, I would like to thank the rest of my committee members: Dr. Scott Bohle, Dr. Gonzalo Cosa, and, Dr. Mark Andrews for their encouragement, insightful comments, and hard questions. My sincere thanks goes to our collaborator Dr. Dusica Maysinger from Faculty of medicine, McGill University.

I would like to thank my fellow labmates, Tina Lam, William Curtis, Mathieu Bedard, Yu Chen, Aurelie Regnaud, Amber Nawaz, and Graeme Cambridge for the stimulating discussions, and for all the fun we have had in the last four years. I would like to thank our former group members Dr. Soren Leth Mejlsoe, Dr. Ghareb Soliman, Vanessa Ng, Elizabeth Ladd, and Kunal Khanna. My special thanks to Rami Hourani for sharing brilliant research ideas, Dr. Annie Castoguay for her kind support and help in writing French version of the abstract of this thesis; and Dr. Aradhana Bachher for having wonderful times together. I would also like to thank Ghareb Soliman, Kevin Neibert, Armen Khatchadourian, Noura Al-Hajaj and Diana Mejia for doing work in collaborations.

I am greatly thankful to Dr. Nadim Saadeh for mass and MALDI-TOF spectroscopy analysis, Frederick Morin for NMR analysis, and Petr Fiurasek for UV-Vis, and Fluorescence trainings. I am grateful to NSERC, CSACS, and Chemistry Department, McGill University for all the financial assistance. My special thanks go to the incredible people in the chemistry department, Sandra,

Karen, Alison, Fay, and Chantal. I thank them from the core of my heart for their support.

Last but not the least, I would like to thank my family, my parents Amrit Kaur and Sadhu Singh, for giving birth to me and supporting me throughout my life, my sisters Manpreet and Kitty, my parents-in-law Ashok Sharma and Manju Sharma to inspire me to pursue higher studies, my husband Rishi Sharma for all his love and support, and my daughter Manya Sharma for being such a wonderful part of my life.

Abstract

The synthesis of well defined multifunctional nanocarriers capable of simultaneously imaging, targeting and delivering therapeutics to specific cellular organelles continues to be a tedious task. The challenge is to develop simple and efficient synthetic methodologies which can allow the incorporation of multiple functional units in a single nanocarrier. Hyperbranched (dendrimers) and branched (miktoarm stars) macromolecules provide an excellent platform to construct such multifunctional nanocarriers. In this thesis, we report the development of versatile and efficient synthetic methodologies for the construction of multifunctional nanocarriers based on dendrimers and miktoarm polymers. The nanocarriers were synthesized using building blocks with orthogonal functional groups on which sequential reactions can be carried out with ease, and different functionalities can be covalently introduced. example, we first developed a synthetic methodology to introduce two different functions in a single dendrimer scaffold. We designed and synthesized bifunctional nanocarrier in which a therapeutic agent, Niacin, in combination with the imaging dye BODIPY were attached, using highly efficient "click" reaction and Steglich esterification. These nanocarriers were evaluated for the delivery of Niacin to lipid droplets, and they were found almost exclusively within cytoplasmic lipid droplets. Biological studies suggested that these multifunctional nanocarriers did not cause significant cell death, and can be suitably used for imaging and for targeting drugs to lipid droplets. The synthetic methodology was then extended to synthesize a variety of bi-functional dendrimers with different combinations of drugs, dye and solubilizing agents. For example, bifunctional dendrimers containing covalently linked α-lipoic acid or the dye BODIPY, together with polyethylene glycol (PEG), were prepared. We subsequently further expanded the versatility of our synthetic approach and designed a tri-functional dendrimer, where we incorporated all the three functionalities, α -lipoic acid, BODIPY and the solubilizing polymer PEG, in a single nanoscaffold. These carriers were internalized into the cells where they were able to reduce H₂O₂ induced reactive oxygen species formation. We have also explored physical entrapment of drugs into miktoarm polymeric micelles. We have designed and constructed multifunctional nanocarriers based on ABC type miktoarm polymers (A = PEG, B = polycaprolactone (PCL), and C = triphenylphosphonium bromide (TPPBr)), to target mitochondria. The miktoarm stars were synthesized using a combination of "click" chemistry with ring-opening polymerization. These were then self-assembled into nanosized micelles, and were employed to load the drug CoQ10. The micelles showed high drug loading capacity, and the studies of the fluorescently labeled polymer analog showed that the carrier did indeed reach mitochondria. The versatility of the "click" chemistry used to prepare these new mitochondria-targeting nanocarriers offers a simple and easily reproducible procedure to develop a wide variety of multifunctional nanocarriers to deliver drugs to mitochondria, or other intracellular locations. As the future of the nanomedicine is progressing towards designing trackable therapeutics, we have developed a synthetic methodology to construct fluorescently labeled dendrimers for detecting these drug carriers at the cellular level. Tetraiodofluorescein, a model fluorescent marker, constitutes the inherent part of these nanocarriers. As proof of concept, one of the hydroxyl-terminated inherently fluorescent dendrimer was utilized to attach the model drug α -lipoic acid. The synthetic tools developed in this thesis provide a general platform to design multifunctional nanocarriers incorporating any desired combination of entities for Theranostics.

Résumé

La synthèse de nanotransporteurs capables de simultanément imager, cibler, de même que d'effectuer la livraison d'agents thérapeutiques à des organites cellulaires spécifiques continue d'être une tâche difficile. Le défi réside dans le développement de méthodologies synthétiques simples et efficaces pouvant permettre l'incorporation de multiples unités fonctionnelles en un simple nanotransporteur. Les macromolécules hyperbranchées (dendrimères) et branchées (étoiles « miktoarms ») procurent une excellente plateforme pour construire de tels nanotransporteurs. Dans cette thèse, nous rapportons le développement de méthodologies synthétiques versatiles et efficaces pour la construction de nanotransporteurs multifonctionnels à base de dendrimères et de polymères « miktoarms ». Les nanotransporteurs ont été synthétisés en faisant usage d'unités de base comprenant des groupes fonctionnels orthogonaux sur lesquels des réactions séquentielles peuvent être facilement effectuées, et différentes fonctionnalités peuvent être introduites de façon covalente. Par exemple, nous avons premièrement développé une méthodologie synthétique pour introduire deux différentes fonctions à un seul dendrimère. Nous avons fait le design et la synthèse de nanotransporteurs bifonctionnels pour lesquels l'agent thérapeutique Niacin et le colorant pour imagerie BODIPY ont été combinés en utilisant une réaction "click" simple et hautement efficace de même qu'une estérification de Steglich. Ces nanotransporteurs ont été évalués pour la livraison du Niacin aux goutelettes lipidiques. Les nanotransporteurs contenant Niacin et BODIPY ont été observés exclusivement à l'intérieur des gouttelettes lipidiques cytoplasmiques. Des études biologiques ont suggéré que ces nanotransporteurs multifonctionnels ne causent pas la mort significative des cellules, et peuvent être utilisés pour l'imagerie ou bien pour livrer des médicaments aux gouttelettes lipidiques. Cette méthodologie synthétique a été étendue pour préparer une variété de dendrimères fonctionnels avec différentes combinaisons de médicaments, colorants et agents de solubilisation. Par exemple, des dendrimères bifonctionnels contenant l'acide lipoïque ou bien le colorant BODIPY, avec du polyéthylène glycolique (PEG), ont été préparés. Nous avons subséquemment étendu davantage la versatilité de notre approche synthétique et avons fait le design d'un dendrimère trifonctionnel, où nous avons incorporé toutes les trois fonctionnalités, soient l'acide liporque, BODIPY, et le polymère solubilisant PEG, en une unique nanostructure. Ces transporteurs ont été introduits à l'intérieur des cellules où ils ont démontré leur potentiel à réduire la formation d'espèces oxygénées réactives, préalablement induites par le peroxyde d'hydrogène. Nous avons exploré l'encapsulation physique de médicaments à l'intérieur de micelles polymériques « miktoarms ». Nous avons effectué le design et avons construit des nanotransporteurs basés sur des polymères « miktoarms » de type ABC (A = PEG, B = polycaprolactone (PCL), et C = bromure de triphenylphosphonium (TPPBr)), pour ensuite les livrer vers le mitochondrie. Les étoiles « miktoarms » ont été synthétisées en utilisant une combinaison de chimie « click » et de polymérisation par ouverture de cycle. Ces étoiles ont alors été auto-assemblées en micelles, et ont été chargées du médicament CoQ10. Les micelles ont démontré une capacité élevée à encaspuler le médicament, et les études d'un polymère fluorescent analogue ont démontré que le transporteur est en effet capable d'atteindre sa cible, le mitochondrie. La versatilité de la chimie "click" utilisée pour préparer ces nouveaux nanotransporteurs capables de cibler le mitochondrie offre une procédure simple et facilement reproductible pour développer une vaste gamme de nanotransporteurs multifonctionnels pour livrer des médicaments au mitochondrie, ou bien à d'autres cibles intracellulaires. Comme le futur de la nanomédecine progresse vers le design d'agents thérapeutiques tractables, nous avons développé une méthodologie synthétique pour construire des dendrimères fluorescents afin de détecter ces livreurs de médicaments au niveau cellulaire. Le tétraiodofluorescéine, un marqueur fluorescent modèle, constitue la partie inhérente de la structure de ces nanotransporteurs. Comme preuve de concept, la périphérie de ces dendrimères (composée de groupements hydroxyles) a été utilisée pour attacher le médicament modèle α-acide lipoïque. Les outils synthétiques développés dans cette thèse procurent une plateforme générale pour effectuer le design de nanotransporteurs pouvant comporter n'importe quelle combinaison d'entités à des fins théranostiques.

Table of Contents

Preface

Dedica	tionii
Acknow	wledgementsiii
Abstrac	ctv
Résumo	évii
Table o	of Contentsx
List of	Figuresxv
List of	Schemes xx
List of	Tablesxxi
List of	Abbreviations and acronymsxxii
Contrib	outions of authors xxv
Licence	es <i>xxviii</i>
Chapter	1
Introduction	and scope of the thesis1
1.1 Inti	oduction to dendrimers and miktoarm polymers2
=	nthetic challenges in the construction of dendrimers and miktoarms dical applications
1.2.1	Challenges in the synthesis of dendrimers4
1.2.2	Challenges in the synthesis of miktoarm polymers8
	ities of drug incorporation into dendrimers and miktoarm polymers
1.3.1	Drug loading by physical incorporation11
1.3.2	Drug loading by chemical conjugation
1.3.2.	-
1.0.2.	1 Direct coupling

1.4 I	Dendrimers and miktoarm polymers for targeted drug delivery 20
1.4.1	Passive targeting21
1.4.2	Active targeting
1.5 I	Dendrimer and miktoarm cytotoxicity
1.6	Conclusions
1.7 F	References
1.8 Upd	ate subsequent to publication of the above review49
1.9 Sco	pe of the thesis
Chapte	r 2 57
-	nt Niacin Nanoconjugates for Delivery to Cytoplasmic Lipid Droplet
	57
2.1 I	ntroduction59
2.2 N	Materials and methods60
2.2.1	Materials60
2.2.2	Synthesis61
2.2.3	Cell cultures
2.2.4	Nitric oxide production:
2.2.5	Measurement of biocompatibility by the MTT reduction assay68
2.2.6	Confocal microscopy69
2.2.7	Flow cytometry69
2.2.8	Statistics70
2.3 F	Results and discussion70
2.3.1	Synthesis of nanocarriers70
2.3.2	Biological studies
2.4	Conclusions83
2.5 F	References84
Chapte	er 3 89
	nstruction of Multifunctional Nanocarriers Using Sequential Click for Applications in Biology89
3.1 I	ntroduction91
3.2 E	Results and discussion 92

3.3	Co	nclusions	102
3.4	Ex	perimental section	102
3.4	l.1	Materials and methods:	102
3.4	1.2	Synthesis:	103
3.4	1.3	Biological studies:	111
	3.4	3.1 Cell culture and media	112
	3.4	3.2 Assessment of cytotoxicity	112
	3.4	3.3.3 Assessment of reactive oxygen species formation	on (ROS)112
		4.3.4 Spectrofluorometric measurements of total intratathione	
	Ū	3.5 Cellular internalization of BODIPY labeled der	
3.5		ferences	
Chap	ter	4	117
Design	and	Evaluation of Multi-functional Nanocarriers for Selection (Page 1978) Evaluation (Pag	ective Delivery
4.1 Iı	ntrod	uction	119
4.2 E	xper	imental section	121
4.2	2.1 M	laterials and methods	121
4.2	2.2 S	ynthesis of ABC miktoarm polymers	122
4.2	2.3 P	reparation of blank and CoQ10-loaded miktoarm mi	celles127
4.2	2.4 C	haracterization	127
4.2	2.5 C	alculation of Flory Huggins interaction parameters (
Co	Q10	and PCL	129
4.2	2.6 C	ritical association concentration (CAC) of ABC mik	toarm micelles
			130
4.2	2.7 St	tability studies	130
2	4.2.7	.1 Micelles colloidal stability	130
2	4.2.7	.2 Photostability of CoQ10	130
4.2	2.8 D	ifferential scanning calorimetry (DSC) studies	131
4.2	2.9 C	ell culture and media	131
4 2	10 (Cells Viability	132

4.2.11	Superoxide anion and reactive oxygen species detection 132
4.2.12	Confocal microscopy
	Fluorescent microscopy for mitochondrial membrane potential rement
4.3 R	esults and discussion
4.3.1	Synthesis and Characterization of ABC miktoarm polymers134
4.3.2	Preparation and characterization of miktoarm polymer micelles 137
4.3.3 micell	CoQ10 incorporation into PEG2-PCL-TPPBr miktoarm polymer es 140
4.3.4	Thermal analysis
4.3.5 \$	Stability studies
4.3.	5.1 Critical association concentration (CAC)146
4.3.	5.2 Physical stability of the CoQ10-containing micelles147
4.3.	5.3 CoQ10 photostability147
4.3.6 biolog	Localization of miktoarm nanocarrier in mitochondria and ical activity of CoQ10 in stressed microglia148
4.4 Conc	clusions
4.5 Refe	rences
Chapte	r 5
•	Evaluation of Multifunctional Inherently Fluorescent Dendrimers ostics
5.1 Intro	duction
5.2 Resu	lts and discussion
5.2.1 \$	Synthesis161
5.2.2 I	Biological studies
5.3 Conc	elusions:
5.4 Expe	rimental
5.4.1 N	Materials and methods
5.4.2 \$	Synthesis:
5.4.3	Cell culture177

5.4.4 Measurement of mitochondrial metabolic activity and cell viability
5.4.5 Spectrofluorometric measurements
5.4.6 Confocal microscopy178
5.4.7 Measurement of nitric oxide release
5.4.8 Data and Statistical analysis179
5.5 References
Chapter 6 183
Conclusions, Contributions to Original Knowledge, and Suggestions for Future Work
6.1 Conclusions and Contributions to Original Knowledge183
6.2 Suggestions for future work
6.2.1. Designing amphiphilic dendritic polymers using Click chemistry186
6.2.2. Designing tetrafunctional dendrimer: Combining Therapeutics, Imaging, Stealth and Targeting
6.2.3. Designing multifunctional trackable dendrimers for theranostic applications
Appendix 1 190
Designing dendritic frameworks using versatile building blocks suitable for Cu ^I -catalyzed alkyne azide 'click' chemistry
Appendix 2
Supporting Information - Chapter 2: Multivalent Niacin Nanoconjugates for Delivery to Cytoplasmic Lipid Droplets
Appendix 3 204
Supporting Information – Chapter 3: Facile Construction of Multifunctional Nanocarriers Using Sequential Click Chemistry for Applications in Biology20
Appendix 4 214
Supporting Information – Chapter 4: Design and Evaluation of Multi-functional Nanocarriers for Selective Delivery of Coenzyme Q10 to Mitochondria. 214

List of Figures

Figure 1.1. Dendrimer and miktoarm polymer architecture4
Figure 1.2. Multifunctional Dendrimer
Figure 1.3. Schematic illustration of physical drug incorporation into dendrimers and micelles of miktoarm polymers with rapid drug release in the blood stream
Figure 1.4. Selective incorporation based on drug molecular size into copolymers of $poly(\beta$ -cyclodextrin) (β -CD)- $poly(N,N$ -dimethylaminoethyl methacrylate) (PDMA)
Figure 1.5. Schematic illustration of biodistribution of intravenously injected nanoparticles showing nanoparticles accumulation in tumors due to the EPR effect, nanoparticles uptake by the RES system, and nanoparticles excretion by the kidney
Figure 1.6. Selective uptake of G4 PAMAM-OH-FITC dendrimer in activated microglia and astrocytes following subarachnoid injection in the cerebral palsy rabbit model. Adapted from ref. 212
Figure 1.7. Colocalization of niacin-and BODIPY-conjugated dendrimer with lipid droplets in human hepatocytes (A) and murine microglia (B) 27
Figure 2.1. Internalization of fluorescent carriers in N9 microglia and HepG2 hepatocytes. Cells cultured in serum (1%) containing media were treated with 7, 10 and 4 for 1, 6, 24 and 48h. For all treatments, the final concentration of the fluorescent dye BODIPY was 1μM. At the indicated time points, cells were washed and prepared for FACS analysis (refer to Experimental procedures). The uptake was determined by measuring the mean fluorescence intensity (MFI) of (A) N9 microglia and (B) HepG2 hepatocytes using 544/590 nm excitation/emission settings. Data were obtained from two independent experiments (n=3) and are expressed as MFI ± standard error of the mean (SEM). Significant differences and p values are discussed in Results and discussion
Figure 2.2. Determination of biocompatibility of fluorescent and non-fluorescent nanocarriers. N9 microglia cultured in serum (1%) containing media were incubated with (A) non-fluorescent polymers (13, 12 and 15) and (B) fluorescent polymers (4, 10 and 7) for 24 and 48h. The final concentration of niacin (NA) in carriers treated cells was 50 μM. Free NA was added at a concentration of 50 or 500 μM. Cell viability was assessed by measuring mitochondrial metabolic activity using the MTT reagent assay (described in

Experimental procedure). Data were obtained from at least two independent experiments and are expressed as mean (%) cell viability \pm standard error of

- **Figure 2.3.** Assessment of nitric oxide (NO) production following treatment with niacin and niacin-conjugated nanocarriers. N9 microglia cultured in serum (1%) were incubated with niacin (NA, 50 μ M), 12, 13 and 15 for 24h with or without LPS (10 μ g/mL). When LPS was also present, cells were first treated with the polymers for 2h, and then incubated with LPS for another 24h. NO production in the supernatants was measured using the Griess reagent assay and expressed as concentration of NO (μ M). Mean values (\pm SEM) were obtained from triplicate analysis and from at least two independent experiments. Statistically different values are indicated by * p<0.005...80
- **Figure 2.4.** Colocalization of niacin-conjugated nanocarriers with lipid droplets in hepatocytes and microglia. Cells seeded in confocal chamber slides were cultured overnight in 1% serum-containing media supplemented with oleic acid (100 μM). Lipid droplets in hepatocytes (A) and microglia (B) were stained with the green fluorescent dye Bodipy 493/503 (20μM) for 10 min. Lipid droplets (green) and carriers (red) (4, 7 and 10) were imaged using a Zeiss LSM 510 confocal microscope soon after (~ 1 min) polymers were added. Z-stacks consisting of a total of 10 Z-slices (each 0.3 μm deep) were acquired for each field. Colocalization of carriers with lipid droplets is indicated by the presence of yellow regions resulting from the overlap between the signal in the green and red channels. Scale bar = 20 μm.....82
- Figure 3.1. Measurement of cellular metabolic activity and inhibition of superoxide formation following exposure to α-lipoic acid conjugated dendrimer and miktoarm nanocarriers in PC12 cells. A) Nanocarrier metabolic activity as assessed by Alamar Blue assay is indicative of cell viability. PC12 cells were treated for 24 hours with equimolar concentrations of various dendrimer and miktoarm nanocarriers with respect to α-lipoic acid (200 µM). Cellular metabolic activity was determined and expressed as a percentage with respect to the untreated control. Data are presented as means ± SEM of three individual experiments of triplicates. No significant differences were detected. **B**) Reactive oxygen species (ROS) generation following acute oxidative (1 hour) insult was assessed using dihydroethidium (DHE), a fluorescent probe sensitive to super oxide radicals. PC12 cells were pretreated with dendrimers and miktoarm nanocarriers for 6 hours prior to 1 hour 300 µM H₂O₂ exposure. DHE fluorescent intensity was determined spectrofluorimetricly and expressed as a change (percentage) with respect to the untreated control cells. Data are presented as means \pm SEM of three individual experiments of triplicates. Statistically significant differences from the H₂O₂ untreated control (first black bar) are shown (** p<0.01, *** p<0.001). Statistically significant differences from free α-lipoic acid are shown (a, p<0.001)......98

- **Figure 3.2.** Assessment of total intracellular glutathione following exposure to α lipoic acid conjugated dendrimer and miktoarm nanocarriers. A) Total intracellular glutathione content was assessed using monochlorobimane (mCBI), a probe which binds specifically to reduced glutathione (GSH) forming the fluorescent mCBi-GSH adduct. Representative fluorescent micrographs of PC12 cells treated for 24 hours with free α -lipoic acid (LA), **9** and **17** in equimolar concentrations with respect to α -lipoic acid (200 µM), were selected from at least three independent experiments of triplicates. The nucleus was stained with Hoechst and is visible in blue. Scale bar represents 10 um. **B**) The fluorescent intensity of the mCBI-GSH adduct was measured using spectrofluorimetry in PC12 cells treated for 24 hours with drug conjugated nanocarriers in equimolar concentrations with respect to α -lipoic acid (200 µM). Data is expressed as a percentage with respect to the untreated control. Data are presented as means \pm SEM of three individual experiments of triplicates. Statistically significant differences from the untreated control are shown (*** p<0.001). Statistically significant differences from free α -lipoic acid are shown (a p<0.001). C) PC12 cells were treated for 6, 24, 48 and 72 hours with drug conjugated nanocarriers. The fluorescent intensity of the mCBi-GSH adduct was measured spectrofluorimetrically and expressed as a mean fluorescent intensity in arbitrary units. Data are presented as means ± SEM of three individual experiments of triplicates. Statistically significant differences from the
- **Figure 4.2.** (A) TEM image of PEG2-PCL7-TPPBr micelles (polymer concentration = 1 g/L). (B) Distribution of the hydrodynamic diameter ($D_{\rm H}$) of PEG2-PCL3.8-TPPBr micelles (Deionized water; polymer concentration: 1 g/L; θ : 90°). (C) Plots of intensity ratio (I_{338}/I_{333}) of pyrene excitation spectra ($\lambda_{\rm em} = 390$ nm) vs concentration of different PEG2-PCL-TPPBr miktoarm copolymers in water. (D) Hydrodynamic diameter of CoQ10-loaded/PEG2-PCL3.8-TPPBr micelles as a function of storage time at 4 °C (Deionized water; polymer concentration : 1 g/L ;CoQ10 loading :10 wt. %).

- Figure 4.7. Mitochondrial membrane potential measured by TMRE in H₂O₂ stressed cells is partially retained upon treatment with CoQ10 alone or released from the nanodelivery system. Primary hippocampal neurons and glia were treated as described in the Materials and methods section. A) Z-Stack confocal micrographs of 9 confocal sections for control cells (CTL) treated only with TMRE (100 nM, 30 min) taken at an interval of 0.3 µm. Insets represent the enlarged area (zoomed) for each corresponding section. Scale bar (20 µm) in control is representative for all panels. Scale bar (2 µm) is representative for all zoomed areas. B) Schematic illustrating the position along the Z-axis with respect to sections shown in A (numbered 1-9). C) Confocal micrograph of live cells showing loss in mitochondrial membrane potential following H₂O₂ exposure (1 mM, 40 min) using TMRE (100 nM, 30 min) that was partially retained in cells pretreated with CoQ10 (1 µM, 24 hr) and CoQ10-Targeted micelle (1 µM, 24 hr) compared to untreated control (CTL). Each image represents a Z-stack consisting of 6-9 confocal sections taken at an interval of 0.3 µm. Scale bar (20 µm) in control is representative for all panels. Scale bar (2 µm) is representative for all zoomed areas. Images were acquired using HeNe (543 nm) excitation laser.
- **Figure 5.2.** Fluorescent dendrimers do not affect N9 or J774.2 cell viability. Microglia and macrophages were assayed for cell viability as measured by the extent of mitochondrial activity with an MTT assay. N9 microglia were

point, MTT was added to cells and formazan crystal formation was measured using a spectrophotometer at 595 nM. Data is represented as mean \pm standard deviation (n=3). Representative brightfield images were acquired for microglia treated for 90 minutes with fluorescent dendrimers C)167
Figure 5.3. Fluorescent intensity of dyes and dendrimers taken up by N9 microglia. Microglia were treated with fluorescent dyes ($10nM-5\mu M$) or dendrimers ($500nM-5\mu M$) for 90 minutes. At treatment end-time point, cells were washed and fluorescence intensity was measured. All data are presented as group means \pm SEM. Values are indicated by * (p <0.05), ** (p<0.01) and *** (p<0.001)
Figure 5.4. Fluorescent dyes are taken up by N9 microglia rapidly and non-specifically. N9 microglia were treated with dyes (100 or 500 nM) for indicated time and fluorescence intensity was measured (A). Representative images of microglia treated with dyes (500 nM $-$ 5 μ M, 90 min) and hoechst (10 μ M, 10 min) are shown (B).
Figure 5.5. Dendrimers are taken up by N9 microglia and show a punctate distribution within the cells. Representative images of microglia treated with dendrimers (1 μM, 90 min) are shown (A). Cells were fixed and nuclei stained with Hoechst (10 uM, 10 min). Confocal images of treated microglia were acquired to confirm dendrimer internalization (B). Figure 5.5. Dendrimers are taken up by N9 microglia and show a punctate distribution within the cells. Representative images of microglia treated with dendrimers (1 μM, 90 min) are shown (A). Cells were fixed and nuclei stained with Hoechst (10 uM, 10 min). Confocal images of treated microglia were acquired to confirm dendrimer internalization (B)
Figure 6.1. Amphiphilic dendritic polymer
Figure 6.2. Tetrafunctional dendrimer with a combinition of therapeutics, imaging, stealth and targeting agents
Figure 6.3. Multifunctional trakable dendrimer

treated with 6-OH dendrimer for 6 and 24 hours B). At treatment end-time

List of Schemes

Scheme 2.1. Synthesis of bifunctional dendrimer 4 containing BODIPY dye and Niacin molecules
Scheme 2.2. Synthesis of linear analog 7 containing covalently linked BP dye and Niacin
Scheme 2.3. Synthesis of trifunctional unit 10
Scheme 2.4. Synthesis of monofunctional dendrimers 12 and 1375
Scheme 2.5 . Synthesis of 15
Scheme 3.1 . Synthesis of bifunctional dendrimer 6 containing BODIPY dye and PEG ₇₅₀ chains
Scheme 3.2 . Synthesis of bifunctional dendrimer 9 (containing α -lipoic acid and PEG ₇₅₀ chains), and trifunctional dendrimer 13 (containing α -lipoic acid, BODIPY dye and PEG ₇₅₀ chains)
Scheme 3.3. Synthesis of miktoarm unit 15 having all the three functionalities PEG ₇₅₀ , BODIPY dye and α-lipoic acid
Scheme 3.4. Synthesis of miktoarm unit 17 having 2 PEG ₇₅₀ chains and a molecule of α-lipoic acid
Scheme 4.1. Synthesis of ABC miktoarm star polymers containing PEG, PCL and triphenylphosphonium bromide
Scheme 4.2. Synthesis of Fluorescein isothiocyanate (FITC) conjugated ABC miktoarm star polymer 9 (non-targeted) and 10 (with targeting moiety TPP ⁺ cation)
Scheme 5.1. Synthesis of building blocks with carboxylic acid or hydroxyl functional groups
Scheme 5.2. Synthesis of fluorescent core with six propargyl functions163
Scheme 5.3. Synthesis of trackable dendrimer 12 with 6 hydroxyl functional groups and 13 with 6 drug molecules
Scheme 5.4. Synthesis of trackable dendrimer 14 with 12 hydroxyl functional functions
Scheme 5.5. Synthesis of linear compounds 15 and 16

List of Tables

Table 4.1 GPC analysis of miktoarm polymers	138
Table 4.2 Properties of blank and CoQ10-loaded miktoarm polym	ers based
micelles	139

List of Abbreviations

AFM Atomic force microscopy

ATRP Atom transfer radical polymerization

bis-MPA Dimethylolpropionic acid

 β -CD β -cyclodextrin

CNS Central nervous system

CROP Controlled ring opening polymerization

CPT Camptothecin

CP Cerebral palsy
CoQ10 Coenzyme Q10

CuAAC Cu (I) catalyzed alkyne-azide click chemistry

COX-2 Cyclooxygenase-2

CIPhIQ 1-(2-chlorophenyl)isoquinoline-3-carboxylic acid

DMPC 1,2-dimyristoyl-sn-glycero-3-phosphocholine

DGAT2 Diacylglycerol acyltransferase 2

DDS Designed delivery systems

DMAP 4(dimethylamino)pyridine

DCC *N,N'* -dicyclohexylcarbodiimide

DMF N,N' -dimethylformamide

DHE Dihydroethidium

DMSO Dimethylsulfoxide

DCM Dichloromethane

Dox Doxorubicin

EDTA Ethylenediaminetetraacetic acid

EDC 1-[3-(Dimethylamino)propyl]-

3ethylcarbodiimidemethiodide

EPR Enhanced permeability and retention

FACS Fluorescence activated cell sorting

FA Folic acid

5-FU 5-fluorouracil

FBS Fetal bovine serum

FITC Fluoresceinisothiocyanate

GSH Glutathione

GPC Gel permeation chromatography

Glu Glutamic acid

HDL-C High density lipoprotein cholesterol

Hz Hertz

HMPA *N*-(2-hydroxylpropyl)methacrylamide (HPMA)

iNOS Inducible nitric oxide synthase

LDH Lactate dehydrogenase

Luc Luciferase

LDs Lipid droplets

LDL-C Low density cholesterol

LA α-Lipoic acid

LL Levofloxacin lactate

MAPs Multiple antigen peptides

MRI Magnetic resonance imaging

mCBi Monochlorobimane

MALDI-TOF Matrix assister lazer desorption ionization-time of flight

MFI Mean fluorescence intensity

MTX Methotrexate

NaAsc Sodium ascorbate

NO Nitric oxide

NAC *N*-acetyl cysteine

NMR Nuclear magnetic resonance

NMP Nitroxide-mediated radical polymerization

O/N Overnight

PEG Poly(ethylene glycol)

PCL Poly(caprolactone)

PAMAM Poly(amidoamine)

PPI Poly(propylene imine)

PAA Poly(acrylic acid)

PEI Poly (ethylene imine)

(PDMA) Poly(*N*,*N*-dimethylaminoethyl methacrylate)

PVP Polyvinylpyrrolidone

PGLSA-OH Poly(glycerol succinic-adipic acid)

PGA Penicillin-G-amidase

PC12 Pheochromocytoma cells

PP Phenolphthalein

RES Reticuloendothelial system

ROS Reactive oxygen species

RT Room temperature

RAFT Reversible addition-fragmentation chain transfer

SEM Standard error of the mean

SK Streptokinase

THF Tetrahydrofuran

TPP Triphenylphosphonium

TEB 1,3,5-triethynyl benzene

TBAF Tetrabutylammonium fluoride

Tf Transferring

WGA Wheat germ agglutinin

Contribution of Authors

"The Faculty of Graduate Studies and Research at McGill University allows, as an alternative to the traditional thesis format, a manuscript-based thesis, where the candidate has the option of including, as part of the thesis, the text of one or more papers submitted, or to be submitted, for publication, or the clearly-duplicated text (not the reprints) of one or more published papers. The thesis must be more than a collection of manuscripts. All components must be integrated into a cohesive unit with a logical progression from one chapter to the next. In order to ensure that the thesis has continuity, connecting texts that provide logical bridges preceding and following each manuscript are mandatory."

"When co-authored papers are included in a thesis, the candidate must be the primary author (the author who has made the most substantial contribution) for all papers included in the thesis. In addition, the candidate is required to make an explicit statement in the thesis as to who contributed to such work and to what extent."

Chapters 1, 2, 3, 4 and appendix 1 of this thesis are reproduced, in part, from published manuscripts, while Chapter 5 of this thesis is reproduced, in part, from manuscript being prepared for publication as the following:

Chapter 1: Soliman G. M. [†], Sharma A. [†], Maysinger D, and Kakkar A., *Chemical Communications*, **2011**, 47, 9572.

This manuscript is a review article written by the author with equal contribution (†) of co-author Ghareb M Soliman, a joint postdoctoral researcher in Dr. Kakkar's and Dr. Maysinger's groups. In addition to this, an update has been provided by the author since the wrting of this review article in 2011. The co-authors Dr. Kakkar and Dr. Maysinger have provided guidance and edited the text of the manuscript.

Chapter 2: Sharma A., Khatchadourian A., Khanna K., Sharma R., Kakkar A. and Maysinger D. *Biomaterials*, **2011**, 32, 1419.

This manuscript is co-authored by Armen Khatchadourian, a Ph.D. student in the Department of Pharmacology & Therapeutics, who performed all the biological experiments; Kunal Khanna, a former MSc. candidate in Kakkar's group, who synthesized 2 compounds (9 and 10); and Rishi Sharma, a former research associate in Kakkar's group, who synthesized 1 compound (15). Apart from that all other dendrimers and intermediates were synthesized and characterized by the author. Dr. Kakkar (my research supervisor) and Dr. Maysinger (collaborator for biology) have given guidance throughout the research work and in writing the manuscript.

Chapter 3: Sharma A., Neibert K., Sharma R., Hourani R., Maysinger D., & Kakkar A., *Macromolecules*, 2011, 44, 521.

This manuscript is co-authored by Kevin Neibert, a Ph.D. student in the Department of Pharmacology & Therapeutics, who performed the biological studies; Rishi Sharma, who synthesized only one compound (17); and Rami Hourani, a former PhD student who helped in developing ideas for this project. All other compounds except compound 17 were synthesized and characterized by the author. The co-authors Dr. Kakkar and Dr. Maysinger provided guidance throughout the work.

Chapter 4: Sharma A., Soliman G. M., Al-Hajaj N., Sharma R., Maysinger D., and Kakkar A., *Biomacromolecules*, 2012, 13, 239.

This manuscript is co-authored by Ghareb M Soliman, who performed the self assembly studies of miktoarm polymers and drug loading; Noura Al-Hajaj from Department of Pharmacology & Therapeutics, who carried out the biological experiments; and Rishi Sharma, who helped the author to perform Ring opening polymerization reaction. All the compounds in the manuscript were synthesized and characterized by the author. Dr. Kakkar and Dr. Maysinger gave suggestions and guidance.

Chapter 5: Sharma A., Mejia D., Maysinger D., and Kakkar A., Manuscript prepared for *Chemistry and Biology*, 2013.

This manuscript is co-authored by Diana Mejia from Department of Pharmacology & Therapeutics, who carried out the biological experiments. All the compounds in this chapter were synthesized and characterized by the author. Dr. Kakkar and Dr. Maysinger have provided guidance throughout the research work.

Appendix 1: Hourani, R.; Sharma, A.; and Kakkar, A. *Tetrahedron Letters* **2010**, 51, 3792-3795.

This manuscript is co-authored by Rami Hourani, a former graduate student in Dr. Kakkar's group. Major work in this manuscript has been done by Rami Hourani. Author contributed in synthesizing convergent building blocks 6a, 6b, 7 and monofunctional dendrimers, 10, 11a, and 11b. Dr. Kakkar provided guidance during research as well as writing of manuscript.



Royal Society of Chemistry Thomas Graham House Science Park Milton Road Cambridge CB4 0WF

Tel: +44 (0)1223 420 066 Fax: +44 (0)1223 423 623 Email: contracts-copyright@rsc.org

www.rsc.org

Acknowledgements to be used by RSC authors

Authors of RSC books and journal articles can reproduce material (for example a figure) from the RSC publication in a non-RSC publication, including theses, without formally requesting permission providing that the correct acknowledgement is given to the RSC publication. This permission extends to reproduction of large portions of text or the whole article or book chapter when being reproduced in a thesis.

The acknowledgement to be used depends on the RSC publication in which the material was published and the form of the acknowledgements is as follows:

- For material being reproduced from an article in New Journal of Chemistry the acknowledgement should be in the form:
 - [Original citation] Reproduced by permission of The Royal Society of Chemistry (RSC) on behalf of the Centre National de la Recherche Scientifique (CNRS) and the RSC
- For material being reproduced from an article Photochemical & Photobiological Sciences the acknowledgement should be in the form:
 - [Original citation] Reproduced by permission of The Royal Society of Chemistry (RSC) on behalf of the European Society for Photobiology, the European Photochemistry Association, and RSC
- For material being reproduced from an article in Physical Chemistry Chemical Physics the acknowledgement should be in the form:
 - [Original citation] Reproduced by permission of the PCCP Owner Societies
- For material reproduced from books and any other journal the acknowledgement should be in the form:
 - [Original citation] Reproduced by permission of The Royal Society of Chemistry

The acknowledgement should also include a hyperlink to the article on the RSC website.

The form of the acknowledgement is also specified in the RSC agreement/licence signed by the corresponding author.

Except in cases of republication in a thesis, this express permission does not cover the reproduction of large portions of text from the RSC publication or reproduction of the whole article or book chapter.

A publisher of a non-RSC publication can use this document as proof that permission is granted to use the material in the non-RSC publication.

VAT Registration Number: GB 342 1764 71 Registered Charity Number: 207890

ELSEVIER LICENSE TERMS AND CONDITIONS

Jul 29, 2013

This is a License Agreement between Anjali Sharma ("You") and Elsevier ("Elsevier") provided by Copyright Clearance Center ("CCC"). The license consists of your order details, the terms and conditions provided by Elsevier, and the payment terms and conditions.

All payments must be made in full to CCC. For payment instructions, please see information listed at the bottom of this form.

Supplier Elsevier Limited

The Boulevard,Langford Lane Kidlington,Oxford,OX5 1GB,UK

Registered Company

Number

1982084

Anjali Sharma Customer name 3450 Hutchison Customer address

Montreal, QC H2X 2G5

License number 3198271001368 License date Jul 29, 2013 Licensed content publisher Elsevier Licensed content Biomaterials

publication

Licensed content title Multivalent niacin nanoconjugates for delivery to cytoplasmic lipid

droplets

Licensed content author Anjali Sharma, Armen Khatchadourian, Kunal Khanna, Rishi

Sharma, Ashok Kakkar, Dusica Maysinger

Licensed content date February 2011

Licensed content volume

number

Licensed content issue

number

5

Number of pages 11 Start Page 1419 **End Page** 1429

Type of Use reuse in a thesis/dissertation

Portion full article

Format both print and electronic

Are you the author of this

Elsevier article?

Will you be translating? No

tps://s100.copyright.com/AppDispatchServlet

7/29/13 Rightslink Printable License

Order reference number

Title of your thesis/dissertation Design and Synthesis of Multifunctional Nanocarriers for Biological applications

Expected completion date Aug 2013

Estimated size (number of 260

pages)

Elsevier VAT number GB 494 6272 12

Permissions price 0.00 USD

0.00 USD / 0.00 GBP VAT/Local Sales Tax

0.00 USD Total

Terms and Conditions





Home

Account Info





Facile Construction of Multifunctional Nanocarriers Using Sequential Click Chemistry for Applications in

Biology

Author:

Anjali Sharma, Kevin Neibert, Rishi Sharma, Rami Hourani, Dusica Maysinger, and Ashok

Kakkar

Publication: Macromolecules

Publisher: American Chemical Society

Date: Feb 1, 2011

Copyright @ 2011, American Chemical Society

Logged in as: Anjali Sharma

LOGOUT

PERMISSION/LICENSE IS GRANTED FOR YOUR ORDER AT NO CHARGE

This type of permission/license, instead of the standard Terms & Conditions, is sent to you because no fee is being charged for your order. Please note the following:

- Permission is granted for your request in both print and electronic formats, and translations.
- If figures and/or tables were requested, they may be adapted or used in part.
- Please print this page for your records and send a copy of it to your publisher/graduate school.
- Appropriate credit for the requested material should be given as follows: "Reprinted (adapted) with permission from (COMPLETE REFERENCE CITATION). Copyright (YEAR) American Chemical Society." Insert appropriate information in place of the capitalized words.
- One-time permission is granted only for the use specified in your request. No additional uses are granted (such as derivative works or other editions). For any other uses, please submit a new request.













Design and Evaluation of Multifunctional Nanocarriers for

Selective Delivery of Coenzyme Q10 to Mitochondria

Author: Anjali Sharma, Ghareb M.

Soliman, Noura Al-Hajaj, Rishi Sharma, Dusica Maysinger, and

Ashok Kakkar

Publication: Biomacromolecules

Publisher: American Chemical Society

Date: Jan 1, 2012

Copyright © 2012, American Chemical Society

Logged in as: Anjali Sharma

LOGOUT

PERMISSION/LICENSE IS GRANTED FOR YOUR ORDER AT NO CHARGE

This type of permission/license, instead of the standard Terms & Conditions, is sent to you because no fee is being charged for your order. Please note the following:

- Permission is granted for your request in both print and electronic formats, and translations.
- If figures and/or tables were requested, they may be adapted or used in part.
- Please print this page for your records and send a copy of it to your publisher/graduate school.
- Appropriate credit for the requested material should be given as follows: "Reprinted (adapted) with permission from (COMPLETE REFERENCE CITATION). Copyright (YEAR) American Chemical Society." Insert appropriate information in place of the capitalized words.
- One-time permission is granted only for the use specified in your request. No additional uses are granted (such as derivative works or other editions). For any other uses, please submit a new request.

ELSEVIER LICENSE TERMS AND CONDITIONS

Aug 12, 2013

This is a License Agreement between Anjali Sharma ("You") and Elsevier ("Elsevier") provided by Copyright Clearance Center ("CCC"). The license consists of your order details, the terms and conditions provided by Elsevier, and the payment terms and conditions.

All payments must be made in full to CCC. For payment instructions, please see information listed at the bottom of this form,

Supplier Elsevier Limited

The Boulevard, Langford Lane

Kidlington, Oxford, OX5 1GB, UK

Registered Company

Number

1982084

Customer name Anjali Sharma Customer address 3450 Hutchison

Montreal, QC H2X 2G5

3206590613547 License number License date Aug 12, 2013

Licensed content publisher Elsevier

Licensed content

publication

Tetrahedron Letters

Designing dendritic frameworks using versatile building blocks suitable for Cu-catalyzed alkyne azide 'click' chemistry Licensed content title

Licensed content author Rami Hourani, Anjali Sharma, Ashok Kakkar

21 July 2010 Licensed content date

Licensed content volume number

Licensed content issue

number

29

Number of pages 4 Start Page 3792 End Page 3795

Type of Use reuse in a thesis/dissertation

Intended publisher of new other

work

Portion full article

Format both print and electronic

Are you the author of this Elsevier article?

https://s100.copyright.com/AppDispatchServiet

Rightslink Printable License

Will you be translating? No

Order reference number

Title of your Design and Synthesis of Multifunctional Nanocarriers for Biological applications

thesis/dissertation applications Expected completion date Aug 2013

Estimated size (number of 260

pages)

8/12/13

Elsevier VAT number GB 494 6272 12

Permissions price 0,00 USD

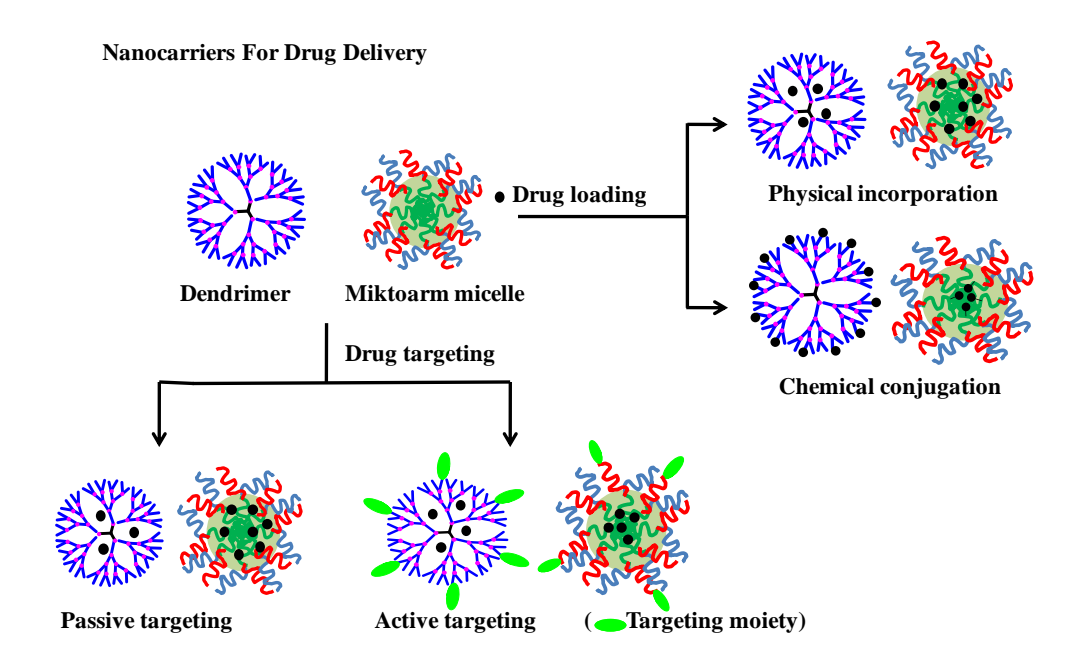
VAT/Local Sales Tax 0,0 USD / 0,0 GBP

Total 0.00 USD

Terms and Conditions

Chapter 1

Introduction and scope of the thesis



Reproduced in part with permission from:

Soliman, G. M.[†]; Sharma, A.[†]; Maysinger, D.; Kakkar, A., *Chemical Communications* **2011**, 47 (34), 9572-9587. († Equal authors)

Copyright, 2011, Royal Society of Chemistry

Dendrimers and Miktoarm Polymers Based Multivalent Nanocarriers for Efficient and Targeted Drug Delivery

The delivery of biologically active agents to the desired site in the body and intracellular organelles is still a big challenge despite efforts made for more than five decades. With the elaboration of synthetic methodologies to branched and hyperbranced macromolecules such as miktoarm stars and dendrimers, the focus has shifted to nanocarriers able to release and direct drug molecules to desired location in a controlled manner. We present here recent developments in the field of targeted drug delivery with a focus on two specific macromolecular nanocarriers, dendrimers and miktoarm stars, and provide examples of these nanocarriers tested in different biological systems. A particular attraction of miktoarm stars is their versatility in achieving superior drug loading within their self-assembled structures. Advantages of dendrimers over linear polymers are that the former provide a platform for development of multivalent and multifunctional nanoconjugates, in addition to their ability to accommodate large number of molecules inside, or at their surfaces.

1.1 Introduction to dendrimers and miktoarm polymers

Some of the current challenges facing theranostics (*i.e.*, combining therapy and diagnostics) include preparing drug carriers which are biologically inert, internalise easily into the cells and remain intact until they reach their intended target with high specificity.^{1, 2} Premature drug release and the inability to monitor the fate of drug carriers *in vivo*, are key issues that need to be addressed in developing drug delivery nanotechnology.^{3, 4} Nanocarriers based on biocompatible and/or biodegradable polymers have shown tremendous potential in addressing these unmet needs, and a significant effort has been devoted in the past to incorporate therapeutic agents into such polymeric nanoparticles using hydrophobic and/or electrostatic interactions.⁵⁻¹⁰ Some of the nanoparticles based on linear block copolymers have advanced well beyond experimental/conceptual phases and many are now in clinical trials, especially for cancer chemotherapy.⁷

^{11, 12} However, there are still several practical aspects of this technology that need to be addressed before any clinical implementation. For instance, micelles of linear block copolymers have low drug loading efficacy (ca. 5 weight %), insufficient stability *in vitro* and *in vivo* and rapid drug release *in vivo*. ¹³⁻¹⁵ In addition, it is becoming increasingly evident that multitasking using a single particle is essential to enhance their efficacy, a feature that is lacking in linear block copolymers. In this regard dendrimers and miktoarm polymers provide a highly useful platform to achieve these goals. ¹⁶

Branched and hyperbranched macromolecules such as miktoarm stars and dendrimers, 17-22 offer distinct structural features, but share a common thread in which arms emanate from a central core (Fig. 1.1). Dendrimers are hyperbranched and globular macromolecules with a well-defined core, backbone and multivalent periphery. The synthetic methodology to construct dendrimers was introduced by Vögtle and coworkers in 1978. However, the first series of dendrimers prepared using a well established method appeared in 1985 with the introduction of poly(amidoamine) (PAMAM) dendrimers by Tomalia. There has been considerable effort in the recent past that has led to synthetic elaboration of dendrimers, and numerous elegant methodologies now exist to construct these hyperbranched macromolecules with a tailor made architecture. Miktoarm polymers that are sometimes also referred to as asymmetric polymers or heteroarm polymers, are star-shaped macromolecues in which a variety of polymeric arms which could vary in chemical identity and/or molecular weight branch out from the core. The star star star star star star identity and/or molecular weight branch out from the core.

The intense interest of the scientific community in exploring the potential of dendrimers and miktoarm polymers for therapeutics delivery has been due to their versatility in structure, multivalency, and low polydispersity. ²⁸⁻³⁰ These features offer real life applications in enhancing drug loading efficiency, and in developing multi-tasking nanoparticle based technology for targeted delivery by conjugating drug, imaging and targeting moieties in the same scaffold. ^{31, 32} DNA and siRNA can also be bound to terminal groups of dendrimers by electrostatic interactions resulting in better transfection efficiency. ³³⁻³⁵ Similarly, hydrophobic

drugs can be solubilised by physical incorporation in the cavities of dendrimers or inside self-assembled structures of miktoarm polymers. This chapter is not intended to be an exhaustive review of the literature on dendrimers and miktoarm polymers. Instead, it will focus on recent developments in their efficacy as targeted drug delivery vehicles.

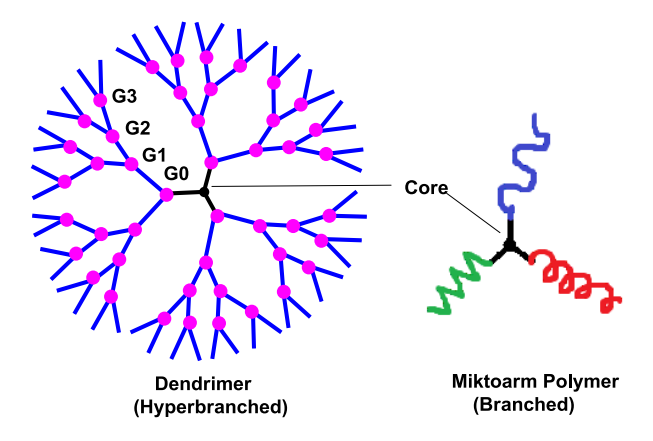


Figure 1.1. Dendrimer and miktoarm polymer architecture

1.2 Synthetic challenges in the construction of dendrimers and miktoarms for biomedical applications

In the recent past, dendrimers and miktoarm star polymers have become prominent in the field of biomedical science due to their unique morphological and physical properties as compared to linear polymers. Synthetic challenges associated with dendrimers and miktoarm polymers have been widely addressed by the chemical community during the last 25 years. A brief summary of this account is provided below.

1.2.1 Challenges in the synthesis of dendrimers

The most important aspect to synthesize a dendrimer for biological applications is to have proper control on the number and types of functional groups present at its periphery, as well as the type of backbone (*i.e.* if it is biodegradable/biocompatible).³⁹ These groups are required to attach diverse functional moieties⁴⁰ such as drug molecules, imaging^{41, 42} and targeting agents⁴³ etc. Historically, dendrimer synthesis has been carried out by either convergent or

divergent strategies, each with its own advantages and disadvantages. The dendrimer synthesis was initiated by Tomalia, ²⁴ Newkome, ⁴⁴ Vögle²³ using a divergent route, in which the construction starts from a core and progresses to the periphery with successive formation of new generations. ⁴⁵ The advantage of a divergent strategy is that one can synthesize higher generation dendrimers such as those reported for poly(amidoamine) or PAMAM and poly(propylene imine) or PPI dendrimers. ⁴⁶ But the drawback is that the dendrimers often have defects at higher generations due to incomplete reactions. To address this problem, often the monomers are added in excess which then requires purification at every step. Accelerated synthetic strategies have been developed by Malkoch *et al.* to reduce the number of steps associated with the divergent synthesis. This methodology involves two different monomers having complementary functionalities, which eliminates the need of deprotection. ⁴⁷

The convergent approach was introduced by Hawker and Fréchet,⁴⁸ and it involves the prior construction of branches of a dendrimer, the so called dendrons, which are then attached to the central core. The convergent approach is synthetically more demanding but the dendrimers can be produced in much higher purity as the number of active sites present per reaction are limited, thus reducing structural defects in the dendrimer. The dendrons can also act as building blocks, and can be attached to the poly-functional cores to synthesize multimodal dendrimers. The disadvantage of convergent approach is that it can be used only for lower generations as the attachment of larger dendrons on the core faces steric hindrances. However, lower generations may not be a limitation for dendrimers to be used for biological applications. ³⁸

The dendrimer synthesis has benefitted from the development of methodologies which involve reactions with fewer steps, high yields, having tolerance to a variety of functional groups, and which could be carried out under mild conditions with minimum purification steps. ^{47,49} Sharpless described a set of reactions which meet above mentioned criteria, and coined the term "Click" chemistry. ⁵⁰ Although a number of reactions come under the category of "click" chemistry, ²⁵ Cu(I) catalyzed Husigen 1,3 dipolar cycloaddition reaction is the

most popular one. Hawker et al. demonstrated the synthesis of dendrimers using this click methodology by reacting an azide terminated dendrimer with an alkyne monomer, followed by halogenation and azido substitution.⁵¹ This group used click reaction to synthesize dendrimers in a convergent manner in which a third generation dendron with azide focal point was constructed and clicked on to the polyacetylene core to obtain a 4th generation dendrimer.⁵² Recently, Hawker et al. used thiol-ene click reaction to construct dendrimers of up to generation 4 using a divergent route. With this method, they constructed dendrimers by an orthogonal strategy that eliminated the use of any solvent and metal catalysts, and it reduced the structural defects related to typical divergent synthesis.⁵³ For biomedical usage, there is still a need to construct dendrimers on large scale in an efficient and reproducible manner, with minimum defects in the structure. These 'fast' reactions would provide a greater control over the synthesis and reduce the need of purification. The development of a wide variety of chemo-selective ligation reactions, 54-56 like Staudinger ligation, 54 Cu(I) catalyzed alkyne-azide, 55 thiolene⁵⁶ and Diels-Alder click⁵⁷ reactions have helped to overcome the synthetic challenges associated with dendrimer synthesis.

The introduction of multiple functionalities in the same dendrimer (Fig. **1.2**) in a controlled manner is a synthetically challenging task, and only a few examples of dendrimers with more than two functionalities have been reported. ^{16, 26, 31, 32, 58-61} Our group recently developed a versatile synthetic methodology to biand tri-functional dendrimers with orthogonal end groups, using sequential Cu(I) catalyzed alkyne-azide click reactions. Using this approach, we synthesized multifunctional dendrimers with the desired combination of therapeutic agent (α lipoc acid or niacin), imaging agent (dipyrromethene boron difluoride) (BODIPY) and solubilising agent (polyethylene glycol) in decent yields. ^{16, 31, 32} An elaboration of this methodology allows covalent linking of any desired combination of functionalities at the periphery of dendrimers. The Cu (I) catalyzed alkyne-azide "click" reaction provides an efficient way to construct dendrimers in good yields with minimum purification. It has been reported that there is no detectable amount of the catalyst in the dendrimer products. In

addition, these dendrimers could be further purified to remove any residual copper by incubation with ethylenediaminetetraacetic acid (EDTA), followed by dialysis, using oxide-capped metallic iron nanoparticles as Cu sequesters. ^{62, 63}

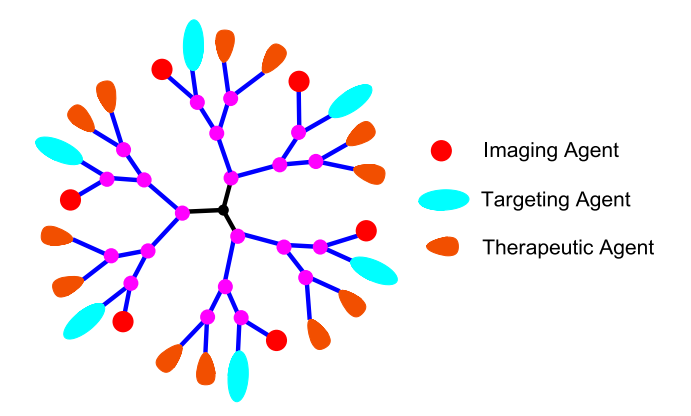


Figure 1.2. Multifunctional Dendrimer

Until now, the most commonly used dendrimers for biomedical applications have been PAMAM based. Introduction of multiple functionalities to commercially available PAMAM dendrimers, is achieved by a random statistical approach by partial functionalization of terminal amines.^{64, 65} Kannan's group has reported nearly complete peripheral modification (87-93%) of G4 PAMAM dendrimers, in which they used one-step synthesis to convert 64 symmetrical end groups into two reactive, distinct, orthogonal and chemo-selective moieties.⁶⁶ Weck and coworkers have introduced a new strategy towards multifunctional dendrimers in which they attached two poly(amide) based dendrons bearing different functionalities and a fluorescent dye on to a tri-functional core.⁶¹

Functionalization of the dendrimers not only provides a route to introduce a variety of drugs, imaging and solubilising agents, but it can also fulfill the objectives of targeted drug delivery^{67, 68}, increase in plasma residence time,⁶⁹ and reduction in cytotoxicity.⁷⁰ For example, cytotoxicity associated with amine terminated dendrimers has been overcome by PEGylation and acetylation.⁷¹⁻⁷⁵ PEGylation makes the dendrimers biocompatible, as well as helps meet other objectives including improved biodistribution and pharmacokinetics, solubility, increase in drug loading, sustained and controlled drug release etc.⁷⁶⁻⁷⁸ Sometimes, surface modifications can lead to problems. For example, Roth and

coworkers were able to decrease toxicity of PAMAM dendrimers to U87 cells, but higher degrees of amine neutralization reduced the gene silencing efficiency of PAMAM/siRNA delivery vectors.^{73, 75} Thus, there are still opportunities for chemists to develop synthetic methodologies that could achieve surface modifications without compromising their overall properties, and achieve functionalization with chemically reactive groups suitable for attachment of desired moieties at a low cost and minimum purification steps.

1.2.2 Challenges in the synthesis of miktoarm polymers

Miktoarm stars continue to attract considerable attention because of their compact architecture. 79-81 These were originally synthesized using living anionic polymerization methodologies. 82-86 However, these often involve stringent polymerization conditions and are restricted to only a few monomers. Recent developments in controlled/living polymerizations such as controlled ring opening polymerization (CROP),⁸⁷ atom transfer radical polymerization (ATRP),⁸⁸⁻⁹⁰ nitroxide-mediated radical polymerization (NMP)⁹¹ and reversible additionfragmentation chain transfer (RAFT) polymerization, 92 have provided efficient ways to design and synthesize well defined and complex miktoarm polymers. This is due to a wide variety of applicable monomers and mild polymerization conditions as compared to living anionic polymerization. Miktoarm stars are usually synthesized via one of the three common strategies: "core-first", "armfirst" or "in-out". 80, 93, 94 The core-first method employs living polymerization from a heteromultifunctional core initiator with different initiating sites.⁹⁵ With this method multiple arms can be grown simultaneously from a single core molecule. The major drawback of this method is that it involves complex multistep syntheses of heteromultifunctional initiators from small molecules, and often involves the use of protection/deprotection strategies which makes the chemistry complex. 96-98 For instance, Webster and coworkers have reported the synthesis of miktoarm stars from propargyl diol which was used to initiate ROP of ε-caprolactone followed by alkyne/azide click reaction of two arm ROP product with an azide functionalized poly(butyl acrylate) polymer. 99 In the "arm-first"

method, the chain ends of many linear macroinitiators formed from different controlled radical polymerization methods are used to polymerize a divinyl compound. The synthesis of miktoarm star polymers becomes problematic with this method when macroinitiators with different activity are used. The "in-out" method involves a living macroinitiator which initiates the polymerization of a cross linking agent to form a homoarm star polymer, with its initiating sites preserved within the core. It is used as a multifunctional initiator for the subsequent growth of second generation of arms. This is an important method for synthesizing miktoarm star copolymers with multiple arms. Its disadvantage is that all the initiating sites cannot participate in the reaction because of congestion around the core, thus decreasing the number of second generation arms as compared to first generation in miktoarm star copolymers. 100 The grafting of second generation arms in the core of star polymers has faced several obstacles such as star-star and intrastar couplings which can lead to broad molecular weight distribution. ¹⁰¹ In order to overcome this problem, Matyjaszewski and co-workers have proposed the synthesis of miktoarm core cross-linked star polymers by copolymerization of linear monomers with cross-linker using low molecular weight ATRP initiator. 102 The number of initiating sites and arms are independently controlled, thus reducing the star-star coupling reactions leading to smaller molecular weight distribution.

For applications in the field of biomedicine and nanotechnology, the miktoarm star polymers with novel architectures are required. The synthesis of A_nB_m multimiktoarm star polymers having more than 10 arms is very complex and these are rarely synthesized by simple controlled living polymerizations. Matyjaszewski and co-workers have reported a new method for the synthesis of multi-miktoarm star copolymers *via* one-pot ATRP cross-linking reaction of several different linear macroinitiators and a divinyl cross-linker. Using this strategy, the average number of arms can be extended to $50.^{100, 103, 104}$ But this strategy could not lead to miktoarm polymers with a precise architecture. The alternate method to synthesize these multi-miktoarm stars with precise arm number and arm length is by designing heteromultifunctional A_nB_m initiators, but

the synthesis of these initiators with more than 10 functionalities is a tedious task. To resolve this issue, polymer chemists started using naturally occurring cyclodextrins having fixed numbers of primary and secondary hydroxyl groups with different reactivities. Shen and co-workers have successfully synthesized $A_{14}B_7$ multimiktoarm star copolymers composed of 14 PCL arms and 7 poly(acrylic acid) (PAA) arms with β -cyclodextrin as core using a combination of CROP and ATRP.

The synthetic methodologies discussed above have their own limitations, and efforts are continually being made to develop facile and efficient routes to the synthesis of miktoarm polymers. Recent addition of "click chemistry" in combination with different living radical polymerization techniques has provided a useful tool in diversifying the synthetic strategy of these miktoarm polymers. ^{50, 93, 94, 109-113} A wide variety of miktoarm star copolymers have been synthesized using Cu(I) catalyzed azide-alkyne click reaction with living radical polymerization techniques. ^{99, 109, 114-121} We have recently reported the synthesis of A₂B and ABC type miktoarm stars containing a combination of polyethylene glycol, polycaprolactone and polystyrene arms, using a core with orthogonal functionalities on which Cu(I) catalyzed alkyne-azide click reactions and ring-opening polymerization are carried out in sequence. ^{114, 115}

Another click methodology is the Diels-Alder reaction, which generally consists of coupling of a diene and a dienophile by intra- or intermolecular reaction. Recently, Tunca and coworkers have synthesized multi-miktoarm star block copolymers where they have employed sequential double click reactions involving azide-alkyne and diels-Alder reactions. Wen-Li Deng and coworkers have synthesized miktoarm star copolymers by a combination of RAFT arm first technique and aldehyde-aminooxy click reaction. The advantage of using this click reaction is that except the reacting reagents no other auxiliaries such as metallic catalysts are required. In summary, numerous methods have been developed for the synthesis of miktoarm polymers, each with its own advantages, and the judicious choice of a synthetic methodology clearly depends on the type of desired miktoarm architecture.

1.3 Modalities of drug incorporation into dendrimers and miktoarm polymers

Active pharmaceutical agents can be either loaded into the internal voids of dendrimers and into self-assembled structures of miktoarm polymers by physical incorporation, or by covalent conjugation into the nanocarrier architecture.

1.3.1 Drug loading by physical incorporation

Due to their inherent architecture, drug molecules can be loaded into dendrimers using their well defined internal crevices by hydrophobic interactions or hydrogen bonding or by electrostatic interactions between drug ionic groups and oppositely charged dendrimer surfaces. The exact location of the solubilised drug and the loading capacity are controlled by several factors, such as dendrimer generation, architecture, characteristics of internal cavities, drug molecular weight and pK_a of drug ionisable groups.^{37, 124-127} A detailed computational and experimental study by Tomalia and coworkers has shown that low generation β alanine dendrimers (G1-G3) exhibit an oblong open structure while higher generations (≥G4) have a densely packed surface that is necessary to produce enclosed internal spaces that can incorporate and solubilise hydrophobic drugs. 128, ¹²⁹ Using poly(amidoamine) (PAMAM) dendrimers of different generations (G2-G6) and four different drugs, Cheng et al. compared the effect of internal hydrophobic interactions versus external electrostatic interactions on hydrophobic drug solubilisation. 130 By combining solubility and NMR studies, they demonstrated that external electrostatic interactions between the dendrimer surface and the drug contributed more to drug solubility enhancement than hydrophobic interactions in the PAMAM cavities. The ability of dendrimers to solubilise a variety of drugs including anticancer, anti-HIV and anti-inflammatory agents, has recently been reviewed. 21, 28, 131, 132

Compared to chemical conjugation, physical incorporation of drugs has the advantage of straightforward, rapid preparation without adversely affecting drug pharmacological activity. Its disadvantages include low stability in terms of storage and premature drug release, variation of the concentration of solubilised drug from batch to batch and low drug loading capacity. *In vitro* release of physically incorporated drugs from dendrimers is usually rapid, and depends on several factors such as drug partition coefficient between hydrophobic and aqueous environments, strength of drug/dendrimer interactions, dendrimer generation and surface groups (Fig. **1.3**). 133-135

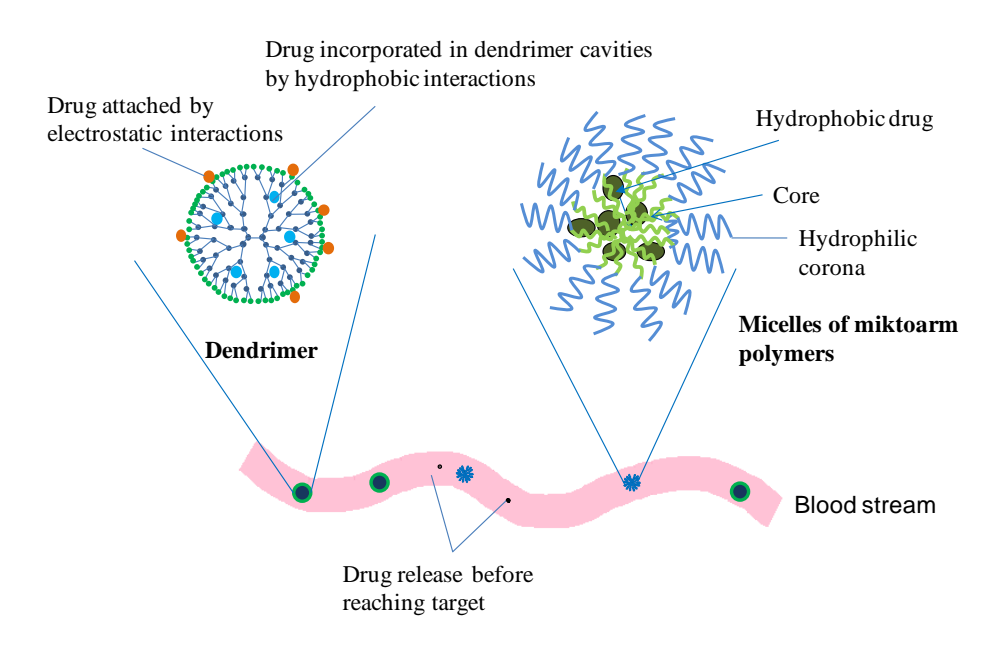


Figure 1.3. Schematic illustration of physical drug incorporation into dendrimers and micelles of miktoarm polymers with rapid drug release in the blood stream.

It has been shown that drug release and loading efficiency can be enhanced by PEGylation of dendrimers. For instance, the anti-cancer drug 5-fluorouracil showed 6-fold lower release rate and 12-fold higher loading capacity in PEGylated G4 PAMAM dendrimers in which 25% of PAMAM surface groups were capped with PEG (5 kDa) compared to non PEGylated dendrimers. ¹³⁶ In addition to PEGylation, entrapment of dendrimers in other nanocarriers, such as liposomes has been shown to sustain drug release. Gardikis *et al.* showed that at 96 h cumulative doxorubicin release from pure liposomes was 74.6±7.8%

compared to 27.9±2.8% when G2 dendrimer was co-encapsulated with doxorubicin in liposomes. Despite this improvement, controlled drug release in physiological media is difficult to achieve for drugs incorporated into dendrimers. Covalently linking drugs to dendrimers may help overcome some of these disadvantages.

Similar to dendrimers, drugs are incorporated into miktoarm stars by hydrophobic interactions (Fig. 1.3). However, miktoarm polymers have to be selfassembled first into nanoparticles since their architecture is different from that of dendrimers. For successful self-assembly in aqueous solutions, miktoarm polymers should have at least one hydrophobic arm with a suitable balance between hydrophilic and hydrophobic arms. The unique self-assembly behaviour of miktoarm polymers has been demonstrated in bulk and in solution, and it is related to their architecture of three or more arms branching out from a central junction point. 138 Based on their structure, chemical composition and length of the arms, miktoarm stars can form different nanoparticle morphologies, such as micelles, polymersomes, worm micelles or multicompartment micelles. 115, 139-141 This lends considerable advantages to miktoarm polymers as drug and gene delivery systems over analogues linear copolymers. For instance, Wang et al. reported that micelles obtained from PCL and PEG-based multiarm star block copolymers, had a loading capacity of 22 weight % for etoposide, a hydrophobic anticancer drug. 142, 143 Yin et al. reported the preparation of a series of Y-shaped AB_2 miktoarm polymers (A = polyethylene glycol (PEG); B = poly(L-lactide)) that mimic natural structure of phospholipids. 140 These polymers formed polymersomes (polymeric vesicles) in aqueous solutions with a size that ranged from 33-75 nm in radius, depending on polymer composition. The polymersomes had an incorporation efficiency of 72 weight% for doxorubicin HCl, a hydrophilic anticancer drug, and sustained its release for more than 48 h. Polymersome formation for the miktoarm polymers was observed at PEG volume fractions of 0.2-0.7 compared to PEG volume fractions of 0.2-0.4 for their linear diblock copolymers counterparts confirming the versatility of miktoarm polymers. We have recently reported the incorporation of nimodipine into polymeric micelles of A₂B miktoarm polymers (A = PEG; B = polycaprolactone (PCL)). 115 Nimodipine is a poorly water soluble drug used primarily for the prevention and treatment of delayed ischemic neurological disorders. The micelles showed nimodipine incorporation efficiency up to 78 weight % and sustained drug release for more than 3 days. Enhanced micellar stability and smaller sizes were obtained for these A₂B miktoarms compared to their linear counterparts of similar composition and molecular weight. Other reports have also suggested that miktoarm polymers selfassemble differently from their linear counterparts. 144, 145 Gou et al. have reported the synthesis and drug loading of ibuprofen-conjugated amphiphilic A₁₄B₇ miktoarm stars composed of 14 PCL arms and 7 PEG arms with β -cyclodextrin $(\beta$ -CD) as core moiety. ¹⁴⁶ These amphiphilic star polymers self-assembled into multimorphological aggregates in aqueous solution and showed higher drug loading capacity compared to the corresponding non-drug conjugated copolymers. Güç et al. showed that a fatty acid-based hyperbranched resin (HBR) formed nanoparticles with an average size ranging from 206-276 nm. ¹⁴⁷ The nanoparticles had loading efficiencies up to 74% for tamoxifen and idarubicin, both hydrophobic anticancer drugs. Compared to free tamoxifen, nanoparticles-loaded drug exhibited up to 13-fold higher cytotoxicity against MCF-7 breast cancer cells, in vitro.

In order to widen the spectrum of drugs that can be incorporated into the same nanodelivery system, Radowski *et al.* prepared a liposome-like nanodelivery dendritic multishell system based on hyperbranched polymeric core surrounded by double layered shell. The core was hyperbranched poly (ethylene imine) (PEI) surrounded by a shell of amphiphilic alkyl dicarboxylic acids and a corona of PEG. Nimodipine and β -carotene were used as model hydrophobic guest molecules whereas congo red and vitamin B_6 monohydrochloride were used as model polar guest molecules. The nanoparticles were able to increase the solubility of these guest molecules. While the incorporation efficiency of the guest molecules was slightly affected by the PEG molecular weight, it was strongly dependent on the size of the PEI polar core and the size of the hydrophobic inner shell. Another interesting amphiphilic hyperbranched

polymeric system suitable for selective incorporation of guest molecules was recently reported. The system is based on a hydrophobic core of poly(β -cyclodextrin) (β -CD) and a hydrophilic corona of poly(N,N-dimethylaminoethyl methacrylate) (PDMA). The authors hypothesized that selective incorporation of two different guest molecules could be achieved due to the presence of two different cavities; the internal cavity of β -CD and the cavity created between the different polymeric arms (Fig. **1.4**). Levofloxacin lactate (LL) and phenolphthalein (PP) showed different release profiles suggesting their incorporation in different molecular cavities with different microenvironments: PP being encapsulated in β -CD cavities and LL in the hyperbranched cavities. The release of LL dominates at early stage in comparison with PP, subsequently the release rate of PP increases to play a determinate role in the release system.

The above mentioned examples show a potential of dendrimers and miktoarm stars as nanodelivery vehicles for drugs by physical drug incorporation which is superior to other carriers. However, premature drug release from these systems is still a hurdle, and chemical conjugation of drugs to dendrimers and miktoarms is one of the promising strategies to overcome it.

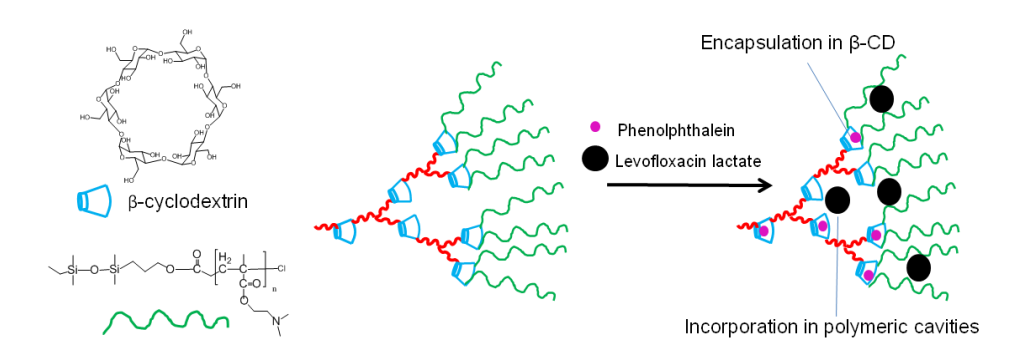


Figure 1.4. Selective incorporation based on drug molecular size into copolymers of $poly(\beta-cyclodextrin)$ ($\beta-CD$)-poly(N,N-dimethylaminoethyl methacrylate) (PDMA)

1.3.2 Drug loading by chemical conjugation

Some of the drawbacks of physical drug incorporation can be reduced by

covalent linking of a drug to the dendrimer or miktoarm polymer framework, using a chemical approach which will also bring about selective drug release *in vivo*. Such an approach can generate structures with pre-measured drug content and enhanced stability. In addition, targeted drug delivery and controlled release can be achieved by attaching the drug to the polymeric scaffold through stimuli responsive bonds where drug release can be obtained by change in the biological microenvironment such as variation in pH, temperature or concentration of a specific enzyme.

1.3.2.1 Direct coupling

The future of drug release from its conjugate depends on the type of linking group used to covalently attach the drug on the surface of dendrimers. Different types of linking bonds or spacers include enzymatically or hydrolytically cleavable esters, amide groups 150-154 and reducible disulfides 155 which can be reduced by glutathione in cytosol. The cleavage of an ester linkage is generally more rapid than that of an amide bond. A detailed study on ester and amide linked naproxen conjugates of G0 PAMAM dendrimers to determine their stability and release, was reported by Najlah et al. 152 The drug-dendrimer ester conjugates show rapid enzyme catalysed hydrolysis ($t_{1/2}$ =51 min) while the amide linked conjugate resisted release in 80% human plasma, and showed stability in plasma and liver homogenate as compared to ester linked conjugate which released the drug rapidly. 152, 156 Recently, Kannan and co-workers have shown similar results where ibuprofen linked through ester bond to G4 PAMAM dendrimers showed higher drug release as compared to their amide counterparts. Same study also proved the importance of presence and absence of linkers between the drug and the dendrimer. The drug release from ibuprofen conjugated by amide linkage through a Gly-Phe-Leu-Gly peptide linker attached to G4 PAMAM, and ibuprofen directly linked by amide linkage to the similar dendrimer was compared. The results showed 40 times more drug release in cathepsin B solution in 48 h in case where the linker was present as compared to the conjugates where the drug was directly attached. 153 Not only the presence of linker but the length of the linker also affects the drug release profile. Baker and co-workers have compared PAMAM dendrimer conjugates having succinic acid ester-linked paclitaxel, folic acid and FITC to their glutaric acid ester-linked counterpart. Quantitative thin layer chromatography revealed that the succinic acid derivatives hydrolyzed in PBS buffer with a half life of approx. 10 h while the glutaric acid derivative showed no hydrolysis in same conditions even after 7 days. ¹⁵⁷ In addition to ester and amide linkages, reducible disulfide bonds can also be used to attach drugs covalently on dendrimer surface which can selectively release the drug at intracellular glutathione (GSH) concentrations which is 10 folds more than the extracellular one. Kannan and co-workers have used reducible disulfide bond to attach *N*-acetyl cysteine (NAC) to PAMAM dendrimers. These conjugates could deliver approximately 60% of NAC payload at intracellular GSH concentration and pH within 1 h, but could not release any NAC at plasma GSH concentrations. Also, the conjugates showed up to an order of magnitude improvement in efficacy of NAC, *in vitro*. ¹⁵⁵

The type of bond linking dendrimer-drug conjugates not only influences the stability as well as release profile of drugs, but it also affects the efficacy of the drug. Methotrexate (MTX), an anticancer drug, has two possible sites for covalent attachment i.e. through its carboxylic acid group forming an ester linkage by reacting with hydroxyl group of the carrier or through amine group by reacting with carboxylic acid present on the carrier producing an amide linkage. MTX linked via an ester bond to acetamide-functionalized G5 PAMAM dendrimer was found to be four times more active than free MTX, whereas MTX conjugated by amide bonds to the same dendrimer was less active than free MTX. 158, 159 Different studies have shown that the conformation of anticancer drugs attached on the dendrimers surface also affects their cytotoxic activity. 150, 158, 160 Kannan and co-workers compared the anticancer activity of MTX when attached through its amine group to the carboxylic acid group of G2.5-COOH dendrimers forming amide linkages with MTX attached through its carboxylic acid group to the primary amines of G3-NH₂ dendrimers. G2.5-MTX conjugates were found to be 3-fold more toxic as compared to free MTX toward lymphoblastic leukaemia cells, whereas G3-MTX conjugates were 10 fold less toxic than the free MTX. 150

Dendrimer conjugation of anticancer drugs, including methotrexate, ^{150, 151, 161} doxorubicin ¹⁶²⁻¹⁶⁵ and camptothecin ^{166, 167} have shown to provide a high payload, due to which the administered dose can be reduced to minimize side effects and maximize therapeutic effect. Also, the retention of efficacy of drug after conjugation to certain scaffold is very important. There are few studies which show that the efficacy depends on the type of scaffold. For instance, some studies showed that there was a considerable reduction in efficacy of streptokinase (SK) upon conjugation to PEG and dextran due to considerable loss in enzymatic activity (67%, 50%) respectively. In contrast, Kannan and co-workers have reported that SK-PAMAM G3.5 conjugates with equimolar ratio of dendrimer to SK retained highest enzymatic activity (80%). ¹⁶⁸ These examples show that a choice of the scaffold is really important in order to retain the activity of the drug after chemical conjugation.

As in the case of dendrimers, the covalent attachment of drugs to miktoarm polymers has also been reported. 31, 32, 169-172 Recently, Zhi-Quan Shen and co-workers have reported that the miktoarm-drug conjugates not only affect the drug release behaviour, but the covalent attachment of drug to these polymers can also change their drug loading and drug incorporation efficiencies. 118, 146 They have developed A₂B₂ miktoarm star copolymers having PEG and PCL chains with ibuprofen attached on PCL chains through ester linkage. The drug loading capacities of miktoarm polymer micelles with/without drug showed better drug loading in drug conjugated miktoarm star copolymers than their non drug counterparts. 118

1.3.2.2 pH sensitive linkages

The incorporation of pH sensitive linkages to dendrimer-drug conjugates can have potential use in pH dependant drug delivery systems, as these linkages can be designed to be stable in the systemic circulation (pH 7.4) but will be hydrolyzed at lower pH (5-6) in the endosome/lysosome, thus releasing the drug inside the cell. Among the pH sensitive linkages are *cis*-aconityl and hydrazone linkages. Although *cis*-aconityl linkage was the first one to be used to conjugate drugs to polymeric carriers¹⁷³ as an acid sensitive linkage, the most widely used

pH sensitive linkages are hydrazones. There are several examples of pH sensitive linkages among dendrimer-drug conjugates. 163, 174-177 For instance, Jiang and coworkers demonstrated the effect of drug conjugation for tumor selective targeting of doxorubicin (Dox). They conjugated Dox to partially PEGylated PAMAM dendrimers by acid sensitive cis-aconityl linkage (PPCD conjugate) or acid insensitive succinic linkage (PPSD conjugate). The drug release from PPCD conjugates followed an acid triggered manner but PPSD conjugates released negligible amount of drug under mildly acidic or neutral pH conditions. PPCD conjugates were more cytotoxic as compared to PPSD conjugates against murine melanoma B16 cells. Although there was more tumor accumulation for PPSD conjugates, the free drug concentration was higher for PPCD conjugates due to acid triggered release as compared to PPSD conjugates. 165 Szoka and co-workers compared pH sensitive hydrazone-linked dendrimer-drug conjugates and pH insensitive carbamate-linked conjugates. Dox was covalently attached to an asymmetric biodegradable polyester dendrimer through pH sensitive acyl hydrazone linkage or through a carbamate linkage. Dendrimer-Dox conjugates with hydrazone linkage were more cytotoxic towards colon carcinoma cells (IC₅₀=1.4μg of Dox/mL) as compared to dendrimer-Dox conjugates with carbamate linkage (IC₅₀=2.0µg of Dox/mL) after incubation of 72 h. 163, 178 Harada and co-workers have developed PAMAM dendrimers with glutamic acid (Glu) residues at every chain end of the dendrimer, the amino group of which was utilized to graft PEG chains. The anticancer drug, Adriamycin, was attached to the side chains of Glu residue through amide or hydrazone bonds. This study showed that for dendrimer-drug conjugates with amide linkage, there was a slight release at pH 7.4 and 5.5, whereas the conjugates with hydrazone linkage showed negligible release at pH 7.4 but a remarkable release at pH 5.5 (pH of endosomes). 175 More recently, similar results were reported by Gu and co-workers for doxorubicin-dendrimer constructs with pH sensitive hydrazine bonds, showing more release of the drug at pH 5.0 as compared to pH 7.0 due to acid cleavage of hydrazine linkage. 177 These pH sensitive dendrimer- drug conjugates have shown significant enhancement in the delivery of anticancer drugs. However, such systems have their own limitations since they can deliver drugs in acidic endosomal environment but cannot distinguish between diseased and healthy cells. An interesting future direction for drug-dendrimer conjugates would require introduction of enzyme-specific bonds/linkages which would be primarily cleaved in sick cells where such enzymes are upregulated. This would leave healthy cells less affected. For instance, Shabat and co-workers have demonstrated enzymatic activation of second generation self-immolative dendrimers with four molecules of anti-cancer drug camptothecin (CPT), two PEG chains to provide aqueous solubility and a trigger that can be activated by penicillin-G-amidase (PGA). This dendritic pro-drug was tested for toxicity against three different cell lines: the human T-lineage acute lymphoblastic leukemia cell line (MOLT-3), the human leukemia T cell line (JURKAT), and the human kidney embryonic cell line (HEK-293). The IC₅₀ of the pro-drug alone was between 100 and - 1000 fold less than free CPT in all cell lines. However, upon treating cells with PGA, the pro-drug was activated and its toxicity reached that of free CPT. These results show that the incorporation of a specific enzyme substrate which would be cleaved by a protease overexpressed in tumor cells can generate a cancer cell specific dendritic prodrug system. 179

1.4 Dendrimers and miktoarm polymers for targeted drug delivery

The ultimate goal of targeted drug delivery is to increase drug's therapeutic index through maximizing its concentration at its site of action while minimizing it in non target tissues. This usually allows administration of lower doses and reduced side effects which is particularly important for anticancer drugs whose accumulation in healthy tissues results in serious side effects. Dendrimers and miktoarm polymers are excellent vehicles for targeted drug delivery by virtue of their small size (5-100 nm) and availability of many surface groups to conjugate drugs, imaging tags and targeting moieties. Drug targeting using dendrimers and miktoarms can be achieved through passive or active targeting.

1.4.1 Passive targeting

Passive targeting of nanoparticles refers to their accumulation at a particular site in the body due to physicochemical and pathophysiological factors. 181 Nanoparticles made of dendrimers and miktoarm polymers can be passively targeted to solid tumors and inflamed tissue via the enhanced permeability and retention (EPR) effect. 182 This effect takes advantage of both tissue pathophysiological properties as well as nanoparticles physicochemical properties. Tumors usually have a leaky vasculature and impaired lymphatic drainage, which allows 10-30 times higher drug concentration in tumors compared to the blood for a longer time. 183-186 The EPR effect was first described in the 1980s by Maeda who demonstrated that Evans blue dye bound to plasma albumin selectively accumulated in tumor tissue after intravenous administration. 182 Moreover, radiolabeled transferrin (~90 kDa) and immunoglobulin G (IgG) (~160 kDa) exhibited similar behavior, whereas small proteins such as neocarzinostatin (~12 kDa) and ovomucoid (~29 kDa) did not accumulate in tumors. Based on this and on evidence accumulated by independent research during the last 25 years, it was concluded that the EPR effect takes place in most solid tumors for biocompatible macromolecules with molecular weight \geq 40 kDa and for nanoparticles of size up to 1 µm. 187 However, for successful EPRmediated-targeting, nanoparticles should have long circulation time in the blood, ideally more than 6 h and their size should be less than 200 nm to avoid uptake by the reticuloendothelial system (RES) (Fig. 1.5). 184, 188, 189 Long circulation properties of nanoparticles can be achieved by surface modification with hydrophilic polymers such as PEG "PEGylation" or polyvinylpyrrolidone (PVP). 190-193 These hydrophilic polymers can decrease the adsorption of opsonin proteins in the blood, help nanoparticles escape recognition by RES and circulate longer in the blood.

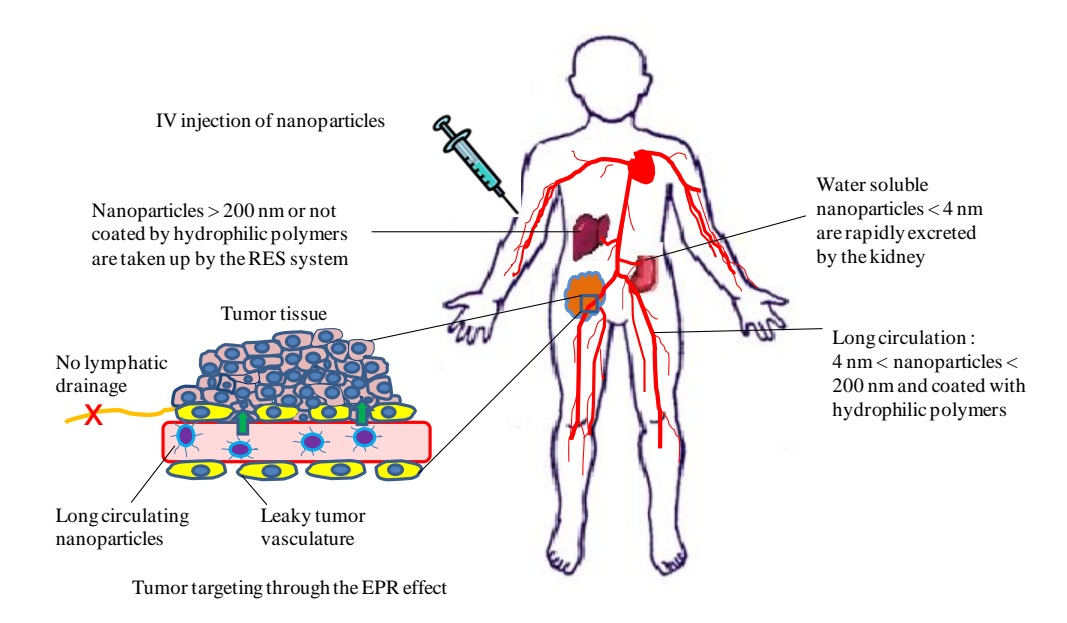


Figure 1.5. Schematic illustration of biodistribution of intravenously injected nanoparticles showing nanoparticles accumulation in tumors due to the EPR effect, nanoparticles uptake by the RES system, and nanoparticles excretion by the kidney.

Nanoparticles should not be filtered in the kidneys in order to attain longevity in the blood. The filtration size cut-off for the kidney is known to range from a hydrodynamic diameter of 3.7 to 6.0 nm.¹⁹⁴ Therefore, water soluble nanoparticles and dendrimers with hydrodynamic diameter less than ~ 4 nm are expected to be rapidly filtered by the kidneys and excreted in the urine (Fig. 1.5). Indeed, Choi *et al.* have shown that quantum dots with hydrodynamic diameter < 5.5 nm were rapidly and efficiently eliminated from the body via urinary excretion.¹⁹⁵ Miktoarm polymers form nanoparticles with hydrodynamic diameters larger than the threshold of renal filtration suggesting their possible extended blood circulation; taking into account surface charge and molecular weight. PAMAM dendrimers, on the other hand have generation and surface group-dependent hydrodynamic diameter. Thus, PAMAM-OH dendrimers were shown to have smaller hydrodynamic size compared to their PAMAM-NH₂ counterparts of the same generation due to a more extended structure of

PAMAM-NH₂. ^{196, 197} G0-G7 PAMAM dendrimers with ethylenediamine core have a hydrodynamic diameter in the range of 1.4-8.8 nm whereas G1-G5 poly(propylene imine) (PPI) dendrimers have hydrodynamic diameter in the range of 0.6-2.0 nm. 198, 199 In addition to the dendrimer hydrodynamic diameter, the nature of their surface groups also affects their residence time in the blood. Thus, PAMAM-NH₂ dendrimers were rapidly eliminated from the blood and accumulated in the liver, lung and spleen possibly due to electrostatic interactions between the surface cationic groups and anionic sulphated proteoglycans on cell surfaces. 200-203 Approaches such as acetylation, succinylation or PEGylation of dendrimers have been effective in prolonging their circulation times and decreasing their accumulation in the liver and kidneys. ^{69, 161, 201, 204} For instance, PEGylated polylysine dendrimers were concentrated ~8-fold and 3-fold in Walker 256 tumors more than in muscle and heart, respectively. 205 Moreover, PEGylated G4 PAMAM-doxorubicin conjugates showed time dependent tumor accumulation after intravenous injection in mice inoculated with SKOV-3 cells. Higher concentration of the conjugates in the tumor tissue was detected as early as 1 h after injection with a maximum at 24 h and small decrease within 48 h post injection. Conjugates with the highest PEG content (~20 PEG molecules per PAMAM molecule) showed the highest accumulation in tumors compared to other conjugates. 162

The EPR effect was more extensively studied with nanoparticulate formulations based on linear copolymers rather than those of branched and hyperbranched polymers.⁷ Recently, Sadekar et al. reported a comparative study on the biodistribution of the linear copolymer N-(2hydroxylpropyl)methacrylamide (HPMA) and a hydroxyl-terminated PAMAM dendrimers of generation 5, 6 and 7 in ovarian-tumor-bearing mice. 196 They reported that molecular weight, hydrodynamic size and polymer architecture were the major factors that influenced the biodistribution profiles of these polymers. G5 PAMAM-OH (hydrodynamic diameter of 4.6 nm) was retained in the kidney over 1 week, whereas linear HPMA copolymer of similar molecular weight (hydrodynamic diameter of 2.8 nm) was excreted through the kidney within 2 h.

G6 PAMAM-OH with hydrodynamic diameter of 6 nm was not filtered in the kidney; instead, it accumulated in the liver. HPMA copolymer of comparable molecular weight had a three times higher plasma circulation time compared to G6 PAMAM-OH. Among the studied polymers, G7 PAMAM-OH dendrimer showed extended plasma circulation, enhanced tumor accumulation, and prolonged retention with the highest tumor/blood ratio. This dendrimer showed a time-dependent accumulation in the tumor with a maximum at 6 h and persisted for up to 1 week with a tumor to blood ratio (T/B ratio) of ~ 12.75. This was attributed to the rigid sphere-like conformation of this dendrimer and its hydrodynamic diameter (i.e., ~ 8 nm) above the filtration size cut-off of the kidney (i.e., 3.7-6 nm). 194, 206 The size of nanoparticles also affects their biodistribution profiles after in vivo administration. Thus, paclitaxel-loaded nanoparticles of amphiphilic telodendrimers (PEG-b-dendritic oligocholic acid) of small size (17-60 nm) accumulated in the tumors in xenograft models whereas larger paclitaxel-loaded micelles (150 nm) were mostly accumulated in the liver and lungs.²⁰⁷ The antitumor efficacy of these paclitaxel-loaded micelles was greater than that of Taxol® and Abraxane® in subcutaneous and intraperitoneal ovarian cancer mouse models.²⁰⁸ In order to overcome the disadvantages of dendrimers small size, several approaches have been reported to facilitate dendrimers self-assembly into larger multimolecular micelles. For instance, Zhang et al. have shown that modification of G1 PAMAM dendrimers by grafting cholic acid to its surface amino group endowed the dendrimer with self-assembly properties.²⁰⁹ The modified PAMAM dendrimer had 2 cholic acid molecules per PAMAM molecule, and self-assembled into micelles with an average size of 50-70 nm. Moreover, the micelles showed pH- dependent incorporation of camptothecin, a hydrophobic anticancer drug. The anticancer activity of micelleincorporated camptothecin was higher than that of free drug, in vitro. The in vivo biodistribution of these camptothecin-containing micelles remains to be determined.

In addition to tumors, dendrimers have also shown passive accumulation in inflamed tissues. Although arthritic joints do not lack lymphatic drainage, indomethacin incorporated in G4 PAMAM dendrimer was 2.29 times more concentrated in inflamed joints compared to free drug. Flurbiprofen incorporated in PAMAM dendrimer had 2-3 fold higher concentration in inflamed tissue of a carrageenan induced paw edema model in male albino rats compared to free drug. Furthermore, Dai *et al.* have shown that G4 PAMAM-OH dendrimers with no targeting moieties exhibit intrinsic targeting properties to activated microglia and astrocytes following subarachnoid administration in newborn rabbits with maternal inflammation-induced cerebral palsy (CP). Using fluorescently labelled PAMAM dendrimers, it was shown that a 15-fold greater PAMAM concentration was observed in the CP rabbits, compared with control (Fig. 1.6). The increased dendrimer uptake in the CP rabbits was attributed to increased phagocytic ability of activated microglia and hypertrophic astrocytes compared to healthy cells. The usefulness of PAMAM dendrimers and other nanoparticles remains to be determined in different neurodegenerative disorders associated with inflammation.

1.4.2 Active targeting

Active targeting of nanoparticles refers to their accumulation at a particular site in the body using specific interactions between tissue or cell components and nanoparticles.¹⁸¹ Active targeting can be achieved by making stimuli-responsive nanoparticles, or by attaching specific targeting ligand molecules to the nanoparticles surface.³ Directing drug-dendrimer conjugates to tumor cells can be achieved by attaching a variety of targeting moieties *e.g.* folic acid (FA),^{72, 158, 159, 204, 213, 214} biotin,^{177, 215} or macromolecules, for example, cell penetrating peptides,²¹⁶⁻²¹⁸ or antibodies.^{151, 219, 220} FA has affinity towards receptors expressed on tumors. FA-bound dendrimer-drug conjugates largely accumulated in the tumor cells, as compared to the free drug,^{217, 221} or the dendrimer-drug conjugates without targeting agent.^{158, 222} For example, Baker and co-workers have reported that FA-acetylated PAMAM-MTX conjugates showed accumulation in tumor and liver tissue over 4 days after intravenous administration into immunodeficient mice with human KB tumors. Treatment

with conjugates led to 10 times higher suppression of tumor growth as compared to free MTX of equivalent dose. Long-ping Wen and co-workers have reported partially acetylated G5 PAMAM dendrimers with biotin as a targeting moiety, and fluoresceinisothiocyanate (FITC) as an imaging agent. PAMAM-biotin-FITC conjugates exhibited much higher cellular uptake in HeLa cells as compared to non-targeted counterparts. More recently, Xin-Ru Jia and co-workers reported PEGylated PAMAM G4 dendrimer with dual targeting drug carrier bearing transferrin (Tf) and wheat germ agglutinin (WGA) as brain-targeting ligands. Dox was loaded in the interior of this dendrimer. PAMAM-PEG-WGA-Tf showed enhanced transport ratio (13.5%) of drug across blood brain barrier, as compared to single targeting carrier, PAMAM-PEG-WGA (8%), PAMAM-PEG-Tf (7%), or free Dox (5%) within 2 h. Dual targeting conjugate significantly decreased cytotoxicity of Dox to healthy cells, but increased the inhibition rate to C6 glioma cells. Load of the control of the control of the conference of the inhibition rate to C6 glioma cells.

Bornhop's group has designed the translocator protein (TSPO) targeted imaging agent based on G4 **PAMAM** dendrimer using 1-(2chlorophenyl)isoquinoline-3-carboxylic acid (CIPhIQ Acid) and lissamine dye. TSPO is a translocator protein expressed on outer mitochondrial membrane in steroid producing cells. These conjugates colocalized with mitotracker green, demonstrating their ability to target mitochondria. 224 More recently, our group has demonstrated targeting of cytoplasmic lipid droplets with dendrimers and miktoarm polymers covalently linked to a therapeutic agent (niacin or α-lipoic acid) and lipohilic fluorescent dye, BODIPY. 16, 31, 32 These conjugates localized in the cytoplasmic lipid droplets in living hepatocytes and microglia cells (Fig. **1.7**).³¹

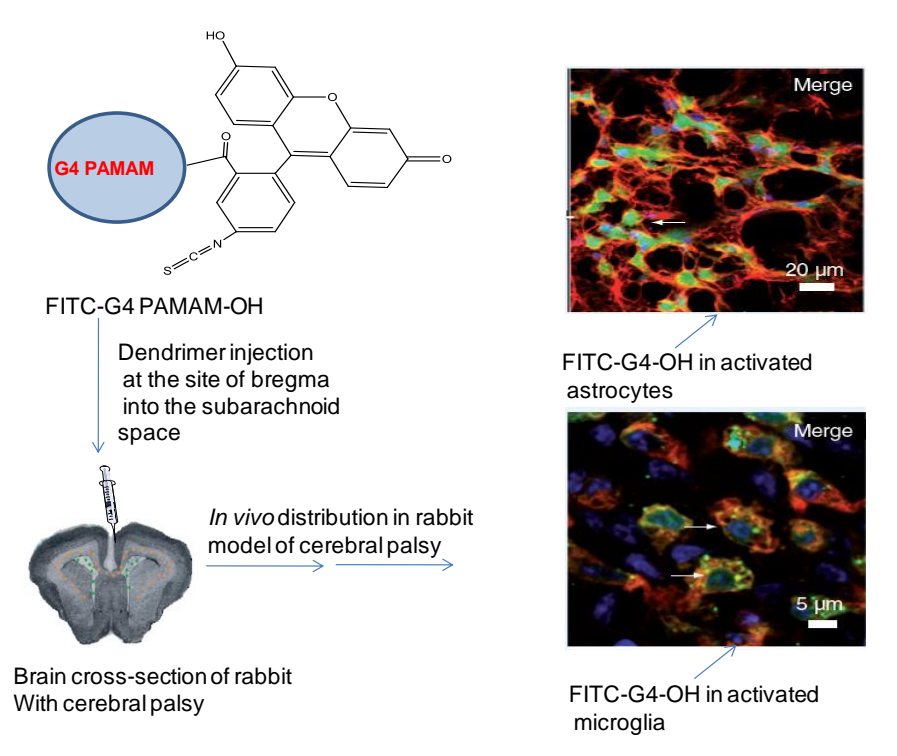


Figure 1.6. Selective uptake of G4 PAMAM-OH-FITC dendrimer in activated microglia and astrocytes following subarachnoid injection in the cerebral palsy rabbit model. Adapted from ref. 212

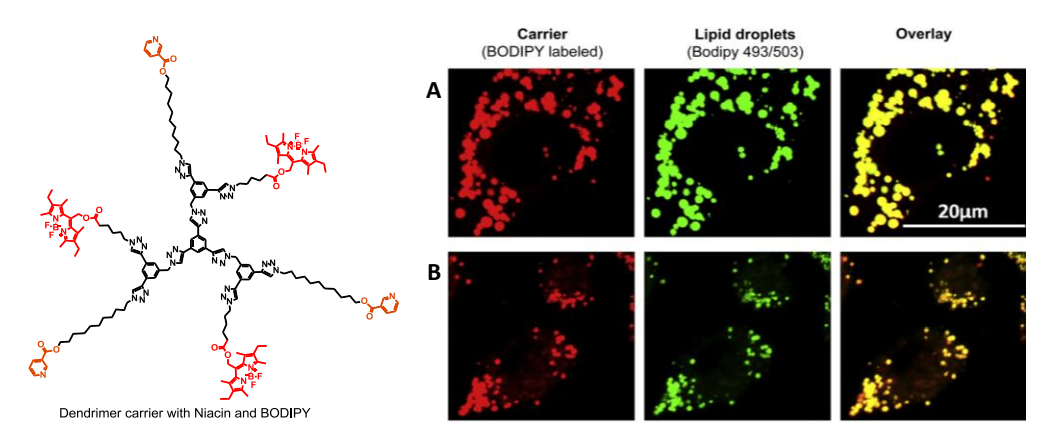


Figure 1.7. Colocalization of niacin-and BODIPY-conjugated dendrimer with lipid droplets in human hepatocytes (A) and murine microglia (B).

Stimuli responsive nanoparticles have offered considerable potential for targeted drug delivery,^{3, 225} since stimuli produced by a diseased state can trigger the release of drug only in the affected area, and thus reducing the side effects.

The drug release can be triggered by various stimuli including temperature, light, pH, redox microenvironment and enzyme overexpression. Dendrimer-drug conjugates with pH sensitive covalent linkages have been discussed in the section on chemical conjugation. The difference in pH can allow the release of drug payload by breaking pH sensitive linkages or by protonation of dendrimer structure to release the incorporated drug. Jain and co-workers reported the release of incorporated aceclofenac, an anti-inflammatory drug from PEGylated PPI dendrimers in a pH responsive manner. ²²⁶ In another study, they demonstrated the release of incorporated histamine H₂ receptor agonist, famotidine from PEGylated PPI dendrimer under acidic pH. 227 pH responsive polymers can also be attached to dendrimers to make pH sensitive drug delivery systems. 228 Recently, Baker and co-workers used a strategy of photocaging, involving the inactivation of the drug using photocleavable protecting group, which upon UV irradiation can irreversibly release the drug in its active form. They used G5 PAMAM dendrimers conjugated to folic acid as a targeting ligand and doxorubicin was attached through a photocleavable group. This doxorubicin-caged nanoconjugate showed toxicity to the KB cells only after exposure to UV light when the drug was released. 229 A novel concept for the simultaneous release of all the peripheral groups on the surface of dendrimers in the presence of an enzymatic trigger has been reported by Shabat and co-workers. 179, 230, 231 Different terms have been used for this type of mechanism, such as, 'dendrimers disassembly', 'cascade release' or 'self immolative dendrimers'. 232-235 Thus, combining the advantages of dendrimers with stimuli responsive modalities can produce smart nanocarriers for site specific drug delivery with increased therapeutic efficacy and reduced side effects.

1.5 Dendrimer and miktoarm cytotoxicity

Nanoparticles intended for biomedical applications and their degradation products should be not cytotoxic. Most miktoarm polymers intended for drug delivery applications are based on biocompatible and/or biodegradable polymers such as PEG, PCL and PLA. We recently reported the synthesis and characterization of a series of A_2B miktoarm polymers (A = PEG and B = PCL)

for the incorporation and delivery of hydrophobic drugs. 115 Micelles of these miktoarm polymers did not induce cytotoxicity in N9 microglia cells at polymer concentrations high enough to produce clinically relevant drug concentrations in aqueous medium. Micelles of star shaped 6sPCL-S-S-PEG were not cytotoxic against MCF-7 cells at concentrations as high as 1000 mg/L. In contrast to miktoarms, a wide range of building blocks including biodegradable and nonbiodegradable blocks is being used in dendrimers synthesis. Dendrimers based on biodegradable backbones such as polylysine, dimethylolpropionic acid (bis-MPA), poly(glycerol succinic-adipic acid) (PGLSA-OH) are preferred for drug applications over non-biodegradable ones.³⁸ delivery administration accumulation of non-biodegradable dendrimers and nanoparticles could result in serious side effects. The dendrimer cytotoxicity is dependent on the dendrimer generation, nature of building blocks, concentration and surface groups. 201, 238-241 Cationic dendrimers such as PAMAM, PLL and PPI have shown significant cytotoxicity both in cell cultures and in vivo models, which certainly limits their clinical utility. 242-244 Naha et al. reported a generation dependent cytotoxicity of PAMAM dendrimers in mouse macrophage cells (J774A.1) where the degree of cytotoxicity followed the order G6> G5> G4. The degree of cytotoxicity was correlated with the number of PAMAM surface amino groups.²⁴⁰ Mechanistic studies showed that the mechanism of PAMAM-NH₂ induced cell death is overproduction of reactive oxygen species (ROS) and proinflammatory cytokines (macrophage inflammatory protein-2 (MIP-2), tumour necrosis factor-α (TNF-α) and interleukin-6, (IL-6)). Cytotoxicity of G5 PAMAM-NH₂ dendrimers was evaluated in mouse embryonic fibroblast cells (NIH 3T3 cells) by measuring the IC₅₀ values (concentration at which 50% of mitochondrial dehydrogenase activity was inhibited).²⁴³ While the IC₅₀ was 0.3 mg/mL for unmodified PAMAM-NH₂, this value increased by 12-105 times by PEGylation of PAMAM amino groups pointing towards the importance of PAMAM surface groups in determining their toxicity. Indeed, cationic dendrimers cytotoxicity has been shown to be due to interactions between the cationic surface groups and the negatively charged cell surface. Hong et al. studied the interactions between

PAMAM-NH₂ and supported 1,2-dimyristoyl-sn-glycero-3-phosphocholine (DMPC) lipid bilayers and KB and Rat2 cell membranes using atomic force microscopy (AFM), enzyme assays, flow cell cytometry, and fluorescence microscopy. GFM, enzyme assays, flow cell cytometry, and fluorescence microscopy. GFMAM-NH₂ dendrimers (10–100 nM) formed holes of 15–40 nm in diameter in aqueous, supported lipid bilayers. In contrast, G5 PAMAM-NH₂ and PAMAM-acetamide dendrimers did not form holes within this concentration range, yet G5 PAMAM-NH₂ expanded holes at existing defects. G5 PAMAM-NH₂ and PAMAM-acetamide dendrimers were not cytotoxic up to a 500 nM concentration in KB and Rat2 cells. However, G5 PAMAM-NH₂ decreased the integrity of the cell membranes as evidenced by a dose dependent release of the cytoplasmic proteins lactate dehydrogenase (LDH) and luciferase (Luc), in contrast to PAMAM-acetamide dendrimer which had little effect on membrane integrity at a concentration up to 500 nM. PAMAM-NH₂ induced permeability was not permanent however, since leaking of cytosolic enzymes returned to normal levels upon dendrimers removal.

In contrast to the detailed and numerous in vitro cytotoxicity studies of dendrimers there are fewer studies dealing with the hazards associated with their in vivo administration. Using zebrafish embryo, Heiden et al. evaluated the developmental toxicity of low generation (G3.5 and G4) PAMAM dendrimers, as well as Arg-Gly-Asp (RGD)-conjugated PAMAM. G4 PAMAM-NH₂ was toxic and attenuated growth and development of zebrafish embryos. Mortality was observed at low dendrimer concentration (0.2 µM) and was dependent on both PAMAM dose and exposure time. In contrast, G3.5 PAMAM-COOH dendrimers were not toxic to zebrafish embryos. Furthermore, RGD-conjugated G4 dendrimers were less toxic than G4 PAMAM-NH₂ dendrimers. RGD-conjugated G3.5 dendrimers did not show toxicity at the highest concentrations tested.²⁴² Neerman et al. studied the acute toxicity of melamine dendrimers by administering 2.5, 10, 40 and 160 mg/kg of dendrimers to mice by i.p. injection. All mice died after 6–12 h when injected 160 mg/kg. Mice treated at a dose of 40 mg/kg showed hepatotoxicity as indicated by increased liver enzyme activity. In subchronic toxicity studies (three i.p. injections of 2.5-40 mg/kg in 3-week interval) did not cause renal damage or mortality, except for the extensive liver necrosis with the highest dose (40 mg/kg) after 48 h. These studies clearly demonstrate the importance of detailed *in vivo* toxicity studies of dendrimers and miktoarm polymers before any clinical implementation.

In view of the great potential of dendrimers in nanomedicine, several strategies have been proposed to eliminate or to reduce their toxicity. The most common approaches include designing biodegradable dendrimers such as polyester-based dendrimers¹⁶⁴ and surface engineering of cationic dendrimers to mask their surface cationic groups by strategies such as PEGylation²⁰⁵, acetylation, and conjugation with amino acids and peptides.²⁴⁶ A detailed review of dendrimers toxicity and strategies to minimize it has been recently published.²⁴⁴

Despite hurdles in the synthesis and biocompatibility of dendrimers several dendrimer-based formulations are in clinical trials or have already made it to the market. For instance, a polylysine dendrimer-based microbiocide topical gel formulation, VivaGelTM, is being developed by Starpharma for the prevention of transmission of HIV and other sexually transmitted diseases during sexual intercourse. SuperFect® of Oiagen is an activated dendrimer used for gene transfection in many cell lines. Another application of dendrimers is in the use of multiple antigen peptides (MAPs). 247-249 The first example of MAPs was based on polylysine dendrimer core reported by Tam and coworkers. Since these first reports, several studies have been carried out where MAP structures have been used to produce peptide-specific antibodies. A MAP based malaria vaccine is in phase I human clinical trials.²⁵⁰ As diagnostic tools, several dendrimer-based systems have been developed. Thus, a polylysine dendrimer functionalized with gadolinium chelates, Gadomer-17 was developed by Schering AG as a magnetic resonance imaging (MRI) contrast agent. Stratus® CS, commercialized by Dade Behring has been used as a rapid detection tool of suspected myocardial ischemia. The system is based on a G5 PAMAM dendrimer used as a linking agent of monoclonal antibodies to a glass fiber matrix.²⁵¹ Moreover, the US army research laboratory has developed a dendrimer-based detection tool of anthrax called Alert

1.6 Conclusions

Macromolecule based drug therapy has come a long way from the use of simple polymer matrices to nano-therapeutics, and it has brought scientists with varied backgrounds to a common goal of achieving high specificity in directing pharmaceutical agents to the tissue, cell and cell-organelle. Considerable progress has been made in this direction, and it suggests that dendrimers and miktoarm stars, relatively new additions to the macromolecular field, are important and key players in this quest. Chemists have stood up to the challenge, and tremendous success has been achieved in streamlining their synthesis and characterization. Introduction of "click" chemistry to the repertoire of chemical reactions available for their construction, has significantly contributed to the rapid pace with which these macromolecules and their conjugates could be synthesized. In this article, we have attempted to highlight some of the recent developments in chemistry and biology of dendrimers and miktoarm stars, and their efficacy as vehicles for different drugs and imaging agents. Biological studies indicate that both dendrimers and miktoarm polymers are promising nanomaterials for biomedical applications. However, stringent criteria and multiple biological assays have to be used to determine which physical and chemical properties, should be considered to minimize/avoid adverse effects in experimental biological systems and eventually humans.

1.7 References

- 1. V. I. Shubayev, T. R. Pisanic Ii and S. Jin, *Adv. Drug Deliv. Rev.*, 2009, **61**, 467-477.
- 2. S. M. Janib, A. S. Moses and J. A. MacKay, *Adv. Drug Deliv. Rev.*, 2010, **62**, 1052-1063.
- 3. C. Kojima, Expert Opin. Drug Deliv., 2010, 7, 307-319.
- 4. S. Ganta, H. Devalapally, A. Shahiwala and M. Amiji, *J. Control Release*, 2008, **126**, 187-204.
- 5. I. K. Voets, A. de Keizer and M. A. C. Stuart, *Adv. Colloid Interface Sci.*, 2009, **147-148**, 300-318.
- 6. V. Torchilin, Eur. J. Pharm. Biopharm., 2009, 71, 431-444.
- 7. Y. Matsumura and K. Kataoka, Cancer Sci., 2009, 100, 572-579.
- 8. M. Wang and M. Thanou, *Pharmacol. Res.*, 2010, **62**, 90-99.
- Z. L. Tyrrell, Y. Q. Shen and M. Radosz, *Prog. Polym. Sci.*, 2010, 35, 1128-1143.
- 10. M. Talelli, C. J. F. Rijcken, C. F. van Nostrum, G. Storm and W. E. Hennink, *Adv. Drug Deliv. Rev.*, 2010, **62**, 231-239.
- 11. Y. Matsumura, *Jpn. J. Clin. Oncol.*, 2008, **38**, 793-802.
- E. Miele, G. P. Spinelli, F. Tomao and S. Tomao, *Int. J. Nanomed.*, 2009,
 4, 99-105.
- 13. A. Agarwal, Y. Lvov, R. Sawant and V. Torchilin, *J. Control Release*, 2008, **128**, 255-260.
- 14. H. Chen, S. Kim, W. He, H. Wang, P. S. Low, K. Park and J.-X. Cheng, *Langmuir*, 2008, **24**, 5213-5217.
- 15. R. Savić, T. Azzam, A. Eisenberg and D. Maysinger, *Langmuir*, 2006, **22**, 3570-3578.
- R. Hourani, M. Jain, D. Maysinger and A. Kakkar, *Chem. Eur. J.*, 2010,
 16, 6164-6168.
- D. A. Tomalia and J. M. J. Frechet, J. Polym. Sci. Pol. Chem., 2002, 40, 2719-2728.

- 18. C. C. Lee, J. A. MacKay, J. M. J. Frechet and F. C. Szoka, *Nat. Biotechnol.*, 2005, **23**, 1517-1526.
- R. Hourani and A. Kakkar, *Macromol. Rapid Commun.*, 2010, 31, 947-974.
- 20. S. Svenson and D. A. Tomalia, *Adv. Drug Deliv. Rev.*, 2005, **57**, 2106-2129.
- 21. S. Svenson, Eur. J. Pharm. Biopharm., 2009, **71**, 445-462.
- 22. C. M. Paleos, D. Tsiourvas, Z. Sideratou and L.-A. Tziveleka, *Expert Opin. Drug Deliv.*, 2010, **7**, 1387-1398.
- 23. E. Buhleier, W. Wehner and F. Vögtle, *Synthesis*, 1978, **1978**, 155,158.
- 24. D. A. Tomalia, H. Baker, J. Dewald, M. Hall, G. Kallos, S. Martin, J. Roeck, J. Ryder and P. Smith, *Polymer J.*, 1985, **17**, 117-132.
- 25. G. Franc and A. K. Kakkar, *Chem. Soc. Rev.*, 2010, **39**, 1536-1544.
- 26. G. Franc and A. Kakkar, *Chem. Commun.*, 2008, 5267-5276.
- K. Khanna, S. Varshney and A. Kakkar, *Polym. Chem.*, 2010, 1, 1171-1185.
- 28. B. K. Nanjwade, H. M. Bechra, G. K. Derkar, F. V. Manvi and V. K. Nanjwade, *Eur. J. Pharm. Sci.*, 2009, **38**, 185-196.
- M. Calderón, M. A. Quadir, S. K. Sharma and R. Haag, *Adv. Mater.*, 2010,
 22, 190-218.
- 30. M. Irfan and M. Seiler, *Ind. Eng. Chem. Res.*, 2010, **49**, 1169-1196.
- 31. A. Sharma, A. Khatchadourian, K. Khanna, R. Sharma, A. Kakkar and D. Maysinger, *Biomaterials*, 2011, **32**, 1419-1429.
- 32. A. Sharma, K. Neibert, R. Sharma, R. Hourani, D. Maysinger and A. Kakkar, *Macromolecules*, 2011, **44**, 521-529.
- 33. P. Wang, X.-H. Zhao, Z.-Y. Wang, M. Meng, X. Li and Q. Ning, *Cancer Lett.*, 2010, **298**, 34-49.
- 34. J. Wang, Z. Lu, M. G. Wientjes and J. L. S. Au, *Aaps J*, 2010, **12**, 492-503.
- 35. C. M. Paleos, L. A. Tziveleka, Z. Sideratou and D. Tsiourvas, *Expert Opin. Drug Deliv.*, 2009, **6**, 27-38.

- 36. J. R. Baker, Jr., *Hematology*, 2009, **2009**, 708-719.
- 37. S. H. Medina and M. E. H. El-Sayed, *Chem. Rev.*, 2009, **109**, 3141-3157.
- 38. M. A. Mintzer and M. W. Grinstaff, *Chem. Soc. Rev.*, 2011, **40**, 173-190.
- 39. L. Röglin, E. H. M. Lempens and E. W. Meijer, *Angew. Chem. Int. Ed.*, 2011, **50**, 102-112.
- N. Fischer-Durand, M. Salmain, B. Rudolf, L. Jugé, V. Guérineau, O. Laprévote, A. Vessières and G. Jaouen, *Macromolecules*, 2007, 40, 8568-8575.
- 41. H. Kobayashi, S. Kawamoto, S.-K. Jo, N. Sato, T. Saga, A. Hiraga, J. Konishi, S. Hu, K. Togashi, M. W. Brechbiel and R. A. Star, *Kidney Int*, 2002, **61**, 1980-1985.
- 42. H. Kobayashi, T. Saga, S. Kawamoto, N. Sato, A. Hiraga, T. Ishimori, J. Konishi, K. Togashi and M. W. Brechbiel, *Cancer Res.*, 2001, **61**, 4966-4970.
- 43. M. Saad, O. B. Garbuzenko, E. Ber, P. Chandna, J. J. Khandare, V. P. Pozharov and T. Minko, *J. Control Release*, 2008, **130**, 107-114.
- 44. G. R. Newkome, Z. Yao, G. R. Baker and V. K. Gupta, *J. Org. Chem.*, 1985, **50**, 2003-2004.
- 45. M. Fischer and F. Vögtle, *Angew. Chem. Int. Ed.*, 1999, **38**, 884-905.
- 46. E. M. M. de Brabander-van den Berg and E. W. Meijer, *Angew. Chem. Int. Ed.*, 1993, **32**, 1308-1311.
- 47. P. Antoni, D. Nystrom, C. J. Hawker, A. Hult and M. Malkoch, *Chem. Commun.*, 2007, 2249-2251.
- 48. C. J. Hawker and J. M. J. Frechet, *J. Am. Chem. Soc.*, 1990, **112**, 7638-7647.
- 49. S. J. E. Mulders, A. J. Brouwer, P. G. J. van der Meer and R. M. J. Liskamp, *Tetrahedron Lett.*, 1997, **38**, 631-634.
- H. C. Kolb, M. G. Finn and K. B. Sharpless, *Angew. Chem. Int. Ed.*, 2001,
 40, 2004-2021.
- 51. M. J. Joralemon, R. K. O'Reilly, J. B. Matson, A. K. Nugent, C. J. Hawker and K. L. Wooley, *Macromolecules*, 2005, **38**, 5436-5443.

- P. Wu, A. K. Feldman, A. K. Nugent, C. J. Hawker, A. Scheel, B. Voit, J. Pyun, J. M. J. Fréchet, K. B. Sharpless and V. V. Fokin, *Angew. Chem. Int. Ed.*, 2004, 43, 3928-3932.
- 53. K. L. Killops, L. M. Campos and C. J. Hawker, *J. Am. Chem. Soc.*, 2008, **130**, 5062-5064.
- 54. M. Köhn and R. Breinbauer, Angew. Chem. Int. Ed., 2004, 43, 3106-3116.
- 55. J.-F. Lutz, Angew. Chem. Int. Ed., 2007, 46, 1018-1025.
- 56. A. Dondoni, Angew. Chem. Int. Ed., 2008, 47, 8995-8997.
- 57. G. Franc and A. K. Kakkar, *Chem.–Eur. J.*, 2009, **15**, 5630-5639.
- P. Wu, M. Malkoch, J. N. Hunt, R. Vestberg, E. Kaltgrad, M. G. Finn, V. V. Fokin, K. B. Sharpless and C. J. Hawker, *Chem. Commun.*, 2005, 5775-5777.
- A. P. Goodwin, S. S. Lam and J. M. J. Fréchet, *J. Am. Chem. Soc.*, 2007,
 129, 6994-6995.
- 60. P. Antoni, Y. Hed, A. Nordberg, D. Nyström, H. von Holst, A. Hult and M. Malkoch, *Angew. Chem. Int. Ed.*, 2009, **48**, 2126-2130.
- 61. C. Ornelas and M. Weck, *Chem. Commun.*, 2009, 5710-5712.
- 62. J. E. Macdonald, J. A. Kelly and J. G. C. Veinot, *Langmuir*, 2007, **23**, 9543-9545.
- 63. C. D. Hein, X. M. Liu and D. Wang, *Pharm. Res.*, 2008, **25**, 2216-2230.
- 64. R. K. Tekade, P. V. Kumar and N. K. Jain, *Chem. Rev.*, 2008, **109**, 49-87.
- 65. D. G. Mullen, E. L. Borgmeier, M. Fang, D. Q. McNerny, A. Desai, J. R. Baker, B. G. Orr and M. M. Banaszak Holl, *Macromolecules*, 2010, 43, 6577-6587.
- 66. R. S. Navath, A. R. Menjoge, B. Wang, R. Romero, S. Kannan and R. M. Kannan, *Biomacromolecules*, 2010, **11**, 1544-1563.
- 67. T. Okuda, S. Kawakami, T. Maeie, T. Niidome, F. Yamashita and M. Hashida, *J. Control Release*, 2006, **114**, 69-77.
- 68. M. L. Patil, M. Zhang, O. Taratula, O. B. Garbuzenko, H. He and T. Minko, *Biomacromolecules*, 2009, **10**, 258-266.

- 69. L. M. Kaminskas, B. J. Boyd, P. Karellas, G. Y. Krippner, R. Lessene, B. Kelly and C. J. H. Porter, *Mol. Pharm.*, 2008, **5**, 449-463.
- 70. K. M. Kitchens, M. E. H. El-Sayed and H. Ghandehari, *Adv. Drug Deliv. Rev.*, 2005, **57**, 2163-2176.
- 71. I. J. Majoros, B. Keszler, S. Woehler, T. Bull and J. R. Baker, *Macromolecules*, 2003, **36**, 5526-5529.
- 72. I. J. Majoros, T. P. Thomas, C. B. Mehta and J. R. Baker, *J. Med. Chem.*, 2005, **48**, 5892-5899.
- 73. R. Qi, Y. Gao, Y. Tang, R.-R. He, T.-L. Liu, Y. He, S. Sun, B.-Y. Li, Y.-B. Li and G. Liu, *AAPS J.*, 2009, **11**, 395-405.
- 74. R. B. Kolhatkar, K. M. Kitchens, P. W. Swaan and H. Ghandehari, *Bioconjugate Chem.*, 2007, **18**, 2054-2060.
- 75. C. Waite, S. Sparks, K. Uhrich and C. Roth, *BMC Biotechnology*, 2009, **9**, 38.
- 76. V. Gajbhiye, P. Vijayaraj Kumar, R. K. Tekade and N. K. Jain, *Eur. J, Med. Chem.*, 2009, **44**, 1155-1166.
- D. Bhadra, A. K. Yadav, S. Bhadra and N. K. Jain, *Int. J. Pharm.*, 2005,
 295, 221-233.
- 78. V. Gajbhiye, P. V. Kumar, R. K. Tekade and N. K. Jain, *Curr. Pharm. Des.*, 2007, **13**, 415-429.
- 79. N. Hadjichristidis, M. Pitsikalis, S. Pispas and H. Iatrou, *Chem. Rev.*, 2001, **101**, 3747-3792.
- 80. A. Blencowe, J. F. Tan, T. K. Goh and G. G. Qiao, *Polymer*, 2009, **50**, 5-32.
- 81. T. Higashihara, T. Sakurai and A. Hirao, *Macromolecules*, 2009, **42**, 6006-6014.
- 82. A. Hirao, M. Hayashi, S. Loykulnant, K. Sugiyama, S. W. Ryu, N. Haraguchi, A. Matsuo and T. Higashihara, *Prog. Polym. Sci.*, 2005, **30**, 111-182.
- 83. N. Hadjichristidis, *J. Polym. Sci., Part A: Polym. Chem.*, 1999, **37**, 857-871.

- 84. H. Iatrou and N. Hadjichristidis, *Macromolecules*, 1993, **26**, 2479-2484.
- 85. A. Mavroudis and N. Hadjichristidis, *Macromolecules*, 2005, **39**, 535-540.
- 86. S. Christodoulou, P. Driva, H. Iatrou and N. Hadjichristidis, *Macromolecules*, 2008, **41**, 2607-2615.
- 87. S. Penczek, M. Cypryk, A. Duda, P. Kubisa and S. Slomkowski, *Prog. Polym. Sci.*, 2007, **32**, 247-282.
- 88. J.-S. Wang and K. Matyjaszewski, *J. Am. Chem. Soc.*, 1995, **117**, 5614-5615.
- 89. M. Kato, M. Kamigaito, M. Sawamoto and T. Higashimura, *Macromolecules*, 1995, **28**, 1721-1723.
- 90. M. Kamigaito, T. Ando and M. Sawamoto, *Chem. Rev.*, 2001, **101**, 3689-3746.
- 91. M. K. Georges, R. P. N. Veregin, P. M. Kazmaier and G. K. Hamer, *Macromolecules*, 1993, **26**, 2987-2988.
- 92. J. Chiefari, Y. K. Chong, F. Ercole, J. Krstina, J. Jeffery, T. P. T. Le, R. T. A. Mayadunne, G. F. Meijs, C. L. Moad, G. Moad, E. Rizzardo and S. H. Thang, *Macromolecules*, 1998, 31, 5559-5562.
- 93. H. Gao and K. Matyjaszewski, *Prog. Polym. Sci.*, 2009, **34**, 317-350.
- M. Ouchi, T. Terashima and M. Sawamoto, *Chem. Rev.*, 2009, **109**, 4963-5050.
- 95. K. Ohno, B. Wong and D. M. Haddleton, *J. Polym. Sci., Part A: Polym. Chem.*, 2001, **39**, 2206-2214.
- 96. D.-H. Han and C.-Y. Pan, *J. Polym. Sci., Part A: Polym. Chem.*, 2007, **45**, 789-799.
- 97. W. Yuan, J. Yuan, M. Zhou and C. Pan, *J. Polym. Sci., Part A: Polym. Chem.*, 2008, **46**, 2788-2798.
- 98. M. Le Hellaye, C. Lefay, T. P. Davis, M. H. Stenzel and C. Barner-Kowollik, J. Polym. Sci., Part A: Polym. Chem., 2008, 46, 3058-3067.
- 99. A. Vora, K. Singh and D. C. Webster, *Polymer*, 2009, **50**, 2768-2774.
- 100. H. Gao and K. Matyjaszewski, *J. Am. Chem. Soc.*, 2007, **129**, 11828-11834.

- J. Du and Y. Chen, J. Polym. Sci., Part A: Polym. Chem., 2004, 42, 2263-2271.
- 102. H. Gao, S. Ohno and K. Matyjaszewski, *J. Am. Chem. Soc.*, 2006, **128**, 15111-15113.
- 103. H. Gao and K. Matyjaszewski, *Macromolecules*, 2006, **39**, 7216-7223.
- 104. H. Gao and K. Matyjaszewski, *Macromolecules*, 2008, **41**, 4250-4257.
- 105. R. Hoogenboom, B. C. Moore and U. S. Schubert, *Chem. Commun.*, 2006, 4010-4012.
- 106. P.-F. Gou, W.-P. Zhu, N. Xu and Z.-Q. Shen, *J. Polym. Sci., Part A: Polym. Chem.*, 2008, **46**, 6455-6465.
- 107. Z. Ge, J. Xu, J. Hu, Y. Zhang and S. Liu, *Soft Matter*, 2009, **5**, 3932-3939.
- P.-F. Gou, W.-P. Zhu, N. Xu and Z.-Q. Shen, J. Polym. Sci., Part A: Polym. Chem., 2010, 48, 2961-2974.
- C. Li, Z. Ge, H. Liu and S. Liu, J. Polym. Sci., Part A: Polym. Chem., 2009, 47, 4001-4013.
- 110. A. Gozgen, A. Dag, H. Durmaz, O. Sirkecioglu, G. Hizal and U. Tunca, *J. Polym. Sci., Part A: Polym. Chem.*, 2009, **47**, 497-504.
- 111. Y. Zhang, H. Liu, H. Dong, C. Li and S. Liu, *J. Polym. Sci., Part A: Polym. Chem.*, 2009, **47**, 1636-1650.
- 112. Q. Fu, G. Wang, W. Lin and J. Huang, J. Polym. Sci., Part A: Polym. Chem., 2009, 47, 986-990.
- 113. H. Durmaz, A. Dag, E. Erdogan, A. L. Demirel, G. Hizal and U. Tunca, *J. Polym. Sci., Part A: Polym. Chem.*, 2010, **48**, 99-108.
- 114. K. Khanna, S. Varshney and A. Kakkar, *Macromolecules*, 2010, **43**, 5688-5698.
- G. M. Soliman, R. Sharma, A. O. Choi, S. K. Varshney, F. M. Winnik, A.
 K. Kakkar and D. Maysinger, *Biomaterials*, 2010, 31, 8382-8392.
- 116. G. Deng, D. Ma and Z. Xu, Eur. Polym. J., 2007, 43, 1179-1187.
- M. R. Whittaker, C. N. Urbani and M. J. Monteiro, J. Am. Chem. Soc., 2006, 128, 11360-11361.

- 118. P.-F. Gou, W.-P. Zhu, N. Xu and Z.-Q. Shen, *J. Polym. Sci., Part A: Polym. Chem.*, 2009, **47**, 6962-6976.
- P.-F. Gou, W.-P. Zhu, N. Zhu and Z.-Q. Shen, J. Polym. Sci., Part A: Polym. Chem., 2009, 47, 2905-2916.
- Y. Zhang, C. Li and S. Liu, J. Polym. Sci., Part A: Polym. Chem., 2009,
 47, 3066-3077.
- 121. A. Dag, H. Durmaz, O. Sirkecioglu, G. Hizal and U. Tunca, *J. Polym. Sci.*, *Part A: Polym. Chem.*, 2009, **47**, 2344-2351.
- 122. A. Dag, H. Durmaz, V. Kirmizi, G. Hizal and U. Tunca, *Polym. Chem.*, 2010, **1**, 621-623.
- 123. Z.-M. Wu, H. Liang, J. Lu and W.-L. Deng, *J. Polym. Sci., Part A: Polym. Chem.*, 2010, **48**, 3323-3330.
- 124. J. Hu, Y. Cheng, Y. Ma, Q. Wu and T. Xu, J. Phys. Chem. B., 2008, 113, 64-74.
- 125. J. Hu, Y. Cheng, Q. Wu, L. Zhao and T. Xu, J. Phys. Chem. B., 2009, 113, 10650-10659.
- 126. L. Zhao, Y. Cheng, J. Hu, Q. Wu and T. Xu, *J. Phys. Chem. B.*, 2009, **113**, 14172-14179.
- 127. X. Feng, Y. Cheng, K. Yang, J. Zhang, Q. Wu and T. Xu, *J. Phys. Chem. B.*, 2010, **114**, 11017-11026.
- 128. A. M. Naylor, W. A. Goddard, G. E. Keifer and D. A. Tomalia, *J. Am. Chem. Soc.*, 1989, **111**, 2339.
- 129. M. T. Morgan, M. A. Carnahan, C. E. Immoos, A. A. Ribeiro, S. Finkelstein, S. J. Lee and M. W. Grinstaff, *J. Am. Chem. Soc.*, 2003, **125**, 15485.
- 130. Y. Cheng, Q. Wu, Y. Li and T. Xu, J. Phys. Chem. B., 2008, 112, 8884-8890.
- 131. S. Svenson and A. S. Chauhan, *Nanomedicine*, 2008, **3**, 679-702.
- 132. P. Sharma and S. Garg, *Adv. Drug Deliv. Rev.*, 2010, **62**, 491-502.
- 133. C. Kojima, K. Kono, K. Maruyama and T. Takagishi, *Bioconj. Chem.*, 2000, **11**, 910.

- 134. A. K. Patri, J. F. Kukowska-Latallo and J. R. Baker, *Adv. Drug Delivery Rev.*, 2005, **57**, 2203.
- 135. M. T. Morgan, Y. Nakanishi, D. J. Kroll, A. P. Griset, M. A. Carnahan, M. Wathier, N. H. Oberlies, G. Manikumar, M. C. Wani and M. W. Grinstaff, *Cancer Res.*, 2006, 66, 11913.
- D. Bhadra, S. Bhadra, S. Jain and N. K. Jain, *Int. J. Pharm.*, 2003, 257, 111-124.
- 137. K. Gardikis, S. Hatziantoniou, M. Bucos, D. Fessas, M. Signorelli, T. Felekis, M. Zervou, C. G. Screttas, B. R. Steele, M. Ionov, M. Micha-Screttas, B. Klajnert, M. Bryszewska and C. Demetzos, *J. Pharm. Sci.*, 2010, **99**, 3561-3571.
- 138. J. Babin, D. Taton, M. Brinkmann and S. Lecommandoux, *Macromolecules*, 2008, **41**, 1384-1392.
- F. Nederberg, E. Appel, J. P. K. Tan, S. H. Kim, K. Fukushima, J. Sly, R.
 D. Miller, R. M. Waymouth, Y. Y. Yang and J. L. Hedrick, *Biomacromolecules*, 2009, 10, 1460-1468.
- 140. H. Yin, S.-W. Kang and Y. H. Bae, *Macromolecules*, 2009, **42**, 7456-7464.
- 141. T. P. Lodge, A. Rasdal, Z. B. Li and M. A. Hillmyer, *J. Am. Chem. Soc.*, 2005, **127**, 17608-17609.
- 142. F. Wang, T. K. Bronich, A. V. Kabanov, R. D. Rauh and J. Roovers, *Bioconjugate Chem.*, 2005, **16**, 397-405.
- 143. F. Wang, T. K. Bronich, A. V. Kabanov, R. D. Rauh and J. Roovers, *Bioconjugate Chem.*, 2008, **19**, 1423-1429.
- 144. J. Yun, R. Faust, L. S. Szilágyi, S. Kéki and M. Zsuga, *Macromolecules*, 2003, **36**, 1717-1723.
- 145. S. Pispas, N. Hadjichristidis, I. Potemkin and A. Khokhlov, *Macromolecules*, 2000, **33**, 1741-1746.
- 146. P.-F. Gou, W.-P. Zhu and Z.-Q. Shen, *Biomacromolecules*, 2010, **11**, 934-943.

- E. Güç, G. Gündüz and U. Gündüz, *Drug Dev. Ind. Pharm.*, 2010, 36, 1139-1148.
- 148. M. R. Radowski, A. Shukla, H. von Berlepsch, C. Böttcher, G. Pickaert, H. Rehage and R. Haag, *Angew. Chem., Int. Ed.*, 2007, **46**, 1265-1269.
- 149. W. Tian, X. Fan, J. Kong, Y. Liu, T. Liu and Y. Huang, *Polymer*, 2010, 51, 2556-2564.
- 150. S. Gurdag, J. Khandare, S. Stapels, L. H. Matherly and R. M. Kannan, *Bioconjugate Chem.*, 2006, **17**, 275-283.
- 151. R. Shukla and et al., Nanotechnology, 2008, **19**, 295102.
- 152. M. Najlah, S. Freeman, D. Attwood and A. D'Emanuele, *Int. J. Pharm.*, 2006, **308**, 175-182.
- Y. E. Kurtoglu, M. K. Mishra, S. Kannan and R. M. Kannan, *Int. J. Pharm.*, 2010, 384, 189-194.
- 154. S.-T. Lo, S. Stern, J. D. Clogston, J. Zheng, P. P. Adiseshaiah, M. Dobrovolskaia, J. Lim, A. K. Patri, X. Sun and E. E. Simanek, *Mol. Pharm.*, 2010, 7, 993-1006.
- 155. Y. E. Kurtoglu, R. S. Navath, B. Wang, S. Kannan, R. Romero and R. M. Kannan, *Biomaterials*, 2009, **30**, 2112-2121.
- 156. M. Najlah, S. Freeman, D. Attwood and A. D'Emanuele, *Int. J. Pharm.*, 2007, **336**, 183-190.
- 157. X. Bi, X. Shi, I. J. Majoros, R. Shukla and J. R. Baker, *J. Comput. Theor. Nanosci.*, 2007, **4**, 1179-1187.
- 158. A. Quintana, E. Raczka, L. Piehler, I. Lee, A. Myc, I. Majoros, A. Patri, T. Thomas, J. Mulé and J. Baker, *Pharm. Res.*, 2002, **19**, 1310-1316.
- 159. T. P. Thomas, I. J. Majoros, A. Kotlyar, J. F. Kukowska-Latallo, A. Bielinska, A. Myc and J. R. Baker, *J. Med. Chem.*, 2005, **48**, 3729-3735.
- 160. J. J. Khandare, S. Jayant, A. Singh, P. Chandna, Y. Wang, N. Vorsa and T. Minko, *Bioconjugate Chem.*, 2006, **17**, 1464-1472.
- L. M. Kaminskas, B. D. Kelly, V. M. McLeod, B. J. Boyd, G. Y. Krippner, E. D. Williams and C. J. H. Porter, *Mol. Pharm.*, 2009, 6, 1190-1204.

- 162. S. Zhu, M. Hong, L. Zhang, G. Tang, Y. Jiang and Y. Pei, *Pharm. Res.*, 2010, **27**, 161-174.
- C. C. Lee, E. R. Gillies, M. E. Fox, S. J. Guillaudeu, J. M. J. Fréchet, E. E. Dy and F. C. Szoka, *Proc. Natl. Acad. Sci. U. S. A.*, 2006, 103, 16649-16654.
- 164. D. G. van der Poll, H. M. Kieler-Ferguson, W. C. Floyd, S. J. Guillaudeu, K. Jerger, F. C. Szoka and J. M. Fréchet, *Bioconjugate Chem.*, 2010, 21, 764-773.
- S. Zhu, M. Hong, G. Tang, L. Qian, J. Lin, Y. Jiang and Y. Pei, Biomaterials, 2010, 31, 1360-1371.
- 166. M. E. Fox, S. Guillaudeu, J. M. J. Fréchet, K. Jerger, N. Macaraeg and F. C. Szoka, *Mol. Pharm.*, 2009, 6, 1562-1572.
- G. Thiagarajan, A. Ray, A. Malugin and H. Ghandehari, *Pharm. Res.*, 2010, 27, 2307-2316.
- 168. X. Wang, R. Inapagolla, S. Kannan, M. Lieh-Lai and R. M. Kannan, *Bioconjugate Chem.*, 2007, **18**, 791-799.
- 169. O. Perumal, J. Khandare, P. Kolhe, S. Kannan, M. Lieh-Lai and R. M. Kannan, *Bioconjugate Chem.*, 2009, **20**, 842-846.
- 170. X. Li, M. Lu, Q. Wu, D.-s. Lv and X.-F. Lin, *J. Polym. Sci., Part A: Polym. Chem.*, 2008, **46**, 117-126.
- 171. Z. Xie, X. Hu, X. Chen, J. Sun, Q. Shi and X. Jing, *Biomacromolecules*, 2007, **9**, 376-380.
- 172. J. Liu, P. Zahedi, F. Zeng and C. Allen, *J. Pharm. Sci.*, 2008, **97**, 3274-3290.
- 173. W.-C. Shen and H. J. P. Ryser, *Biochem. Bioph. Res. Co.*, 1981, **102**, 1048-1054.
- 174. S. J. Guillaudeu, M. E. Fox, Y. M. Haidar, E. E. Dy, F. C. Szoka and J. M. J. Fréchet, *Bioconjugate Chem.*, 2008, **19**, 461-469.
- 175. K. Kono, C. Kojima, N. Hayashi, E. Nishisaka, K. Kiura, S. Watarai and A. Harada, *Biomaterials*, 2008, **29**, 1664-1675.

- 176. H. R. Ihre, O. L. Padilla De Jesús, F. C. Szoka and J. M. J. Fréchet, *Bioconjugate Chem.*, 2002, **13**, 443-452.
- 177. H. Yuan, K. Luo, Y. Lai, Y. Pu, B. He, G. Wang, Y. Wu and Z. Gu, *Mol. Pharm.*, 2010, **7**, 953-962.
- 178. O. L. Padilla De Jesús, H. R. Ihre, L. Gagne, J. M. J. Fréchet and F. C. Szoka, *Bioconjugate Chem.*, 2002, **13**, 453-461.
- A. Gopin, S. Ebner, B. Attali and D. Shabat, *Bioconjugate Chem.*, 2006,
 17, 1432-1440.
- 180. S. R. MacEwan, D. J. Callahan and A. Chilkoti, *Nanomedicine*, 2010, **5**, 793-806.
- 181. M. C. Garnett, Adv. Drug Deliv. Rev., 2001, **53**, 171-216.
- 182. Y. Matsumura and H. Maeda, *Cancer Res.*, 1986, **46**, 6387-6392.
- 183. S. A. Skinner, P. J. M. Tutton and P. E. O'Brien, *Cancer Res.*, 1990, **50**, 2411-2417.
- 184. K. Greish, J. Fang, T. Inutsuka, A. Nagamitsu and H. Maeda, *Clin. Pharmacokinet.*, 2003, **42**, 1089-1105.
- 185. H. Maeda, G. Y. Bharate and J. Daruwalla, *Eur. J. Pharm. Biopharm*, 2009, **71**, 409-419.
- 186. R. Gref, Y. Minamitake, M. T. Peracchia, V. Trubetskoy, V. Torchilin and R. Langer, *Science*, 1994, **263**, 1600-1603.
- 187. H. Maeda, *Bioconjugate Chem.*, 2010, **21**, 797-802.
- 188. S. Stolnik, L. Illum and S. S. Davis, *Adv. Drug Deliv. Rev.*, 1995, **16**, 195-214.
- 189. V. C. F. Mosqueira, P. Legrand, A. Gulik, O. Bourdon, R. Gref, D. Labarre and G. Barratt, *Biomaterials*, 2001, **22**, 2967-2979.
- 190. F. Ravenelle, S. Gori, D. Le Garrec, D. Lessard, L. Luo, D. Palusova, J. Sneyd and D. Smith, *Pharm. Res.*, 2008, **25**, 313-319.
- H. Otsuka, Y. Nagasaki and K. Kataoka, *Adv. Drug Deliv. Rev.*, 2003, 55, 403-419.
- 192. D. E. Owens and N. A. Peppas, *Int. J. Pharm.*, 2006, **307**, 93-102.

- L. M. Kaminskas, Z. Wu, N. Barlow, G. Y. Krippner, B. J. Boyd and C. J.
 H. Porter, *J. Pharm. Sci.*, 2009, 98, 3871-3875.
- 194. C. Rippe, D. Asgeirsson, D. Venturoli, A. Rippe and B. Rippe, *Kidney Int*, 2006, **69**, 1326-1332.
- 195. H. Soo Choi, W. Liu, P. Misra, E. Tanaka, J. P. Zimmer, B. Itty Ipe, M. G. Bawendi and J. V. Frangioni, *Nat Biotech*, 2007, **25**, 1165-1170.
- 196. S. Sadekar, A. Ray, M. Janàt-Amsbury, C. M. Peterson and H. Ghandehari, *Biomacromolecules*, 2010, **12**, 88-96.
- 197. S. Uppuluri, S. E. Keinath, D. A. Tomalia and P. R. Dvornic, *Macromolecules*, 1998, **31**, 4498-4510.
- 198. D. A. Tomalia, A. M. Naylor and W. A. Goddard, *Angew. Chem. Int. Ed.*, 1990, **29**, 138-175.
- 199. R. Scherrenberg, B. Coussens, P. van Vliet, G. Edouard, J. Brackman, E. de Brabander and K. Mortensen, *Macromolecules*, 1998, **31**, 456-461.
- S. Nigavekar, L. Sung, M. Llanes, A. El-Jawahri, T. Lawrence, C. Becker,
 L. Balogh and M. Khan, *Pharm. Res.*, 2004, 21, 476-483.
- N. Malik, R. Wiwattanapatapee, R. Klopsch, K. Lorenz, H. Frey, J. W. Weener, E. W. Meijer, W. Paulus and R. Duncan, *J. Control. Release*, 2000, 65, 133-148.
- 202. M. Bernfield, M. Gotte, P. W. Park, O. Reizes, M. L. Fitzgerald, J. Lincecum and M. Zako, *Annu. Rev. Biochem.*, 1999, **68**, 729-777.
- B. J. Boyd, L. M. Kaminskas, P. Karellas, G. Krippner, R. Lessene and C.
 J. H. Porter, *Mol. Pharm.*, 2006, 3, 614-627.
- 204. J. F. Kukowska-Latallo, K. A. Candido, Z. Cao, S. S. Nigavekar, I. J. Majoros, T. P. Thomas, L. P. Balogh, M. K. Khan and J. R. Baker, *Cancer Res.*, 2005, 65, 5317-5324.
- 205. L. M. Kaminskas, B. D. Kelly, V. M. McLeod, G. Sberna, D. J. Owen, B. J. Boyd and C. J. H. Porter, *J. Control. Release*, In Press, Uncorrected Proof.
- D. A. Tomalia, L. A. Reyna and S. Svenson, *Biochem. Soc. Trans.*, 2007,
 35, 61-67.

- 207. J. Luo, K. Xiao, Y. Li, J. S. Lee, L. Shi, Y.-H. Tan, L. Xing, R. Holland Cheng, G.-Y. Liu and K. S. Lam, *Bioconjugate Chem.*, 2010, 21, 1216-1224.
- K. Xiao, J. Luo, W. L. Fowler, Y. Li, J. S. Lee, L. Xing, R. H. Cheng, L. Wang and K. S. Lam, *Biomaterials*, 2009, 30, 6006-6016.
- 209. K. Zhang, Y. Wang, A. Yu, Y. Zhang, H. Tang and X. X. Zhu, *Bioconjugate Chem.*, 2010, **21**, 1596-1601.
- A. S. Chauhan, N. K. Jain, P. V. Diwan and A. J. Khopade, *J. Drug Target.*, 2004, 12, 575-583.
- 211. A. Asthana, A. S. Chauhan, P. V. Diwan and N. K. Jain, *AAPS PharmSciTech*, 2005, **6**.
- 212. H. Dai, R. S. Navath, B. Balakrishnan, B. R. Guru, M. K. Mishra, R. Romero, R. M. Kannan and S. Kannan, *Nanomedicine*, 2010, 5, 1317-1329.
- 213. Y. Zhang, T. P. Thomas, A. Desai, H. Zong, P. R. Leroueil, I. J. Majoros and J. R. Baker, *Bioconjugate Chem.*, 2010, **21**, 489-495.
- 214. Z. Sideratou, C. Kontoyianni, G. I. Drossopoulou and C. M. Paleos, *Bioorg. Medicinal Chem. Lett.*, 2010, **20**, 6513-6517.
- 215. W. Yang, Y. Cheng, T. Xu, X. Wang and L.-p. Wen, Eur. J, Med. Chem., 2009, 44, 862-868.
- 216. H. Yang and W. J. Kao, Int. J. Nanomed., 2007, 2, 89-99.
- A. Myc, A. K. Patri and J. R. Baker, *Biomacromolecules*, 2007, 8, 2986-2989.
- 218. L. Han, R. Huang, S. Liu, S. Huang and C. Jiang, *Mol. Pharm.*, 2010, **7**, 2156-2165.
- 219. C. Wängler, G. Moldenhauer, M. Eisenhut, U. Haberkorn and W. Mier, *Bioconjugate Chem.*, 2008, **19**, 813-820.
- 220. T. Miyano, W. Wijagkanalan, S. Kawakami, F. Yamashita and M. Hashida, *Mol. Pharm.*, 2010, **7**, 1318-1327.
- 221. I. J. Majoros, A. Myc, T. Thomas, C. B. Mehta and J. R. Baker, *Biomacromolecules*, 2006, **7**, 572-579.

- 222. A. K. Patri, J. F. Kukowska-Latallo and J. J. R. Baker, *Adv. Drug Deliv. Rev.*, 2005, **57**, 2203-2214.
- 223. H. He, Y. Li, X.-R. Jia, J. Du, X. Ying, W.-L. Lu, J.-N. Lou and Y. Wei, *Biomaterials*, 2011, **32**, 478-487.
- 224. L. E. Samuelson, M. J. Dukes, C. R. Hunt, J. D. Casey and D. J. Bornhop, *Bioconjugate Chem.*, 2009, **20**, 2082-2089.
- M. Calderón, M. A. Quadir, M. Strumia and R. Haag, *Biochimie*, 2010, 92, 1242-1251.
- 226. V. Gajbhiye, P. V. Kumar, A. Sharma and N. K. Jain, *Current Nanoscience*, 2008, **4**, 267-277.
- 227. V. Gajbhiye, P. V. Kumar, R. K. Tekade and N. K. Jain, *Eur. J. Med. Chem.*, 2009, **44**, 1155-1166.
- 228. W. Yuan, J. Yuan, S. Zheng and X. Hong, *Polymer*, 2007, **48**, 2585-2594.
- 229. S. Ki Choi, T. Thomas, M.-H. Li, A. Kotlyar, A. Desai and J. J. R. Baker, *Chem. Commun.*, 2010, **46**, 2632-2634.
- 230. K. Haba, M. Popkov, M. Shamis, R. A. Lerner, C. F. Barbas and D. Shabat, *Angew. Chem. Int. Ed.*, 2005, **44**, 716-720.
- 231. M. Avital-Shmilovici and D. Shabat, Soft Matter, 2010, 6, 1073-1080.
- 232. D. V. McGrath, Mol. Pharm., 2005, 2, 253-263.
- 233. F. M. H. de Groot, C. Albrecht, R. Koekkoek, P. H. Beusker and H. W. Scheeren, *Angew. Chem. Int. Ed.*, 2003, **42**, 4490-4494.
- 234. R. J. Amir, N. Pessah, M. Shamis and D. Shabat, *Angew. Chem. Int. Ed.*, 2003, **42**, 4494-4499.
- 235. S. Li, M. L. Szalai, R. M. Kevwitch and D. V. McGrath, *J. Am. Chem. Soc.*, 2003, **125**, 10516-10517.
- 236. X. Zhang, J. Cheng, Q. Wang, Z. Zhong and R. Zhuo, *Macromolecules*, 2010, **43**, 6671-6677.
- 237. T.-B. Ren, Y. Feng, Z.-H. Zhang, L. Li and Y.-Y. Li, *Soft Matter*, 2011, **7**, 2329-2331.
- 238. D. Q. McNerny, P. R. Leroueil and J. R. Baker, *Wiley Interdiscip. Rev. Nanomed. Nanobiotechnol.*, 2010, **2**, 249-259.

- J. C. Roberts, M. K. Bhalgat and R. T. Zera, *J. Biomed. Mater. Res.*, 1996,
 30, 53-65.
- 240. P. C. Naha, M. Davoren, F. M. Lyng and H. J. Byrne, *Toxicol. Appl. Pharmacol.*, 2010, **246**, 91-99.
- 241. H. B. Agashe, T. Dutta, M. Garg and N. K. Jain, *J. Pharm. Pharmacol.*, 2006, **58**, 1491-1498.
- 242. T. C. King Heiden, E. Dengler, W. J. Kao, W. Heideman and R. E. Peterson, *Toxicol. Appl. Pharmacol.*, 2007, **225**, 70-79.
- 243. W. Wang, W. Xiong, J. L. Wan, X. H. Sun, H. B. Xu and X. L. Yang, *Nanotechnology*, 2009, **20**, 7.
- K. Jain, P. Kesharwani, U. Gupta and N. K. Jain, *Int. J. Pharm.*, 2010,
 394, 122-142.
- 245. S. Hong, A. U. Bielinska, A. Mecke, B. Keszler, J. L. Beals, X. Shi, L. Balogh, B. G. Orr, J. R. Baker and M. M. Banaszak Holl, *Bioconjugate Chem.*, 2004, **15**, 774-782.
- 246. Y. Cheng, L. Zhao, Y. Li and T. Xu, Chem. Soc. Rev., 2011.
- 247. C. Rao and J. P. Tam, *J. Am. Chem. Soc.*, 1994, **116**, 6975-6976.
- 248. K. Sadler and J. P. Tam, Rev. Mol. Biotechnol., 2002, **90**, 195-229.
- 249. J. Ziegler, R. T. Chang and D. W. Wright, *J. Am. Chem. Soc.*, 1999, **121**, 2395-2400.
- 250. E. H. Nardin, J. M. Calvo-Calle, G. A. Oliveira, R. S. Nussenzweig, M. Schneider, J.-M. Tiercy, L. Loutan, D. Hochstrasser and K. Rose, J. Immunol., 2001, 166, 481-489.
- P. Singh, F. Moll, 3rd, S. Lin, C. Ferzli, K. Yu, R. Koski, R. Saul and P. Cronin, *Clin. Chem.*, 1994, 40, 1845-1849.
- 252. R. Yin, M. S. Bratcher, A. L. Jenkins, R. P. Hydutsky, R. Cheng, H. D. Durst, P. A. Emanuel and G. L. Hagnauer, Abstracts of Papers, 221st ACS National Meeting, San Diego, CA, United States, April 1-5, 2001, 2001, PMSE-474.

1.8 Update subsequent to publication of the above review

Macromolecules based multifunctional nanocarriers for biological applications continue to constitute a topical area of research. Since the writing of the above mentioned review article in 2011, a fair amount of work has been carried out in the design of new nacromolecules based nanoconjugates. A brief summary of the developments in this area is provided below as an update to this review.

Major developments in dendrimer nanoconjugates over the last two years have been in designing bifunctional dendrimers.^{3, 5-13} Multitasking with nanocarriers requires that the scaffolds with low polydisopersity and high purity are assembled, especially when the synthesis is carried out at large scales. In order to resolve this issue, Baker and coworkers have recently reported a proof of concept to construct bifunctional dendrimers where the two functionalities have been introduced in fixed ratios.¹⁴ The synthesis was achieved via one step 'click' reaction using triazine as a trifunctional molecule, in which two sites were coupled to a targeting ligand, Folic acid (FA), and a drug, Methotrexate (MTX) in 1:1 ratio, while an azido focal point is created at the third functional site. Using this strategy they were able to synthesize bifunctional dendrimer conjugates with an exact 1:1 ratio of the two ligands. It prevented the production of dendrimer populations containing only FA or MTX as in their previous procedure, ¹⁵ and reduced the need of extensive purifications. In another study, Baker's group has reported the synthesis of a trifunctional dendrimer with a targeting moiety (FA), a therapeutic agent (MTX) and an imaging agent (fluoresein) using copper free click chemistry.¹⁶ The synthesis was achieved using G5 PAMAM dendrimer based platform with cyclooctyne molecules at the surface to perform copper free click reaction. Mono-, di-, and tri-functionalized G5 PAMAM dendrimer conjugates were obtained by reacting azido modified functionalities simultaneously or sequentially with PAMAM dendrimer scaffold. Wang and coworkers¹⁷ have reported a multifunctional tumor targeted and pH responsive drug release system, based on FA conjugated polyethylene glycol (PEG) modified G3.5 PAMAM dendrimers. Iron oxide nano particles (IONPs) were stabilized by this FA-PEG-G3.5 PAMAM dendrimer and the anticancer drug doxorubicin (DOX) was conjugated to the dendrimer segments of amino-stabilized IONPs using hydrazine as the linker via hydrazone bonds. These hydrazone linkages are acid sensitive and make the nanocarrier an ideal pH-responsive drug release system. Conjugation with oleylamine stabilized IONPs provide better cancer imaging ability as an MR contrast agent *in vivo* and combined FA and the EPR effect can improve the overall efficacy towards cancer treatment.

There are several recent reports where internal cavities of dendrimers have been used to physically encapsulate drug molecules. 18-22 The encapsulation of DOX within the dendrimers is not very efficient method in general due to the problem of rapid drug release, thus limiting the use of this method for DOX loading into dendrimers.³ Recently, Jiang and coworkers have developed a more stable DOX release system based on a PEGylated G5 PAMAM dendrimer in pH 7.4 by complexing the drug to a codelivered apoptosis-inducing gene (TRAIL) prior to the encapsulation into the dendrimer.²³ The complexation of DOX to the gene makes its release more dependent on the liberation of the gene from the dendrimer rather than the electrostatic interactions with the scaffold. Only 20% of DOX release was observed over the period of 120 hours. In another report, Khoa and coworkers have designed a PEGylated G3 PAMAM dendrimer based system to load anti-cancer drug fluorouracil (5-FU).²⁴ The generation 3 PAMAM dendrimer was synthesized and subsequently PEGylated with PEGylation degree of around 31% for peripheral amine groups of the dendrimer. TEM results confirmed the spherical shape of the PEGylated dendrimer with size ranging from 30-40 nm. The studies showed a slow release profile for the loaded 5-FU from PEGylated dedrimer. The PEGylated PAMAM dendrimer exhibited less toxicity as compared to non-PEGylated counterpart in MCF-7 cells in in vitro studies. For in vivo tumor xenograft study, MCF-7 cells-derived cancer tumors were generated on mice and the 5-FU encapsulated pegylated dendrimer showed a significant decrease in tumors generated by MCF-7 cancer cells.

Miktoarm polymers for drug delivery applications have already been discussed in detail in the review article described above as the part of this chapter,

and only a little work has been carried out in this area in the past two years. 25-27 Jérôme and coworkers have reported the evaluation of stealth properties of multifunctional poly(ethylene oxide) (PEO) based ABC miktoarm star terpolymer and ABC triblock copolymer, which combined three different polymer blocks, i.e. hydrophobic poly(\varepsilon-caprolactone), PEO and poly(2-vinylpyridine) (P2VP).²⁷ Biotin was grafted at P2VP chain end as a model targeting molecule in order to check the effect of pH on the exposure of targeting ligand as well as on the micelles. At physiological pH, biotin as well as the positive charges should be shielded by PEO corona of the micelles, and should become exposed on the surface upon protonation of P2VP chains. The results showed that the complement protein adsorption and macrophage uptake were low at physiological pH when the P2VP was un-protonated and the biotin was shielded by PEO shell. The selection of copolymer concentration was a key factor to provide stability to the micelles until they reach their target sites. You Han Bae and colleagues have designed and synthesized histidine-based AB2 miktoarm polymer (mPEG-b-(polyHis)₂) that mimics phospholipid structures.²⁵ The polymer was synthesized using "core-first" click chemistry and ring opening polymerization reactions, and which could self-assemble in aqueous solutions to form nano-sized polymersomes with strong proto-buffering ability and low cytotoxicity. The polymersomes were stable above pH 7.4, but transformed from vesicles to micelles in between pH 6.8 to 5.0 due to gradual protonation of imidazole groups. These polymers could be used as potential pH dependent drug delivery systems.

References

- 1. J. Lazniewska, K. Milowska and T. Gabryelak, Wiley Interdisciplinary Reviews: Nanomedicine and Nanobiotechnology, 2012, **4**, 469-491.
- 2. S.-T. Lo, A. Kumar, J.-T. Hsieh and X. Sun, *Molecular Pharmaceutics*, 2013, **10**, 793-812.
- 3. L. M. Kaminskas, V. M. McLeod, C. J. H. Porter and B. J. Boyd, *Molecular Pharmaceutics*, 2012, **9**, 355-373.

- 4. M. A. Mintzer, E. L. Dane, G. A. O'Toole and M. W. Grinstaff, *Molecular Pharmaceutics*, 2011, **9**, 342-354.
- H. Arima, A. Yoshimatsu, H. Ikeda, A. Ohyama, K. Motoyama, T. Higashi, A. Tsuchiya, T. Niidome, Y. Katayama, K. Hattori and T. Takeuchi, *Molecular Pharmaceutics*, 2012, 9, 2591-2604.
- 6. A. Choksi, K. V. L. Sarojini, P. Vadnal, C. Dias, P. K. Suresh and J. Khandare, *International Journal of Pharmaceutics*, 2013, **449**, 28-36.
- L. M. Kaminskas, B. D. Kelly, V. M. McLeod, G. Sberna, D. J. Owen, B. J. Boyd and C. J. H. Porter, *Journal of Controlled Release*, 2011, 152, 241-248.
- 8. J. Lim, S.-T. Lo, S. Hill, G. M. Pavan, X. Sun and E. E. Simanek, *Molecular Pharmaceutics*, 2012, **9**, 404-412.
- 9. T. P. Thomas, B. Huang, S. K. Choi, J. E. Silpe, A. Kotlyar, A. M. Desai, H. Zong, J. Gam, M. Joice and J. R. Baker, *Molecular Pharmaceutics*, 2012, **9**, 2669-2676.
- L. Zheng, J. Zhu, M. Shen, X. Chen, J. R. Baker, S. H. Wang, G. Zhang and X. Shi, *MedChemComm*, 2013, 4, 1001-1005.
- 11. A. L. Acton, C. Fante, B. Flatley, S. Burattini, I. W. Hamley, Z. Wang, F. Greco and W. Hayes, *Biomacromolecules*, 2013, **14**, 564-574.
- 12. X. Ma, Q. Sun, Z. Zhou, E. Jin, J. Tang, E. Van Kirk, W. J. Murdoch and Y. Shen, *Polymer Chemistry*, 2013, **4**, 812-819.
- 13. Y. Chang, Y. Li, X. Meng, N. Liu, D. Sun, H. Liu and J. Wang, *Polymer Chemistry*, 2013, **4**, 789-794.
- H. Zong, T. P. Thomas, K.-H. Lee, A. M. Desai, M.-h. Li, A. Kotlyar, Y. Zhang, P. R. Leroueil, J. J. Gam, M. M. Banaszak Holl and J. R. Baker, *Biomacromolecules*, 2012, 13, 982-991.
- 15. D. G. Mullen, M. Fang, A. Desai, J. R. Baker, B. G. Orr and M. M. Banaszak Holl, *ACS Nano*, 2010, **4**, 657-670.
- B. Huang, J. F. Kukowska-Latallo, S. Tang, H. Zong, K. B. Johnson, A. Desai, C. L. Gordon, P. R. Leroueil and J. R. Baker Jr, *Bioorganic & Medicinal Chemistry Letters*, 2012, 22, 3152-3156.

- 17. Y. Chang, N. Liu, L. Chen, X. Meng, Y. Liu, Y. Li and J. Wang, *Journal of Materials Chemistry*, 2012, **22**, 9594-9601.
- 18. K. Rouhollah, M. Pelin, Y. Serap, U. Gozde and G. Ufuk, *Journal of Pharmaceutical Sciences*, 2013, **102**, 1825-1835.
- 19. V. Gajbhiye, N. Ganesh, J. Barve and N. K. Jain, *European Journal of Pharmaceutical Sciences*, 2013, **48**, 668-679.
- S. K. Yandrapu, P. Kanujia, K. B. Chalasani, L. Mangamoori, R. V. Kolapalli and A. Chauhan, *Nanomedicine: Nanotechnology, Biology and Medicine*, 2013, 9, 514-522.
- 21. S. L. Kuan, B. Stöckle, J. Reichenwallner, D. Y. W. Ng, Y. Wu, M. Doroshenko, K. Koynov, D. Hinderberger, K. Müllen and T. Weil, *Biomacromolecules*, 2012, **14**, 367-376.
- S. R. Cerqueira, J. M. Oliveira, N. A. Silva, H. Leite-Almeida, S. Ribeiro-Samy, A. Almeida, J. F. Mano, N. Sousa, A. J. Salgado and R. L. Reis, Small, 2013, 9, 738-749.
- 23. L. Han, R. Huang, J. Li, S. Liu, S. Huang and C. Jiang, *Biomaterials*, 2011, **32**, 1242-1252.
- 24. T. U. Ly, N. Q. Tran, T. K. D. Hoang, K. N. Phan, H. N. Truong and C. K. Nguyen, *Journal of Biomedical Nanotechnology*, 2013, **9**, 213-220.
- 25. H. Yin, H. C. Kang, K. M. Huh and Y. H. Bae, *Journal of Materials Chemistry*, 2012, **22**, 19168-19178.
- 26. T. Liu, Y.-f. Zhang and S.-y. Liu, *Chin J Polym Sci*, 2013, **31**, 924-937.
- K. Van Butsele, M. Morille, C. Passirani, P. Legras, J. P. Benoit, S. K. Varshney, R. Jérôme and C. Jérôme, *Acta Biomaterialia*, 2011, 7, 3700-3707.

1.9 Scope of the thesis

The delivery of therapeutic agents to the desired site in the body with simultaneous imaging of their targeted intracellular locations has always been a challenging task. Among various nanostructures being evaluated for theranostic applications, dendrimers and miktoarm polymers offer a great potential because of their unique morphological and physical properties. There are several examples of mono-functional nanocarriers available in the literature, but there are a few reports of nanocarriers with multiple functionalities on them. This is due to the synthetic challenges associated with their synthesis. For biomedical applications it is very important to construct nanocarriers which are multitasking with a combination of a variety of functionalities e.g. drug molecules, targeting ligands, imaging dyes or stealth agents. The purpose is to deliver the therapeutics as well as to track and target the drugs at the same time. So, there is a need to develop versatile and efficient synthetic strategies which allow the incorporation of different functional ligands in the nanocarriers making them multitasking. Click chemistry¹⁻⁵ that encompasses e.g. alkyne-azide cycloaddition, Diels-Alder and thiol-ene reactions, (Scheme 1) provides an excellent platform to construct hyperbranched and branched macromolecules that find applications in a variety of areas including biology. For the scope of this thesis, Cu(I) catalyzed alkyne-azide coupling is the main reaction that is employed for building multifunctional nanocarriers. The thesis explores the design and development of facile, efficient and convenient synthetic methodologies to construct multifunctional nanocarriers using dendrimers and miktoarm polymers for biological applications. This methodology will allow incorporation of any desired number and types of functionalities into macromolecules based nanocarriers in a highly precise manner, and in any required combination. Both chemical conjugation of the drugs in dendrimers, and physical entrapment of drugs in the hydrophobic core of the miktoarm polymer micelles were explored. The choice of miktoarm polymers was based on their branched structure to attach different functionalities on them as well as due to their better drug loading as compared to the linear polymers. The detailed evaluation of these nanocarriers for biological applications has also been carried out. A brief description of the results presented in this thesis is given below:

Scheme 1: Click methodologies for the construction of branched and hyperbranched macromolecules.

Chapter 2: This chapter describes the development of an efficient synthetic strategy to incorporate two functionalities into a single dendrimer scaffold; a therapeutic agent and an imaging dye. The detailed synthesis of bifunctional nanoconjugates based on designing of an orthogonal molecular system which allows covalent linking of two different functional moieties in a single dendrimer for the simultaneous delivery of therapeutics with targeting of an intracellular location (lipid droplets), is presented. This is followed by an evaluation of their effects in biological systems.

Chapter 3: Together with combining delivery of drugs with imaging or targeting, it is also important to provide stability and aqueous solubility to the nanocarriers. This chapter describes the design and synthesis of multifunctional dendrimers by developing a synthetic methodology using orthogonal building blocks to incorporate multiple functional moieties in any desired number and combination in dendrimers based nanocarriers. A detailed synthesis of bi-functional dendrimers with different combination of functionalities (*i.e.* imaging and stealth agent or therapeutics and solubilising agent), and a tri-functional dendrimer having a combination of all these three moieties *i.e.* imaging, therapeutic and

stealth agent in a single nano-scaffold is presented. The evaluation of their biological results is also discussed.

Chapter 4: It is not always possible to link drugs covalently on to the nanocarriers due to the lack of appropriate functional groups or due to the poor aqueous solubility of the drugs. This chapter describes the construction and evaluation of the use of miktoarm polymer based micelles for physical encapsulation of drugs with simultaneous intracellular targeting. A mitochondriatargeted nanodelivery system based on ABC miktoarm polymers is presented. A detailed synthetic methodology to construct a library of miktoarm polymers along with their self assembly and biological evaluation is discussed.

Chapter 5: This chapter describes a novel approach towards the synthesis of multifunctional trackable nanocarriers based on dendrimer backbones with inherent imaging capabilities. Dendrimers of different generations are built on a fluorescent dye that forms their core. The peripheries of these hydroxyl terminating fluorescent dendrimers were subsequently functionalized with drug molecules. The detailed synthetic elaborations as well as their biological results are discussed.

Chapter 6: This chapter describes the summary of our results as well as the future perspectives of the research in the field of multifunctional nanocarriers for drug delivery applications.

References:

- 1. G. Franc and A. K. Kakkar, *Chemistry A European Journal*, 2009, **15**, 5630-5639.
- 2. G. Franc and A. K. Kakkar, *Chemical Society Reviews*, 2010, **39**, 1536-1544.
- 3. R. K. Iha, K. L. Wooley, A. M. Nyström, D. J. Burke, M. J. Kade and C. J. Hawker, *Chemical Reviews*, 2009, **109**, 5620-5686.
- 4. H. C. Kolb, M. G. Finn and K. B. Sharpless, *Angewandte Chemie International Edition*, 2001, **40**, 2004-2021.
- 5. B. T. Worrell, J. A. Malik and V. V. Fokin, *Science*, 2013, **340**, 457-460.

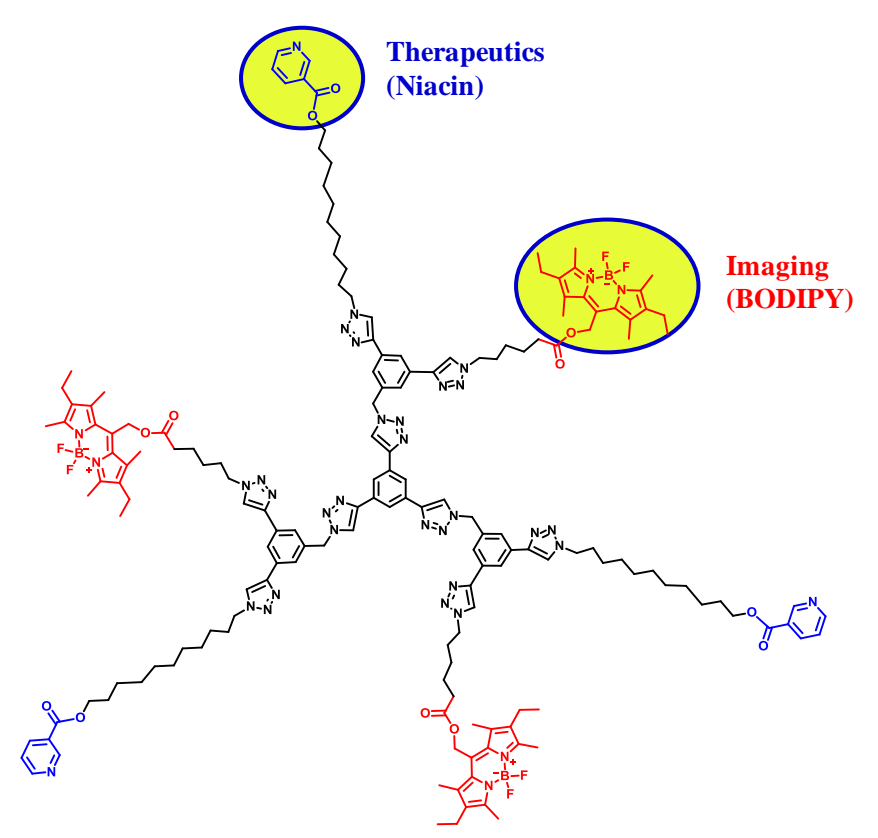
Chapter 2

Multivalent Niacin Nanoconjugates for Delivery to Cytoplasmic Lipid Droplets

Before carrying out the complex chemistry of incorporating multiple functionalities into dendrimers, we first standardized the methodology by constructing monofunctional dendrimers (Hourani, R.; Sharma, A.; Kakkar, A. *Tetrahedron Letters* **2010**, 51, 3792, Appendix 1). The dendrimers with acetylene surface groups were constructed via both convergent and divergent methodologies using Cu (I) catalyzed alkyne-azide click (CuAAC) chemistry. The surface of these dendrimers was then decorated using a variety of azides through click reaction to get monofunctional dendrimers with imaging dyes or cationinc groups on the surface.

Once the construction of monofunctional dendrimers along with the functionalization of their periphery was successfully demonstrated, the next step was to design and construct multitasking nanocarriers for biological applications. The major challenge of the project was to develop a convenient and efficient

synthetic methodology which allows us to incorporate multiple functional moieties in a single nano-scaffold and to construct dendrimers in high yields and purities. This chapter describes an elegant synthetic approach to construct bifunctional nanocarriers for targeted delivery of therapeutics to intracellular lipid droplets. In order to construct bifunctional nanocarriers, orthogonal bifunctional building blocks were constructed which allow the covalent linking of two different functional moieties (drug and dye) in a single nanoscaffold using CuAAC chemistry. The choice of click reaction was based on its high yield, no side products, tolerance to a variety of functional groups, and easy purification. Linear and branched counterparts of the dendrimers were also constructed in order to see the dendritic effect. The potential of these nanoconjugates in theranostics is also discussed in detail.



Reproduced in part with permission from:

Sharma A., Khatchadourian A., Khanna K., Sharma R., Kakkar A. and Maysinger D. *Biomaterials*, **2011**, 32, 1419.

Copyright, 2011, Elsevier

2.1 Introduction

Efficient delivery of therapeutics and simultaneous imaging of their targeted intracellular locations using materials of nanodimensions continues to be a topical area of research in biotechnology.[1-2] Challenges in the design and construction of such multivalent carriers have included developing synthetic methodologies that could deliver orthogonally functionalized architectures, an evaluation of their biocompatibility, monitoring the delivery to specific sites across cell membranes, and determining their therapeutic efficiency with improved pharmacokinetics.[3] Among numerous nanostructures that have been currently studied for combining drug delivery with tissue imaging, functionalized dendrimers and miktoarm polymers offer tremendous potential due to their unique architecture and properties.[4] Dendrimers are hyperbranched macromolecules, structurally versatile (can be tailored to a wide range of nanodimensions), and are monodisperse in nature with well-defined particle size.[5] Dendrimers are a recent addition to the field of nanomedicine, and they are currently being developed together with polymeric macromolecules as nanodevices for therapeutic applications.[6] We demonstrate here that such biocompatible nanovectors that can carry a combination of therapeutics and organelle imaging agents can be easily constructed using a highly efficient synthetic methodology based on Cu¹ catalyzed alkyne-azide cycloaddition "click" chemistry.[7-10] This 1,3-dipolar Huisgen cycloaddition is a versatile synthetic tool in constructing multifunctional nanomaterials with orthogonal functionalities which offer tremendous potential for applications in biology.[11]

Targeting of drugs by designed delivery systems (DDS) to specific subcellular compartments could prove a valid approach to achieve greater drug efficacy and specificity.[12-14] Herein, we describe a novel macromolecule-based nanodelivery system for niacin to specifically target lipid droplets (LDs). In the context of liver cells (hepatocytes), a designed DDS may provide specificity by carrying niacin directly to its target, DGAT2, localized on LDs. The mechanism of transport of niacin in hepatocytes was studied and shown to be regulated by specific membrane carriers systems.[15] Niacin, covalently attached to the

nanocarrier by an ester bond, can only be released when the bond is cleaved off by cellular esterases. The detection of the polymers at the subcellular level was made possible by attaching a lipophilic fluorescent dye, BODIPY. One particular non-polar derivative of BODIPY, Bodipy 493/503, is commonly used for staining intracellular LDs.[16]

Niacin/nicotinic acid (Vitamin B₃) is well known for its potential to improve lipid profile in patients with abnormalities including hyperlipidemia [17], and to treat atherosclerosis and reduce risks for cardiovascular disease.[18-20] Niacin is the most effective agent for increasing high density lipoprotein cholesterol (HDL-C) levels and concomitantly reducing low density cholesterol (LDL-C) and triglycerides in patients with dyslipidemia.[18] Niacin exerts most of its biological effects in cells by binding with high affinity to the G-protein coupled receptor GPR109a/HM74a.[21-24] Mechanisms of action [19] of Niacin include the inhibition of lipolysis in adipocytes and inhibition of hepatic diacylglycerol acyltransferase 2 (DGAT2), the enzyme involved in the final step of triglyceride biosynthesis.[25] Triglycerides are stored in intracellular lipid droplets (LDs), organelles specialized in lipid storage and fatty acid mobilization.[26] DGAT2 was shown to co localize with LDs in adipoctes [27-28] Excessive LD accumulation linked with hepatic steatosis and inflammation [29] could likely be reduced by targeting LD or LD-associated proteins with suitable nanocarriers. The objective of the study reported here was to develop multifunctional materials for targeting niacin to LDs and to show if the designed nanocarriers co-localized with these organelles.

2.2 Materials and methods

2.2.1 Materials

Copper (II) sulfate pentahydrate (CuSO₄.5H₂O) (>98.0%), sodium ascorbate (NaAsc) (crystalline) (98%), 6-bromohexanoic acid (97%), 11-bromo-1-undecanol (98%), niacin (NA) (>99%), 1-[3-(dimethylamino)propyl]-3-ethylcarbodiimidemethiodide(EDC), 4(dimethylamino)pyridine (DMAP) (99%), and sodium azide (NaN₃) (>99.5%) were purchased from Sigma-Aldrich Canada,

and used as received. 8-Acetoxymethyl-2,6-diethyl -1,3,5,7-tetramethyl pyrromethene fluoroborate (PM605) was purchased from Exciton Inc, and used as received. All other solvents were used as received in their anhydrous forms. NMR spectra were recorded on a 400 or 500 MHz (as specified) spectrometer at ambient temperatures. The chemical shifts in ppm are reported relative to tetramethylsilane as an internal standard for ¹H and ¹³C{¹H} NMR spectra. Mass spectra were recorded on Thermo Scientific Orbitrap mass analyzer (ES) and Kratos MS25 (EI) mass spectrometers, and MALDI-TOF spectra on Autoflex III Mass Spectrometer (Bruker) using LiBr-dithranol as the matrix.

2.2.2 Synthesis

The following compounds were synthesized by adaptation of the previously published procedure as follows: 1,3,5-triethynylbenzene [30], 11-Azido-undecan-1-ol [31], PEG₇₅₀-Azide [32], Miktoarm carrier containing PEG₇₅₀, acetylene and benzylic alcohol.[32] Miktoarm carrier containing two PEG₇₅₀ chains and a benzylic alcohol group.[33] BODIPY-Azide, Linear unit containing long chain alcohol and an acetylenic arm, and the dendrimer containing the long chain alcohol arms and free acetylenic groups.[31]

2.2.2.1 Synthesis of dendrimer containing niacin and free acetylenic arms (3): To a solution of dendrimer containing long chain alcohol and free acetylene (100 mg, 0.073 mmol), 1-[3-(dimethylamino)propyl]-3-ethylcarbodiimide methiodide (130.5 mg, 0.439 mmol), 4-(dimethylamino)pyridine (14 mg, 0.115 mmol), pyridine (1 mL) in anhydrous (2 mL) DMF, nicotinic acid (54.11 mg, 0.439 mmol) was added, and the solution was stirred at room temperature for 24h. Water (40 mL) was then added, and extraction of the product was carried using dichloromethane (3 x 20 mL). The combined organic extracts were then washed with water and brine, dried over sodium sulphate and concentrated under reduced pressure. The crude product was then passed through a column of silica gel. The pure fractions of product were obtained using 5% methanol in dicholoromethane (DCM) as an eluent. The fractions were then concentrated to give the desired product as a white solid. (120 mg, 100%). ¹H NMR (400 MHz, CDCl₃): δ (ppm)

1.21-1.44 (m, 42H, -CH₂-), 1.62-1.82 (m, 6H, -CH₂CH₂OH), 1.82-2.02 (m, 6H, -CH₂CH₂-triazole), 3.11 (s, 3H, ArCCH), 4.22-4.34 (m, 6H, -CH₂OCO-), 4.34-4.42 (m, 6H, -CH₂CH₂-triazole), 5.58 (s, 6H, -ArCH₂-triazole), 7.36 (s, 3H, ArH), 7.36-7.41 (m,3H, ArH), 7.79 (s, 3H, triazoleH), 7.82 (s, 3H, ArH), 7.86 (s, 3H, ArH), 7.93 (s, 3H, ArH, core), and 8.19 (s, 3H, triazoleH, core), 8.25-8.30 (m, 3H, ArH), 8.75-8.77 (m, 3H, ArH) and 9.20-9.21 (m, 3H, ArH). ¹³C{¹H} NMR (125 MHz, CDCl₃): δ (ppm) 25.9, 26.4, 28.6, 28.9, 29.2, 29.3, 29.4, 30.3, 50.5, 53.8, 50.5, 53.8, 65.5, 78.6, 82.4, 120.0, 120.2, 122.4, 123.3, 123.9, 125.6, 129.6, 130.9, 131.6, 132.1, 135.4, 136.9, 145.9, 147.6, 150.9, 153.3 and 165.3. ESI-MS: m/z 1701.82 ([M+Na]⁺).

2.2.2.2 Synthesis of dendrimer containing niacin and BODIPY (4): Compound 3 (102 mg, 0.062 mmol) and BODIPY-azide (131.7 mg, 0.278 mmol) were dissolved in 2 mL of THF, followed by addition of sodium ascorbate (5 mg, 0.03 mmol). An aqueous solution (1 mL) of CuSO₄.5H₂O (3.0 mg, 0.01 mmol) was added dropwise to the solution. The reaction mixture was left to stir overnight at room temperature. THF was then evaporated, and the remaining solution was extracted with DCM (3 x 20 mL), and then the organic layer was extracted with brine (3 x 50 mL). It was dried over MgSO₄, and the solvent was evaporated. Silica-gel column chromatography was used to isolate the product with 5% methanol in DCM. The solvent was evaporated to yield the product as a red solid (120 mg, 65%). ¹H NMR (400 MHz, CDCl₃): δ (ppm) 0.98 (t, 18H, -ArCH₂CH₃), 1.20-1.40 (m, 48H, -CH₂-), 1.60-1.70 (m, 6H, -CH₂CH₂OH), 1.70-1.80 (m, 6H, -CH₂CH₂CH₂-triazole), 1.80-1.96 (m, 12H, -CH₂CH₂-triazole), 2.18 (s, 18H, -ArCH₃), 2.24-2.38 (m, 18H, -CH₂-), 2.46 (s, 18H, -ArCH₃), 4.28-4.35 (m, 6H, -CH₂OH), 4.35-4.40 (m, 12H, -CH₂CH₂-triazole), 5.27 (s, 6H, -ArCH₂OOCCH₂-), 5.60 (s, 6H, -ArCH₂-triazole), 7.39 (s, 3H, ArH), 7.35-7.40 (m, 3H, ArH), 7.76 (s, 3H, triazole**H**), 7.79 (s, 3H, Ar**H**, core), 7.87 (s, 6H, Ar**H**), 8.14 (s, 3H, triazole**H**, BODIPY arm), 8.14-8.29 (m, 3H, ArH), 8.29 (s, 3H, triazoleH,core), 8.75-8.76 (m, 3H, Ar**H**) and 9.20-9.21(m, 3H, Ar**H**). $^{13}C\{^{1}H\}$ NMR (125 MHz, CDCl₃): δ (ppm) 12.6, 14.7, 17.1, 22.7, 24.2, 24.9, 25.6, 25.9, 26.5, 28.6, 28.9, 29.2, 29.3, 29.4, 29.7, 29.9, 30.3, 31.9, 33.6, 33.9, 50.1, 50.5, 54.1, 58.2, 65.6, 120.2, 120.3,

122.3, 124.8, 131.6, 132.2, 132.4, 133.5, 135.8, 136.5, 137.0, 146.5, 146.6, 147.4, 150.8, 153.3, 154.9, 165.3 and 172.8. MALDI: m/z 3074.34 ([M+Li]⁺).

2.2.2.3 Synthesis of the linear compound containing niacin and free acetylene (6): To a solution of the linear compound containing long chain alcohol and the free 0.590 (200)mmol), 1-[3-(dimethylamino)propyl]-3acetylene mg, ethylcarbodiimide methiodide (350.4)mg, 1.180mmol), 4-(dimethylamino)pyridine (36 mg, 0.295 mmol), pyridine (0.5 mL) in anhydrous (2 mL) DMF, nicotinic acid (145.3 mg, 1.180 mmol) was added, and the solution was stirred at room temperature for 24h. Water (30mL) was then added, and the product was extracted using DCM (3 x 20 mL). The combined organic extracts were then washed with water and brine, dried over sodium sulphate and concentrated under reduced pressure. The crude mixture was then passed through a column of silica gel. The pure fractions of product were obtained using 5% methanol in DCM as an eluent. The fractions were then concentrated to afford the product as a white solid. (260 mg, 94%). ¹H NMR (400 MHz, CDCl₃): δ (ppm) 1.34-1.40 (m, 12H, -CH₂-), 1.40-1.43(m, 2H, -CH₂CH₂OH), 1.75-1.80 (m, 2H, -CH₂CH₂-triazole), 1.92-1.96 (m, 2H, -CH₂CH₂-triazole), 3.13 (s, 1H, -CCH), 4.34 (t, 2H, -CH₂OCO-), 4.40 (t, 2H, -CH₂-triazole), 7.39-7.42(m,1H, ArH), 7.55 (d, 2H, ArH), 7.78 (d, 2H, ArH), 7.81 (s, 1H, triazoleH), 8.28-8.31 (m, 1H, ArH), 8.76-8.78(m,1H, Ar**H**), and 9.22-9.93(m,1H, Ar**H**). 13 C{ 1 H} NMR (125 MHz, CDCl₃): δ (ppm) 25.9, 26.5, 28.6, 29.0, 29.2, 29.3, 29.4, 30.3, 50.5, 65.5, 77.8, 83.5, 119.7, 121.6, 123.2, 125.4, 126.3, 131.1, 132.6, 137.0, 147.0, 150.9, 153.3 and 165.3. ESI-MS: m/z 467.24 ([M+Na]⁺), 445.26 ([M+H]⁺).

2.2.2.4 Synthesis of the linear compound containing niacin and BODIPY dye (7): Linear compound containing niacin and free acetylene (6) (60 mg, 0.135 mmol) and BODIPY-azide (96 mg, 0.203 mmol) were dissolved in 2 mL of THF, followed by addition of sodium ascorbate (5 mg, 0.03 mmol). An aqueous solution (1 mL) of CuSO₄.5H₂O (3.0 mg, 0.01 mmol) was added dropwise to the solution. The reaction mixture was left to stir overnight at room temperature. THF was then evaporated, and the remaining solution was extracted with DCM (3

x 20 mL), and then the organic layer was extracted with brine (3 x 50 mL). It was dried over MgSO₄, and the solvent was evaporated. Silica-gel column chromatography was used to isolate the product with 5% methanol in DCM. The solvent was evaporated to yield the product as a red solid (100 mg, 81%). ¹H NMR (400 MHz, CDCl₃): δ (ppm) 1.02 (t, 6H, -ArCH₂CH₃), 1.25-1.34 (m, 14H, -CH₂-), 1.34-1.42 (m, 2H, -CH₂CH₂OH), 1.50-1.70 (m, 4H, -CH₂CH₂CH₂-triazole), 1.70-2.00 (m, 4H, -CH₂CH₂-triazole), 2.22 (s, 6H, -ArCH₃), 2.30-2.40 (m, 6H, -OOCCH₂-, -ArCH₂CH₃), 2.49 (s, 6H, -ArCH₃), 3.64 (t, 2H, -CH₂OH), 4.32-4.40 (m, 4H, -CH₂-triazole), 5.30 (s, 2H, -ArCH₂OOCCH₂-), 7.39(m, 1H, ArH), 7.79 (s, 2H, triazoleH), 7.89 (s, 4H, ArH), 8.27-8.30 (m, 1H, ArH), 8.76-8.77 (m, 1H, ArH) and 9.21-9.23 (m, 1H, ArH), ; ¹³C{¹H} NMR (125 MHz, CDCl₃): δ (512.6, 14.7, 15.3, 17.1, 24.2, 25.9, 26.5, 28.6, 29.2, 29.3, 29.4, 29.9, 30.3, 33.7, 50.0, 50.5, 58.2, 65.6, 119.4, 119.5, 123.3, 126.0, 130.3, 130.4, 131.5, 132.2,133.6, 136.4, 136.9, 147.3, 147.4, 150.8, 153.3, 155.0 and 172.9. ESI-MS: m/z 940.52 ([M+Na]⁺).

2.2.2.5 Synthesis of miktoarm carrier containing PEG₇₅₀, BODIPY and benzylic alcohol (9): A concentrated solution of the miktoarm carrier containing PEG₇₅₀, acetylene and benzylic alcohol (0.196 g, 0.201 mmol) and BODIPY-azide (0.1 g, 0.211 mmol) in THF (2.5 mL) was prepared and stirred to dissolution in a roundbottom flask. Sodium L-ascorbate (4.190 mg, 0.021 mmol) was then added to the flask. CuSO_{4.5}H₂O (3.70 mg, 0.148 mmol) was dissolved in 0.5 mL of distilled water and added dropwise to the above mixture. A condenser was attached to the apparatus; reaction was placed under nitrogen and allowed to stir for 36 hours in the dark. The contents of the flask were then added directly to a column where it was purified by silica gel column chromatography using a mixture of methanol and dichloromethane (1:5). The solvent was then evaporated and dark red oil was recovered (0.150 g, 53%). ¹H NMR (500 MHz, CDCl₃): δ (ppm) 1.02 (t, 6H, - CH_2CH_3), 1.41 (m, 2H, -OCO- CH_2CH_2 -), 1.72 (m, 2H, -OCO- CH_2 - CH_2 -), 1.97 (m, 2H, -Tri-Az-CH₂-CH₂), 2.22 (s, 6H, CH₃-), 2.36 (m, 2H, -OCO-CH₂-), 2.38 (m, 4H, CH_3CH_2 -), 2.48 (s, 6H, CH_3 -), 3.25 (t, 2H, -Triazole- CH_2 -), 3.36 (s, 3H, -PEG-OCH₃), 3.53-3.63 (m, PEGH), 3.91 (t, 2H, -PEG-CH₂-CH₂-triazole-), 4.59 (t, 2H, -PEG-CH₂-CH₂-triazole-), 4.77 (s, 2H, -ArCH₂OH), 5.31 (s, 2H, -CH₂-OCO), 7.81 (s, 1H, ArH), 7.85 (s, 1H, ArH), 7.91 (s, 1H, ArH), 8.14 (s, 1H, triazole-H), 8.23 (s, 1H, triazole-H); ¹³C{¹H} NMR (125 MHz, CDCl₃): δ (ppm) 12.6, 13.6, 14.7, 17.1, 19.7, 24.0, 24.2, 25.9, 29.9, 33.6, 50.0, 50.4, 58.3, 59.0, 64.7, 69.4, 70.3, 70.5, 72.0, 72.5, 120.1, 121.5, 121.8, 123.5, 123.7, 131.3, 131.5, 132.2, 133.6, 136.5, 142.7, 147.2, 147.4, 154.9, and 172.9.

2.2.2.6 Synthesis of miktoarm carrier containing PEG₇₅₀, BODIPY and niacin (10): To a solution of 9 (0.150 g, 0.1068 mmol) and 4-dimethylaminopyridine (13 mg, 0.1068 mmol) in DCM (3 mL), nicotinic acid (19.7 mg, 0.1602 mmol) was added. Once the solid was fully dissolved, 1-ethyl-3-(3dimethylaminopropyl)carbodiimide (63 mg, 0.2136 mmol) was added and the solution was stirred under nitrogen overnight at room temperature in the dark. The reaction mixture was then added directly into a column and purified by silica gel column chromatography using a mixture of methanol and dichloromethane (1:20). The solvent was evaporated to yield red oil (25 mg, 16%). ¹H NMR (400 MHz, CDCl₃): δ (ppm) 1.04 (t, 6H, -CH₂C**H**₃), 1.46 (m, 2H, -OCO-CH₂C**H**₂), 1.69 (m, 2H, -OCO-CH₂-CH₂-CH₂-), 1.99 (m, 2H, -Triazole-CH₂-CH₂), 2.22 (s, 6H, CH₃-), 2.36 (m, 2H, -OCO-CH₂-), 2.38 (m, 4H, CH₃CH₂), 2.49 (s, 6H, CH₃-), 3.25 (t, 2H, -Triazole-C**H**₂-), 3.36 (s, 3H, -PEG-OC**H**₃), 3.53-3.63 (m, PEG**H**), 3.94 (t, 2H, -PEG-CH₂-CH₂-triazole-), 4.59 (t, 2H, -PEG-CH₂-CH₂-triazole-), 5.31 (s, 2H, -CH₂-OCO-), 5.52 (s, 2H, -ArCH₂OH), 7.50 (s, 1H, Pyr-H), 7.94 (s, 1H, ArH), 7.96 (s, 2H, ArH), 8.14 (s, 1H, triazole-H), 8.26 (s, 1H, triazole-H), 8.42 (s, 1H, Pyr-**H**), 8.8 (s, 1H, Pyr-**H**), 9.27 (s, 1H, Pyr-**H**); ¹³C{¹H} NMR (125 MHz, CDCl₃): δ (ppm) 12.6, 13.7, 14.7, 17.1, 19.9, 24.3, 30.9, 59.0, 59.3, 70.5, and 105.0.

2.2.2.7 Synthesis of monofunctional dendrimer containing long chain alcohol undecan-1-ol (11): 1,3,5-triethynyl benzene (TEB) (30 mg, 0.2 mmol) and 11-Azido-undecan-1-ol (140.4 mg, 0.66 mmol) were dissolved in 2 mL of THF, followed by addition of sodium ascorbate (12 mg, 0.06 mmol). An aqueous solution (1 mL) of CuSO₄.5H₂O (7.5 mg, 0.03 mmol) was added dropwise to the solution which was left to stir overnight at 40°C. THF was then evaporated, and

the remaining solution was extracted with DCM (3 x 30 mL), and dried over MgSO₄. The solvent was evaporated, and the crude product was then purified by flash chromatography eluting the product with 4% MeOH in DCM. The solvent was evaporated to yield the product as white solid (150 mg, 97%). ¹H NMR (400 MHz, CDCl₃): δ (ppm) 1.20-1.45 (m, 42H, -CH₂-), 1.48-1.55 (m, 6H, -CH₂CH₂OH), 1.90-2.02 (m, 6H, -CH₂CH₂-triazole), 3.63 (t, 6H, -CH₂CH₂OH), 4.43 (t, 6H, -CH₂CH₂-triazole), 7.99 (s, 3H, ArH) and 8.32 (s, 3H, triazoleH); 13 C{ 1 H} NMR (125 MHz, CDCl₃): δ (ppm) 25.6, 26.3, 28.8, 29.2, 29.3, 29.4, 30.2, 32.8, 50.5, 62.9, 120.2, 122.1, 131.8 and 147.1. ESI-MS: m/z 812.59 ([M+Na]⁺), 790.60 ([M+H]⁺).

2.2.2.8 Synthesis of monofunctional dendrimer containing niacin (12): To a stirring solution of 11 (375 mg, 0.475 mmol), 1-[3-(dimethylamino)propyl]-3-2.139 ethylcarbodiimide methiodide (635.2 mg, mmol), (dimethylamino)pyridine (87 mg, 0.713 mmol), pyridine (1 mL) in anhydrous N,N-dimethyl formamide (DMF) (2 mL), added nicotinic acid (263.3 mg, 2.139 mmoles) and solution was stirred at room temperature for 24 hrs. Water (30 mL) was added and extraction was done using dichloromethane (3 x 20 mL). The combined organic extracts were then washed with water and brine, dried over sodium sulphate and concentrated under reduced pressure. The crude was then passed through a column of silica gel. The pure fractions of product were obtained using 7% methanol in DCM as an eluent. The fractions were then concentrated to afford the product as white solid. (340mg, 65%). H NMR (400 MHz, CDCl₃): δ (ppm) 1.20-1.45 (m, 42H, -CH₂-),1.70-1.76 (m, 6H, -CH₂CH₂OCO-), 1.77-2.02 (m, 6H, -C**H**₂CH₂-triazole), 4.33(t,6H, - CH₂C**H**₂OCO-), 4.43 (t, 6H, - CH₂C**H**₂triazole), 7.35-7.40 (m, 3H, ArH), 7.96 (s, 3H, ArH), 8.25-8.30 (m, 6H, ArH), 8.75-8.77 (m, 3H, ArH) and 9.22 (s, 3H, ArH). ¹³C{¹H} NMR (75 MHz, CDCl₃): δ 25.6, 26.5, 28.6, 29.0, 29.2, 29.3, 29.4, 30.3, 50.5, 65.6, 120.1, 122.1, 123.3, 131.8, 137.0, 147.1, 150.9, 153.3 and 165.3. MALDI: m/z 1111.54 ([M+Li]⁺).

2.2.2.9 Synthesis of monofunctional dendrimer containing PEG₇₅₀ (13): 1,3,5-Triethynylbenzene (15 mg, 0.1 mmol) and PEG₇₅₀-N₃ (232.22 mg, 0.3 mmol)

were dissolved in 2 mL of THF followed by addition of sodium ascorbate (6 mg, 0.03 mmol). An aqueous solution (1 mL) of CuSO₄.5H₂O (3.5 mg, 0.014 mmol) was added dropwise to the solution which was left to stir overnight at 40°C. THF was then evaporated, and the remaining solution was extracted with DCM (3x30 mL), and dried over MgSO₄. The solvent was evaporated, and the crude product was then purified by flash chromatography eluting the product with 5% MeOH in DCM. The solvent was evaporated to yield the product as transparent liquid (200 mg,80.9 %). ¹H NMR (400 MHz, CDCl₃): δ (ppm) 3.37 (s, 9H, -OCH₃), 3.30-3.70 (m, PEG-H), 3.95 (t, 6H, - CH₂CH₂-PEG), 4.63 (t, 6H, -CH₂CH₂-triazole), 8.20(s, 3H, ArH) and 8.34(s, 3H, triazole H). ¹³C{¹H} NMR (125 MHz, CDCl₃): δ (ppm) 25.6, 29.6, 50.5, 53.4, 58.9, 67.9, 69.5, 70.6, 71.9, 72.6, 114.5, 122.2, 128.8, 129.5, 130.9, 131.9, 161.0 and 200.9.

2.2.2.10 Synthesis of miktoarm carrier containing two PEG₇₅₀ units and niacin (15): To a flame dried two neck round bottom 100 mL flask, nicotinic acid (35 mg, 0.27 mmol), EDC (100 mg, 0.33 mmol), DMAP (27 mg, 0.22 mmol) and miktoarm containing two PEG molecules and benzylic alcohol (400 mg, 0.22 mmol) were added and dissolved in dry DMF (5 mL) under nitrogen atmosphere. The reaction mixture was stirred at room temperature overnight. Reaction completion was monitored with the help of TLC. The reaction mixture was diluted with water (5 mL) and extracted 3 times with dichloromethane. The organic layer was separated and washed with brine. It was then dried over anhydrous sodium sulphate and concentrated under reduced pressure. compound was obtained as off white solid. (310 mg, 73%) ¹H NMR(400 MHz, CDCl₃): δ (ppm) 3.36 (s, -OCH₃ PEG), 3.42-3.74 (m, PEG H), 3.86 (t, J = 10Hz, PEG H), 4.53 (t, J = 10 Hz, PEG CH₂), 5.16 (s, 4H), 5.29 (d, J = 6.4Hz, 2H, - OCH_2), 6.58-6.70 (m, 3H, Ar**H**), 7.40 (t, J = 6.2Hz, 1H, Ar**H**), 7.783 (s, 2H, triazole), 8.32 (d, J = 16Hz, 2H, Ar**H**), 8.76 (d, 6.4Hz, 1H, Ar**H**) and 9.23 (s, 1H). ¹³C{¹H} NMR (100 MHz, CDCl₃): δ (ppm) 50.3,59.0, 62.0, 66.7, 69.3, 70.4, 70.5,71.8, 101.6, 107.1, 123.3, 124.1, 137.2, 137.8, 143.4, 151.0, 153.5, 159.6 and 164.9.

2.2.3 Cell cultures

Murine microglia (N9) were cultured in Iscove's modified Dulbecco's medium (IMDM; Gibco # 12440) supplemented with 5% (v/v) fetal bovine serum (FBS; Gibco) and 1% (v/v) penicillin/streptomycin (Gibco). Human HepG2 hepatocytes were cultured in high glucose Dulbecco's Modified Eagle Medium (DMEM; Gibco #11995) supplemented with 5% (v/v) fetal bovine serum (FBS; Gibco) and 1% (v/v) penicillin/streptomycin (Gibco).

2.2.4 Nitric oxide production:

Release of nitric oxide (NO) from microglial cultures was measured using the Griess reagent (Sigma, G-4410). Cells seeded at a density of 2 X 10^5 in 24-well culture plates (Sarstedt) were treated with the drugs and the polymers for 24h in 1% FBS containing media. At the end of treatments, supernatants (50 μ l) were collected and incubated with the Griess reagent (50 μ l) for 15 min, after which the absorbance (540 nm) was measured with a spectrophotometer. A standard curve with different concentrations of nitrite was created.

2.2.5 Measurement of biocompatibility by the MTT reduction assay

N9 microglia were seeded in 24-well plates (5 x 10⁴ cells/well) and cultured for 24h in 5% FBS containing culture media. Cells were treated with the drugs and the polymers for 24 and 48 h in 1% FBS containing culture media. The vehicle treatment consisted of 0.5 % DMSO. The polymers **15** and **12** were added at a concentration of 50 μM (calculated to account for the concentration of niacin). **4**, **10** and **7** were added at a concentration of 1 μM (accounting for the final concentration of BODIPY). MTT (Thiazolyl blue tetrazolium bromide) assay was performed to assess the mitochondrial metabolic activity. MTT reagent (M2128, Sigma) was dissolved in phosphate buffered saline (PBS) (5 mg/mL). Following treatments (24 or 48h), old media was removed from culture plates. Cells were incubated in fresh media (1% FBS) containing MTT (0.5 mg/mL) for 30 min at 37 °C. Subsequently, cells were lysed with 500 μl of dimethyl sulfoxide (Sigma, 154938). Absorbance was measured at 595 nm using a Benchmark

microplate reader (Bio-Rad, Mississauga, ON, Canada). All measurements were performed in quadruplicates.

2.2.6 Confocal microscopy

Images were acquired with a Zeiss LSM 510 NLO inverted confocal microscope using a Plan Achromat 63X/1.4 Oil DIC objective. Microglial cells were seeded at a density of 1.5 X 10^4 cells/well on confocal chamber slides (Lab-Tek, Nalge Nunc International, Rochester, NY, USA) and cultured for 24h prior to experiments. LDs were stained with the neutral lipid staining fluorophore Bodipy 493/503 (4,4-difluoro-1,3,5,7,8-pentamethyl-4- bora-3a,4a-diaza-s-indacene) for 10 min (20 μ M). The polymers **4, 10** and **7** were added to living microglia at a final concentration of 1 μ M and imaged after 2 min. Images of LDs and fluorescent polymers were acquired at a resolution of 1024 X 1024 using the Argon 488 nm (4%) and the HeNe 543 nm (100%) excitation lasers, respectively. For each Z-stack, a total of 10 Z-slices were acquired using a scaling of 0.07 X 0.07 X 0.30 μ m (x, y, z).

2.2.7 Flow cytometry

N9 microglial cells and HepG2 hepatocytes were seeded at a density of 3 X 10⁵ cells and 1 X 10⁶, respectively, in 12 well plates (Sarstedt). Cells were treated with fluorescent polymers **4**, **10** and **7** for 1, 6, 24 and 48 h in 1% FBS containing media. The final concentration of the polymers in the culture was 1 μM (accounting for the final concentration of BODIPY). Following treatments, plates were washed with PBS, followed by a mild acidic (PBS at pH 5.5) wash. Cells were removed from plates mechanically by scraping and kept in 0.5% BSA containing PBS until analysis by flow cytometry. Samples were analyzed using a Becton Dickinson FACS scan flow cytometer. The fluorescence of the polymers was measured using the 544/590 (excitation/emission) setting and was expressed as mean fluorescence intensity (MFI).

2.2.8 Statistics

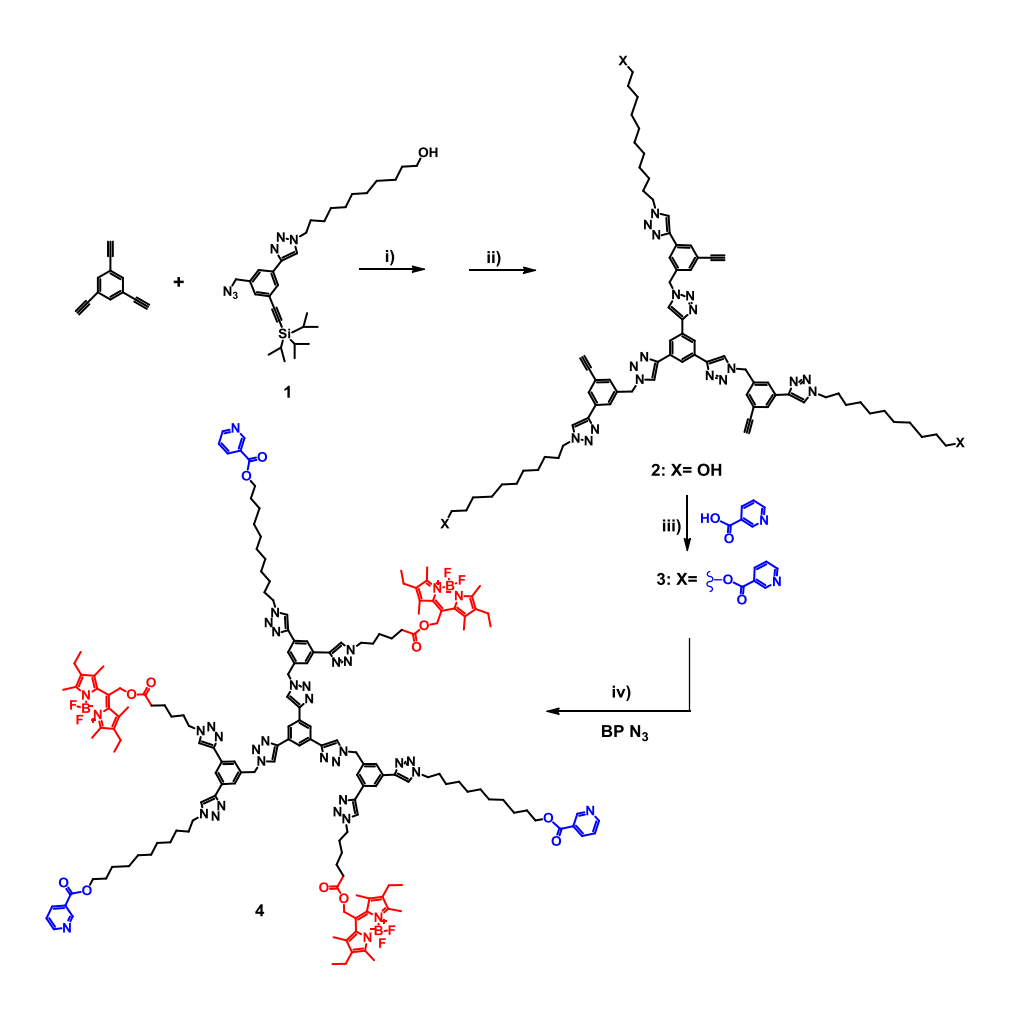
Statistical analysis was performed using Systat (version 10.2). Comparisons between multiple groups were done using t-tests followed by a Bonferroni correction. All data are presented as group means \pm SEM. p<0.05 was considered significant.

2.3 Results and discussion

2.3.1 Synthesis of nanocarriers

The development of a bifunctional nanocarrier to target LD was based on designing an orthogonal molecular system that would allow covalent linking of two different functional units using Cu(I) catalyzed alkyne-azide "click" chemistry.[7-10] Such a building block contains an azide group and two acetylenes protected with trimethylsilyl and triisopropyl groups respectively.[34] Upon selectively deprotecting the trimethylsilyl-acetylene, it was clicked with 11azido-undecan-1-ol to give compound 1 (Scheme 2.1).[31] The latter was covalently linked to the 1,3,5-triethynylbenzene core using the "click" reaction, and the triisopropylsilylacetylene was then deprotected (2, Scheme 2.1). The primary alcohol on this compound was employed for the attachment of the drug niacin using a simple esterification reaction. It should be noted that it was essential to remove the bulky triisopropyl groups from the acetylene first, since it was not possible to carry out the subsequent esterification reaction cleanly in their presence. The free acetylene groups on compound 3 were then clicked with azidefunctionalized BODIPY dye using copper sulphate and sodium ascorbate in a THF/water mixture, to give the desired bifunctional dendrimer 4 (Scheme **2.1**).[31] The reaction was monitored easily using ¹H NMR which showed the disappearance of acetylene peak at 3.11 ppm, and the appearance of BODIPY protons. It is important to follow this sequence of reactions since if BODIPY is clicked first, followed by esterification with niacin, it leads to very poor yield of the product. Dendrimer size could be an important variable in designing dendrimer based conjugates depending on their intended application.[35] For instance, smaller generations such as in **4** which is estimated to be about 3-4 nm in size [36], with tailored active sites, are in fact desirable for nanodelivery carriers targeting different intracellular locations. It should also be noted that the copper (I) compounds used in the "click" reactions are in catalytic amounts, and the "clicked" products contain non-measureable amount of copper.[37] It is also ascertained by the biocompatibility of the nanoconjugates reported here.

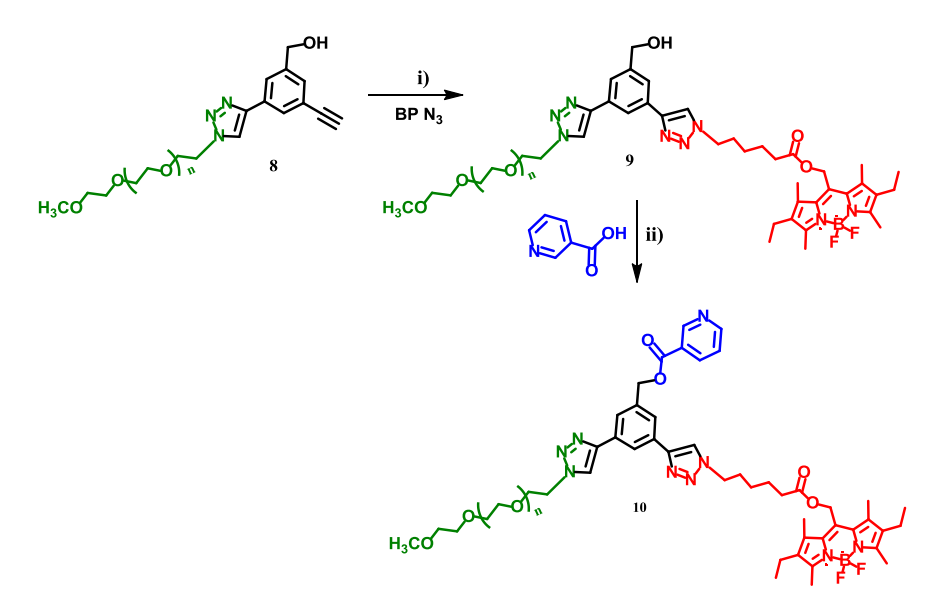
A linear model of the bifunctional dendrimer **4** was synthesized starting from (4-ethynyl-phenylethynyl)-triisopropyl-silane, on which two click reactions were carried out in sequence. 11-Azido-undecan-1-ol was first clicked using the free acetylene arm of (4-ethynyl-phenylethynyl)-triisopropyl-silane to give compound **5** (Scheme **2.2**). The second acetylenic arm of this molecule was then deprotected, and the drug niacin was covalently linked through the primary alcohol using the esterification reaction (**6**, Scheme **2.2**). The free acetylene arm was subsequently used to click the BODIPY dye molecule to get the desired compound **7** (Scheme **2.2**). The reaction could be once again easily monitored using ¹H NMR.



Scheme 2.1. Synthesis of bifunctional dendrimer 4 containing BODIPY dye and Niacin molecules i) CuSO₄•5H₂O/sodium ascorbate, H₂O/THF, 50⁰C, 48 h; ii) tetrabutylammonium fluoride (TBAF)/THF; iii) 1-[3-(Dimethylamino)propyl]-3-ethylcarbodiimidemethiodide (EDC), 4-dimethylaminopyridine (DMAP), Pyridine, DMF, RT, 24h; iv) CuSO₄•5H₂O / sodium ascorbate, H₂O/THF, RT, Overnight (O/N).

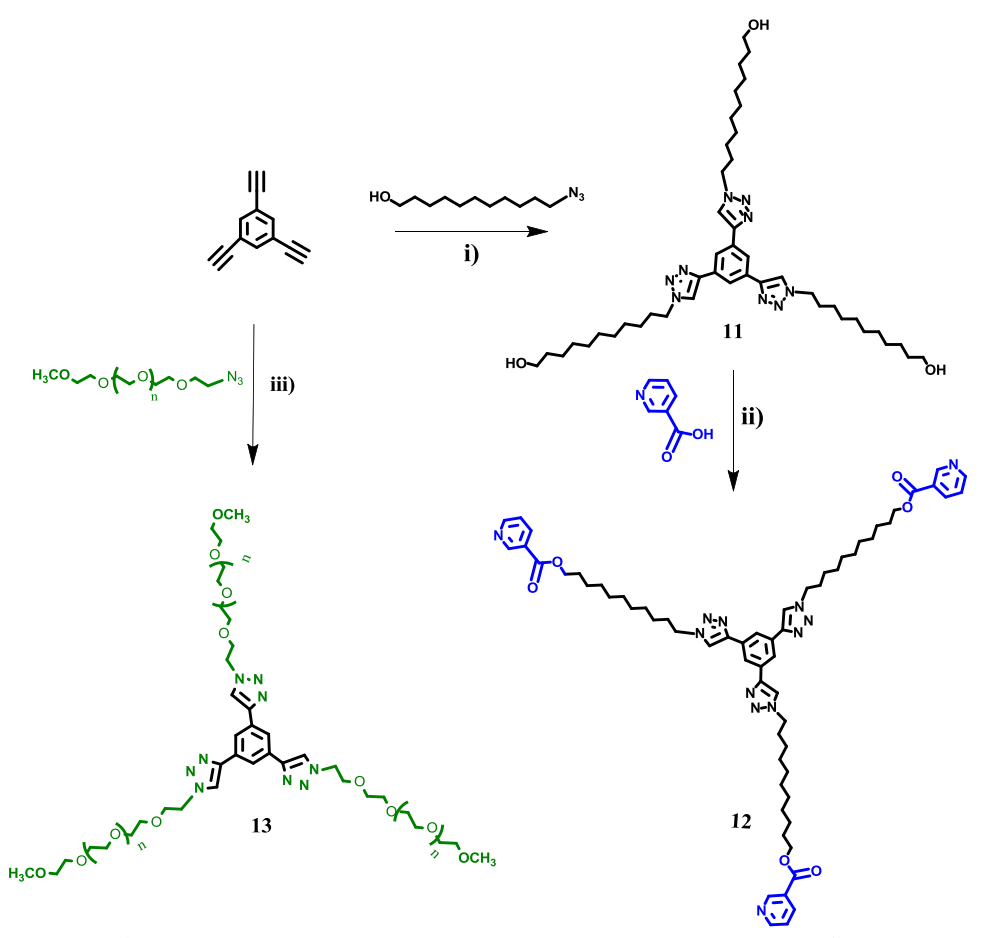
Scheme2.2. Synthesis of linear analog **7** containing covalently linked BP dye and Niacin: i) EDC, DMAP, Pyridine, DMF, RT, 24h.; ii) CuSO₄.5H₂O, Sodium Ascorbate, THF/H₂O, O/N, RT.

To examine the role of the carrier structure on the internalization process, we synthesized a trifunctional molecular unit containing BODIPY dye, niacin, and polyethylene glycol (PEG₇₅₀) covalently linked to the central core. This miktoarm carrier is structurally different from the dendrimer. The core molecule containing PEG, an unprotected acetylene and benzylic alcohol (8, Scheme 2.3) was first prepared using a literature procedure.[32] The free acetylene in compound 8 was then reacted with BODIPY-azide using copper sulfate pentahydrate and sodium ascorbate as catalysts. For this reaction to go to completion, the use of an extremely concentrated solution was necessary. This reaction can also be monitored by ¹H NMR in which the loss of the acetylene peak at 3.11 ppm, and the appearance of BODIPY protons provided evidence for the completion of the "click" reaction (9, Scheme 2.3). Finally, nicotinic acid was linked to 9 by esterification using EDC/DMAP to yield the desired compound 10 (Scheme 2.3). The conjugation of nicotinic acid in 10 was evidenced by a shift in the ¹H NMR of the aryl ring's benzylic methylene from 4.77 ppm to 5.52 ppm, as well as the absence of any carboxylic acid peaks.



Scheme 2.3. Synthesis of trifunctional unit **10:** i) CuSO₄.5H₂O, Sodium Ascorbate, THF/H₂O, RT, 36h.; ii) EDC, DMAP, DCM, O/N, RT.

We also synthesized a monofunctional dendrimer containing three drug molecules attached to it. For that purpose, we started with the trifunctional core with three free acetylene arms available for click reaction, and first clicked this core molecule with 11-azido-undecan-1-ol to obtain 11 with three terminal hydroxyl groups. Niacin was then coupled with these primary alcohol groups using esterification reaction (12, Scheme 2.4).



Scheme 2.4. Synthesis of monofunctional dendrimers **12** and **13:** i) CuSO₄.5H₂O, Sodium Ascorbate, THF/H₂O, O/N, RT; ii) EDC, DMAP, Pyridine, DMF, RT, 24h; iii) CuSO₄.5H₂O, Sodium Ascorbate, THF/H₂O, O/N, RT.

Similarly, we synthesized dendrimer containing only the polyethylene glycol arms (13), and a miktoarm carrier containing two PEG chains and a niacin molecule (15). Azide functionalized PEG-750 was first synthesized using a literature procedure [38], and it was then clicked with 1,3,5-triethynylbenzene core using conditions described earlier to give compound 13 (Scheme 2.4). Again the disappearance of acetylene peak and appearance of PEG protons in ¹H NMR was used to confirm the completion of the reaction. For the synthesis of the miktoarm carrier with two PEG arms and one niacin molecule, we started with miktoarm core molecule with two PEG arms and a benzylic alcohol which was synthesized using a literature procedure.[32] The benzylic hydroxyl group of this

core molecule was used to attach the drug molecule using the esterification reaction resulting in compound 15 (Scheme 2.5).

Scheme 2.5. Synthesis of 15: i) EDC, DMAP, DMF, O/N, RT.

2.3.2 Biological studies

We subsequently examined the uptake of the fluorescent carriers 4, 7 and 10 by fluorescence activated cell sorting (FACS) analysis. The uptake was monitored in microglia and in hepatocytes. All carriers were taken up by the cells in a time-dependent manner (Figure 2.1). The uptake of all three compounds seemed to take place at a faster rate in hepatocytes (Figure 2.1B) than in microglia (Figure 2.1A). In fact, the equilibrium in their uptake was reached earlier (after 6h) in the hepatocytes than in microglia (not before 24h). The maximal uptake value for 4 in both microglia and hepatocytes (966 \pm 30 and 467 \pm 42 MFI) was smaller than the maximal value for 10 (1366 \pm 52 and 1403 \pm 56 MFI, p<0.05) and 7 (1773 \pm 36 and 947 \pm 36) MFI respectively, p<0.05). In order to demonstrate that this was not due to the intrinsic fluorescence properties of 4, we measured the relative fluorescence intensity (RFI) of the 4, 7 and 10 in pure dimethyl sulfoxide using a spectrofluorometer (Figure S2.1, Appendix 2). The relative fluorescence intensity (shown as absolute values) of 4 was higher at all concentrations examined (1, 5 and 20 µM) than that of 10, which in turn had a greater fluorescence intensity than 7.

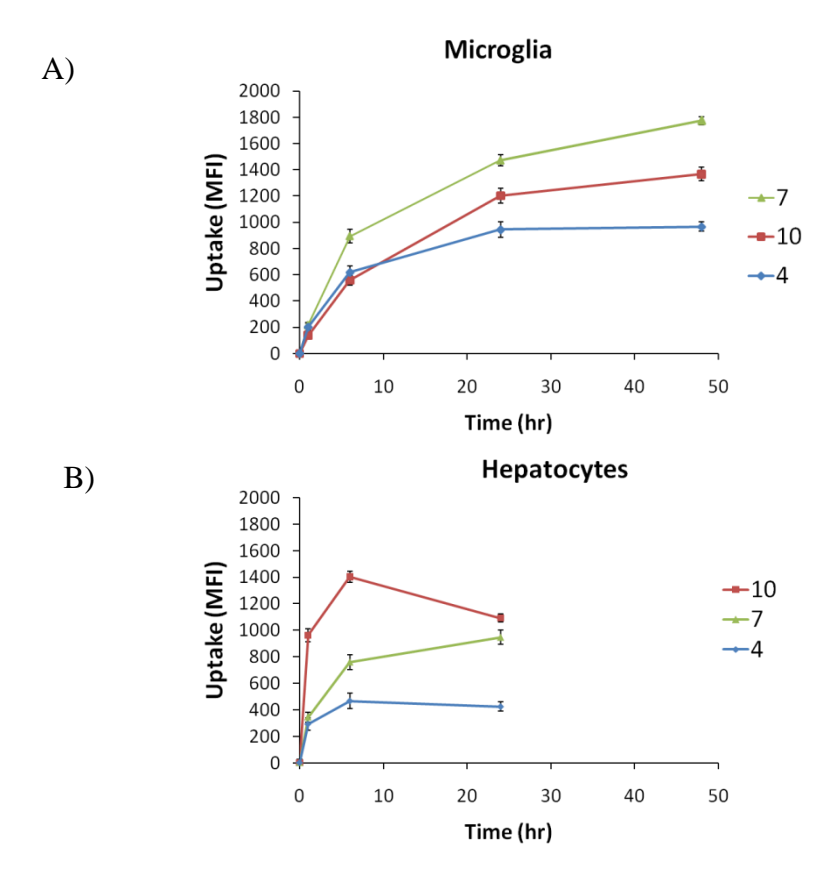


Figure 2.1. Internalization of fluorescent carriers in N9 microglia and HepG2 hepatocytes. Cells cultured in serum (1%) containing media were treated with 7, 10 and 4 for 1, 6, 24 and 48h. For all treatments, the final concentration of the fluorescent dye BODIPY was 1μM. At the indicated time points, cells were washed and prepared for FACS analysis (refer to Experimental procedures). The uptake was determined by measuring the mean fluorescence intensity (MFI) of (A) N9 microglia and (B) HepG2 hepatocytes using 544/590 nm excitation/emission settings. Data were obtained from two independent experiments (n=3) and are expressed as MFI ± standard error of the mean (SEM). Significant differences and p values are discussed in Results and discussion.

To gain an insight into the biocompatibility of the nanocarriers, microglial cells were treated with **12**, **13** and **15** (50 μ M) for either 24 or 48h (Figure **2.2A**). We selected microglia because these cells are critically involved in the environmental surveillance" and they promptly respond to an insult or exposure to nanoparticles.[39-40] Moreover, they release both cytokines and trophic factors

depending of the stimulus). We have previously shown that even extremely small amounts of nanoparticles in the central nervous system (CNS) cause an activation of microglia and astrocytes in mice.[41-42] None of the carriers used in the present studies markedly changed microglia morphology or enhanced their activity. Similarly, there was no significant decrease in cell viability when compared with the vehicle treatment after either 24 or 48 h, as determined by measurements of the mitochondrial metabolic activity. In addition, fluorescent nanocarriers were also not cytotoxic (Figure 2.2B); Treatment of microglia with niacin (50 μ M) significantly increased mitochondrial metabolic activity after 48h (11%, p<0.05) confirming that free niacin does not cause functional impairment of these cells.

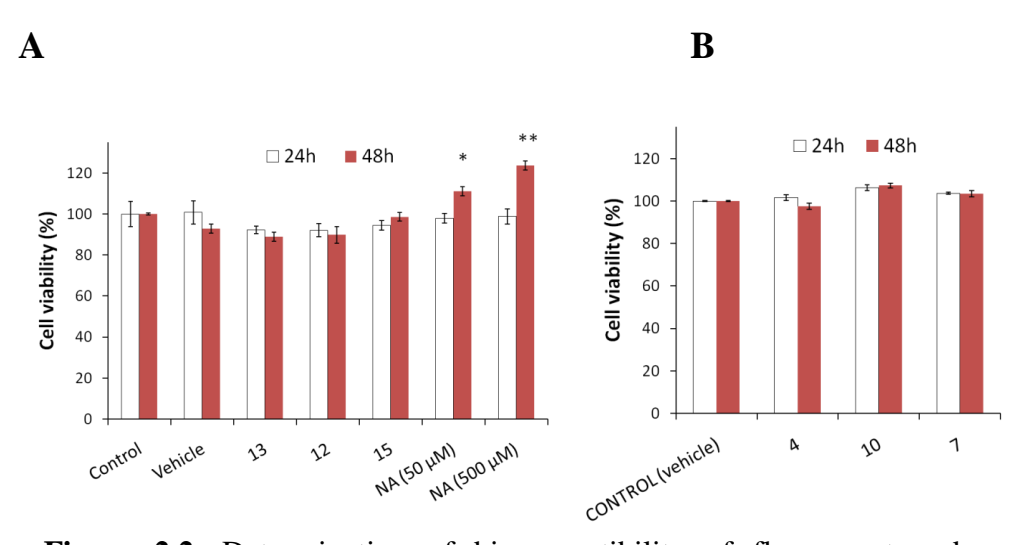


Figure 2.2. Determination of biocompatibility of fluorescent and non-fluorescent nanocarriers. N9 microglia cultured in serum (1%) containing media were incubated with (A) non-fluorescent polymers (13, 12 and 15) and (B) fluorescent polymers (4, 10 and 7) for 24 and 48h. The final concentration of niacin (NA) in carriers treated cells was 50 μM. Free NA was added at a concentration of 50 or 500 μM. Cell viability was assessed by measuring mitochondrial metabolic activity using the MTT reagent assay (described in Experimental procedure). Data were obtained from at least two independent experiments and are expressed as mean (%) cell viability \pm standard error of the mean (SEM). Statistically significant differences are indicated by * p<0.05 and ** p<0.005.

To examine the physiological response of microglia to niacin nanodelivery systems, cells were challenged with bacterial endotoxin lipopolysaccharide (LPS), a well established inducer of nitric oxide (NO) release.[43] NO was measured both in non-challenged and LPS-exposed cells and the extent of NO induced by LPS served as a positive control for microglia activation. Excessive microglial activation (reactive microgliosis) may be responsible for neurotoxicity and is involved in the progression of neurodegenerative diseases.[44] Importantly, microglia may express the inducible nitric oxide synthase (iNOS), an enzyme critical for NO production during inflammation. The production of NO following niacin (50 μM) treatment was significantly increased (9.7 μM, p< 0.005), as compared to vehicle-treated (0.5% DMSO) control (0.4 µM). There seemed to be an additive (p<0.005) effect when niacin and LPS were present together in the cell culture medium. The combination resulted in a large production of NO (48.3 µM) significantly higher than NO produced by LPS alone (37.7 μM, p<0.005). The carriers alone (50 µM) did not stimulate NO production in cells when compared to the cells treated with the vehicle (0.5 % DMSO v/v). Production of NO in cells treated with both the carriers and LPS appeared to be lower than in the cells exposed to LPS alone, suggesting that the carriers by themselves could partly prevent LPS-induced NO release.

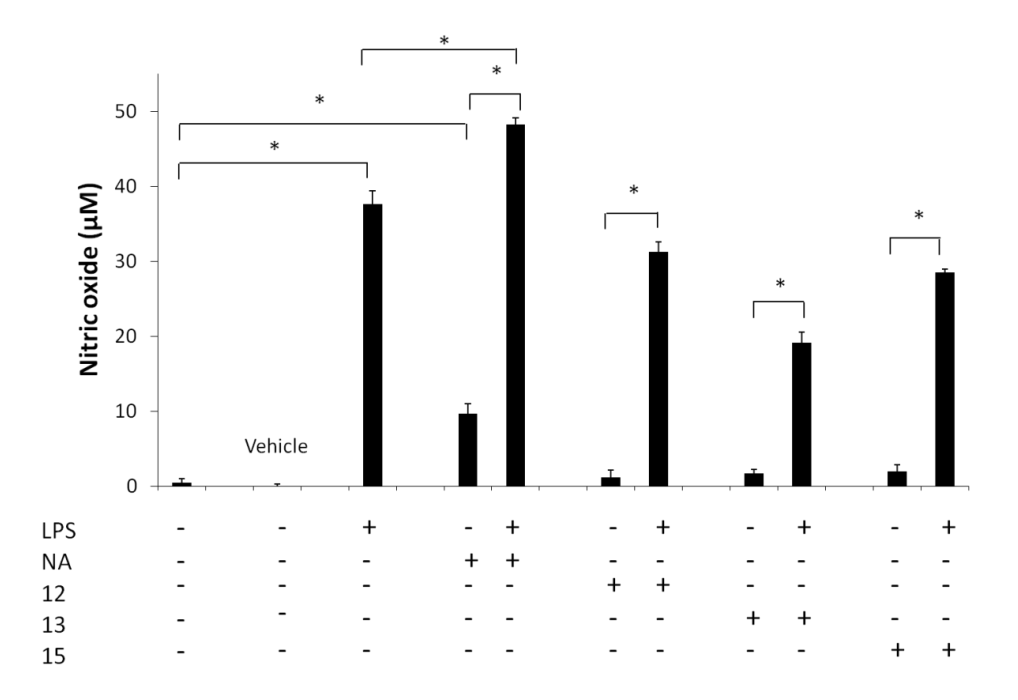


Figure 2.3. Assessment of nitric oxide (NO) production following treatment with niacin and niacin-conjugated nanocarriers. N9 microglia cultured in serum (1%) were incubated with niacin (NA, 50 μ M), 12, 13 and 15 for 24h with or without LPS (10 μ g/mL). When LPS was also present, cells were first treated with the polymers for 2h, and then incubated with LPS for another 24h. NO production in the supernatants was measured using the Griess reagent assay and expressed as concentration of NO (μ M). Mean values (\pm SEM) were obtained from triplicate analysis and from at least two independent experiments. Statistically different values are indicated by * p<0.005.

In order to assess the efficacy of the niacin-conjugated nanocarriers as a lipid droplet targeting drug delivery system, we examined their colocalization with these organelles by confocal microscopy. The intracellular LDs were stained with the fluorescent dye Bodipy 493/503 (green), which selectively stains neutral lipids. The carriers, labelled with a different Bodipy (red), were added separately following the staining of LDs. Within seconds, the fluorescent carriers were detected in the cytosol and within cytoplasmic LDs (Figure 2.4). The colocalization of the carrier with the lipid droplets was indicated by the droplets appearing yellow instead of the green observed in the absence of the carrier. Carriers 4 and 7 seemed to be entirely colocalized with the LDs. The colocalization of 4 with LDs is shown in hepatocyte (Figure 2.4A) and microglia LDs (Figure 2.4B). The trifunctional polymer 10, however, partially colocalized

with the LDs (Figure **2.4B**). The presence of polyethylene glycol (PEG) in structure **10** (but not in **4** or **7**) could reduce colocalization with highly lipophilic organelles, *i.e.* lipid droplets. Molecular modeling studies are necessary to examine the possibility that conformational differences between the structures **4**, **7** and **10** could also contribute to the differences in their co-localization with LDs and to their modes of internalization.

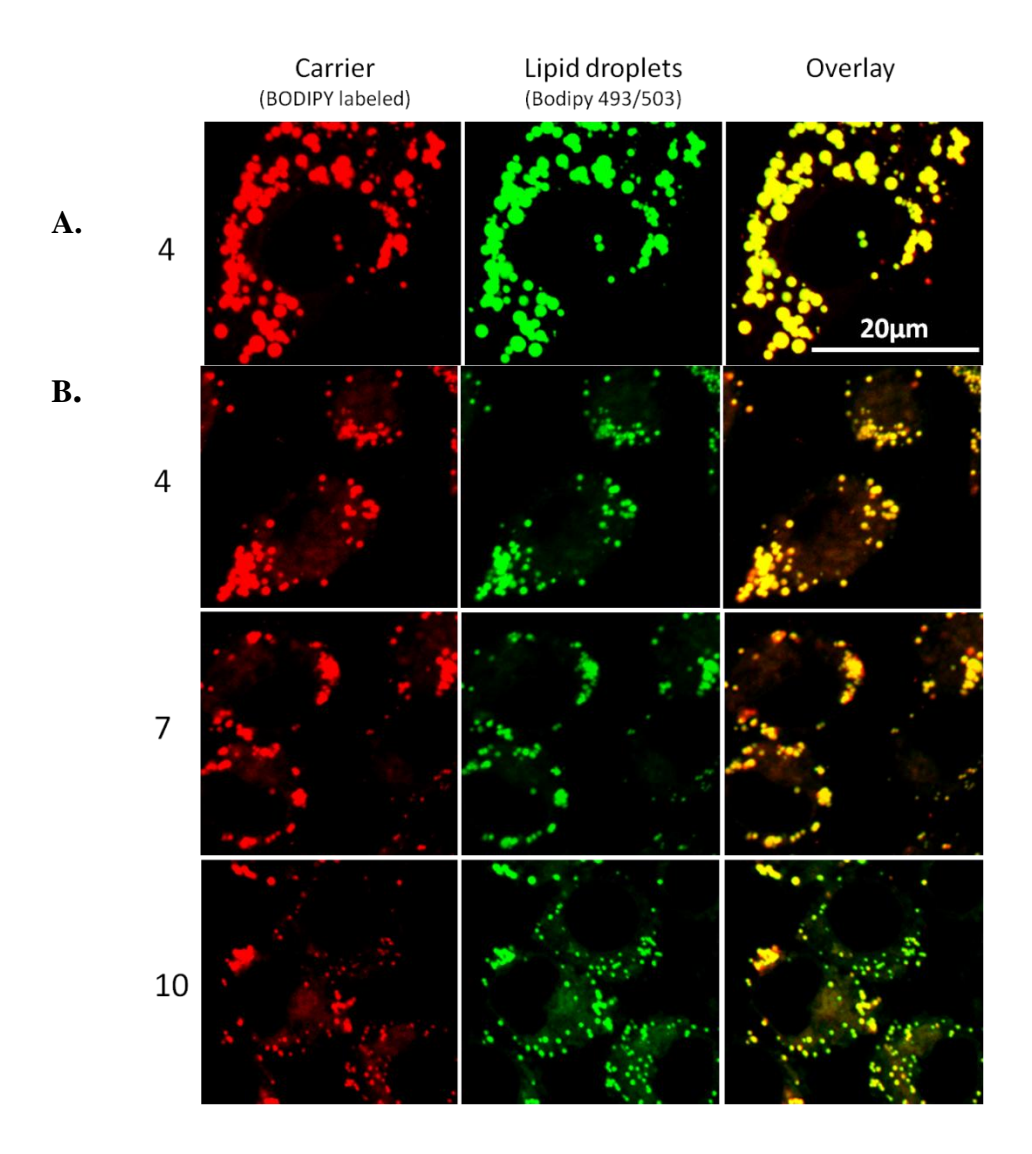


Figure 2.4. Colocalization of niacin-conjugated nanocarriers with lipid droplets in hepatocytes and microglia. Cells seeded in confocal chamber slides were cultured overnight in 1% serum-containing media supplemented with oleic acid (100 μM). Lipid droplets in hepatocytes (A) and microglia (B) were stained with the green fluorescent dye Bodipy 493/503 (20μM) for 10 min. Lipid droplets (green) and carriers (red) (4, 7 and 10) were imaged using a Zeiss LSM 510 confocal microscope soon after (~ 1 min) polymers were added. Z-stacks consisting of a total of 10 Z-slices (each 0.3 μm deep) were acquired for each field. Colocalization of carriers with lipid droplets is indicated by the presence of yellow regions resulting from the overlap between the signal in the green and red channels. Scale bar = 20 μm

2.4 Conclusions

In summary, results from this study show localization of niacin-conjugated carriers to lipid droplets (LDs), a new organelle considered for subcellular targeting by nanostructures. Herein, we aimed at delivering niacin to LDs by means of dendrimeric and other polymeric structures, synthesized using "click" chemistry, in order to inhibit the activity of LD-localized enzyme, DGAT2, which is a critical enzyme in triglyceride biosynthesis. Such an approach will possibly give rise to the emergence of new strategies in nanomedicine in the treatment of diseases characterized by excessive accumulation of triglycerides (*i.e* LDs), such as obesity, hepatic steatosis and atherosclerosis.[26,45] The versatility of the click chemistry approach described here uniquely enables the design and construction of a variety of tunable nanomaterials with orthogonal functionalities, to target drugs, fluorophores or sensors to other organelles.

2.5 References

- [1] Haag R, Kratz F. Polymer therapeutics: concepts and applications. Angew. Chem. Int. Ed. Engl. 2006; 45 (8): 1198-1215.
- [2] Rudin M, Weissleder R. Molecular imaging in drug discovery and development. Nat. Rev. Drug Discov. 2003; 2 (2): 123-131.
- [3] Maeda H, Seymour LW, Miyamoto Y. Conjugates of anticancer agents and polymers: advantages of macromolecular therapeutics in vivo. Bioconjug. Chem. 1992; 3 (5): 351-362.
- [4] Lee CC, MacKay JA, Frechet JM, Szoka FC. Designing dendrimers for biological applications. Nat. Biotechnol. 2005; 23 (12): 1517-1526.
- [5] Bayele HK, Ramaswamy C, Wilderspin AF, Srai KS, Toth I, Florence AT. Protein transduction by lipidic peptide dendrimers. J. Pharm. Sci. 2006; 95 (6): 1227-1237.
- [6] Astruc D, Boisselier E, Ornelas C. Dendrimers designed for functions: from physical, photophysical, and supramolecular properties to applications in sensing, catalysis, molecular electronics, photonics, and nanomedicine. Chem. Rev. 2010; 110 (4): 1857-1959.
- [7] Franc G, Kakkar A. Dendrimer design using Cu(I)-catalyzed alkyne-azide "click-chemistry". Chem. Commun. 2008; 42: 5267-5276.
- [8] Franc G, Kakkar AK. Diels-Alder "click" chemistry in designing dendritic macromolecules. Chem. Eur. J. 2009; 15 (23): 5630-5639.
- [9] Franc G, Kakkar AK. "Click" methodologies: efficient, simple and greener routes to design dendrimers. Chem. Soc. Rev. 2010; 39 (5): 1536-1544.
- [10] Kolb HC, Finn MG, Sharpless KB. Click chemistry: diverse chemical function from a few good reactions. Angew. Chem. Int. Ed. Engl. 2001; 40 (11): 2004-2021.
- [11] DeForest CA, Polizzotti BD, Anseth KS. Sequential click reactions for synthesizing and patterning three-dimensional cell microenvironments, Nature Materials, 2009; 8: 659 664.
- [12] Rajendran L, Knolker HJ, Simons K. Subcellular targeting strategies for drug design and delivery. Nat. Rev. Drug Discov. 2010; 9 (1): 29-42.

- [13] Savic R, Luo L, Eisenberg A, Maysinger D. Micellar nanocontainers distribute to defined cytoplasmic organelles. Science. 2003; 300 (5619): 615-618.
- [14] Boddapati SV, D'Souza GG, Erdogan S, Torchilin VP, Weissig V. Organelle-targeted nanocarriers: specific delivery of liposomal ceramide to mitochondria enhances its cytotoxicity in vitro and in vivo. Nano Lett. 2008; 8 (8): 2559-2563.
- [15] Said HM, Nabokina SM, Balamurugan K, Mohammed ZM, Urbina C, Kashyap ML. Mechanism of nicotinic acid transport in human liver cells: experiments with HepG2 cells and primary hepatocytes. Am. J. Physiol. Cell Physiol. 2007; 293 (6): C1773-1778.
- [16] Listenberger LL, Brown DA. Fluorescent detection of lipid droplets and associated proteins. Curr. Protoc. Cell Biol. 2007, Chapter 24, Unit 24 2
- [17] McKenney J. New perspectives on the use of niacin in the treatment of lipid disorders. Arch Intern Med. 2004; 164 (7): 697-705.
- [18] McKenney J. Niacin for dyslipidemia: considerations in product selection. Am J Health Syst. Pharm. 2003; 60 (10): 995-1005.
- [19] Kamanna VS, Kashyap ML. Mechanism of action of niacin on lipoprotein metabolism. Curr. Atheroscler Rep. 2000; 2 (1): 36-46.
- [20] Brown BG, Zhao XQ. Nicotinic acid, alone and in combinations, for reduction of cardiovascular risk. Am. J. Cardiol. 2008; 101 (8A): 58B-62B.
- [21] Benyo Z, Gille A, Kero J, Csiky M, Suchankova M.C, Nusing RM, Moers A, Pfeffer K, Offermanns S. GPR109A (PUMA-G/HM74A) mediates nicotinic acid-induced flushing. J. Clin. Invest. 2005; 115 (12): 3634-3640.
- [22] Pieper JA. Understanding niacin formulations. Am. J. Manag. Care 2002; 8 (12 Suppl), S308-314.
- [23] Kamanna VS, Ganji SH, Kashyap ML. The mechanism and mitigation of niacin-induced flushing. Int. J. Clin. Pract. 2009; 63 (9); 1369-1377
- [24] Penberthy WT. Nicotinic acid-mediated activation of both membrane and nuclear receptors towards therapeutic glucocorticoid mimetics for treating multiple sclerosis. PPAR Res 2009; 2009: 853707

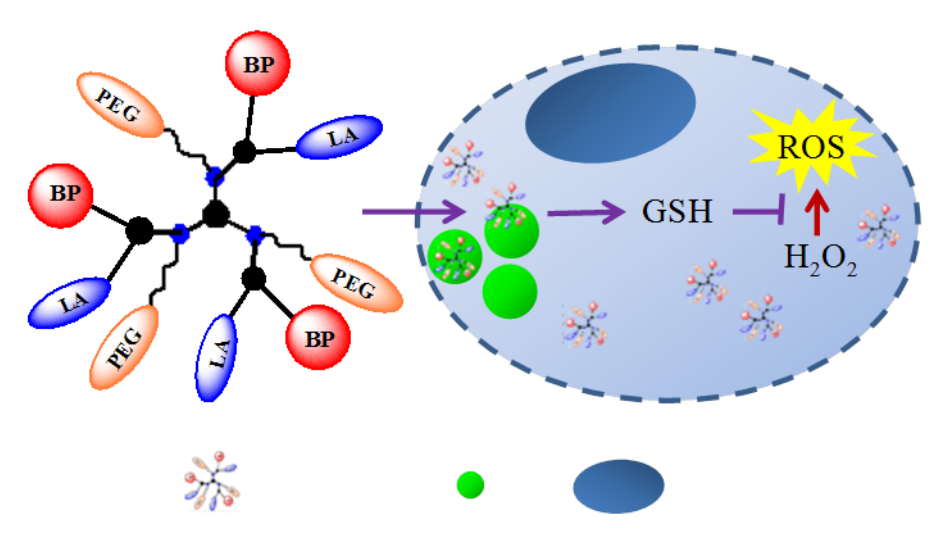
- [25] Ganji SH, Tavintharan S, Zhu D, Xing Y, Kamanna VS, Kashyap ML. Niacin noncompetitively inhibits DGAT2 but not DGAT1 activity in HepG2 cells. J. Lipid Res. 2004; 45 (10): 1835-1845.
- [26] Martin S, Parton RG. Lipid droplets: a unified view of a dynamic organelle. Nat. Rev. Mol. Cell Biol. 2006; 7 (5): 373-378.
- [27] Stone SJ, Levin MC, Zhou P, Han J, Walther TC, Farese RV Jr. The endoplasmic reticulum enzyme DGAT2 is found in mitochondria-associated membranes and has a mitochondrial targeting signal that promotes its association with mitochondria. J. Biol. Chem. 2009; 284 (8): 5352-5361.
- [28] Kuerschner L, Moessinger C, Thiele C. Imaging of lipid biosynthesis: how a neutral lipid enters lipid droplets. Traffic. 2008; 9 (3): 338-352.
- [29] Farese RV Jr., Walther TC. Lipid droplets finally get a little R-E-S-P-E-C-T. Cell. 2009; 139 (5): 855-860.
- [30] Weber E, Hecker M, Koepp E, Orlia W, Czugler M, Csöregh I. New trigonal lattice hosts: stoicheiometric crystal inclusions of laterally trisubstituted benzenes-X-ray crystal structure of 1,3,5-tris-(4-carboxyphenyl)benzene·dimethylformamide. J. Chem. Soc., Perkin Trans. 1988; 2: 1251-1258.
- [31] Hourani R, Jain M, Maysinger D, Kakkar A. "Multi-tasking with single scaffold dendrimers for targeting sub-cellular microenvironments", Chem. Eur. J. 2010; 16(21): 6164-6168.
- [32] Khanna K, Varshney S, Kakkar A. Designing miktoarm polymers using a combination of "click" reactions in sequence with ring opening polymerization. Macromolecules. 2010; 43: 5688-5698.
- [33] Soliman GM, Sharma R, Choi AO, Varshney SK, Winnik FM, Kakkar AK. Maysinger, D., Tailoring the efficacy of nimodipine drug delivery using nanocarriers based on A₂B miktoarm star polymers. Biomaterials. 2010; 31: 8382-8392.
- [34] Hourani R, Sharma A, Kakkar A. "Designing dendritic frameworks using versatile building blocks suitable for Cu^I catalyzed alkyne azide "click" chemistry," Tett. Lett. 2010; 51(29): 3792-3795.

- [35] Wängler C, Moldenhauer G, Eisenhut M, Haberkorn U, Mier W. Antibodydendrimer conjugates: the number, not the size of the dendrimers, determines the immunoreactivity, Bioconjugate Chem. 2008; 19: 813–820.
- [36] Hourani R, Kakkar AK, Whitehead MA. 3,5-Dihydroxybenzylalcohol based dendrimers: structure evaluation and molecular encapsulation in generations 1-5, J. Mater. Chem. 2005; 15: 2106-2113.
- [37] Hein CD, Liu X-M, Wang, D. Click chemistry, a powerful tool for pharmaceutical sciences. Pharm Res. 2008; 25 (10): 2216-2230.
- [38] Gao H, Matyjaszewski K. Synthesis of molecular brushes by "grafting onto" method: combination of ATRP and click reactions. J. Am. Chem. Soc. 2007; 129 (20): 6633-6639.
- [39] Block ML, Hong JS. Microglia and inflammation-mediated neurodegeneration: multiple triggers with a common mechanism. Prog. Neurobiol. 2005; 76 (2): 77-98.
- [40] Hanisch UK, Kettenmann H. Microglia: active sensor and versatile effector cells in the normal and pathologic brain. Nat. Neurosci. 2007; 10 (11): 1387-1394.
- [41] Lalancette-Hebert M, Moquin A, Choi AO, Kriz J, Maysinger D. Lipopolysaccharide-QD micelles induce marked induction of TLR2 and lipid droplet accumulation in olfactory bulb microglia. Mol. Pharm. 2010; 7 (4): 1183-1194.
- [42] Maysinger D, Behrendt M, Lalancette-Hébert M, Kriz J. Real-time imaging of astrocyte response to quantum dots: in vivo screening model system for biocompatibility of nanoparticles. Nano Lett. 2007; 7: 2513-2520
- [43] abd-el-Basset E, Fedoroff S. Effect of bacterial wall lipopolysaccharide (LPS) on morphology, motility, and cytoskeletal organization of microglia in cultures. J. Neurosci. Res. 1995; 41 (2): 222-237.
- [44] Block ML, Zecca L, Hong JS. Microglia-mediated neurotoxicity: uncovering the molecular mechanisms. Nat. Rev. Neurosci. 2007; 8 (1): 57-69.
- [45] Choi CS, Savage DB, Kulkarni A, Yu XX, Liu ZX, Morino K, Kim S, Distefano A, Samuel VT, Neschen S, Zhang D, Wang A, Zhang XM, Kahn M, Cline GW, Pandey SK, Geisler JG, Bhanot S, Monia BP, Shulman GI.

Suppression of diacylglycerol acyltransferase-2 (DGAT2), but not DGAT1, with antisense oligonucleotides reverses diet-induced hepatic steatosis and insulin resistance. J. Biol. Chem. 2007; 282 (31): 22678-22688.

Chapter 3

Facile Construction of Multifunctional Nanocarriers Using Sequential Click Chemistry for Applications in Biology



Tri-functional dendrimer Lipid droplets Nucleus

In the previous chapter, we described the synthetic methodology to construct bifunctional nanoconjugates, where the therapeutic agent and the imaging dye were covalently linked to a dendrimer. The focus of research in this chapter is to design and develop an efficient and versatile synthetic strategy to construct multifunctional nanocarriers; which allow covalent linking of any desired combination of functional moieties. This approach can be utilized in designing potential nanocarriers for biological applications where multitasking is required. In this chapter, details of the synthetic methodology to construct a variety of bifunctional nanocarriers, showing the versatility of this approach is discussed. The construction of bifunctional dendrimers with a combination of drug and PEG molecules; and a combination of an imaging dye and PEG molecules is discussed.

The choice of PEG as a functionality was made to provide biocompatibility and aqueous solubuility to the dendrimers. α -Lipoic acid is used as a model drug and BODIPY is used as an imaging dye.

It is important to have more than two functional moieties in a single nanocarrier for various biological applications. There is a need to develop nanocarriers which can deliver the therapeutics along with their simultaneous tracking in the cells, and at the same time, the nanocarriers should be stable enough so that they should not be degraded in the body prior to reaching their site of action. Considering the need for multitasking nanocarriers for drug delivery applications, we further elaborated our chemistry from the construction of bifunctional dendrimers to a trifunctional dendrimer. In this chapter, along with the bifunctional dendrimers we have also demonstrated the synthesis of a trifunctional dendrimer with a combination of covalently linked model drug (α -lipoic acid), fluorescent dye (BODIPY) and polyethylene glycol (PEG), using a core with orthogonal functional groups, on which Husigen alkyne-azide "click" reactions are performed in sequence. These carriers are internalized into the cells where they reduce H_2O_2 induced reactive oxygen species formation. The biological results are dicussed in detail.

Reproduced in part with permission from Sharma A., Neibert K., Sharma R., Hourani R., Maysinger D., & Kakkar A., *Macromolecules*, **2011**, 44, 521.

Copyright 2011 American Chemical Society

3.1 Introduction

Designing well defined multifunctional nanocarriers into which a combination of the desired drug, an imaging dye and a solubilising agent can be covalently introduced, continues to be a focus of current research in theranostics.¹⁻ ³ Dendrimers⁴ constitute an intriguing class of macromolecules that are increasingly being evaluated for applications in biology. 1-4 Dendrimers are hyperbranched and monodisperse in nature, and numerous synthetic methodologies have been developed to expand the scope of these complex and yet highly elegant nanomaterials.⁵ Many dendrimers are now available in which the core, backbone or peripheral groups have been modified to contain a single functionality. Introduction of multiple covalent functionalities into a single dendrimer has faced synthetic challenges, and the effort has been largely limited to bifunctional dendrimers. However, there are few reports of dendrimers with more than two functionalities, ⁷ and there remains a need for a simple and versatile synthetic methodology which can be used to incorporate desired functionalities in a controlled manner. We report here a versatile synthetic route to bi- and trifunctional nanocarriers, using "click" chemistry which involves Cu^I catalyzed coupling of an alkyne with an azide, 5d,8 in sequence, on building blocks with orthogonal reactive moieties. This simple methodology allows facile, high yield synthesis of multifunctional dendrimers in which any desired combination of functionalities such as therapeutic (α-lipoic acid), solubilising (PEG) and imaging (BODIPY dye) agents can be incorporated with relative ease.

 α -Lipoic acid is a multimodal antioxidant tested in a number of preclinical and clinical trials involving subjects with neurodegenerative, cardiovascular and liver disease as well as diabetes and diabetic neuropathy. $^{10-12}$ It is a naturally occurring, amphipathic compound with a low redox potential (-0.29 V) and contains a disulfide group which allows α -lipoic acid to function as a metabolic antioxidant, cystein precursor and heavy metal chelator. 13,14 Administration of antioxidant compounds such as α -lipoic acid which contains disulfide group capable of being reduced to thiol group, leads to the enhancement and regeneration of several intracellular antioxidant molecules including

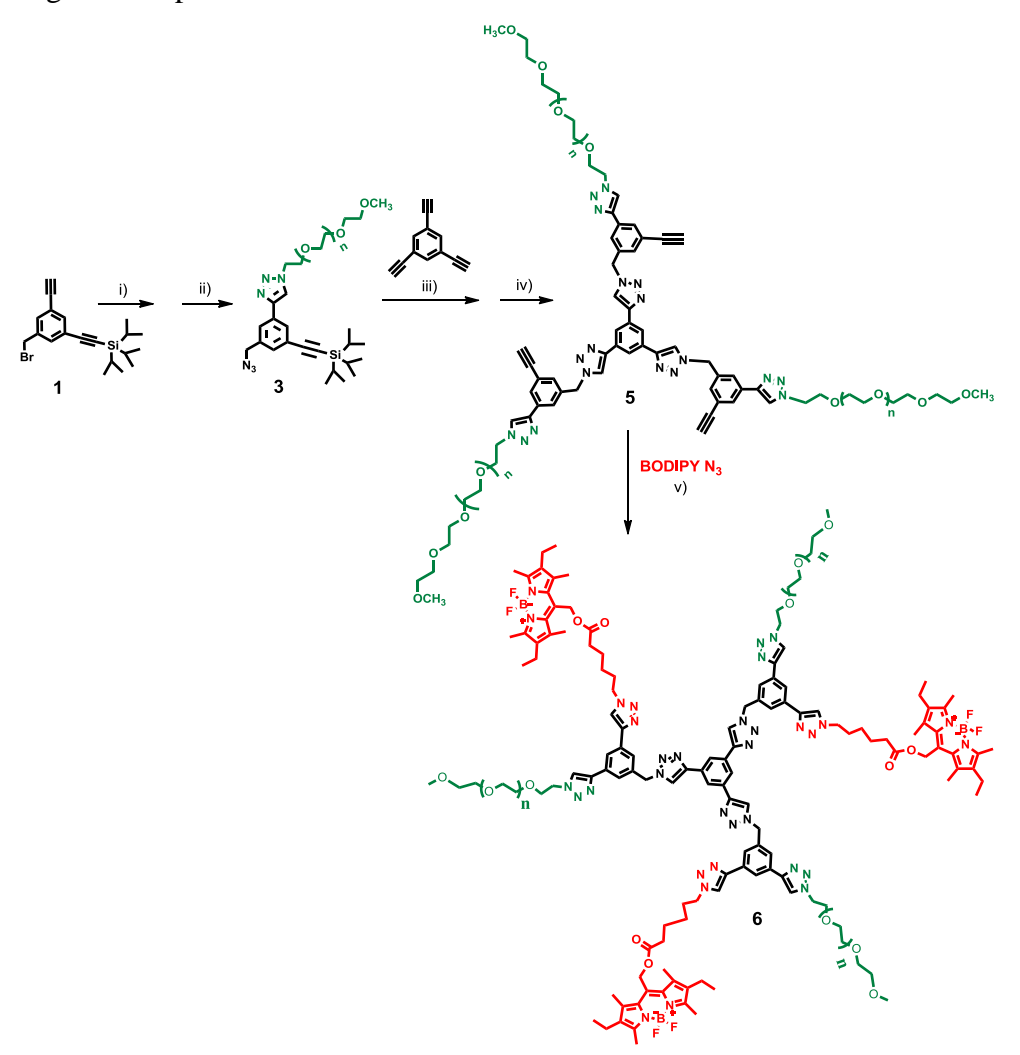
glutathione, thioredoxins and vitamin E which protect against oxidative stress.¹⁵ Glutathione (GSH) is the most abundant of the endogenous thiol containing antioxidants and plays a key role in the maintenance of cellular homeostasis.

Through the use of an appropriate delivery vehicle, the stability and efficacy of a therapeutic agent can be significantly improved. Dendrimers and miktoarms are an emerging class of polymeric nanocarriers for controlled intracellular delivery of drugs owing to the tailored density of reactive functional groups, carrying capacity, well defined structure and monodispersity. Several recent findings have reported the unique benefits of introducing anti-oxidant moieties into dendrimer scaffoldings, and GSH-inducing antioxidant drugs such as *N*-Acetyl-L-cysteine (NAC) have been previously coupled to the dendrimers. We demonstrate that the conjugated dendrimer and miktoarm carriers reported here are noncytotoxic within micromolar concentrations, and are effective in reducing reactive oxygen species in pheochromocytoma (PC12) cells. Interestingly, the miktoarm carrier also enhances glutathione concentrations in these cells. Tri-functional and bi-functional carriers containing the imaging probe BODIPY are internalized into these cells and tend to accumulate in the cytoplasmic lipid droplets.

3.2 Results and discussion

The synthesis of multifunctional nanocarriers is carried out on building blocks that allow covalent linking of different functionalities using Cu(I) catalyzed alkyne-azide "click" chemistry, in sequence. The construction of the bifunctional dendrimer 6 containing three PEG₇₅₀ chains and three BODIPY dye molecules was carried out using the core compound 1 (Scheme 3.1). The latter molecule with free and protected acetylene centres was synthesized using a procedure developed earlier in our group. The free acetylene arm of 1 was first used to covalently bind a PEG chain using "click" reaction with PEG₇₅₀-azide in the presence of copper sulfate pentahydrate and sodium ascorbate. This is a clean and straight forward reaction with a high yield. The bromo focal point of the resulting compound was then converted to azide via an azidation reaction with sodium azide to give compound 3 in a good yield. The latter was then clicked on

the triethynylbenzene core, followed by deprotection of triisopropylsilyl-acetylene groups. The corresponding free acetylene centers were subsequently clicked with the azide-functionalized BODIPY dye to yield bifunctional dendrimer **6**. It should be noted that the PEG arm has to be attached first on **1**, and then the dye, since the azidation reaction in the presence of BODIPY on the molecule degrades the dye. It is essential to follow this particular sequence of reactions to avoid this degradation process.

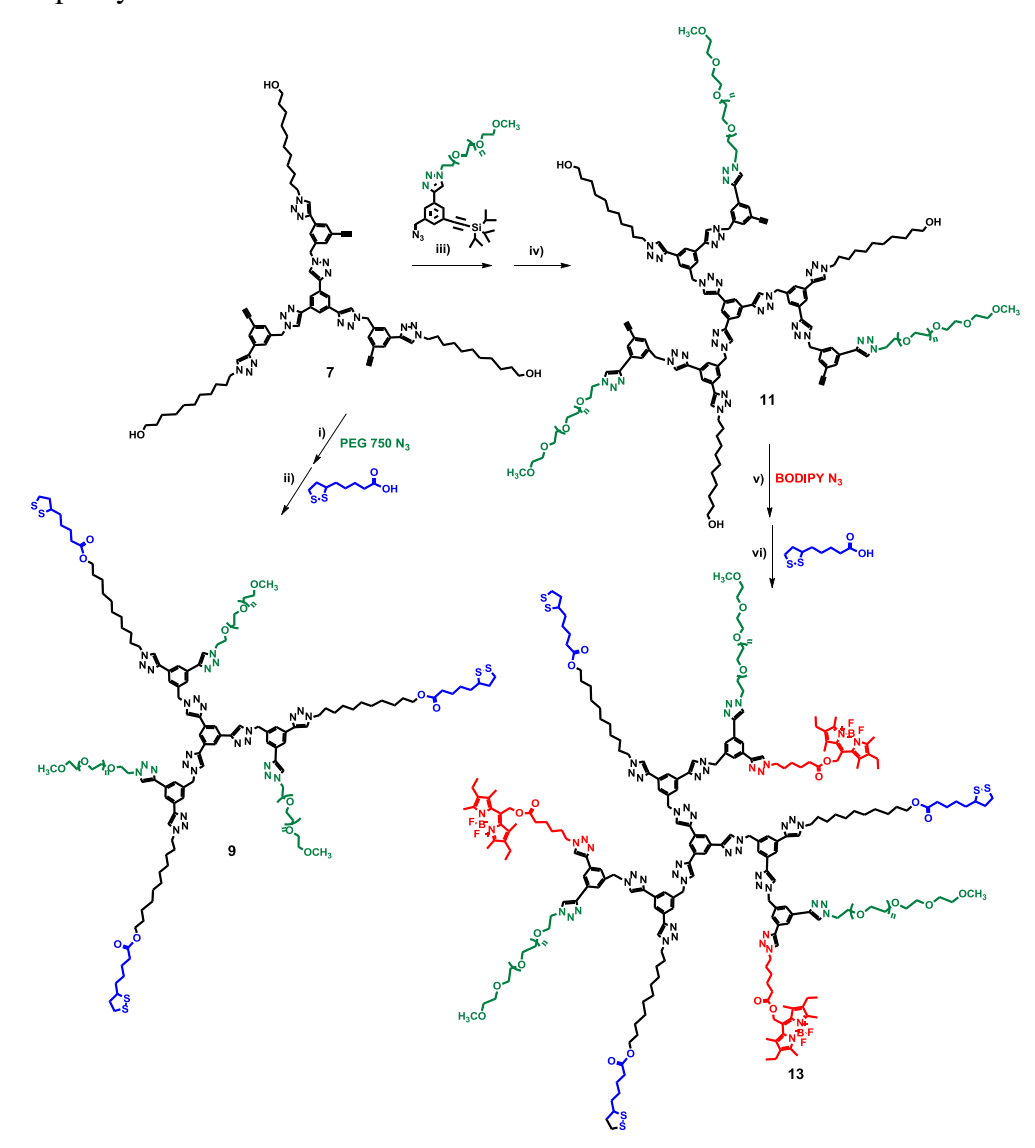


Scheme 3.1. Synthesis of bifunctional dendrimer **6** containing BODIPY dye and PEG₇₅₀ chains: i) PEG₇₅₀N₃, CuSO₄·5H₂O/sodium ascorbate, H₂O/THF, RT, Overnight (O/N), 73% yield; ii) NaN₃, DMF, RT, 3H, 79% yield iii) CuSO₄·5H₂O/sodium ascorbate, H₂O/THF, RT, O/N, 90% yield iv) tetrabutylammonium fluoride (TBAF)/THF O/N, 65% yield; v) CuSO₄·5H₂O / sodium ascorbate, H₂O/THF, RT, O/N, 92% yield.

The synthesis of another bifunctional dendrimer 9 with a combination of the drug α -lipoic acid and PEG₇₅₀ was begun from 7, which contains three terminal alcohols for the attachment of the drug and three free acetylenes available for the subsequent click reaction. Compound 7 was synthesized by clicking azido compound with long chain alcohol on triethynylbenzene core, followed by the deprotection of triisopropylsilyl-acetylene groups. ^{6e} PEG₇₅₀-azide was first clicked on 7 using the same procedure as described above, followed by the reaction of hydroxyl terminated arms with α -lipoic acid using a quantitative esterfication reaction, leading to the formation of the desired bifunctional dendrimer 9 (Scheme 3.2). To carry out the synthesis of this dendrimer, one must first attach long chain alcohols followed by PEG chains. We could not achieve this synthesis the other way by covalently linking three PEG chains on the dendrimer first, followed by long chain alcohols. This may be due to the steric hinderance caused by long PEG chains. Another important point is the attachment of α -lipoic acid, which should always be the last step as the sulphur of this drug interferes with click reaction leading to very poor yields. Thus, it is important to follow a particular sequence of reactions to synthesize bifunctional dendrimers with good yields.

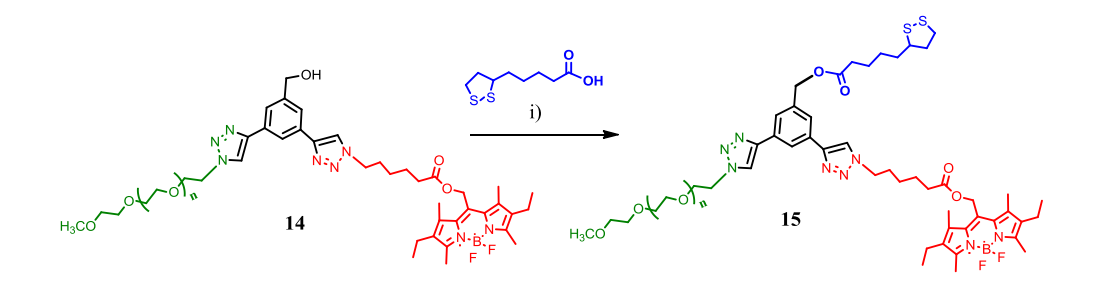
A similar synthetic approach was used to synthesize the trifunctional dendrimer 13. Starting with compound 7, we first clicked compound 3 containing PEG and a protected acetylene (Scheme 3.2). In this reaction, the product was isolated only in 43% yield. This is because the click reaction did not go efficiently, probably due to steric hindrance as the bulkier azide 3 is being clicked on to the compound 7, which contains long chain alcohols. The triisopropylsilylacetylene groups were then deprotected followed by a second "click" reaction with the azide-functionalized BODIPY dye. The primary alcohols were then reacted with α -lipoic acid via an esterfication reaction to yield the desired trifunctional dendrimer 13. Following this particular sequence of reactions is essential as there are now three functionalities which can interfere with each other. We attempted other sequences (*e.g.* PEG first followed by alcohols and

dye), but the above mentioned sequence gave the best results in terms of yields and purity.



Scheme 3.2. Synthesis of bifunctional dendrimer 9 (containing α -lipoic acid and PEG₇₅₀ chains), and trifunctional dendrimer 13 (containing α-lipoic acid, BODIPY dye and PEG₇₅₀ chains) i) CuSO₄·5H₂O/sodium ascorbate, H₂O/THF, O/N, 62% yield; ii) N,N' Dicyclohexylcarbodiimide (DCC), 4dimethylaminopyridine (DMAP), DCM, RT, 3H, 78% yield; iii) CuSO₄·5H₂O/sodium ascorbate, H₂O/THF, RT, O/N, 43% yield iv) tetrabutylammonium fluoride (TBAF)/THF O/N, 70% yield; CuSO₄·5H₂O/sodium ascorbate, H₂O/THF, RT, O/N, 69% yield vi) 1-[3-(Dimethylamino)propyl]-3-ethylcarbodiimidemethiodide (EDC), DMAP, DCM, RT,O/N, 70% yield.

Since the macromolecular structure may influence the overall behavior of the carriers, we decided to construct two miktoarm structures: **15**, a trifunctional carrier containing PEG, BODIPY and α -lipoic acid, and **17** with PEG and α -lipoic acid. To synthesize the miktoarm carrier **15** we started with compound **14** containing a PEG chain, a molecule of BODIPY dye, and benzylic alcohol. This compound was synthesized starting from a compound similar to **1** but having benzyl alcohol instead of benzyl bromide, a free acetylene and a protected acetylene. PEG₇₅₀ azide was clicked on the free acetylene followed by deprotection of triisopropylsilyl group of another acetylene which was then utilised to click BODIPY dye. The resulting compound was then reacted with α -lipoic acid to yield compound **15** (Scheme **3.3**).



Scheme 3.3. Synthesis of miktoarm unit **15** having all the three functionalities PEG₇₅₀, BODIPY dye and α -lipoic acid: i) EDC, DMAP, DCM, RT, O/N, 66% yield.

The miktoarm carrier 17 was synthesized starting with compound 16 containing two PEG chains and a benzylic alcohol (Scheme 3.4). Compound 16 was synthesized by carrying out o-alkylation at 3 and 5 positions of 3,5-dihydroxybenzyl alcohol using propargyl bromide. The two acetylenes were then used to "click" PEG₇₅₀ chains.²⁰ The benzylic alcohol was then reacted with α -lipoic acid using simple esterification reaction to yield compound 17.

Scheme 3.4. Synthesis of miktoarm unit **17** having 2 PEG₇₅₀ chains and a molecule of α -lipoic acid: i) EDC, DMAP, DCM, RT, O/N, 75% yield.

The bi- and tri-functional dendrimer and miktoarm carriers were developed for the intracellular delivery of redox-regulating and anti-apoptotic agents. α -Lipoic acid was used as a model drug for this purpose because it acts as a multimodal antioxidant. In addition to its direct function in the synthesis and/or regeneration of endogenous antioxidants, α -lipoic acid functions indirectly via transcriptional activation or inhibition of specific transcription factors (*e.g.* Nrf2 and NF-kappa B), leading to the expression or repression of a wide range of proteins. As such, the therapeutic potential of α -lipoic acid greatly exceeds the strict definition of an antioxidant.²¹

To track the uptake and cellular localization, dendrimer and miktoarm nanocarriers were conjugated with α-lipoic acid and BODIPY, a fluorescent probe with high affinity for lipid membranes. Fluorescent microscopy revealed that **6**, **13** and **15** were rapidly internalized and diffusely distributed following 30 minute exposure in PC12 cells (supplemental Fig. **3.1**, Appendix 3). In some cases, conjugated nanocarriers appear to be localized in subcellular compartments, presumably lipid droplets. ^{22,6e}

Prior to the evaluation of the various macromolecule carriers as antioxidant agents and GSH inducers, nanocarrier cytotoxicity was assessed. Pheochromocytoma (PC12) cells were treated with equimolar concentrations of dendrimers and miktoarms with respect to α -lipoic acid (200 μ M) and incubated for 24 hours. There was no significant reduction in cellular metabolic activity following exposure to the nanocarriers (Fig. 3.1A). Pretreatment with nontoxic concentrations of α -lipoic acid conjugated nanocarriers reduced H_2O_2 induced

reactive oxygen species formation in PC12 cells, ranging from 37.8 ± 1.89 % for free α -lipoic acid and 61.6 ± 3.08 % for **17** with respect to untreated H_2O_2 control (Fig. **3.1B**). Interestingly, all the dendrimers and miktoarm nanocarriers tested reduced H_2O_2 induced formation of superoxide, irrespective of conjugated drug, and did so more effectively than free α -lipoic acid.

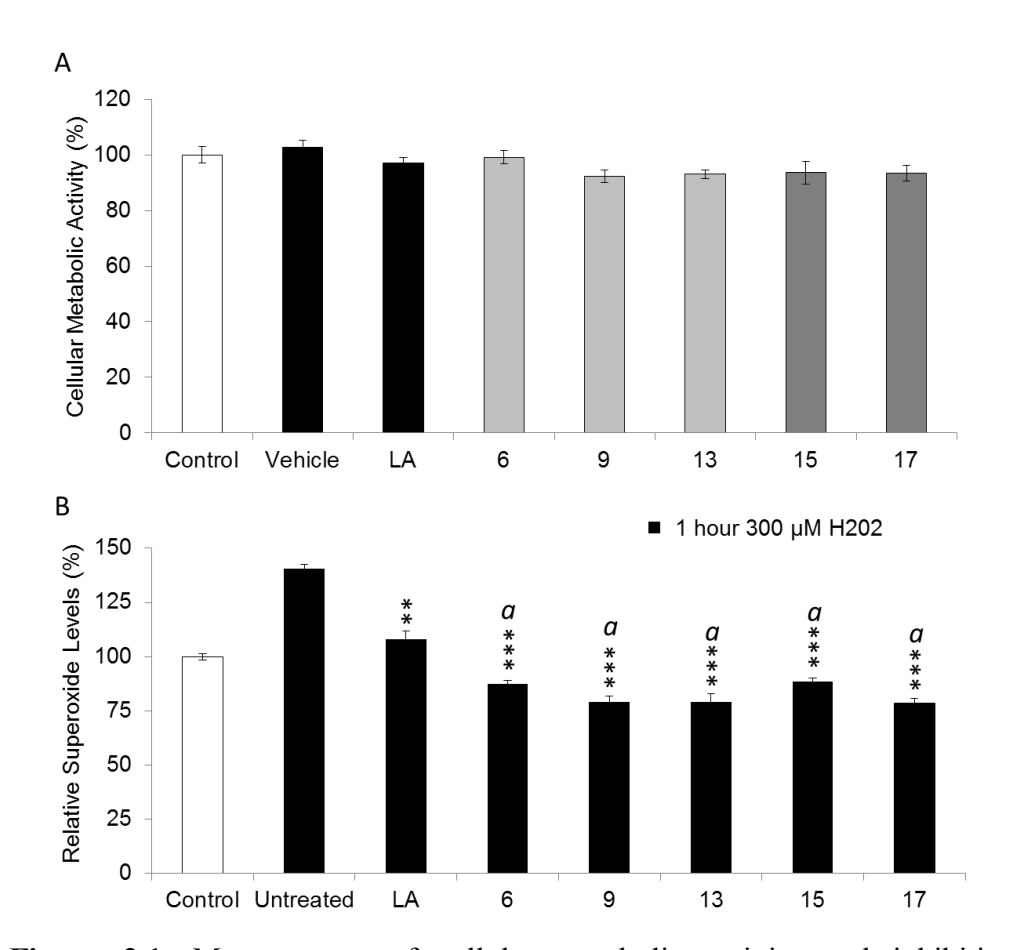


Figure 3.1. Measurement of cellular metabolic activity and inhibition of superoxide formation following exposure to α-lipoic acid conjugated dendrimer and miktoarm nanocarriers in PC12 cells. A) Nanocarrier metabolic activity as assessed by Alamar Blue assay is indicative of cell viability. PC12 cells were treated for 24 hours with equimolar concentrations of various dendrimer and miktoarm nanocarriers with respect to α-lipoic acid (200 μM). Cellular metabolic activity was determined and expressed as a percentage with respect to the untreated control. Data are presented as means \pm SEM of three individual experiments of triplicates. No significant differences were detected. **B**) Reactive oxygen species (ROS) generation following acute oxidative (1 hour) insult was assessed using dihydroethidium (DHE), a fluorescent probe sensitive to super oxide radicals. PC12 cells were pretreated with dendrimers and miktoarm nanocarriers for 6 hours prior to 1 hour 300 μM H₂O₂ exposure. DHE fluorescent

intensity was determined spectrofluorimetricly and expressed as a change (percentage) with respect to the untreated control cells. Data are presented as means \pm SEM of three individual experiments of triplicates. Statistically significant differences from the H_2O_2 untreated control (first black bar) are shown (** p<0.01, *** p<0.001). Statistically significant differences from free α -lipoic acid are shown (a, p<0.001).

We subsequently investigated the capacity of α -lipoic acid conjugated nanocarriers to deliver the drug by measuring intracellular glutathione content. PC12 cells were treated with equimolar concentrations of α -lipoic acid conjugated dendrimer 9 and miktoarm 17 nanocarriers with respect to free α -lipoic acid (200 μM) for 24 hours, and then incubated with mCBi, a fluorescent probe for GSH. Fluorescent micrographs suggested that free α -lipoic acid and 17 enhanced total intracellular glutathione concentrations were above those detected in untreated control cells (Fig. 3.2A). Intracellular glutathione concentrations were quantified spectrofluormetrically following 24 hour exposure to α-lipoic acid conjugated nanocarriers 9, 13, 15 and 17 (Fig. 3.2B). Only free α -lipoic acid and 17 significantly enhanced intracellular glutathione in PC12 cells with respect to control (204.3±4.08% and 151.1±3.78% respectively). There was a significant difference in intracellular glutathione between free α-lipoic acid and 17 treated cells, with the former having a 53% increase over the latter (indicated by a). Even two or three day exposure to the α-lipoic acid conjugated nanocarriers did not increase intracellular glutathione concentrations above those measured in cells treated with unconjugated α-lipoic acid (Fig. 3.2C). These findings suggest that the cleavage of α -lipoic acid from the drug nanocarrier is too slow to achieve effective intracellular concentrations of thiol residues necessary for enhanced synthesis of intracellular glutathione.

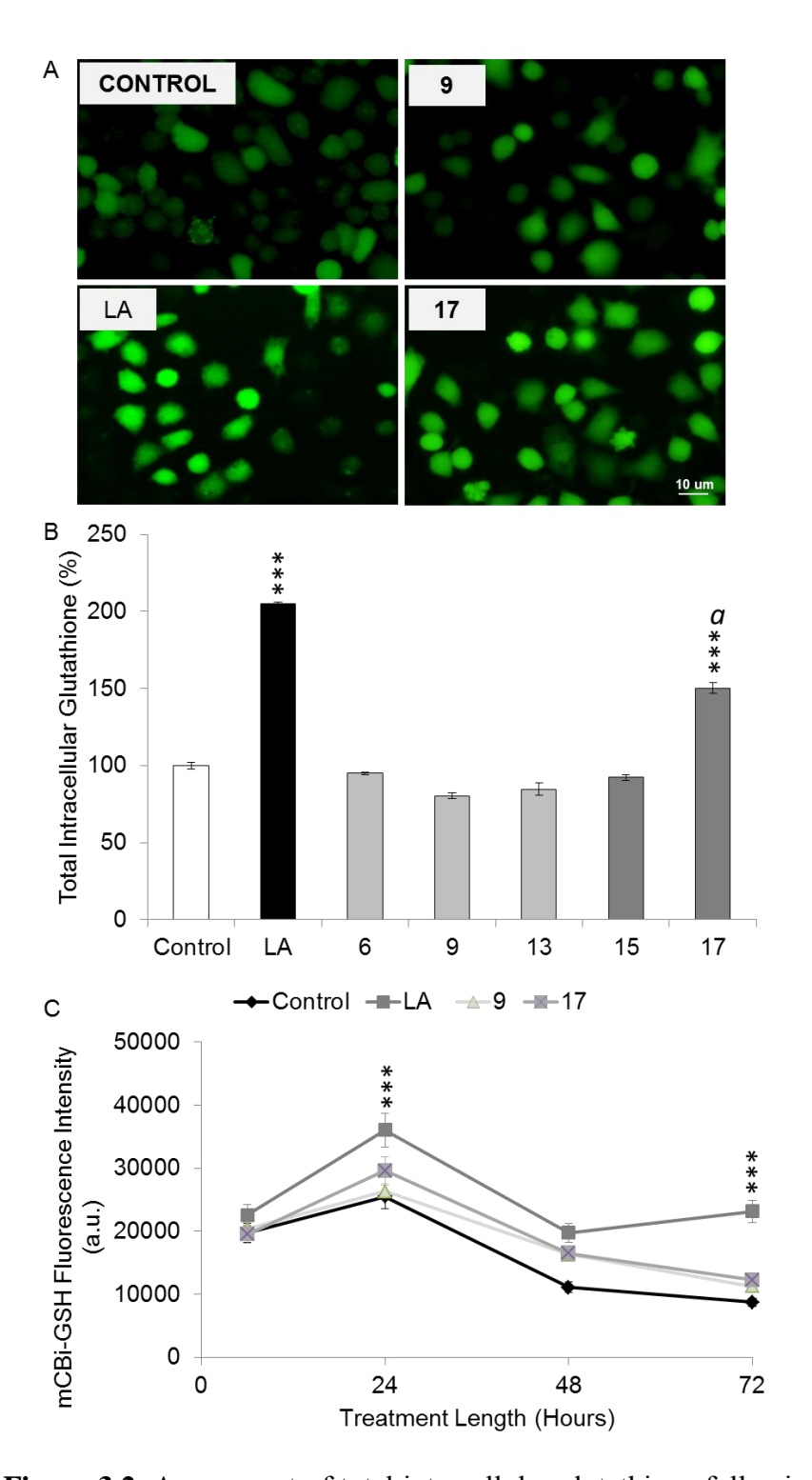


Figure 3.2. Assessment of total intracellular glutathione following exposure to α-lipoic acid conjugated dendrimer and miktoarm nanocarriers. A) Total intracellular glutathione content was assessed using monochlorobimane (mCBI), a probe which binds specifically to reduced glutathione (GSH) forming the fluorescent mCBi-GSH adduct. Representative fluorescent micrographs of PC12 cells treated for 24 hours with free α-lipoic acid (LA), **9** and **17** in equimolar

concentrations with respect to α -lipoic acid (200 μ M), were selected from at least three independent experiments of triplicates. The nucleus was stained with Hoechst and is visible in blue. Scale bar represents 10 um. B) The fluorescent intensity of the mCBI-GSH adduct was measured using spectrofluorimetry in PC12 cells treated for 24 hours with drug conjugated nanocarriers in equimolar concentrations with respect to α -lipoic acid (200 μ M). Data is expressed as a percentage with respect to the untreated control. Data are presented as means ± SEM of three individual experiments of triplicates. Statistically significant differences from the untreated control are shown (*** p<0.001). Statistically significant differences from free α -lipoic acid are shown (a p<0.001). C) PC12 cells were treated for 6, 24, 48 and 72 hours with drug conjugated nanocarriers. The fluorescent intensity of the mCBi-GSH adduct was measured spectrofluorimetrically and expressed as a mean fluorescent intensity in arbitrary units. Data are presented as means ± SEM of three individual experiments of triplicates. Statistically significant differences from the untreated control at each time point are shown (*** p<0.001).

The results presented here suggest that dendrimer and miktoarm nanocarriers are readily internalized by PC12 cells. Both BODIPY and α -lipoic acid (lipophilic moiety) contribute to the rapid diffusion of conjugated nanocarriers through cellular membranes. Limited information is currently available concerning the mechanisms of transport and trafficking of dendrimers across biological barriers. In this regard, knock-down experiments employing specific siRNAs and specific pharmacological inhibitors of proteins participating in internalization processes, should be used to elucidate the modes of α -lipoic acid and BODIPY conjugated nanocarrier entry. Fluorescent microscopy in conjunction with specific pharmacological inhibitors of endocytosis has thus far revealed rapid, clathrin-dependent endocytosis of FITC labeled dendrimers. However, internalization by specific endocytic mechanisms appear to be highly dependent on nanocarrier size and charge.

Once taken up into the cell, dendrimers and miktoarms nanocarriers reduce reactive oxygen species formation more efficiently than free α -lipoic acid. Interestingly α -lipoic acid conjugated dendrimers and miktoarms do not enhance intracellular glutathione concentrations above that of equimolar free α -lipoic acid (200 μ M). α -Lipoic acid is not readily released from its carriers, likely due to the

low concentration of enzymes required to cleave the covalent bond between the drug and the carriers in the cell culture system employed. Thus, an alternative approach that employs GSH sensitive bond cleavage and which should provide rapid delivery from the dendrimer-drug carriers, could be employed. This approach takes advantage of differences between intracellular and extracellular GSH concentrations (mM and μ M respectively) allowing the drug to be released primarily upon entry into the cells. 18b

3.3 Conclusions

We have developed a general and simple methodology for the construction of multifunctional carriers in which desired functionalities can be introduced using a combination of "click" reactions in sequence with esterification. Use of molecular building blocks with orthogonal functionalities facilitates the synthesis of noncytotoxic carriers with any combination of a therapeutic agent with an imaging dye and/or solubilizing polymeric chains. Our results show that the multifunctional dendrimer and miktoarm nanocarriers reduce H₂O₂-induced oxidative stress in PC12 cells. Interestingly, the reduction of superoxide did not depend on α-lipoic acid moiety, suggesting that non-conjugated or "naked" dendritic structures themselves could exert some antioxidant activity. Indeed, several dendrimers showed an anti-inflammatory effect superior to that produced by anti-inflammatory agents attached to the dendrimers. These effects were ascribed to the ability of dendrimers to inhibit cyclooxygenase-2 (COX-2).24 Studies to reveal the mechanisms involved in the antioxidant and inflammatory effects of naked dendrimers and miktoarms presented in the current study are under investigation both in *in vitro* and *in vivo* systems in our laboratory.

3.4 Experimental section

3.4.1 Materials and methods:

Copper (II) sulfate pentahydrate (CuSO₄.5H₂O) (>98.0%), sodium ascorbate (NaAsc) (crystalline) (98%), 6-bromohexanoic acid (97%), tetrabutylammonium fluoride (Bu4NF) (1.0 M in THF), 11-bromo-1-undecanol (98%), α-lipoic acid (>99%), N,N'-dicyclohexylcarbodiimide (DCC) (99%),1-[3-

(dimethylamino)propyl]-3-ethylcarbodiimidemethiodide(EDC),

4(dimethylamino)pyridine (DMAP) (99%), and sodium azide (NaN₃) (>99.5%) were purchased from Sigma-Aldrich Canada, and used as received. 8-Acetoxymethyl-2,6-diethyl-1,3,5,7-tetramethyl pyrromethene fluoroborate (PM605) was purchased from Exciton Inc, and used as received. All other solvents were used as received in their anhydrous forms. NMR spectra were recorded on a 400 or 500MHz (as specified) spectrometer at ambient temperatures. The chemical shifts in ppm are reported relative to tetramethylsilane as an internal standard for ¹H and ¹³C{¹H} NMR spectra. Gel permeation chromatography (GPC) analyses were performed in THF. A Waters 510 liquid chromatography pump, equipped with two (HR1 and HR4) Styragel columns connected in series, and a refractive index detector (Varian RI-4) were used at room temperature. Polystyrene standards (Scientific Polymer Products, Inc., NY) with a narrow molecular weight distribution were used for calibration. The same instrument was used for all the compounds except 12, 13 and 15, for which GPC analyses were carried out in DMF on a Viscogel G-MBLMW-3078 column equipped with a Waters 410 refractive index detector that was calibrated with polyethylene glycol standards.

3.4.2 Synthesis:

The following compounds were synthesized by adaptation of the previously published procedures: 1,3,5-triethynylbenzene,²⁵ 11-Azido-undecan-1-ol,^{6e} PEG₇₅₀-Azide,²⁶ BODIPY-Azide, miktoarm carrier containing PEG₇₅₀, BODIPY dye and benzylic alcohol,¹⁹ and another miktoarm carrier containing two PEG₇₅₀ chains and a benzylic alcohol group²⁰ and the dendrimer containing the long chain alcohol arms and free acetylenic groups.^{6e}

Compound 2: Compound **1** (1g, 2.59 mmol) and PEG₇₅₀-azide (2.01g, 2.59 mmol) were dissolved in 3 mL of tetrahydrofuran (THF), followed by the addition of sodium ascorbate (0.051g, 0.259 mmol). An aqueous solution (1 mL) of CuSO₄.5H₂O (0.032g, 0.129 mmol) was added dropwise to the solution. The reaction mixture was left to stir overnight at room temperature. THF was then

evaporated, and the remaining solution was extracted with ethyl acetate (3x30 mL), and then the organic layer was washed with brine (3x50 mL). It was dried over MgSO₄, and the solvent was evaporated. Silica-gel column chromatography was done and the product was flushed through the column with 5% methanol in dichloromethane (DCM). The solvent was evaporated to yield the product as a transparent liquid (2.20g, 73%). ¹H NMR (400 MHz, CDCl₃): δ (ppm) 1.13 (br s, 21H, -Si(C₃H₇)), 3.38 (s, 3H,-OCH₃), 3.54-3.64 (m, (-OCH₂CH₂-)_n), 3.91 (t, 2H,-CH₂OCH₃), 4.48 (s, 2H, -CH₂Br), 4.60 (t, 2H, -OCH₂CH₂triazole), 7.44 (s, 1H, ArH), 7.86 (s, 2H, ArH) and 8.10 (s, 1H, triazoleH). ¹³C{¹H} NMR (125 MHz, CDCl₃): δ (ppm) 11.3, 18.7, 32.5, 50.5, 59.0, 69.4, 70.5, 71.9, 91.6, 105.97, 121.6, 124.6, 126.2, 129.0, 131.6, 131.8, 138.5, 146.2. GPC: Mn=1820 g/mol. Mw/Mn=1.09.

Compound 3: To a solution of 2 (1.54g, 1.33 mmol) in N,N-dimethyl formamide (DMF), NaN₃ (0.431g, 6.63 mmol) was added. The reaction mixture was left to stir at room temperature for 3h. The solution was extracted with ethylacetate (3x50 mL), and the organic phase was washed with brine (3x70 mL). It was dried over MgSO₄ and followed by removal of the solvent. The product was flushed through a short silica-gel column with 5% methanol in DCM to yield a transparent liquid (1.18g, 79%). ¹H NMR (400 MHz, CDCl₃): δ (ppm) 1.13 (br s, 21H, -Si(C₃H₇)), 3.37 (s, 3H,-OCH₃), 3.54-3.64 (m, (-OCH₂CH₂-)_n), 3.92 (t, 2H,-CH₂OCH₃), 4.39 (s, 2H, -CH₂N₃), 4.60 (t, 2H, -OCH₂CH₂triazole), 7.37 (s, 1H, ArH), 7.79 (s, 1H, ArH), 7.88 (s, 1H, ArH) and 8.10 (s, 1H, triazoleH). ¹³C{¹H} NMR (125 MHz, CDCl₃): δ (ppm) 11.5, 18.9, 50.7, 57.4, 59.3, 69.7, 70.8, 72.1, 91.9, 105.9, 121.8, 124.9, 125.4, 129.1, 131.2, 131.8, 136.5, 146.2. GPC: Mn=1900 g/mol. Mw/Mn=1.13.

Compound 4: 1,3,5-triethynylbenzene (TEB) (0.050g, 0.33 mmol) and compound **3** (1.12g, 1.0 mmol) were dissolved in 2 mL of THF, followed by addition of sodium ascorbate (0.020g, 0.10 mmol). An aqueous solution (1 mL) of CuSO₄.5H₂O (0.013g, 0.05 mmol) was added dropwise to the solution. The reaction mixture was left to stir overnight at room temperature. THF was then evaporated, and the remaining solution was extracted with ethyl acetate (3x30)

mL), and then the organic layer was extracted with brine (3x50 mL). It was dried over MgSO₄, and the solvent was evaporated. Silica-gel column chromatography was used to isolate the product with 5% methanol in DCM. The solvent was evaporated to yield the product as a thick viscous liquid (1.05g, 90%). ¹H NMR (400 MHz, CDCl₃): δ (ppm) 1.11 (br s, 63H, -Si(C₃H₇)), 3.37(s, 9H,-OCH₃), 3.54-3.64(m, (-OCH₂CH₂-)_n), 3.91(t, 6H,-CH₂OCH₃), 4.59(t, 6H, -OCH₂CH₂triazole), 5.59(s, 6H,-CH₂-), 7.41(s, 3H, ArH), 7.79(s, 3H, ArH), 7.97(s, 6H, ArH), 8.09(s, 3H, triazoleH) and 8.26(s, 3H, triazoleH). ¹³C{¹H} NMR (125 MHz, CDCl₃): δ (ppm) 11.3, 18.7, 50.4, 53.8, 59.0, 69.4, 70.5, 71.9, 92.3, 105.7, 120.5, 121.7, 122.4, 125.1, 124.4, 129.5, 131.1, 131.6, 132.1, 135.2, 145.9 and 147.6. GPC: Mn=3500 g/mol. Mw/Mn=1.11.

Compound 5: To a solution of compound 4 (0.53g, 0.15 mmol) in THF (3 mL) in a dry ice/acetone bath, a solution of Bu₄NF-1M solution in THF (0.75mL, 0.75 mmol) was added in a dropwise fashion. The reaction mixture was allowed to warm to room temperature and left to stir overnight. The solvent was removed under vacuum, water (10 mL) was added, and the mixture was extracted with ethyl acetate (3x20ml). The extract was then dried over MgSO₄, and solvent was evaporated. Silica-gel column chromatography was used to isolate the product with 5% methanol in DCM. The solvent was evaporated to yield the product as a transparent liquid (0.30g, 65%). ¹H NMR (400 MHz, CDCl₃): δ (ppm) 3.14 (s, 3H,-CCH-), 3.36 (s, 9H, -OCH₃), 3.54-3.64 (m, (-OCH₂CH₂-)_n), 3.89 (t, 6H,- CH_2OCH_3), 4.58 (t, 6H, -OCH₂CH₂triazole), 5.60 (s, 6H,-CH₂-), 7.36 (s, 3H, ArH), 7.88 (s, 3H, ArH), 7.94 (s, 3H, ArH), 7.99 (s, 3H, ArH), 8.10 (s, 3H, triazole**H**) and 8.24 (s, 3H, triazole**H**). $^{13}C\{^{1}H\}$ NMR (125 MHz, CDCl₃): δ (ppm) 13.6, 19.7, 24.0, 50.4, 53.7, 58.9, 70.4, 70.6, 71.9, 78.7, 82.5, 120.7, 121.8, 122.4, 123.7, 125.7, 129.4, 130.9, 131.6, 132.2, 135.6, 145.8, 147.6. GPC: *Mn*=3400 g/mol. *Mw/Mn*=1.10.

Bifunctional dendrimer 6: Compound **5** (0.100g, 0.03 mmol) and BODIPY-N₃ (0.062g, 0.13 mmol) were dissolved in 2 mL of THF, followed by addition of sodium ascorbate (0.005g, 0.03 mmol). An aqueous solution (1 mL) of CuSO₄.5H₂O (0.003g, 0.01 mmol) was added dropwise to the solution. The

reaction mixture was left to stir overnight at room temperature. THF was then evaporated, and the remaining solution was extracted with DCM (3x20 mL), and then the organic layer was extracted with brine (3x50 mL). It was dried over MgSO₄, and the solvent was evaporated. Silica-gel column chromatography was used to isolate the product with 7% methanol in DCM. The solvent was evaporated to yield the product as a red liquid (0.135g, 92%). ¹H NMR (400 MHz, CDCl₃): δ (ppm) 1.05 (t, 18H, -ArCH₂CH₃), 1.40-1.42 (m, 6H, -OOCCH₂CH₂-), 1.60-1.68 (m, 6H, -CH₂CH₂CH₂traizole), 1.72-1.98 (m, 6H, -CH₂CH₂triazole), 2.19 (s, 18H, -ArCH₃), 2.30-2.45(m, 18H, -OOCCH₂- and - $ArCH_2CH_3$), 2.47 (s, 18H, $-ArCH_3$), 3.36 (s, 9H, $-OCH_3$), 3.54-3.64 (m, (- $OCH_2CH_2-)_n$, 3.91 (t, 6H,-CH₂OCH₃), 4.38 (t, 6H, -CH₂CH₂CH₂triazole), 4.58 (t, 6H, -OCH₂CH₂triazole), 5.28 (s, 6H, ArCH₂OOCCH₂-), 5.64 (s, 6H, -CH₂-), 7.80 (s, 3H, ArH), 7.83 (s, 3H, ArH), 7.94 (s, 3H, ArH), 8.04 (s, 3H, ArH), 8.14 (s, 3H, triazole**H**), 8.21 (s, 3H, triazole**H**) and 8.31 (s, 3H, triazole**H**). ¹³C{¹H} NMR (125 MHz, CDCl₃): δ ppm 12.6, 13.8, 14.7, 17.1, 19.9, 24.2, 25.9, 29.7, 29.9, 33.7, 50.1, 50.5, 58.2, 59.0, 69.4, 70.5, 71.9, 120.9, 122.3, 125.1, 131.5, 132.2, 133.6, 135.9, 136.5, 146.4, 154.9, 172.9. GPC: *Mn*=3300 g/mol. Mw/Mn=1.10.

Compound 8: Compound **7** (0.150g, 0.11 mmol) and PEG₇₅₀-N₃ (0.255g, 0.33 mmol) were dissolved in 2 mL of THF, followed by addition of sodium ascorbate (0.008g, 0.04 mmol). An aqueous solution (1 mL) of CuSO₄.5H₂O (0.005g, 0.02 mmol) was added dropwise to the solution. The reaction mixture was left to stir overnight at room temperature. THF was then evaporated, and the remaining solution was extracted with DCM (3x20 mL), and then the organic layer was extracted with brine (3x50mL). It was dried over MgSO₄, and the solvent was evaporated. Silica-gel column chromatography was used to isolate the product with 8% methanol in DCM. The solvent was evaporated to yield the product as a viscous liquid (0.250g, 62%). ¹H NMR (400 MHz, CDCl₃): δ (ppm) 1.21-1.34 (m, 42H, -CH₂-), 1.49-1.51 (m, 6H, -CH₂CH₂OH), 1.87-1.91 (m, 6H, -CH₂CH₂-triazole), 3.36 (s, 9H, -OCH₃), 3.54-3.64 (m,(-OCH₂CH₂-)_n and 6H,-CH₂OH), 3.90 (t, 6H,-CH₂OCH₃), 4.37 (t, 6H, -CH₂CH₂-triazole), 4.58 (t, 6H, -CH₂-triazole), 4.58 (t, 6H, -CH₂-triazole),

OCH₂CH₂triazole), 5.62 (s, 6H,-CH₂-), 7.77 (s, 3H, ArH), 7.83 (s, 3H, ArH), 7.94 (s, 3H, ArH), 8.07 (s, 3H, ArH), 8.14 (s, 3H, triazoleH), 8.21 (s, 3H, triazoleH) and 8.29 (s, 3H, triazoleH). 13 C{ 1 H} NMR (125 MHz, CDCl₃): δ (ppm) 25.7, 26.4, 28.8, 29.1, 29.2, 29.4, 29.7, 30.2, 32.8, 50.5, 53.4, 59.0, 62.9, 69.4, 70.4, 70.5, 71.9, 108.7, 123.1, 124.8, 124.9, 131.7, 132.4, 132.5, 135.9, 172.6. GPC: Mn=3450 g/mol. Mw/Mn=1.17.

Bifunctional dendrimer 9: To a solution of compound **8** (0.080g, 0.022 mmol), α-lipoic acid (0.015g, 0.07 mmol), and DMAP (0.005g, 0.04 mmoles) in DCM (10 mL), DCC (0.023g, 0.11 mmol) was added, and the solution was stirred at room temperature for 2h. It was filtered, and the solid was washed with more DCM (10 mL). The filtrate was washed with a saturated solution of NaHCO₃ (3x30 mL) and dried over MgSO₄. The solvent was then evaporated, and the residue was flushed on a silica column using 5% methanol in DCM. The solvent was evaporated again to yield viscous liquid (0.065g, 78%). ¹H NMR (400 MHz, CDCl₃): δ (ppm) 1.21-1.34 (m, 42H, -C**H**₂-), 1.38-1.50 (m, 6H, -C**H**₂-), 1.49-1.51 (m, 12H, -CH₂-), 1.87-1.91 (m, 12H, -CH₂-), 2.30 (t,6H,-CH₂COO-), 2.39-2.50 (m, 6H, -SCHCH₂-), 3.05-3.22 (m, 9H, -SSCH₂ and -SSCHCH₂-), 3.37 (s, 9H, - OCH_3), 3.54-3.64 (m,(- OCH_2CH_2 -)_n), 3.91 (t, 6H,- CH_2OCH_3), 4.02 (t, 6H, -CH₂OCO-), 4.39 (t, 6H, -CH₂CH₂-triazole), 4.59 (t, 6H, -OCH₂CH₂triazole), 5.65 (s, 6H,-CH₂-), 7.80 (s, 6H, ArH), 7.91 (s, 3H, ArH), 7.99 (s, 3H, ArH), 8.12 (s, 3H, triazole**H**), 8.23 (s, 3H, triazole**H**) and 8.32 (s, 3H, triazole**H**). ¹³C{¹H} NMR (125 MHz, CDCl₃): δ (ppm) 25.1, 25.9, 26.5, 28.6, 28.7, 29.4, 30.3, 34.1, 34.6, 38.5, 40.2, 50.4, 54.1, 56.3, 58.9, 64.5, 69.4, 70.5, 71.9, 120.3, 121.7, 122.4, 123.1, 124.8, 131.7, 132.4, 135.8, 146.4,146.5, 147.5, 173.5. GPC: Mn=2715 g/mol. Mw/Mn=1.14.

Compound 10: Compound 7 (0.150g, 0.11 mmol) and compound 3 (0.442g, 0.39 mmol) were dissolved in 3 mL of THF, followed by addition of sodium ascorbate (0.008g, 0.04 mmol). An aqueous solution (1 mL) of CuSO₄.5H₂O (0.005g, 0.02 mmol) was added dropwise to the solution. The reaction mixture was left to stir for 48h at room temperature. THF was then evaporated, and the remaining solution was extracted with DCM (3x20 mL), and then the organic layer was

extracted with brine (3x50 mL). It was dried over MgSO₄, and the solvent was evaporated. Silica-gel column chromatography was used to isolate the product with 8% methanol in DCM. The solvent was evaporated to yield the product as a viscous liquid (0.227g, 43%). ¹H NMR (400 MHz, CDCl₃): δ (ppm) 1.09 (br s, 63H, $-Si(C_3H_7)$), 1.21-1.34 (m, 42H, $-CH_2$ -), 1.49-1.51 (m, 6H, $-CH_2CH_2OH$), 1.97-2.01 (m, 6H, -C**H**₂CH₂-triazole), 3.36 (s, 9H, -OC**H**₃), 3.54-3.64 (m,(- OCH_2CH_2 -)_n and $6H_2CH_2OH_3$, 3.88 (t, $6H_2OCH_3$), 4.36 (t, $6H_2CH_2$ triazole), 4.56 (t, 6H, -OCH₂CH₂triazole), 5.58 (s, 6H,-CH₂-), 5.62 (s, 6H,-CH₂-), 7.43 (s, 3H, ArH), 7.76 (s, 3H, ArH), 7.79(s, 3H, ArH), 7.83 (s, 3H, ArH), 7.92 (s, 3H, ArH), 7.99 (s, 3H, ArH), 8.09 (s, 3H, ArH), 8.12 (s, 3H, triazole**H**), 8.18 (s, 3H, triazole**H**), 8.22 (s, 3H, triazole**H**) and 8.30 (s, 3H, triazole**H**). ¹³C{¹H} NMR (125 MHz, CDCl₃): δ (ppm) 11.2, 18.6, 25.6, 26.3, 28.8, 29.1, 29.2, 29.3, 30.1, 32.7, 50.4, 53.7, 53.9, 58.9, 62.6, 69.3, 70.4, 71.8, 92.2, 105.7, 120.6, 120.8, 120.9, 121.8, 122.9, 124.6, 124.7, 124.8, 124.9, 125.4, 129.3, 131.1, 131.4, 131.9, 132.0, 132.2, 135.4, 135.9, 154.9, 146.3, 146.4, 146.9, 147.2. GPC: *Mn*=4300 g/mol. Mw/Mn=1.17.

Compound 11: To a solution of compound **10** (0.227g, 0.05 mmol) in THF (3 mL) in a dry ice/acetone bath, a solution of Bu₄NF-1M solution in THF (0.14mL, 0.14 mmol) was added in a dropwise fashion. The reaction mixture was allowed to warm to room temperature and left to stir overnight. The solvent was removed under vacuum and the residue was extracted with DCM. The extract was then dried over MgSO₄, and solvent was evaporated. Silica-gel column chromatography was used to isolate the product with 8% methanol in DCM. The solvent was evaporated to yield the product as a transparent liquid (0.142g, 70%). ¹H NMR (400 MHz, CDCl₃): δ (ppm) 1.21-1.34 (m, 42H, -C**H**₂-), 1.49-1.53 (m, 6H, -CH₂CH₂OH), 1.90-1.99 (m, 6H, -CH₂CH₂-triazole), 3.15 (s,3H,-CCH-) 3.37 (s, 9H, $-OCH_3$), 3.54-3.64 (m,($-OCH_2CH_2$ -)_n and 6H, $-CH_2OH$), 3.89 (t, 6H,-CH₂OCH₃), 4.36 (t, 6H, -CH₂CH₂-triazole), 4.56 (t, 6H, -OCH₂CH₂triazole), 5.60 $(s, 6H, -CH_2), 5.64 (s, 6H, -CH_2), 7.37 (s, 3H, ArH), 7.79 (s, 3H, ArH), 7.83 (s, 4H, -CH_2), 5.64 (s, 6H, -CH_2), 5.64 (s, 6H, -CH_2), 7.87 (s, 3H, ArH), 7.79 (s, 3H, ArH), 7.83 (s, 4H, -CH_2), 5.64 (s, 6H, -CH_2), 7.87 (s, 3H, ArH), 7.79 (s, 3H, ArH), 7.83 (s, 4H, -CH_2), 7.87 (s, 3H, ArH), 7.89 (s, 3H, ArH),$ 3H, ArH), 7.93 (s, 3H, ArH), 7.94 (s, 3H, ArH), 8.03 (s, 3H, ArH), 8.12 (s, 3H, ArH), 8.16 (s, 3H, triazoleH), 8.20 (s, 3H, triazoleH), 8.26 (s, 3H, triazoleH) and 8.32 (s, 3H, triazole**H**). ¹³C{¹H} NMR (125 MHz, CDCl₃): δ (ppm) 13.5, 19.6, 23.8, 25.7, 26.3, 28.9, 29.1, 29.2, 29.3, 30.1, 32.7, 50.4, 53.6, 53.9, 54.0, 58.9, 62.7, 69.3, 70.4, 70.5, 71.9, 78.7, 82.5, 120.5, 120.6, 120.8, 121.8, 122.9, 123.6, 124.8, 125.7, 128.8, 129.3, 130.9, 131.4, 131.5, 131.9, 132.3, 135.7, 135.9, 140.0, 145.8, 146.4, 147.0, 147.3. GPC: *Mn*=3970 g/mol. *Mw/Mn*=1.14.

Compound 12: Compound **11** (0.075g, 0.018 mmol) and BODIPY-N₃ (0.034g, 0.07 mmol) were dissolved in 2 mL of THF, followed by addition of sodium ascorbate (0.004g, 0.02 mmol). An aqueous solution (1 mL) of CuSO₄.5H₂O (0.003g, 0.01 mmol) was added dropwise to the solution. The reaction mixture was left to stir overnight at room temperature. THF was then evaporated, and the remaining solution was extracted with DCM (3x20 mL), and then the organic layer was extracted with brine (3x50 mL). It was dried over MgSO₄, and the solvent was evaporated. Silica-gel column chromatography was used to isolate the product with 7% methanol in DCM. The solvent was evaporated to yield the product as a red liquid (0.069g, 69%). ¹H NMR (400 MHz, CDCl₃): δ (ppm) 0.99 (t, 18H, -ArCH₂CH₃), 1.19-1.34 (m, 42H, -CH₂-), 1.47-1.51 (m, 6H, - CH_2CH_2OH), 1.52-1.65 (m, 6H, -OOCCH₂CH₂-), 1.66-1.71 (m, 6H, -CH₂CH₂CH₂traizole), 1.72-1.98 (m, 12H, -CH₂CH₂triazole), 2.19 (s, 18H, -ArCH₃), 2.30-2.45(m, 18H, -OOCCH₂- and -ArCH₂CH₃), 2.47 (s, 18H, -ArCH₃), 3.37 (s, 9H, $-OCH_3$), 3.54-3.64 (m,($-OCH_2CH_2$ -)_n and 6H, $-CH_2OH$), 3.89 (t, 6H,-CH₂OCH₃), 4.16 (t, 6H, -CH₂CH₂triazole), 4.36 (t, 6H, -CH₂CH₂-triazole), 4.56 (t, 6H, -OCH₂CH₂triazole), 5.27 (s, 6H, ArCH₂OOCCH₂-) 5.57 (s, 6H, -CH₂-), 5.62 (s, 6H,-C**H**₂-), 7.73 (s, 3H, Ar**H**), 7.76-7.82 (m, 6H, ArH), 7.89 (s, 3H, ArH), 7.83 (s, 3H, ArH), 7.92 (s, 6H, ArH), 7.99 (s, 6H, ArH), 8.09-8.14 (m, 7H, ArH), 8.20 (s, 2H, triazole**H**) and 8.22-8.29 (m, 3H, triazole**H**). ¹³C{¹H} NMR (125 MHz, CDCl₃): δ (ppm) 12.6, 13.6, 14.7,17.1, 19.7, 23.9, 24.2, 24.9, 25.6, 25.7, 26.3, 28.2, 28.8, 29.4, 32.7, 33.6, 33.9, 34.1, 34.4, 34.9, 35.3, 49.7, 50.5, 59.0, 70.5, 70.6, 71.9, 104.9, 124.4, 124.9, 125.7, 125.9, 126.1, 131.1, 131.6, 131.9, 132.2, 133.3, 133.4, 133.6, 135.4, 136.3, 136.5, 136.9, 137.0, 146.4, 154.9, 172.9. GPC: *Mn*=3266 g/mol. *Mw/Mn*=1.02.

Trifunctional dendrimer 13: To a solution of compound **12** (0.055g, 0.01mmol), α-lipoic acid (0.010g, 0.05mmol), and DMAP (0.004g, 0.03 mmol) in DCM (3mL), 1-ethyl-3-(3-dimethylaminopropyl)carbodiimide (EDC) (0.015g, 0.05 mmol) was added, and the solution was stirred at room temperature for 12h. It was diluted with DCM (10 mL), and washed with water (2x20 mL), organic layer was dried over MgSO₄. The solvent was then evaporated, and the residue was purified on a silica column using 5% methanol in DCM. The solvent was evaporated again to yield viscous red liquid (42mg, 70%). ¹H NMR (400 MHz, CDCl₃): δ (ppm) 0.94 (t, 18H, -ArCH₂CH₃), 1.19-1.34 (m, 42H, -CH₂-),1.34-1.40 $(m, 6H, -OOCCH_2CH_2-), 1.42-1.48 (m, 6H, -CH_2-), 1.60-1.70 (m, 18H, -CH_2-),$ 1.80-2.00 (m, 18H, $-CH_2$ -), 2.19 (s, 18H, $-ArCH_3$), 2.30-2.45 (m, 18H, $-OOCCH_2$ and -ArCH₂CH₃), 2.46 (s, 18H, -ArCH₃), 3.05-3.22 (m, 9H, -SSCH₂ and -SSCHCH₂-), 3.22-3.27 (m, 6H, -CH₂OCO-), 3.36 (s, 9H, -OCH₃), 3.54-3.64 (m,(-OCH₂CH₂-)_n), 3.89 (t, 6H, -CH₂OCH₃), 4.17 (t, 6H, -CH₂CH₂CH₂triazole), 4.36 (t, 6H, -CH₂C**H**₂-triazole), 4.56 (t, 6H, -OCH₂C**H**₂triazole), 5.27 (s, 6H, $ArCH_2OOCCH_2$ -), 5.58 (s, 6H,-C H_2 -), 5.64 (s, 6H,-C H_2 -), 7.80-7.86 (m, 12H, ArH), 7.95-8.05 (m, 6H, ArH), 8.10-8.18 (m, 8H, ArH), 8.20-8.25 (m, 5H, ArH), and 8.25-8.32 (m, 5H, triazole**H).** ¹³C{¹H} NMR (125 MHz, CDCl₃): δ ppm 12.6, 13.6, 14.7, 17.1, 19.7, 24.1, 24.5, 24.7, 25.9, 26.5, 28.6, 28.7, 29.4, 29.7, 30.3, 34.1, 34.6, 38.5, 40.2, 50.1, 50.4, 50.5, 54.1, 56.3, 58.2, 58.9, 59.0, 64.5, 69.3, 70.4, 70.5, 71.9, 104.9, 121.9, 123.1, 123.2, 124.9, 125.0, 131.6, 132.1, 132.2, 132.3, 132.4, 133.5, 133.6, 135.9, 136.5, 146.4, 154.9, 172.9,173.6. GPC: *Mn*=2860 g/mol. *Mw/Mn*=1.06.

Miktoarm carrier 15: To a solution of compound 14 (0.035 g, 0.025 mmol) and DMAP (0.003g, 0.025 mmol) in DCM (3 mL) was added α-lipoic acid (0.008g, 0.04 mmol). Once the solution was fully dissolved, EDC (0.011g, 0.04 mmoles) was added and the solution was stirred under nitrogen overnight at room temperature in the dark. The reaction mixture was then added directly into a column and purified by silica gel column chromatography in a mixture of 5% methanol in DCM. The solvent was then evaporated to yield a red liquid (0.026g, 66%). 1 H NMR (400 MHz, CDCl₃): δ (ppm) 1.03 (t, 6H, -ArCH₂CH₃), 1.40-1.52

(m, 4H, -CH₂-), 1.60-1.80 (m, 4H, -CH₂-), 1.80-1.88 (m, 2H, -CH₂-),1.88-2.05 (m, 2H, -CH₂-), 2.23 (s, 6H, -ArCH₃), 2.35-2.45 (m, 10H, -CH₂-), 2.49 (s, 6H, -ArCH₃), 3.05-3.08 (m, 1H, -SSCHCH₂-), 3.36 (s, 3H, -OCH₃), 3.51-3.54 (m, 2H, -SSCH₂), 3.54-3.64 (m,(-OCH₂CH₂-)_n), 3.93 (t, 2H, -CH₂OCH₃), 4.40 (t, 2H, -CH₂CH₂CH₂triazole), 4.61 (t, 2H, -OCH₂CH₂triazole), 5.19 (s, 2H, ArCH₂OOCCH₂-), 5.32 (s, 2H, -CH₂-), 7.82 (s, 1H, ArH), 7.85 (s, 1H, ArH), 7.92 (s, 1H, ArH), 8.11(s, 1H, triazoleH) and 8.26 (s, 1H, triazoleH). ¹³C{¹H} NMR (125 MHz, CDCl₃): δ (ppm) 12.6, 14.7, 17.1, 24.2, 24.7, 25.9, 28.7, 29.9, 33.7, 34.0, 34.5, 38.5, 40.2, 50.1, 50.5, 56.4, 58.3, 59.0, 64.2, 65.9, 69.5, 70.5, 70.6, 71.9, 120.1, 121.5, 122.7, 124.9, 125.1, 131.5, 131.7, 132.2, 133.6, 136.4, 137.4, 154.9, 172.9, 173.3. GPC: *Mn*=840 g/mol. *Mw/Mn*=1.13.

Miktoarm carrier 17: The solution of compound **16** (300mg, 0.16 mmol), α lipoic acid (40mg, 0.18 mmol), EDC (60mg, 0.2 mmol), DMAP (20mg, 0.16 mmol) in DCM (5 mL) in a flame dried two neck round bottom flask was stirred under nitrogen atmosphere for 12h. The reaction mixture was diluted with water (10 mL) and extracted with dichloromethane (3x10 mL). The organic layer was separated and washed with brine (2x10 mL). It was then dried over anhydrous sodium sulphate and concentrated under reduced pressure. The compound was obtained as off white solid (250mg, 75%). ¹H NMR (400 MHz, CDCl₃): δ (ppm) 1.38-1.48 (m, 2H, $-CH_{2}$ -), 1.60-1.75 (m, 2H, $-CH_{2}$ -), 1.85-1.98 (m, 2H, $-CH_{2}$ -), 2.38 (t,2H,-C \mathbf{H}_2 COO-), 2.40-2.48 (m, 3H, -SCHC \mathbf{H}_2 -), 3.05-3.22 (m, 3H, - $SSCH_{2}$ - and $-SSCHCH_{2}$ -), 3.37 (s, 3H, $-OCH_{3}$), 3.54-3.64 (m,($-OCH_{2}CH_{2}$ -)_n), 3.90 (t, 6H, -C**H**₂OCH₃), 4.60 (t, 6H, -OCH₂C**H**₂triazole), 5.03 (s, 2H, -C**H**₂OCO), $5.15(s,4H,-OCH_2-)$, 6.59-6.63 (m, 3H, ArH), 7.95 (s, 2H, TriazoleH). $^{13}C\{^{1}H\}$ NMR (100 MHz, CDCl₃): δ (ppm) 24.6, 28.7, 30.9, 34.0, 34.5, 38.4, 40.2, 50.2, 56.3, 59.0, 61.9, 65.8, 69.9, 101.4, 107.1, 124.3, 138.4, 143.4, 159.5 and 173.2. GPC: *Mn*=1700 g/mol. *Mw/Mn*=1.05.

3.4.3 Biological studies:

3.4.3.1 Cell culture and media

Undifferentiated rat pheochromocytoma cells (PC12) were cultured in RPMI 1640 media (Invitrogen) containing 5% fetal bovine serum (Gibco), 1% penicillin–streptomycin (Gibco) and free of phenol-red. Cells were maintained at 37 °C, 5% CO₂ in a humidified incubator. Cells were seeded at 25,000 cells/well in 96 back well, clear bottom plates (Costar) and at 50,000 cell/well in 24 well plates (Costar). All cell treatments were performed in serum free media for the times indicated.

3.4.3.2 Assessment of cytotoxicity

To assess nanocarrier cytotoxicity, cells were incubated with Alamar Blue diluted in serum free media (10% vol/vol) for 1 hour following 24 hour exposure to dendritic nanocarriers. Mean fluorescent intensity was measured with a FLUOROstar Optima fluorimeter (BGM, Labtech) with filters were set to Ex/Em = 544/590 nm and employed 3x3 matrix well scanning.

3.4.3.3 Assessment of reactive oxygen species formation (ROS)

ROS formation was measured using dihydroethidium (DHE) (Molecular Probes), a fluorescent probe sensitive to super oxygen species. Following 6 hour pretreatment with nanocarriers, oxidative stress was induced with 300 μ M H₂O₂ for 1 hour. Cells were then washed and incubated in the dark for 30 mins with 10 μ M DHE. The conversion of DHE into highly fluorescent ethidium bromide was measured spectrofluoremetrically with a FLUOROstar Optima fluorimeter (BGM, Labtech) with filters set to Ex/Em = 544/612 nm and employed 3x3 matrix well scanning.

3.4.3.4 Spectrofluorometric measurements of total intracellular glutathione

GSH reacts specifically with non-fluorescent membrane permeable dye monochlorobimane (mCBi) to form a fluorescent adduct (mCBi-GSH). Following treatment, cells were washed and incubated at 37 °C with 50 μ M mCBi for 1 hour. mCBi containing media was aspirated, cells were washed with PBS and fresh serum free media was added. Fluorescence images were acquired with a Leica DFC350FX monochrome digital camera connected to a Leica DMI4000B

inverted fluorescence microscope. Fluorescent intensity of the mCBi-GSH adduct was measured with a FLUOROstar Optima fluorimeter (BGM, Labtech). Filters were set to Ex/Em = 380/460 nm and employed 3x3 matrix well scanning.

3.4.3.5 Cellular internalization of BODIPY labeled dendrimers

To assess cellular internalization, cells were treated with equimolar concentrations (1 μ M) of BODIPY conjugated dendritic compounds for 1 hour. Following treatment, the nucleus was labeled with Hoechst 33258 (10 μ M; 10 mins) and lipid droplets were labeled with free BODIPY 493/503 (20 μ M; 10 mins). Fluorescence images were acquired with a Leica DFC350FX monochrome digital camera connected to a Leica DMI4000B inverted fluorescence microscope.

3.5 References

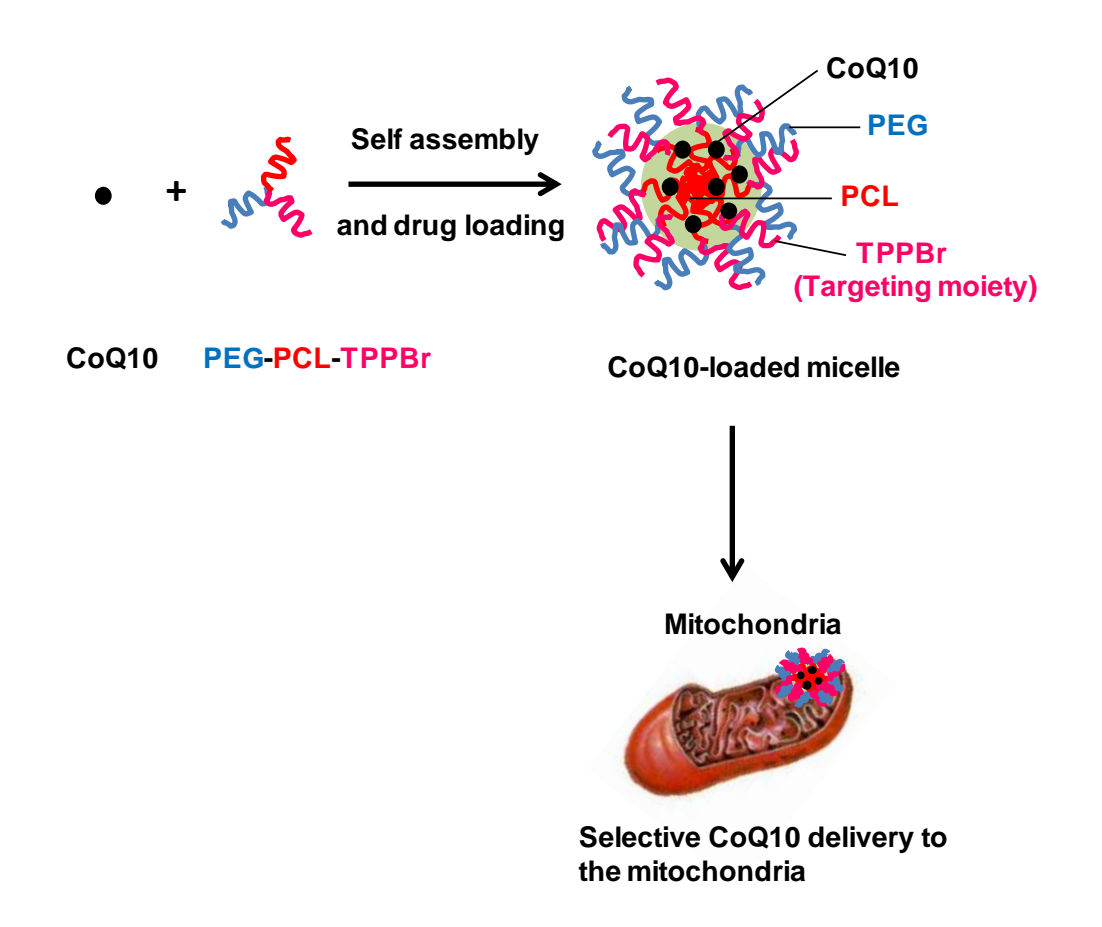
- (1) Tekade, R. K.; Kumar, P. V.; Jain, N. K. Chem. Rev. 2009, 109, 49–87.
- (2) (a) Wolinsky, J. B.; Grinstaff, M. W. Adv. Drug Delivery Rev. **2008**, 60, 1037–1055. (b) Menjoge, A. R.; Kannnan, R. M., Tomalia, D. A. Drug Discovery Today, **2010**, 15, 171-185.
- (3) Majoros, I. J.; Williams C. R.; Baker, J. R. Curr. Top. Med. Chem. **2008**, 8, 1165–1179.
- (4) Hourani, R.; Kakkar, A. Macromolecular Rapid Communications, **2010**, 31(11), 947-974.
- (5) (a) Tomalia, D. A.; Baker, H.; Dewald, J. R.; Hall, M.; Kallos, G.; Martin, S.; Roeck, J.; Ryder, J.; Smith, P. *Polym. J.* **1985**, *17*, 117–132. (b) Hawker, C. J.; Fréchet, J. M. J. *J. Am. Chem. Soc.* **1990**, *112*, 7638–7647. (c) Launay, N.; Caminade, A-M.; Majoral, J-P. *J. Am. Chem. Soc.* **1995**, *117*, 3282–3283. (d) Wu, P.; Feldman, A. K.; Nugent, A. K.; Hawker, C. J.; Scheel, A.; Voit, B.; Pyun, J.; Frechet, J. M. J.; Sharpless K. B.; Fokin, V. V. *Angew. Chem. Int. Ed.* **2004**, *116*, 4018–4022. (e) Franc, G.; Kakkar, A. K. *Chem. Eur. J.* **2009**, 15(23), 5630-5639.
- (6) (a) Wu, P.; Malkoch, M.; Hunt, J. N.; Vestberg, R.; Kaltgrad, E.; Finn, M. G.; Fokin, V. V.; Sharpless, K. B.; Hawker, C. J. Chem. Comm. 2005, 5775–5777.
 (b) Goodwin, A. P.; Lam S. S.; Fréchet, J. M. J. J. Am. Chem. Soc. 2007, 129, 6994–6995. (c) Franc, G.; Kakkar, A. Chem. Comm. 2008, 5267-5276. (d) Antoni, P.; Hed, Y.; Nordber, A.; Nystrom, D.; von Holst, H.; Hult, A.; Malkoch, M. Angew. Chem. Int. Ed. 2009, 48, 2126-2130. (e) Hourani, R.; Jain, M.; Maysinger, D.; Kakkar, A. Chem. Eur. J. 2010, 16(21), 6164-6168.
- (7) (a) Steffensen, M. B.; Simanek, E. E. Angew Chem Int Ed Engl. 2004, 43(39), 5178-5180.
 (b) Sivanandan, K.; Vutukuri, D.; Thayumanavan, S. J. Org. Chem. 2004, 69, 2937-2944.
 (b) Ornelas, C.; Weck, M. Chem. Comm. 2009, 38, 5710-5712.
 - (8) Franc, G.; Kakkar, A. K. Chem. Soc. Rev. 2010, 39(5), 1536 1544.
 - (9) Hourani, R.; Sharma, A.; Kakkar, A. Tett. Lett. **2010**, 51(29), 3792-3795.

- (10) Salinthone, S.; Yadav, V.; Bourdette, D. N.; Carr, D. Q. *Endocr. Metab. Immune Disord. Drug Targets*, **2008**, *8*, 132-142.
- (11) Ghibu, S.; Richard, C.; Vergely, C.; Zeller, M.; Cottin, Y.; Rochette, L. J. Cardiovasc. Pharmacol. **2009**, *54*(*5*), 391-398
- (12) Mijnhout, G. S.; Alkhalaf, A.; Kleefstra, N.; Bilo, H. J. *Biochim. Neth. J. Med.* **2010**, *68*(*4*), 158-162.
- (13) Jain, M. P.; Choi, A. O.; Neibert, K. D.; Maysinger, D. *Nanomedicine*, **2009**, *4*(*3*), 277-290.
- (14) Shay, K. P.; Moreau, R. F.; Smith, E. J.; Smith, A. R.; Hagen, T. M. *Biochim. Biophys. Acta.* **2009**, *1790*(*10*), 1149-1160.
- (15) Suh, J. H.; Shenvi, S. V.; Dixon, D. M.; Liu, H.; Jaiswal, A.K.; Liu, R. M.; Hagen, T. M. *PNAS*, **2004**, *101*(*10*). 3381-3386.
 - (16) Svenson, S. Eur. J. Pharm. Biopharm. 2009, 71, 445-462.
- (17) (a) Chung, J. E.; Kurisawa, M.; Uyama, H.; Kobayashi, S. 1st International Conference on Polyphenols and Health, Vichy, France, November 2003. (b) Lee, C. Y.; Sharma, A.; Uzarski, R. L.; Cheong, J. E.; Xu, H.; Held, R. A.; Upadhaya, S. K.; Nelson, J. L. *Free Radic. Biol. Med.* **2010**, DOI:10.1016/j.freeradbiomed.2010.10.699.
- (18) (a) Navath, R. S.; Kurtoglu, Y. E.; Wang, B.; Kannan, S.; Romero, R.; Kannan, R. M. *Bioconjugate Chem.* **2008**, *19*, 2446-2455. (b) Wang, B.; Navath, R. S.; Romero, R.; Kannan, S.; Kannan, R. *Int. J. Pharm.* **2009**, *337*, 159-168.
- (19) Sharma, A.; Khatchadourian, A.; Khanna, K.; Sharma, R.; Kakkar, A.; Maysinger, D. *Biomaterials*, **2011**, *32*, 1419-1429.
- (20) Soliman, G. M.; Sharma, R.; Choi, A. O.; Varshney, S. K.; Winnik, F. M.; Kakkar, A. K.; Maysinger, D. *Biomaterials*, **2010**, *31*, 8382-8392.
- (21) Shay, K. P.; Moreau, R. F.; Smith, E. J.; Smith A. R.; Hagen, T. M. *Biochim. Biophys. Acta*, **2009**, *1790*(*10*), 1149-1160.
 - (22) Khatchadourian, A.; Maysinger, D. Mol. Pharm. 2009, 6(4), 1125-1137.
- (23) (a) Kitchens, K. M.; Forker, A. B.; Kolhatkar, R. B.; Swaan, P. W.; Ghandehari, H. *Phar. Res.* **2007**, *24*(*11*), 2138-2145. (b) Shen, M.; Shi, X. *Nanoscale*, **2010**, 2, 1596-1610

- (24) Chauhan, A. S.; Diwan, P. V.; Jain, N. K.; Tomalia, D. A. *Biomacromolecules*, **2009**, *10*(*5*), 1195-1202.
- (25) Weber, E.; Hecker, M.; Koepp, E.; Orlia, W.; Czugler, M.; Csöregh, I. *J. Chem. Soc.*, *Perkin Trans.* **1988**, 2, 1251-1258.
- (26) Khanna, K.; Varshney, S.; Kakkar, A., *Macromolecules*, **2010**, *43*, 5688-5698.

Chapter 4

Design and Evaluation of Multi-functional Nanocarriers for Selective Delivery of Coenzyme Q10 to Mitochondria



In chapters 2 and 3, we have demonstrated the construction of multitasking dendrimers with the drug molecules covalently attached on their surface. Sometimes, the covalent attachment of drugs is not feasible due to several reasons; the drugs do not have appropriate functional groups to make covalent linkages, the drugs lose their biological response on making chemical changes in their structures, and some drugs are poorly water soluble and physical loading into the core of micelles can improve their aqueous solubility, as well as absorption

profile. The focus of research in this chapter is to explore the physical encapsulation of the drug molecules into hydrophobic core of miktoarm polymer micelles. The choice of miktoarm polymers over linear polymers is made due to their branched structure which can be utilized to attached a variety of targeting ligands or imaging molecules to make them multitasking. Miktoarm polymers have better drug loading capacities as compared to linear polymers.

Impairment of mitochondrial functions has been associated with failure of cellular functions in different tissues leading to various pathologies. In this chapter, we present a mitochondria–targeted nanodelivery system for coenzyme Q10 (CoQ10) which can reach mitochondria, and deliver CoQ10 in adequate quantities. CoQ10 is highly lipophilic and unstable when exposed to light. To overcome these limitations, a library of multifunctional nanocarriers based on ABC miktoarm polymers (A= PEG, B = polycaprolactone (PCL) and C = triphenylphosphonium bromide (TPPBr)) is synthesized. The polymers are self-assembled into nano-sized micelles, and employed for CoQ10-loading. Drug loading capacity, micelle size and stability are determined using a variety of techniques. Combined results from chemical, and biological experiments are discussed in detail. The versatility of the click chemistry used to prepare this new mitochondria-targeting nanocarrier offers a widely applicable, simple and easily reproducible procedure to deliver drugs to mitochondria or other intracellular organelles.

Reproduced in part with permission from Sharma, A.; Soliman, G. M.; Al-Hajaj, N.; Sharma, R.; Maysinger, D.; Kakkar, A. *Biomacromolecules* **2012**, 13, 239

Copyright, 2012, American Chemical Society

4.1 Introduction

Mitochondria, the power house of the cell, play a pivotal role in the homeostasis of vital physiological functions, including electron transfer, apoptosis, and calcium storage.^{1, 2} Mitochondrial dysfunction is associated with a variety of human disorders, such as neurodegenerative and neuromuscular diseases, obesity and diabetes, ischemia–reperfusion injury, cancer, and inherited mitochondrial diseases.² In many of these diseases a major cause of damage is mitochondrial overproduction of reactive oxygen species (ROS).^{3, 4} Therapeutics, such as creatine, coenzyme Q10 (CoQ10), N-acetyl cysteine (NAC), and α-lipoic acid have shown promising neuroprotective effects in *in vitro* and *in vivo* models of several neurodegenerative diseases.⁵⁻⁸

CoQ10, also known as ubiquinone, is a naturally occurring lipid-soluble, vitamin-like substance that is found in the inner mitochondrial and cellular membranes and in blood; both in high- and in low-density lipoproteins. CoQ10 is a benzoquinone derivative with 10 mono-unsaturated *trans*-isoprenoid units in the side chain (Figure 4.1). It functions primarily as a cofactor for the mitochondrial enzymes (complexes I-III) for the oxidative phosphorylation production of adenosine triphosphate (ATP), and is involved in several aspects of cellular metabolism. In its reduced form (CoQ10H₂, ubiquinol), it acts as a potent antioxidant and free radical scavenger, protecting membranes and lipoproteins from protein oxidation and lipid peroxidation. In vitro studies have shown that CoQ10 pre-treatment prevented a decrease in mitochondrial transmembrane potential and reduced mitochondrial ROS generation.

Several nanocarriers are currently being investigated for targeting drugs to specific sites with improved efficacy and reduced toxicity. 14-17 Polymeric micelles consist of a core-shell architecture: the core with the inner hydrophobic part of amphiphilic copolymer, which can encapsulate poorly water-soluble drugs and control their release, and the outer shell or corona is generally hydrophilic, which provides aqueous solubility and prevents the recognition of micelles by reticuloendothelial system (RES). In this regard, biocompatible and biodegradable polymers have been of specific interest in designing micelles for drug delivery.

Although polymeric micelles have been extensively studied for biomedical applications, most of the research has been focused on utilizing linear block copolymers. Amphiphilic miktoarm star-copolymers have gained considerable interest recently due to their unique aggregated morphologies in bulk, and self-assembly behavior in solution. Miktoarm polymers are branched macromolecules with linear polymeric chains emanating from a common central core, and these polymeric arms can vary in chemical identity and/or molecular weight. The composition of both the core as well as arms can be fine-tuned based on the desired application. The presence of multiple arms in miktoarm stars become advantageous for biological applications, as one could introduce multifunctionality, and covalently link targeting moieties and/or imaging molecules. In a covalently link targeting moieties and/or imaging molecules.

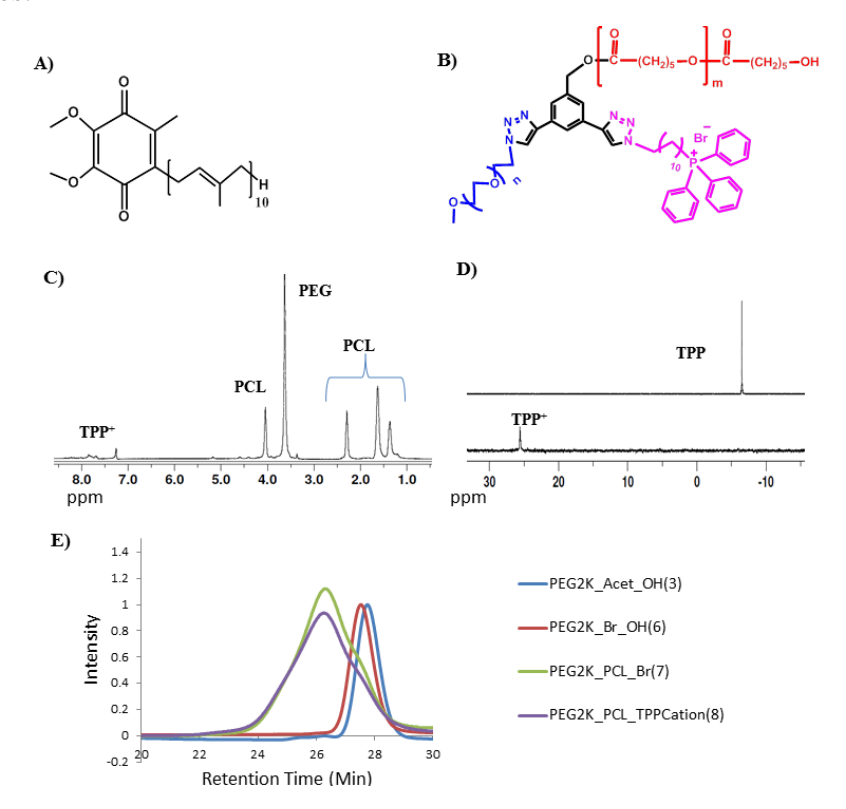


Figure 4.1. A) Chemical structure of CoQ10. B) Structure of ABC miktoarm polymer having PEG, PCL and TPP⁺. C) ¹H NMR of polymer with PEG, PCL and TPP⁺. D) ³¹P NMR of polymer with PEG, PCL and TPP⁺ and of free TPP alone showing a complete shift after attachment to polymer. E) GPC chromatogram showing a shift with increase in molecular weights upon addition of each arm.

We report here the design and construction of a mitochondria-targeting nanodelivery system for CoQ10 using ABC miktoarm star polymers which were constructed using "click" chemistry²²⁻²⁴ in combination with ring-opening polymerization. The synthesis was achieved by designing a molecular building block with three orthogonal functionalities which facilitated the performance of sequential "click" and ring-opening polymerization reactions. These star polymers self-assemble into micelles in an aqueous medium, in which the hydrophilic poly(ethylene glycol) (PEG) arm forms a corona, and the hydrophobic polycaprolactone (PCL) arm the core. Due to the ease and versatility of the CoQ10 loading and release from the miktoarm polymer micelles, as well as its extraordinary loading capacity, this carrier system can be exploited for other drugs with primary site of action within mitochondria.

4.2 Experimental section

4.2.1 Materials and methods

Water was deionized using a Millipore Milli-Q system. Coenzyme Q10 was obtained from Medisca Pharmaceutical Inc., Montreal, Quebec, Canada. Lipopolysaccharides, \(\epsilon\)-caprolactone (99%) and 3-(4,5-dimethylthiazol-2-yl)-2,5diphenyl tetrazolium bromide (MTT), copper (II) sulfate pentahydrate (CuSO_{4.5}H₂O) (>98.0%), sodium ascorbate (NaAsc, crystalline, 98%), tetrabutylammonium fluoride (Bu₄NF; 1M in THF) , 11-bromo-1-undecanol (98%), tetrabromomethane (CBr₄) (99%), triphenylphosphine (TPP), 1-[3-(dimethylamino)propyl]-3-ethylcarbodiimidemethiodide (EDC), (dimethylamino)pyridine (DMAP; 99%), and sodium azide (NaN₃; >99.5%) were purchased from Sigma Aldrich, St. Louis, MO, and used as received. All reactions were performed under dry conditions in an inert environment using dry and distilled solvents. Flash chromatography was performed using 60 Å (230-400 mesh) silica gel from EMD Chemicals Inc. Dialysis membranes (Spectra/por, MWCO: 6-8 kDa, unless otherwise indicated) were purchased from Fisher Scientific (Rancho Dominguez, CA). Penicillin, streptomycin and Griess reagent (1% sulphanilamide, 0.1% N-(1-naphthyl)-ethylenediaminedihydrochloride, 5% phosphoric acid) and fetal bovine serum were purchased from Invitrogen

(Carlsbad, CA). Murine microglia (N9) cell lines were obtained from ATCC. ε-Caprolactone was dried over calcium hydride for 24 h and distilled under reduced pressure prior to use. Fluorescein isothiocyanate (FITC; 95%) was purchased from Alfa Aesar.

4.2.2 Synthesis of ABC miktoarm polymers

The compounds, 3-(triisopropylsilylethynyl)-5-ethynylbenzyl alcohol (**1**) ²⁵, 11-azido-undecan-1-ol (**4**) ²⁶ and PEG 2K-azide ²⁷ were synthesized by adaptation of the previously published procedures.

Compound 2: 3-(Triisopropylsilylethynyl)-5-ethynylbenzyl alcohol (1) (0.50 g, 1.60 mmol) and PEG 2K-azide (2.57 g, 1.29 mmol) were dissolved in 3 mL of tetrahydrofuran (THF), followed by the addition of sodium ascorbate (0.031g, 0.16mmol). An aqueous solution (1 mL) of CuSO₄.5H₂O (0.020g, 0.16mmol) was added drop wise to the solution. The reaction mixture was left to stir overnight at room temperature. THF was then evaporated, and the remaining solution was extracted with dichloromethane (DCM), (3x20 mL), and the organic layer was washed with brine (20 mL). It was dried over Na₂SO₄, and the solvent was evaporated. The product was flushed through a silica gel column with 5% methanol in DCM. The solvent was evaporated to yield the product as a white solid (2.8 g, 75%). ¹H NMR (400 MHz, CDCl₃): δ (ppm) 1.13 (br s, 21H, - $Si(C_3H_7)$), 3.37 (s, 3H,-OCH₃), 3.54-3.87 (m, (-OCH₂CH₂-)n), 3.95 (t, 2H,-CH₂OCH₃), 4.64 (t, 2H, -OCH₂CH₂triazole), 4.80 (d, 2H, -CH₂OH), 7.47-7.49 (m, 3H, ArH), and 7.94 (s, 1H, triazoleH). ${}^{13}C\{{}^{1}H\}$ NMR (125 MHz, CDCl₃): δ (ppm) 11.3, 12.1, 18.8, 59.0, 63.0, 64.5, 69.3, 69.6, 70.5, 71.9, 90.9, 106.6, 124.3, 128.0, 130.0, 142.3 and 160.9.

Compound 3: To a solution of compound 2 (2.13 g, 0.92 mmol) in THF (3 mL) which was placed in a dry ice/acetone bath, a solution of Bu₄NF-1M solution in THF (1.8 mL, 1.85 mmol) was added in a drop wise fashion. The reaction mixture was allowed to warm to room temperature and left to stir overnight. The solvent was removed under vacuum, followed by the addition of water (10 mL), and the mixture was extracted with DCM (3x20mL). The extract was dried over Na₂SO₄, filtered and then the solvent was evaporated. Silica-gel column chromatography

was performed with 7% methanol in DCM. The solvent was evaporated to yield the product as a white solid (1.9 g, 95%). 1 H NMR (400 MHz, CDCl₃): δ (ppm) 3.11 (s, AcetH), 3.37 (s, 3H,-OCH₃), 3.54-3.87 (m, (-OCH₂CH₂-)n), 3.89 (t, 2H,-CH₂OCH₃), 4.59 (t, 2H, -OCH₂CH₂triazole), 4.70 (d, 2H, -CH₂OH), 7.44 (s, 1H, ArH), 7.86 (s, 1H, ArH), 7.91 (s, 1H, ArH), and 7.94 (s, 1H, triazoleH). 13 C{ 1 H} NMR (125 MHz, CDCl₃): δ (ppm) 50.6, 59.0, 64.2, 69.3, 69.6, 70.5, 70.6, 71.5, 71.9, 83.2, 122.0, 122.8, 124.5, 128.2, 129.9, 130.9, and 142.5.

Compound 5: To a solution of 11-Azido-undecan-1-ol (4) (2.00 g, 9.39 mmol) in DCM (2 mL), carbon tetrabromide (CBr₄) (4.04 g, 12.2 mmol) was added, followed by the addition of triphenylphosphine (TPP) (3.2 g, 12.2 mmol). The reaction mixture was left to stir at room temperature overnight. It was subsequently diluted with DCM (30mL), and the organic phase was washed with brine (3x30 mL). It was then dried over Na₂SO₄, and upon filtration solvent was removed under vacuum. The crude was then passed through a silica column using 10% ethylacetate in hexanes to yield a transparent liquid (2.0g, 77%). ¹H NMR (200 MHz, CDCl₃): δ (ppm) 1.22-1.50 (m, 10H, -CH₂-), 1.52-1.65 (m, 4H, -CH₂-), 1.79-1.90 (m, 4H, -CH₂-), 3.26 (t, 2H, -CH₂N₃) and 3.41 (t, 2H, -CH₂Br). ¹³C{¹H} NMR (125 MHz, CDCl₃): δ (ppm) 26.7, 28.1, 28.7, 28.8, 29.1, 29.4, 32.8 34.0, and 51.5.

Compound 6: Compounds **3** (0.90 g, 0.42 mmol) and **5** (0.14 g, 0.50 mmol) were dissolved in 3 mL of tetrahydrofuran (THF), followed by the addition of sodium ascorbate (0.008 g, 0.04 mmol). An aqueous solution (1mL) of CuSO₄.5H₂O (0.005 g, 0.04 mmol) was added dropwise to the solution. The reaction mixture was left to stir overnight at room temperature. THF was then evaporated, and the remaining solution was extracted with dichloromethane (DCM) (3x20 mL). The organic layer was washed with brine (20 mL) dried over Na₂SO₄, and upon filtration the solvent was evaporated. The product was flushed through a silica gel column with 5% methanol in DCM. The solvent was evaporated to yield the product as a white solid (0.90 g, 89%). ¹H NMR (400 MHz, CDCl₃): δ (ppm) 1.22-1.50 (m, 12H, -CH₂-), 1.52-1.95 (m, 6H, -CH₂-), 3.37 (s, 3H,-OCH₃), 3.53-3.70 (m, (-OCH₂CH₂-)n) & (m, 2H, -CH₂Br), 3.83 (t, 2H,-CH₂OCH₃), 4.41 (t, 2H,

-OCH₂CH₂triazole), 4.62 (t, 2H, -OCH₂CH₂triazole), 4.79 (br s, 2H, -CH₂OH), 7.83 (s, 1H, ArH), 7.89 (s, 1H, ArH), 7.93 (s, 1H, ArH), 8.19 (s, 1H, triazoleH) and 8.27 (s, 1H, triazoleH). ¹³C{¹H} NMR (125 MHz, CDCl₃): δ (ppm) 13.7, 19.8, 24.1, 26.4, 27.8, 28.1, 28.7, 28.9, 29.3, 29.6, 30.2, 30.9, 32.6, 32.8, 34.0, 50.5, 59.0, 61.6, 64.6, 68.5, 69.0, 69.2, 69.4, 69.6, 70.4, 70.5, 70.8, 71.5, 71.9, 72.6, 120.1. 121.7, 123.5, 130.8, 131.3, 142.8, 147.2, and 206.9.

Compound 7: General procedure for ring-opening polymerization (PEG2-PCL3.5-Br): A solution of compound 6 (50mg, 0.02mmol) in dry toluene (2 mL) was placed in a flame-dried two neck round bottom flask fitted with a condenser. The solution was degassed by evacuation, and distilled ε-caprolactone (0.07 mL, 0.67 mmol) was added with a syringe through rubber septa. A nitrogen purged solution of Sn(II) 2-ethylhexanoate (catalytic) in toluene (1 mL) was added to the reaction flask and the solution was refluxed for 24 h. The reaction mixture was then cooled to room temperature, and the solvent was removed under vacuum. The product was dissolved in dichloromethane and precipitated in cold methanol. The precipitated polymer was filtered and washed with diethylether to yield a white powder (102 mg, 83% yield). ¹H NMR (400 MHz, CDCl₃): δ (ppm) 1.22-1.50 (m, 12H, -CH₂-) & (m, -CH₂PCL), 1.52-1.95 (m, 6H, -CH₂-) & (m,-CH₂PCL), 2.30 (t, - CH₂PCL), 3.37 (s, 3H,-OCH₃), 3.54 (t, 2H, -CH₂Br), 3.55-3.72 (m, (-OCH₂CH₂-)n) & (m, 2H, -CH₂Br), 3.81 (t, 2H, -CH₂OCH₃), 3.93 (t, 2H, -CH₂), 4.05 (t, -CH₂PCL), 4.41 (t, 2H, -OCH₂CH₂triazole), 4.61 (t, 2H, -OCH₂CH₂triazole), 5.19 (s, 2H, -CH₂PCL), 7.77 (s, 1H, ArH), 7.85 (s, 1H, ArH), 7.90 (s, 1H, ArH), 8.10 (s, 1H, triazoleH) and 8.23 (s, 1H, triazoleH). ¹³C{¹H} NMR (125 MHz, CDCl₃): δ (ppm) 11.8, 13.9, 22.6, 22.9, 24.4, 24.5, 24.7, 25.2, 25.3, 25.5, 25.6, 26.4, 28.1, 28.2, 28.3, 28.5, 28.7, 29.0, 29.3, 29.5, 30.3, 31.6, 32.3, 32.8, 33.4, 34.1, 34.2, 34.3, 34.5, 46.8, 50.5, 59.0, 62.6, 63.4, 63.7, 64.0, 64.1, 64.2, 65.8, 69.3, 69.4, 70.5, 71.9, 120.1, 121.6, 122.7, 125.0, 125.1, 131.6, 137.4, 146.9, 147.0, 173.3, 173.5, 173.8, 173.7, 174.1, 175.9, and 179.4.

Compound 8 - General procedure for PEG2-PCL3.5-TPP⁺Br⁻: A solution of compound **7** (PEG2-PCL3.5-Br, 100 mg, 0.02 mmol) and triphenylphosphine (TPP) (8.8 mg, 0.03 mmol) in acetonitrile (ACN) was refluxed for 48 h. The

solvent was then evaporated and the residue was washed several times with hexanes and diethylether to remove excess of TPP. The white solid was then dried under vacuum to remove the solvents (88 mg, 85% yield). ¹H NMR (400 MHz, CDCl₃): δ (ppm) 1.20-1.50 (m, 12H, -CH₂-) & (m, -CH₂PCL), 1.52-1.95 (m, 6H, -CH₂-) & (m, -CH₂PCL), 2.29 (t, -CH₂PCL), 3.36 (s, 3H,-OCH₃), 3.55-3.80 (m, (-OCH₂CH₂-)n), (m, 2H, -CH₂Br) & (t, 2H, -CH₂Br), 3.80 (t, 2H,-CH₂OCH₃), 3.92 (t, 2H, -CH₂), 4.05 (t, -CH₂PCL), 4.41 (t, 2H, -OCH₂CH₂triazole), 4.59 (t, 2H, -OCH₂CH₂triazole), 5.17 (s, 2H, -CH₂PCL), 7.68-7.85 (m, 15 H, TPP⁺ & 2H, ArH), 8.01 (s, 1H, ArH), 8.16 (s, 1H, triazoleH) and 8.22 (s, 1H, triazoleH). ¹³C{¹H} NMR (125 MHz, CDCl₃): δ (ppm) 22.6, 1124.5, 25.4, 25.5, 26.3, 28.3, 28.9, 30.2, 32.3, 34.0, 34.1, 50.4, 59.0, 62.6, 64.0, 64.1, 65.9, 69.5, 70.5, 70.6, 71.9, 118.8, 121.6, 122.7, 122.8, 130.4, 130.5, 133.8, 135.0, 146.9, 173.4, 204.2, and 205.9. ³¹P NMR (200 MHz, CDCl₃): δ (ppm) 25.5.

Compound 9 (PEG2-PCL4.4-FITC-Br): A solution of FITC (8.5 mg, 0.01 mmoles) in DMSO (1mL) was stirred with 1-[3-(Dimethylamino)propyl]-3ethylcarbodiimidemethiodide (EDC) (4.02 mg, 0.02 mmoles) and 4dimethylaminopyridine (DMAP) (1.71 mg, 0.01 mmoles) for 20 minutes at room temperature, followed by the addition of PEG2-PCL4.4-Br (100 mg, 0.01 mmoles), and stirred at room temperature overnight. The reaction mixture was then dialyzed against DMSO for 48 h by changing DMSO every 8 h to remove excess FITC. It was then dialyzed against water for 12 h. The water was then removed under vacuum and the residue was washed several times with methanol to afford orange colored solid (42 mg, 43%). ¹H NMR (400 MHz, CDCl₃): δ (ppm) 1.22-1.50 (m, 12H, -CH₂-) & (m, -CH₂PCL), 1.52-1.95 (m, 6H, -CH₂-) & (m,- CH₂PCL), 2.30 (t, - CH₂PCL), 3.37 (s, 3H,-OCH₃), 3.54 (t, 2H, -CH₂Br), 3.55-3.72 (m, (-OCH₂CH₂-)n) & (m, 2H, -CH₂Br), 3.81 (t, 2H, -CH₂OCH₃), 3.93 (t, 2H, -CH₂), 4.05 (t, -CH₂PCL), 4.41 (t, 2H, -OCH₂CH₂triazole), 4.61 (t, 2H, -OCH₂CH₂triazole), 5.19 (s, 2H, -CH₂PCL), 6.57-6.85 (m, 6H, FITC ArH), 7.02-7.18 (m, 3H, FITC ArH), 7.77 (s, 1H, ArH), 7.85 (s, 1H, ArH), 7.90 (s, 1H, ArH), 8.10 (s, 1H, triazoleH) and 8.23 (s, 1H, triazoleH). ¹³C{¹H} NMR (125 MHz, CDCl₃): δ (ppm)13.6, 18.1, 24.4, 24.6, 24.7, 25.3, 25.4, 25.5, 25.6, 26.5, 26.8,

28.2, 28.3, 28.5, 28.8, 29.0, 29.3, 29.4, 29.7, 30.4, 30.9, 32.3, 32.6, 33.9, 34.1, 34.2, 36.3, 45.2, 46.8, 50.6, 52.6, 55.9, 59.1, 62.6, 64.1, 65.3, 65.9, 69.6, 70.6, 71.9, 85.6, 86.2, 118.8, 124.9, 125.0, 131.6, 137.4, 146.9, 157.1, 159.3, 171.1, 171.8, 173.3, 173.5, 173.6, 173.8, 196.4, 201.8, 207.1, 208.1, 213.1, 218.5, and 219.7.

Compound 10 (PEG2-PCL4.4-FITC-TPPBr): A solution of FITC (8.5 mg, 0.01 mmoles) in DMSO (1 mL) was stirred with 1-[3-(Dimethylamino)propyl]-3ethylcarbodiimidemethiodide (EDC) (4.02 mg, 0.02 mmoles) and 4dimethylaminopyridine (DMAP) (1.71 mg, 0.01 mmoles) for 20 minutes at room temperature, followed by the addition of PEG2-PCL4.4-TPPBr (100 mg, 0.01 mmoles) and was stirred at room temperature overnight. The reaction mixture was then dialyzed against DMSO for 48 h by changing DMSO every 8 h to remove excess FITC. It was then dialyzed against water for 12 h. The water was then removed under vacuum and the residue was washed several times with methanol to afford an orange colored solid (38 mg, 36%). ¹H NMR (400 MHz, CDCl₃): δ (ppm) 1.20-1.50 (m, 12H, -CH₂-) & (m, -CH₂PCL), 1.52-1.95 (m, 6H, -CH₂-) & (m,- CH₂PCL), 2.29 (t, - CH₂PCL), 3.36 (s, 3H,-OCH₃), 3.55-3.80 (m, (-OCH₂CH₂-)n), (m, 2H, -CH₂Br) & (t, 2H, -CH₂Br), 3.80 (t, 2H, -CH₂OCH₃), 3.92 (t, 2H, -CH₂), 4.05 (t, -CH₂PCL), 4.41 (t, 2H, -OCH₂CH₂triazole), 4.59 (t, 2H, -OCH₂CH₂triazole), 5.17 (s, 2H, -CH₂PCL), 6.57-6.85 (m, 6H, FITC ArH), 7.02-7.18 (m, 3H, FITC ArH), 7.68-7.85 (m, 15 H, TPP+& 2H, ArH), 8.01 (s, 1H, ArH), 8.16 (s, 1H, triazoleH) and 8.22 (s, 1H, triazoleH). ¹³C{¹H} NMR (125) MHz, CDCl₃): δ (ppm) 12.5, 13.1, 18.6, 24.4, 24.6, 24.7, 25.3, 25.5, 27.5, 28.3, 29.0, 29.2, 32.3, 33.9, 34.1, 34.2, 37.0, 37.6, 45.7, 47.1, 59.0, 59.6, 62.2, 62.6, 64.1, 67.7, 70.5, 71.9, 73.3, 76.0, 79.3, 81.3, 84.3, 86.6, 97.8, 124.0, 145.9, 155.1, 164.4, 170.1, 171.9, 173.6, 173.8, 184.4, 185.2, 187.1, 195.4, 201.1, 214.7, 217.2, 218.5, and 219.6.

Detailed synthesis and characterization of a series of targeted and non-targeted polymers are provided in the Supplementary section (Appendix 3).

4.2.3 Preparation of blank and CoQ10-loaded miktoarm micelles

Blank and CoQ10-loaded miktoarm micelles were prepared by the cosolvent evaporation method.¹⁷ Specific weights of the polymer and drug (drug/polymer ratio of 5-200 wt. %) were dissolved in 1.5 mL acetone. The solution was added drop-wise (1 drop/ 10 sec) to 3 mL of magnetically stirred deionized water. The mixture was stirred in the dark for 24 h to remove acetone and trigger micelle formation. The mixture was filtered through a 0.45 μm PVDF filter to remove the free (unencapsulated) drug. Aliquots of the micellar solutions were tested by dynamic light scattering (DLS) to determine the hydrodynamic diameter (*D*_H) and polydispersity index (PDI) of the micelles. Aliquots of the solution were freeze dried and used to determine drug content of the micelles by an HPLC assay.

4.2.4 Characterization

NMR spectra were recorded on a 200, 400 or 500MHz (as specified) Varian spectrometers at ambient temperatures. The chemical shifts in ppm are reported relative to tetramethylsilane as an internal standard for 1 H and 13 C { 1 H} NMR spectra. Molecular weight and polydispersity index (PDI) were obtained from GPC (Waters Breeze) using THF as the mobile phase. The GPC was equipped with three Waters Styragel HR columns (molecular weight measurement ranges: HR1: $10^{2} - 5 \times 10^{3}$ g mol $^{-1}$, HR2: $5 \times 10^{2} - 2 \times 10^{4}$ g mol $^{-1}$, HR3: $5 \times 10^{3} - 6 \times 10^{5}$ g mol $^{-1}$) and a guard column. The columns were operated at 40 °C and a mobile phase flow rate of 0.3 mL min $^{-1}$ during analysis. The GPC was also equipped with both ultraviolet (UV 2487) and differential refractive index (RI 2410) detectors. The molecular weight measurements were calibrated relative to poly(styrene) narrow molecular weight standards in THF at 40 °C.

FT-IR measurements were carried out on a Perkin Elmer Instrument equipped with ATR. Transmission electron microscopy (TEM) was used to capture images of the micelles using a Phillips CM200 electron microscope equipped with an AMT 2k x 2k CCD camera at an acceleration voltage of 80 kV. TEM samples were prepared by adding 10 µL of the aqueous micelle solutions onto a formvar-coated 400 mesh grid stabilized with evaporated carbon

film. The micelles were negatively stained by adding 10 μ L of 1% aqueous uranyl acetate solution. The samples were allowed to dry overnight at room temperature. Dynamic light scattering (DLS) measurements were carried out at a wavelength of 532 nm on a Brookhaven photon correlation spectrometer equipped with a BI9000 AT digital correlator and a compass 315M-150 laser (Coherent Technologies). Measurements were made at ~ 25 °C and at a 90° scattering angle. Mean hydrodynamic diameter measurements were obtained from a Gaussian fit of the CONTIN analysis mode from three averaged measurements of aqueous micellar solutions. Samples were filtered through a 0.45 μ m Millex Millipore PVDF membrane prior to measurements. Steady-state fluorescence spectra were recorded using a Fluoromax-2 spectrometer. Zeta potential measurements were performed using a Brookhaven ZetaPlus Zeta Potential Analyzer. Twenty zeta potential measurements were carried out at 25 °C on aqueous solution of polymeric micelles having 1.0 mM NaCl.

HPLC analysis of CoQ10 was performed on a Waters chromatography system equipped with Waters 1525μ binary HPLC pump, Waters 717plus autosampler, Waters Symmetry® C18 5 μm 4.6x150 mm column, Waters 2487 dual λ absorbance detector, and an IBM computer equipped with the Breeze® software. The assay was carried out at 25 °C using a 6:4 v/v mixture of ethanol-methanol at a flow rate of 1.0 mL/min. The injection volume was 20 μl and the run time was 12 min. CoQ10, monitored by its absorbance at 275 nm, and had a retention time \sim 8.9 min. A calibration curve ($r^2 \ge 0.999$) of CoQ10 was prepared using standard solutions ranging in concentration from 0.1 to 0.7mg/mL prepared immediately prior to the assay. To assay CoQ10 content of different miktoarm micelles, a given volume of aqueous micellar solution was diluted 10 times by the mobile phase. The solution was filtered through 0.2 μm Millex Millipore nylon filters and assayed by HPLC. Given volume of blank polymeric micelles was treated similarly and used as a control. CoQ10 encapsulation efficiency and loading capacity were calculated from the following equations:

4.2.5 Calculation of Flory Huggins interaction parameters (χ_{sm}) between CoQ10 and PCL

The Flory Huggins interaction parameter (χ_{sm}) between the micelle core and CoQ10 was calculated using equation

$$\chi_{\rm sm} = \frac{(\delta_{\rm CoQ10} - \delta_{\rm PCL})^2 V_{\rm CoQ10}}{RT}$$
(3)

 δ_{CoQ10} and δ_{PCL} are solubility parameters for CoQ10 and PCL, respectively; V_{CoQ10} is the molar volume of drug, R is the universal gas constant, and T is the Kelvin temperature. The solubility parameters were calculated by Hansen's approach²⁸, which uses partial solubility parameters to calculate the total solubility parameters according to equation^{29,30}:

$$\delta = (\delta_d^2 + \delta_p^2 + \delta_h^2)^{1/2}$$

where δ_d , δ_p , and δ_h refer to the partial solubility parameters accounting for van der Waals dispersion forces between atoms, dipole-dipole interactions between molecules, and proclivity of hydrogen bonding between molecules, respectively. The partial solubility parameters for CoQ10 and for PCL (Table 4.1, supporting information, Appendix 3) were estimated by the Hansen theory of solubility group contribution method (GCM) using Molecular Modeling Pro software (Chem SW) (Fairfield, CA).

4.2.6 Critical association concentration (CAC) of ABC miktoarm micelles

Given volumes of pyrene stock solution in acetone (180 μ M) were added to a series of 4 mL vials and the acetone was allowed to evaporate overnight in the dark. Blank miktoarm micelles were prepared following the general procedure described above. Specified volumes of the micellar solutions were added to the vials having pyrene so that polymer concentration varied from 0.025 to 200 μ g/mL while pyrene concentration was kept constant at 6 μ M. The pyrene/micellar solutions were equilibrated overnight in the dark. Excitation spectra were recorded from 260-360 nm at λ_{em} =390 nm (excitation and emission bandpass: 2 and 4 nm; respectively). The ratios of the pyrene fluorescence intensities at λ =338 and 333 nm (I_{338}/I_{333}) were calculated and plotted versus polymer concentration. The critical association concentration (CAC) values were determined from the graphs as the intersections of two straight lines (the horizontal line with an almost constant value of the ratio I_{338}/I_{333} and the vertical line with a steady increase in the ratio value).

4.2.7 Stability studies

4.2.7.1 Micelles colloidal stability

CoQ10-loaded micelles were prepared by the co-solvent evaporation method in de-ionized water and stored at 4 °C for 3 months. The particle size of micelles was measured on the freshly prepared sample and on weekly intervals after storage. The micelles were also periodically examined for signs of aggregation/precipitation.

4.2.7.2 Photostability of CoQ10

CoQ10 photostability was studied in a 35 x 35x 30 cm photoreactor equipped with 8 RPR-2537 Å UV lamps operating at λ_{max} of 253 nm (Southern New England Ultraviolet Co., Branford, CT). The studied samples were CoQ10 solution (0.5 mg/mL in 1:1 v/v ethanol acetone mixture) and CoQ10/PEG2-PCL3.8-TPPBr micelles (CoQ10 concentration: 0.5 mg/mL, polymer concentration 1 mg/mL, % CoQ10 loading: 33.34 wt. %). The samples were placed at the center of the UV chamber and 4 UV lamps were turned on. Samples

were withdrawn at predetermined time intervals and analyzed by HPLC for CoQ10 content as described above.

4.2.8 Differential scanning calorimetry (DSC) studies

Thermal analysis was carried out with a TA Q2000 differential scanning calorimeter (DSC) (TA Instruments, Newcastle, DE). The instrument was calibrated against an indium standard. The samples (2–5 mg) were accurately weighed into DSC aluminum pans. Empty pans were used as reference. The samples were heated at rate of 10 °C/min from 20 °C to 80 °C under nitrogen flushing (flow rate of 50 mL/min).

4.2.9 Cell culture and media

Murine microglia (N9) cells obtained from ATCC were seeded in Iscove's Modified Dulbecoo's Medium (IMDM) (Gibco) containing 5% of fetal bovine serum (Gibco) and1% penicillin–streptomycin (Gibco). For all experiments, unless otherwise stated, cells were seeded in 96-well plate (Costar) at a density of 2.5×10^4 cells/well maintained at 37 °C, 5% CO₂ in a humidified atmosphere and were grown in serum containing media for 24 hours before cell treatments to attain confluency. Cells were used between 10 and 30 passages.

For confocal microscopy experiments, primary hippocampal neurons and glia from 3-day-old mouse pups were isolated, mechanically and enzymatically (0.25% Trypsin, Gibco) dissociated. Cells were seeded at a density of 1×10⁵ cells/well onto coated glass coverslips. Coverslips were coated initially with laminin (0.587 ug/mL, Invitrogen) overnight. Cells were grown at 37 °C and 5% CO₂ in a 24-well coated cell culture plate (Corning), initially in phenol-free Dulbecco's Modified Eagle's Medium (Invitrogen) with 1 mm 1-Glutamine, sodium pyruvate and 1% (v/v) PSN (Invitrogen). On the second day-in-vitro (DiV), cells are cultured in Neurobasal A medium without phenol red (Invitrogen) supplemented with 2% (v/v) B-27 supplement (Invitrogen), 1% (v/v) PSN (Invitrogen), and 1 mm 1-Glutamine (Sigma). Half of the culture media was changed every 5 days (note that L-Glutamine was not added to the medium after

DiV 6). Cultures were maintained for 22 days in vitro prior to treatment and imaging.

4.2.10 Cells Viability

Mitochondrial metabolic activity of cells was measured using MTT assay. Media was aspirated and cells were treated in serum-free media with CoQ10/PEG2-PCL3.8-TPPBr (CoQ10-Targeted micelle), CoQ10, PEG2-PCL3.8-TPPBr (empty micelle) or CoQ10/PEG-PCL3.8-Br (CoQ10-Non targeted micelle) (0-50 μ M, calculated in equimolar concentrations with respect to CoQ10 for 24 h).

Following treatment media was removed and replaced with fresh serum-free media (200 μ l/well). MTT solution (0.5 mg/mL, Sigma) was added to each well and incubated for 30 min at 37° C. Formazan crystals were formed then dissolved by adding dimethylsulphoxide (DMSO, Sigma) and quantified by measuring the absorbance of the solution at 595 nm using Benchmark microplate reader (Bio-Rad, Canada). The extent of formazan conversion is expressed in percentages relative to the untreated control. Results are expressed as mean \pm SEM obtained from at least three independent experiments performed in triplicate.

4.2.11 Superoxide anion and reactive oxygen species detection

Superoxide anion and reactive oxygen species were detected using dihydroethidium (DHE, Molecular probes) and 2′,7′dichlorodihydrofluorescein diacetate (DCFH-DA, Molecular probes) respectively. Briefly, Media was aspirated and cells were treated in fresh serum-free media with methyl viologen dichloride (Paraquat, 10 μM, Sigma), or hydrogen peroxide (H₂O₂, 2 mM, EMD) followed by CoQ10/PEG2-PCL3.8-TPPBr (CoQ10-Targeted micelle), CoQ10 or CoQ10/PEG2-PCL3.8-Br (CoQ10-Non targeted micelle) (5 μM with respect to CoQ10 concentration for 24 hr). Following treatment, media were replaced with fresh media containing DHE (20 μM) or DCFH-DA (20 μM) and incubated for 30 min at 37°C. After which, cells were washed once with media (200 μl/well) and fresh serum free media was added. Fluorescence of ethidium and 2′,7′-dichlorodihydrofluorescein (DCF) was determined with Fluostar Optima

spectrofluorometer (BMG, LabTech) using excitation/emission wavelengths= 544/590 and 485/520 nm respectively. Results are expressed as mean ± SEM obtained from at least three independent experiments performed in triplicate. Representative fluorescent images of cells were acquired at 40x with a Leica DFC350FX monochrome digital camera connected to a Leica DMI4000B inverted fluorescence microscope.

4.2.12 Confocal microscopy

For mitochondrial membrane potential measurement experiments, primary cultures were treated with CoQ10/PEG2-PCL3.8-TPPBr (CoQ10-Targeted micelle), CoQ10 or CoQ10/PEG2-PCL3.8-Br (CoQ10-Non targeted micelle) 1 μM with respect to CoQ10 concentration for 24 h. Cells were then exposed to H₂O₂ (1 mM, 40 min). Media were aspirated and cells were incubated with media containing TMRE (tetramethylrhodamine ethyl ester, 100 nM, 30 min). To maintain the equilibrium of TMRE during live cells imaging, cells were incubated with fresh media containing 20 nM TMRE during imaging period. Images were acquired with a Zeiss LSM 710 confocal microscope using a W Plan Achromat 63X/1.0 M27 objective. Images were acquired at a resolution of 940 X 940 using HeNe (543 nm) and pinhole=92 μm. For each Z-stack, a total of 6-9 Z-slices were acquired using a scaling of 0.14 X 0.14 X 0.30 μm (x, y, z).

For FITC-mitochondria-targeted experiments, primary cultures were treated with FITC-PEG2-PCL3.8-TPPBr (FITC-Targeted micelles) or FITC-PEG2-PCL3.8-Br (FITC- Non targeted micelles) (1 μ M, 3 h). Cells were then treated with Mitotracker 633 (Molecular probes, 100 nM, 3 min). Images were acquired with a Zeiss LSM 710 confocal microscope using a W Plan Achromat 63X/1.0 M27 objective. Images were acquired at a resolution of 940 X 940 using HeNe (633 nm) and Argon (488 nm) lasers for detection of deep red and green respectively. Pinhole= 90 μ m. For each Z-stack, a total of 6-8 Z-slices were acquired using a scaling of 0.14 X 0.14 X 0.30 μ m (x, y, z).

4.2.13 Fluorescent microscopy for mitochondrial membrane potential measurement

N9 cells were co-treated with CoQ10/PEG2-PCL3.8-TPPBr (CoQ10-Targeted micelle), CoQ10 or CoQ10/PEG2-PCL3.8-Br (CoQ10-Non targeted micelle) 5 μM with respect to CoQ10 concentration or antimycin A (A.A, 1 μM) for 24 h. Following treatment, media were aspirated and cells were incubated with media containing TMRE (tetramethylrhodamine ethyl ester, 200 nM, 30 min). To maintain the equilibrium of TMRE during live cells imaging, cells were incubated with fresh media containing 50 nM TMRE during imaging period. Fluorescent images of cells were acquired at 40x with a Leica DFC350FX monochrome digital camera connected to a Leica DMI4000B inverted fluorescence microscope. Image analysis (mean fluorescence intensity measurements) was performed using Image J software. Results are expressed as mean ± SEM obtained from at least three independent experiments performed in triplicate.

4.3 Results and discussion

4.3.1 Synthesis and Characterization of ABC miktoarm polymers

ABC amphiphilic miktoarm stars were constructed on a three arm core (1) by performing "click" and ring opening polymerization reactions, in sequence. One arm of the core building block was used to attach a hydrophilic polymer (PEG) whose molecular weight (2000) was kept constant. Another arm was conjugated with a mitochondria targeting moiety, triphenylphosphonium (TPP⁺), and the third arm was used to carry out ring opening polymerization of caprolactone (Scheme **4.1**). This led to a series of miktoarm stars with variable molecular weights of polycaprocatone arm. The key building block (1) with free and protected acetylenes was synthesized using a procedure developed earlier in our group.^{25, 32} The free acetylene arm of 1 was utilized to covalently bind a PEG 2K chain using "click" reaction with PEG2K-azide in the presence of copper sulfate pentahydrate and sodium ascorbate. This click reaction was clean and simple, and gave a good yield of compound **2**. The ¹H NMR spectrum showed the disappearance of the alkyne proton, and appearance of PEG and triazole protons. It was then followed by the deprotection of triisopropylsilyl-acetylene group

which made the second acetylene available in compound 3 for the next click reaction. For the attachment of the targeting moiety TPP⁺, we clicked a linear azide (5) containing a bromo terminal point. The latter was synthesized from 11-Azido-undecan-1-ol (4), by converting its hydroxyl group to bromo, using carbon tetrabromide and triphenylphosphine. The ¹H NMR spectrum confirmed the formation of product **6** with the disappearance of acetylene proton and appearance of a triazole proton, along with protons in aliphatic region. The compound 6 with a PEG 2K chain, a bromo functional group and a third arm with free hydroxyl group, was then utilized to perform ring opening polymerization reactions using variable amounts of caprolactone monomer to get a range of molecular weights of polycaprolactone. Once again, the reaction was monitored by ¹H NMR which showed the appearance of PCL protons. These polymers containing PEG, PCL and –Br units (general structure, 6) were used as non-targeting polymers without triphenylphosphonium cation. Finally, the targeting moiety was attached to 6 by reacting with excess of triphenylphosphine. ¹H, ¹³C{¹H} and ³¹P{¹H} NMR spectra confirmed the attachment of triphenylphosphonium cation. A shift in ³¹P NMR was observed for TPP+ as compared to free TPP, and it also clearly indicated the absence of any excess (free) TPP (Figure 4.1D). GPC chromatogram showed clear shift with the addition of each arm on the core (Figure 4.1E). In addition, we coupled targeted and non-targeted polymers to an imaging dye, Fluorescein isothiocyanate (FITC) to trace these polymers in the cells (Scheme 4.2)

Scheme 4.1. Synthesis of ABC miktoarm star polymers containing PEG, PCL and triphenylphosphonium bromide.

i) $CuSO_4 \cdot 5H_2O/Sodium$ ascorbate, H_2O/THF , RT, over night (O/N); ii) tetrabutylammoniumfluoride (TBAF)/THF, O/N; iii) NaN_3/DMF , RT, O/N; iv) CBr_4 , Triphenylphosphine (TPP), DCM, O/N; v) $CuSO_4 \cdot 5H_2O/Sodium$ ascorbate, $H_2O/THF/DMF$, RT, O/N; vi) Toluene, Sn(II) 2-ethylhexanoate, Reflux, 24 h; vii) TPP, ACN, Reflux, 48 h.

Scheme 4.2. Synthesis of Fluorescein isothiocyanate (FITC) conjugated ABC miktoarm star polymer **9** (non-targeted) and **10** (with targeting moiety TPP⁺ cation)

i) 1-[3-(Dimethylamino)propyl]-3-ethylcarbodiimidemethiodide (EDC), 4-dimethylaminopyridine (DMAP), DMSO, RT, 12 h.

4.3.2 Preparation and characterization of miktoarm polymer micelles

We selected PEG as the hydrophilic arm of the ABC miktoarm polymers on the basis of its biocompatibility, hydrophilicity and ability to stabilize nanoparticles in aqueous solutions, whereas PCL was used as the hydrophobic arm due to its biocompatibility and ability to solubilize hydrophobic drugs in the micelle core, sustain their release and protect them against degradation. The lipophilic cation triphenylphosphonium (TPP⁺) was employed as the mitochondriotropic moiety, since its conjugates with antioxidant drugs CoQ10 (MitoQ) and α-tocopherol (MitoVitE)) have been shown to enhance drug accumulation in mitochondria. Empty and CoQ10-loaded miktoarm micelles were prepared in deionized water by the co-solvent evaporation method which is simple and easy to scale up. To optimize the size of the micelles, colloidal stability and CoQ10 loading capacity, a series of ABC miktoarm polymers were prepared in which the chain length of PEG arm was kept constant at 2 kDa, whereas that of the PCL arm was varied from 3.5 to 7.8 kDa (Table 4.1).

Table 4.1 GPC analysis of miktoarm polymers

^a:Determined from GPC measurements

Polymer	Mn ^a (g/mol)	Mw ^a (g/mole)	PDI
PEG2-PCL3.5-Br	5992	7339	1.22
PEG2-PCL3.5-TPPBr	6022	8126	1.34
PEG2-PCL3.8-Br	6252	8561	1.36
PEG2-PCL3.8-TPPBr	6284	8992	1.43
PEG2-PCL4.4-Br	6911	9150	1.32
PEG2-PCL4.4-TPPBr	7353	9863	1.34
PEG2-PCL5.5-Br	7932	11272	1.42
PEG2-PCL5.5-TPPBr	8374	11939	1.42
PEG2-PCL7.0-Br	9574	12999	1.35
PEG2-PCL7.0-TPPBr	11140	18693	1.67
PEG2-PCL7.8-Br	10247	12819	1.25
PEG2-PCL7.8-TPPBr	12072	20356	1.68

Polymers without triphenylphosphonium bromide (non-targeted polymers) were also prepared and used as control. Direct evidence of micelle formation was obtained from TEM measurements of PEG2-PCL7.0-TPPBr, which showed the presence of spherical, well-dispersed particles with an average diameter of 51.74±7.6 nm (Figure 4.2A). DLS measurements further confirmed the formation of monodispersed micelles as demonstrated in Figure 2B for PEG2-PCL3.8-TPPBr micelles. We subsequently studied the effect of polymer composition on

micelle size (Table **4.2**) by DLS. Increasing the chain length of PCL from 3.5 to 5.5 kDa did not result in a significant change in the hydrodynamic diameter of the micelles which remained around 30 nm (Table **4.2**). However, the hydrodynamic diameter increased from 30.9±2.5 to 65.5±1.9 nm when the PCL chain length was increased from 3.5 to 7.8 kDa. Longer PCL chains usually lead to the formation of bigger micelles due to their incorporation in the core of the micelles.^{17, 36}

Table 4.2 Properties of blank and CoQ10-loaded miktoarm polymers based micelles.

Polymer	Micelles diameter ^a		%DL ^b	%LE ^c	CoQ10 St ^d
	Blank micelles	CoQ10 micelles	-		(μg/mL)
PEG2-PCL3.5-Br	30.9 ± 2.5	40.2 ± 2.2	9.3	93	93
PEG2-PCL3.5- TPPBr	43.0 ± 1.9	57.7 ± 2.3	8.3	83	83
PEG2-PCL3.8-Br	31.8 ± 3.2	40.26 ± 1.9	9.2	92	92
PEG2-PCL3.8- TPPBr	36.5 ± 3.4	44.2 ± 2.7	8.5	85	85
PEG2-PCL5.5-Br	30.5 ± 3.2	40.26 ± 1.9	9.2	92	92
PEG2-PCL5.5- TPPBr	26.7 ± 3.4	39.7 ± 2.7	8.5	85	85

^a Hydrodynamic diameter (nm), mean of three measurements ±SD; ^bPercent drug loading = weight of CoQ10 in micelles x100/weight of micelles tested;

^cPercent loading efficiency = weight of CoQ10 in micelles x100/weight of CoQ10 used in micelles preparation. ^dCoQ10 solubility in water.

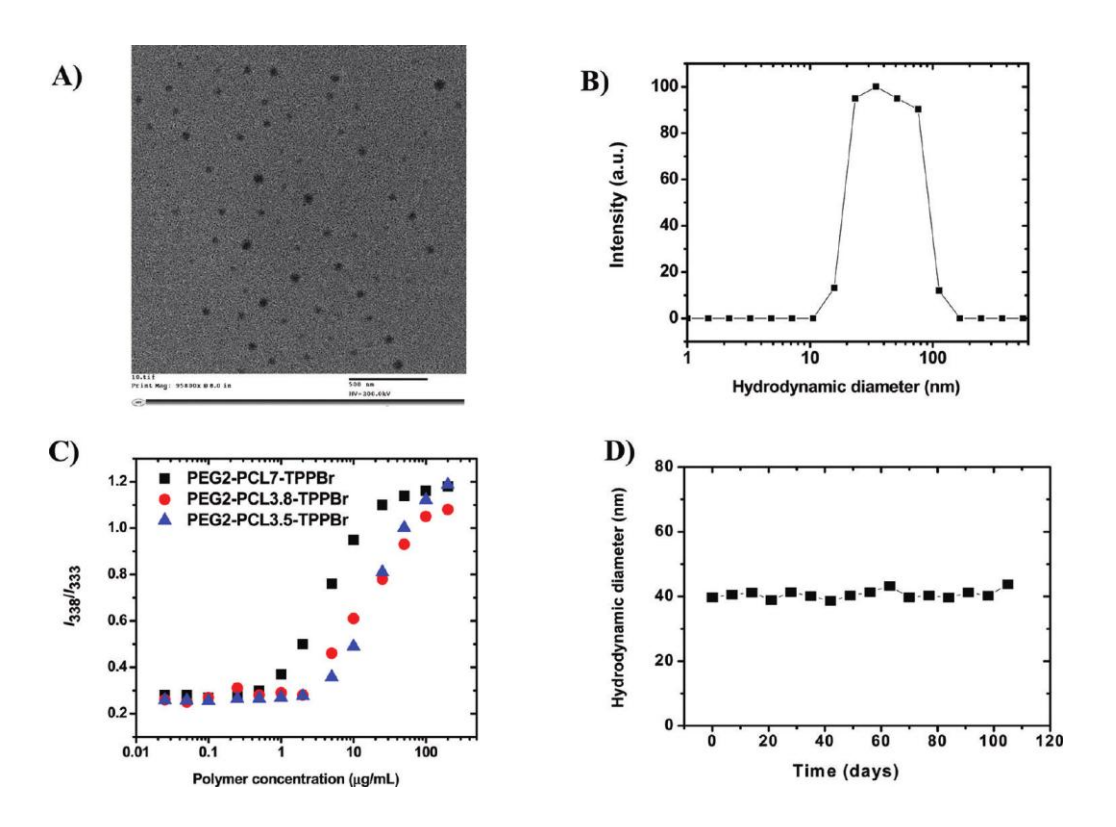


Figure 4.2. (A) TEM image of PEG2-PCL7-TPPBr micelles (polymer concentration = 1 g/L). (B) Distribution of the hydrodynamic diameter ($D_{\rm H}$) of PEG2-PCL3.8-TPPBr micelles (Deionized water; polymer concentration: 1 g/L; θ : 90°). (C) Plots of intensity ratio (I_{338}/I_{333}) of pyrene excitation spectra ($\lambda_{\rm em}$ = 390 nm) vs concentration of different PEG2-PCL-TPPBr miktoarm copolymers in water. (D) Hydrodynamic diameter of CoQ10-loaded/PEG2-PCL3.8-TPPBr micelles as a function of storage time at 4 °C (Deionized water; polymer concentration: 1 g/L; CoQ10 loading: 10 wt. %).

4.3.3 CoQ10 incorporation into PEG2-PCL-TPPBr miktoarm polymer micelles

CoQ10-loaded PEG2-PCL-TPPBr miktoarm polymer micelles were prepared by a co-solvent evaporation method. Confirmation of CoQ10 incorporation in the micelles core was obtained by ¹H NMR spectroscopy. ¹H NMR spectra of CoQ10, PEG2-PCL3.8-TPPBr and their mixture in CDCl₃,

together with the blank and CoQ10-loaded micelles in D₂O are shown in Figure 4.3. Characteristic signals of CoQ10 and PEG2-PCL3.8-TPPBr were observed when they were dissolved in CDCl₃ (Figure **4.3A** and **B**). A similar spectrum was observed for the CoQ10/PEG2-PCL3.8-TPPBr mixture in CDCl₃ (Figure **4.3C**) since it is a good solvent for both of them. In contrast, the spectrum of blank PEG2-PCL3.8-TPPBr micelles in D₂O showed signals characteristic of PEG protons (δ 3.26 and 3.57 ppm) confirming that they are well hydrated and reserved their mobility (Figure 4.3D). In this spectrum the characteristic signals of the PCL arm protons appear weak and broad due to incorporation into the micelles core and severe loss of movement (Figure 4.3D). Similarly, the spectrum of CoQ10/PEG2-PCL3.8-TPPBr showed weak and broad CoQ10 and PCL signals and strong well-resolved PEG signals. Taken together, these results confirmed the formation of nanoparticles in D₂O with core-corona structure. The core of the micelles is made up of PCL chains incorporating CoQ10, whereas PEG chains form the corona. Similar behavior has been reported earlier for other drug-loaded polymeric micelles.³⁷ It was also important to verify the location of the TPP cation since it should be at the micelle surface to direct them to the mitochondria. Signals at δ 7.4-7.8 ppm in Figure **4.3D** and **E** confirmed that the TPP cation is located in the corona of the micelles. This observation was further confirmed by zeta potential measurements of PEG2-PCL3.8-Br and PEG2-PCL3.8-TPPBr micelles in aqueous solution. The zeta potentials (-19.58 mV for PEG2-PCL3.8-Br micelles and +12.1 mV for PEG2-PCL3.8-TPPBr micelles) clearly suggested that the TPP cation is located on the surface of PEG2-PCL3.8-TPPBr micelles.³⁸

The incorporation of CoQ10 into the core of PEG2-PCL-Br and PEG2-PCL-TPPBr micelles increased the micelle hydrodynamic diameter (Table **4.2**). For instance, PEG2-PCL3.8-TPPBr had hydrodynamic diameters of 36.5 ± 3.4 and 44.2 ± 2.7 nm for empty and CoQ10-loaded micelle, respectively. Other mitochondria-targeted and non-targeted miktoarm polymers with PCL chain length of 3.5-5.5 kDa showed similar results (Table **4.2**), as well as CoQ10 loading efficiency of ≥ 83 % (Table **4.2**). However, aggregates with a hydrodynamic diameter > 600 nm were detected for CoQ10-loaded micelles with

a PCL chain length ≥ 6 kDa. The chain length of the hydrophilic PEG arm in these polymers (*i.e.*, 2 kDa) might not be enough to stabilize the nanoparticles with a much longer hydrophobic PCL arm (\geq 6kDa) and bulky triphenylphosphonium group. This hypothesis is supported by the observation that identical non-targeted polymers formed more stable nanoparticles. For instance, no aggregates were detected for PEG2-PCL7.0-Br and PEG2-PCL7.8-Br and the hydrodynamic diameters of their micelles were 46.8±3.2 and 60.2±1.5 nm, respectively. Based on these results, the miktoarm polymer PEG2-PCL3.8-TPPBr was selected for further studies.

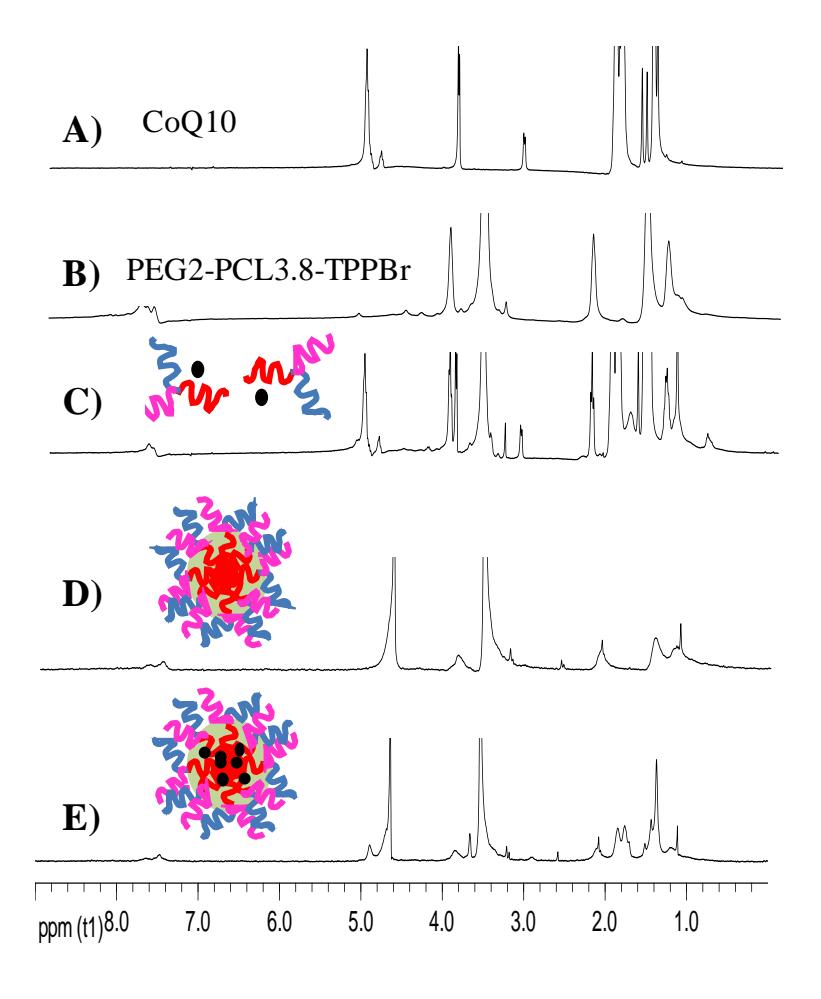


Figure 4.3. ¹H NMR spectra of CoQ10 in CDCl₃ (A), PEG2-PCL3.8-TPPBr miktoarm in CDCl₃ (B), CoQ10/PEG2-PCL3.8-TPPBr mixture in CDCl₃ (C), blank PEG2-PCL3.8-TPPBr miktoarm micelles in D₂O (D) and CoQ10-loaded PEG2-PCL3.8-TPPBr micelles in D₂O (E).

The effect of CoQ10/PEG2-PCL3.8-TPPBr weight feed ratio on the actual drug loading and micelle size was studied by preparing CoQ10-loaded micelles at CoQ10/polymer feed weight ratio varying from 0 to 200%. Micelle size increased linearly ($R^2 = 0.977$) with the CoQ10/polymer feed weight ratio (Figure 4.4A). For instance, the micelles hydrodynamic diameter increased from 30.97±1.5 to 102.3±1.9 nm when the CoQ10/polymer weight ratio increased from 0 to 125%. The increase in micelle size with the CoQ10/polymer ratio is possibly due to drug incorporation in the micelle core which results in core expansion to accommodate the loaded drug molecules.^{39, 40} The micelle size leveled off at CoQ10/polymer weight ratio of 125% and it remained unchanged thereafter and up to a weight ratio of 200%. Similar trend was observed for the effect of CoQ10/polymer feed weight ratio on the actual percent CoQ10 loading. Thus, the relationship between CoQ10/polymer feed weight ratio and actual CoQ10 loading was linear (R² = 0.997) for CoQ10/polymer weight ratio of 5-150%. The actual drug loading remained unchanged at CoQ10/polymer weight ratio ≥ 150%, indicating that maximum drug loading has been achieved at CoQ10/polymer weight ratio of 150%. The CoQ10 encapsulation efficiency was in the range of 72-99% for CoQ10/polymer feed weight ratio of 5-150%. No CoQ10 precipitation was observed for micellar solutions with CoQ10/polymer feed weight ratio of 5-150% after storage at room temperature for several weeks. This indicates that this high CoQ10 loading is not due to temporary supersaturation of the micelle. The CoQ10 content of the micelle at drug/polymer feed weight ratio of 150% is 60 weight%. This corresponds to CoQ10 concentration in aqueous solution of 1.5 mg/mL at polymer concentration of 1 mg/mL. CoQ10 is practically insoluble in water and this represents remarkable improvement in its aqueous solubility. 41

The CoQ10 content in these miktoarm polymer micelles is significantly higher than that obtained for other nanoparticulate formulations. For example, poly(lactide-co-gylcolide) (PLGA) nanoparticles had a maximum CoQ10 content of 19 and 38 weight%; poly(methyl methacrylate) (PMMA) nanoparticles had a CoQ10 content of 37 weight%, whereas nanoparticles based on chitosan and N-carboxymethylchitosan cross-linked with tripolyphosphate had a CoQ10 loading

capacity of 20 weight%. 42-44 Moreover, we have recently found that the maximum loading capacity of nimodipine, a hydrophobic calcium channel blocker into PCL-based linear and miktoarm polymers was ca. 3-5 weight% and was not affected by polymer architecture. The extent of drug loading into a given polymeric micelle formulation is dependent on many factors; the most important of which is the compatibility between the drug and the polymer. Several recent studies have shown that polymer-drug compatibility is a key factor in determining the performance of polymeric micelle as drug delivery systems where high compatibility results in higher drug solubility, loading capacity and controlled drug release. 30, 31, 45, 46

To explain the exceptionally high CoQ10 loading into PEG2-PCL3.8-TPPBr micelles, we used the Flory Huggins interaction parameter (γsm) to estimate the CoQ10-PCL compatibility, since it has been shown to be a good indicator of polymer-drug compatibility. 31, 47 The Hansen partial solubility parameters for CoQ10, nimodipine and PCL were obtained based on the group contribution method using the Molecular Modeling Pro software (Table 4.1, supporting information, Appendix 4). The Flory Huggins interaction parameter was calculated using equation 3, as described above. Maximum drug-polymer compatibility is achieved when the total solubility parameters for the drug and polymer are equal, resulting in γsm= 0. Smaller γsm values therefore indicate good compatibility between a given drug and polymer. The γsm was found to be 4.57 and 2.54 for nimodipine-PCL and CoQ10-PCL, respectively (Table 4.1, supporting information, Appendix 4) confirming that CoQ10 is more compatible with PCL compared to nimodipine. This in turn explains, at least in part the superior CoQ10 loading into PEG2-PCL3.8-TPPBr micelles. The Flory Huggins theory does not take into consideration any specific interactions between the polymer and drug, and assumes that the orientation of molecules within the polymer-drug mixture is completely random. Although this may not be true for either CoQ10-PCL or nimodipine-PCL systems, the calculated xsm values could serve as a guide in evaluating the relative compatibility between a given polymer and different drugs.

4.3.4 Thermal analysis

To get insight into the status of CoQ10 when it is loaded into PEG2-PCL3.8-TPPBr micelle, differential scanning calorimetry (DSC) thermograms were recorded for CoQ10-and polymer alone, their physical mixture at CoQ10 content of 34 weight%, and the micelle with CoQ10 loading of 34 weight%. The crystallinity of the incorporated drug affects several aspects of the performance of the drug delivery system, such as drug loading capacity, micelles stability and drug release profile. The thermogram of CoQ10 alone shows a sharp endothermic peak at 50.48°C ascribed to the melting of CoQ10 (Figure **4.4B**). The thermogram of CoQ10 (Figure **4.4B**).

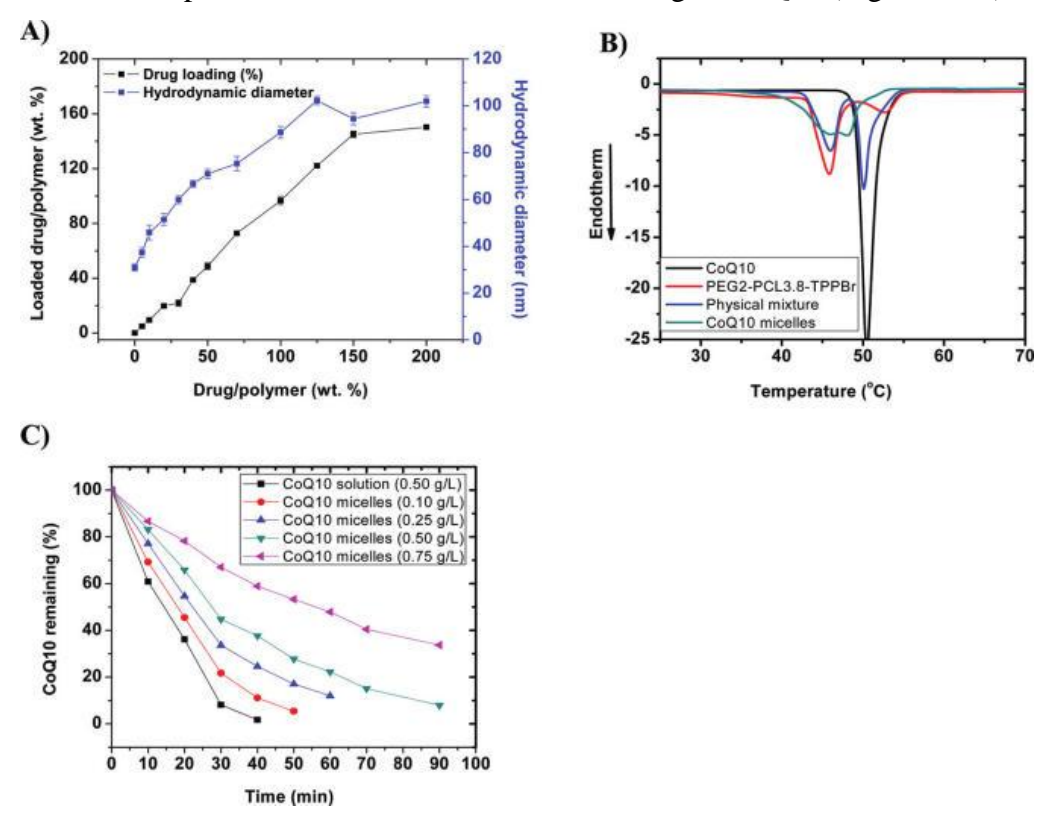


Figure 4.4. (A) Effect of drug/polymer weight feed ratio on drug loading capacity and micelles hydrodynamic diameter of CoQ10/PEG2-PCL3.8-TPPBr micelles prepared in deionized water at polymer concentration of 1 mg/mL. (B) DSC thermograms of CoQ10 alone, PEG2-PCL3.8-TPPBr alone, their physical mixture and micelles prepared at 35 wt% CoQ10 loading. (C) Percentage remaining of different CoQ10 samples as a function of storage time under UV light ($\lambda = 254$ nm).

The thermogram of PEG2-PCL3.8-TPPBr alone shows two distinct endothermic peaks at 45.85 and 52.79 °C, attributed respectively to the melting of PEG and PCL.⁵¹ These two melting events suggest the existence of two distinct crystalline domains in the miktoarm polymer.³⁰ CoQ10/PEG2-PCL3.8-TPPBr physical mixture shows the same characteristic melting peaks for both CoQ10 and PEG2-PCL3.8-TPPBr copolymer (Figure **4.4B**). In contrast, the DSC thermogram of the lyophilized CoQ10/PEG2-PCL3.8-TPPBr micelle shows a bimodal endothermic peak at 45.40 and 48.31 °C corresponding, respectively to the melting of PEG and CoQ10 (Figure **4.4B**).

Crystallization of CoQ10 in the micelles is presumably due to the high drug content of the micelle (*i.e.* 34 weight %). It has been reported that lidocaine and clonazepam also showed crystallization in the micelle core at drug content of 30 weight%.^{52, 53} A broad endothermic shoulder is centered at 51 °C and could be attributed to the melting of PCL. The shift in the melting point of CoQ10 along with the weak melting endotherm of PCL in the thermogram of the lyophilized micelle suggest unique molecular interactions between CoQ10 and PCL arm of the miktoarm polymers. No interaction was detected between CoQ10 and PEG arm of the polymers as indicated by the unchanged melting point of PEG in the thermogram of lyophilized micelle (Figure **4.4B**). Similar results were reported for quercetin/PEG-PCL micelles where the decrease in the PCL melting point in the drug-loaded micelle was attributed to quercetin-PCL hydrophobic interactions.⁵⁴

4.3.5 Stability studies

4.3.5.1 Critical association concentration (CAC)

Polymeric micelles are subjected to extensive dilution in the blood stream following intravenous administration resulting in pre-mature drug release if the micelle concentration falls below their CAC. Low CAC values therefore ensure that micelles remain stable while in circulation till they reach their target and deliver their payload. CACs of PEG2-PCL-TPPBr were measured using pyrene as a fluorescent probe. Excitation spectra of aqueous polymer solutions containing 6

μM pyrene and increasing polymer concentrations were recorded from 260-360 nm at λem=390 nm. Pyrene photophysical properties depend on its microenvironment; its excitation spectrum undergoes a red shift from 333 to 338 nm when it passes from hydrophilic to hydrophobic media. Semi-logarithmic plots of the I_{338}/I_{333} ratios versus the concentration of PEG2-PCL-TPPBr miktoarm polymers having different PCL chain lengths are shown in Figure 4.2C. The I_{338}/I_{333} ratio remained almost constant at low polymer concentration and increased sharply when the polymer concentration reached its CAC. The CAC values determined from the graphs were 3.23, 1.91 and 0.27μg/mL for PEG2-PCL3.5-TPPBr, PEG2-PCL3.8-TPPBr and PEG2-PCL7.0-TPPBr miktoarm polymers, respectively. The decrease in the CAC values with increasing PCL molecular weight at a given PEG molecular weight is consistent with other reports, and suggests increased micellar thermodynamic stability against dilution.

4.3.5.2 Physical stability of the CoQ10-containing micelles

CoQ10/PEG2-PCL3.8-TPPBr micelles with a CoQ10 content of 10 weight% were kept at 4 °C and their hydrodynamic diameter was determined by DLS as a function of storage time. The micelles were also visually inspected for signs of precipitation/aggregation. As shown in Figure **4.2D**, no noticeable change in micelle size was observed and micelle diameter of about 40 nm was maintained for more than 3 months. Moreover, no signs of drug precipitation/micelle aggregation were observed during this period. This confirms micelle stability upon storage at 4 °C.

4.3.5.3 CoQ10 photostability

CoQ10 is known to be susceptible to degradation when exposed to UV irradiation, heat or oxygen. ^{43, 57} CoQ10 incorporated in PEG2-PCL3.8-TPPBr micelles ([CoQ10] = 0.1-0.7 mg/mL), as well as CoQ10 solution in a mixture of ethanol-acetone 1:1 v/v ([CoQ10] = 0.5 mg/mL) were exposed to UV irradiation (λ = 254 nm) at ambient temperature, and the residual CoQ10 content was determined by HPLC. As illustrated in Figure **4.4C**, CoQ10 concentration in

ethanol-acetone mixture rapidly decreased upon exposure to UV irradiation and less than 2% CoQ10 remained after 40 min. In contrast, CoQ10 incorporated in the micelle at different concentrations was much more resistant to UV degradation. For instance, after 40 min UV irradiation of the micelle with a CoQ10 concentration of 0.5 mg/mL, around 25% CoQ10 remained intact. To determine the reaction rate constant (K) and half-life ($T_{0.5}$) of CoQ10 degradation, the data was fitted to zero and first order kinetics. CoQ10 degradation was found to follow first order kinetics as indicated by its higher correlation coefficient (R^2) compared to that of zero order kinetics (Table 4.2, supplementary information, Appendix 4). For the same CoQ10 concentration of 0.5 mg/mL, the degradation rate constant was more than three-fold higher for CoQ10 solution compared to micelle-incorporated CoQ10 (Table 4.2, supplementary information, Appendix 4). This was also reflected by more than 3-fold increase in the $T_{0.5}$ for the micelleentrapped CoQ10 (Table 4.2, supplementary information, Appendix 4). The enhanced stability of micelle-incorporated CoQ10 could be attributed to the entrapment of the drug in the hydrophobic micelle core which isolates CoQ10 from the aqueous environment. Moreover, the polymeric nanoparticles could act as a barrier preventing the UV rays from reaching the incorporated drug. Stability of micelle-entrapped CoQ10 was also dependent on the CoQ10 concentration in solution: higher CoQ10 concentrations had lower degradation rates (Figure 4.4C, Table 4.2, supplementary information, Appendix 4). UV lamps used in this study has constant intensity of UV radiations which degrade certain amount of CoQ10 during a given time period. This results in lower degradation rates for higher CoQ10 concentrations. Other nanoparticulate formulations have also shown higher CoQ10 stability against degradation by UV irradiation compared to CoQ10 solution in capryliccapric triglycerides oil or dispersion in sodium dodecyl sulfate. 43, 57

4.3.6 Localization of miktoarm nanocarrier in mitochondria and biological activity of CoQ10 in stressed microglia

The first aim in biological experiments was to show that miktoarm polymer-targeted to mitochondria indeed reaches this intracellular site. To this

end, we synthesized, characterized and tested in living cells micelles made of FITC-labeled miktoarm analog. Neural primary cultures were exposed to fluorescent micelles (1 μ M, 3 h) and live cell imaging using confocal microscope was performed (Figure **4.5** and supplemental Figure **4.1**, Appendix 4). Analyses of z-stacks collected from confocal microscopy with cells co-labeled with Mitotracker 633, indicated partial co-localization (yellow fluorescence in Figure **4.5**, see zoomed inset) of the carrier (green) with mitochondria (deep red). Micelles with non-covalently bound FITC were used as controls. Measurements of the overlap coefficients suggest consistently an increased co-localization (10-30%) of the micelles with mitochondria for the targeted micelles.

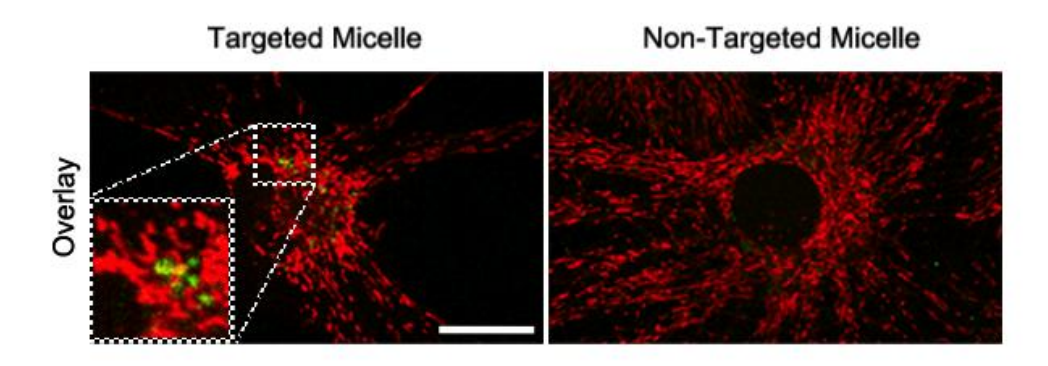


Figure 4.5. Confocal micrographs of primary hippocampal neurons and glia cells treated with FITC-PEG2-PCL3.8-TPPBr (1 μ M, 3 h, green fluorescence) or FITC-PEG2-PCL3.8-Br (1 μ M, 3 h, green fluorescence) and Mitotracker 633 (100 nM, 3 min, deep red fluorescence). More details provided in the Supplementary section, Appendix 4.

We subsequently investigated the effects of nanocarriers on mitochondrial metabolic activity using MTT assay (Supplemental Figure **4.2**, Appendix 4) and generation of reactive oxygen species (Figures **4.6A-D**). Results from the MTT assay showed that targeted micelles containing CoQ10 as well as CoQ10 alone in low micromolar concentrations (< 5 µM) enhance mitochondrial metabolic activity within 24 h. This increase is significant when compared with untreated cells or those treated with the carrier without the drug. In contrast, high concentrations of polymeric micelles and CoQ10 impaired mitochondrial activity

(Supplemental Figure **4.2**, Appendix 4). It is well known that there is an optimal therapeutic window for each drug which differs in different cell types. We have attempted to find this therapeutic window in neural cells of interest, and it turned out to be in relatively low concentration ranges (less than 5 uM), a desirable feature of the described nanosystem containing CoQ10. An excess of CoQ10 (as well as higher carrier concentrations) is deleterious to microglia because an excessive matrix uptake of CoQ10 can depolarize mitochondria.

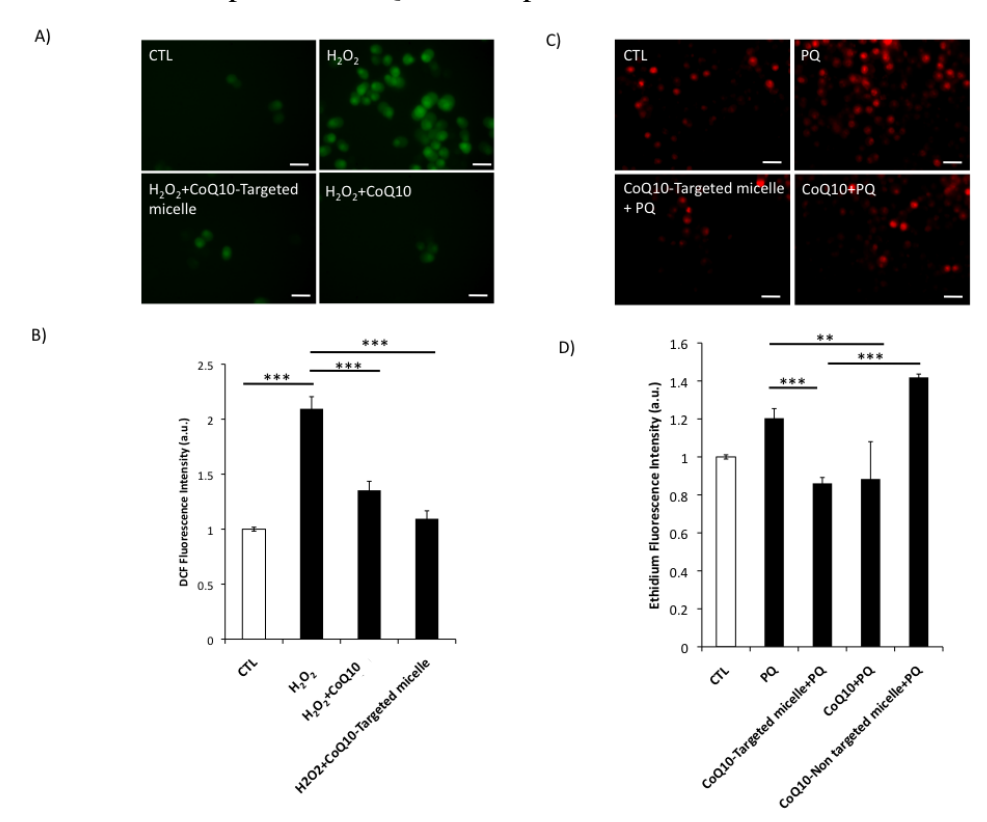


Figure 4.6. Production of reactive oxygen species (ROS), (A) Fluorescent micrographs showing ROS generation following H_2O_2 exposure. (B) Spectrofluorometric detection and quantification of ROS. (C) Fluorescent micrographs showing superoxide anion generation. (D) Spectrofluorometric detection and quantification of ethidium fluorescence intensity. More details are provided in the Supplementary section, Appendix 4.

We next examined if CoQ10, liberated from the nanodelivery system, can reduce the impairment of mitochondria caused by H_2O_2 in primary hippocampal cultures. Confocal micrographs of neural cells (neurons and glia) treated with CoQ10 prior to the exposure to H_2O_2 (1 mM, 40 min) showed that CoQ10

treatment was effective (Figure 4.6), as measured by the fluorescence intensity of TMRE. TMRE fluorescence was consistently stronger in the presence of CoQ10 as compared to H_2O_2 insult alone suggesting the effectiveness of CoQ10 to maintain normal mitochondrial potential (Figure 4.7).

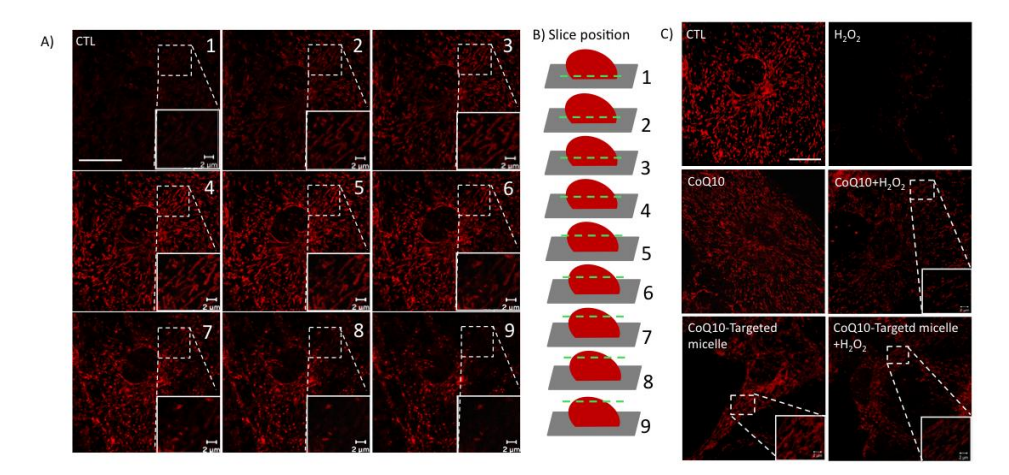


Figure 4.7. Mitochondrial membrane potential measured by TMRE in H₂O₂ stressed cells is partially retained upon treatment with CoQ10 alone or released from the nanodelivery system. Primary hippocampal neurons and glia were treated as described in the Materials and methods section. A) Z-Stack confocal micrographs of 9 confocal sections for control cells (CTL) treated only with TMRE (100 nM, 30 min) taken at an interval of 0.3 µm. Insets represent the enlarged area (zoomed) for each corresponding section. Scale bar (20 µm) in control is representative for all panels. Scale bar (2 µm) is representative for all zoomed areas. B) Schematic illustrating the position along the Z-axis with respect to sections shown in A (numbered 1-9). C) Confocal micrograph of live cells showing loss in mitochondrial membrane potential following H₂O₂ exposure (1 mM, 40 min) using TMRE (100 nM, 30 min) that was partially retained in cells pretreated with CoQ10 (1 µM, 24 hr) and CoQ10-Targeted micelle (1 µM, 24 hr) compared to untreated control (CTL). Each image represents a Z-stack consisting of 6-9 confocal sections taken at an interval of 0.3 µm. Scale bar (20 µm) in control is representative for all panels. Scale bar (2 µm) is representative for all zoomed areas. Images were acquired using HeNe (543 nm) excitation laser.

To prove that micelles prepared from miktoarm-carrying CoQ10 retained the drug biological activity within the low micromolar concentrations, we used three different stress paradigms: (1) H_2O_2 exposure (2 mM, 3 h), (2) paraquat treatment (10 μ M, 24 h) and (3) exposure to antimycin A (A.A, 1 μ M, 24 h; Figures **4.6A-D** and supplemental Figure **4.3**, Appendix 4). Results from these

studies clearly show that the treatment with CoQ10 with or without carrier in two stress models *i.e.* H_2O_2 treatment and exposure to paraquat, significantly reduced their impact of these insults in microglia cells, supporting previous findings that CoQ10 is an effective antioxidant agent. However, a strict control over the intracellular concentration range is required to achieve optimal mitochondrial protection and retention of physiological functions^{13, 58}. Exposure of microglia cells to antimycin A (A.A, 1 μ M, 24 h) led to a significant reduction in mitochondrial potential as measured by TMRE fluorescence (200 nM, 30 min). CoQ10 treatment alone and CoQ10 from the targeted micelle, corrected this mitochondrial impairment, whereas CoQ10 in non-targeted micelles was ineffective.

4.4 Conclusions

We have developed an easy and efficient way of constructing multifunctional miktoarm polymer-based nanocarriers for the delivery of CoQ10, using a combination of click chemistry with ring-opening polymerisation. Results from our studies demonstrate that miktoarm polymers form micelles in an aqueous medium and are able to incorporate extraordinarily large quantities of CoQ10, not commonly seen with other carrier systems. CoQ10 micelles are suitable means of drug delivery to mitochondria, exerting beneficial antioxidant effects in insulted neural cells. The described miktoarm-based polymers provide versatile and widely applicable nanocarriers to overcome several CoQ10 limitations. In addition, they can be exploited for other novel site-directed nanodelivery systems and accommodate different pharmacological agents, individually or in combination. The latter is of particular interest for further pharmacological interventions in pathologies where multiple factors contribute to the mitochondrial impairment.

4.5 References

- 1. Moreira, P. I.; Zhu, X.; Wang, X.; Lee, H.-g.; Nunomura, A.; Petersen, R. B.; Perry, G.; Smith, M. A., *Biochim. Biophys. Acta, Mol. Basis Dis.* **2010,** *1802*, 212-220.
- 2. Yamada, Y.; Harashima, H., Adv. Drug Delivery Rev. **2008**, 60, 1439-1462.
- 3. Moreira, P. I.; Santos, M. S.; Oliveira, C. R., *Antioxid. Redox Signaling* **2007**, *9*, 1621-1630.
- 4. Finkel, T., *Nat. Rev. Mol. Cell Biol.* **2005**, *6*, 971-976.
- 5. Brewer, G. J.; Wallimann, T. W., J. Neurochem. 2000, 74, 1968-1978.
- 6. Moreira, P. I.; Harris, P. L. R.; Zhu, X. W.; Santos, M. S.; Oliveira, C. R.; Smith, M. A.; Perry, G., *J. Alzheimers Dis.* **2007**, *12*, 195-206.
- 7. Yang, X. F.; Yang, Y.; Li, G.; Wang, J. Z.; Yang, E. S., *J. Mol. Neurosci.* **2008**, *34*, 165-171.
- 8. Weissig, V., *Pharm. Res.* **2011**, 28, 2633-2638.
- 9. Villalba, J. M.; Parrado, C.; Santos-Gonzalez, M.; Alcain, F. J., *Expert Opin. Invest. Drugs* **2010**, *19*, 535-554.
- 10. Wolf, D. E.; Hoffman, C. H.; Trenner, N. R.; Arison, B. H.; Shunk, C. H.; Linn, B. O.; McPherson, J. F.; Folkers, K., *J. Am. Chem. Soc.* **1958**, *80*, 4752-4752.
- 11. Littarru, G.; Tiano, L., Mol. Biotechnol. 2007, 37, 31-37.
- 12. Åberg, F.; Appelkvist, E.-L.; Dallner, G.; Ernster, L., *Arch. Biochem. Biophys.* **1992**, 295, 230-234.
- 13. Somayajulu, M.; McCarthy, S.; Hung, M.; Sikorska, M.; Borowy-Borowski, H.; Pandey, S., *Neurobiol. Dis.* **2005**, *18*, 618-627.
- 14. Weissig, V., *Pharm. Res.* **2011**, 28, 2657-2668.
- 15. Boddapati, S. V.; D'Souza, G. G. M.; Erdogan, S.; Torchilin, V. P.; Weissig, V., *Nano Lett.* **2008**, *8*, 2559-2563.
- 16. D'Souza, G. G. M.; Wagle, M. A.; Saxena, V.; Shah, A., *Biochim. Biophys. Acta, Bioenerg.* **2011**, *1807*, 689-696.

- 17. Soliman, G. M.; Sharma, R.; Choi, A. O.; Varshney, S. K.; Winnik, F. M.; Kakkar, A. K.; Maysinger, D., *Biomaterials* **2010**, *31*, 8382-8392.
- 18. Gaucher, G.; Dufresne, M.-H.; Sant, V. P.; Kang, N.; Maysinger, D.; Leroux, J.-C., *J. Controlled Release* **2005**, *109*, 169-188.
- 19. Babin, J.; Taton, D.; Brinkmann, M.; Lecommandoux, S., *Macromolecules* **2008**, *41*, 1384-1392.
- 20. Khanna, K.; Varshney, S.; Kakkar, A., *Polym. Chem.* **2010,** *1*, 1171-1185.
- 21. Soliman, G. M.; Sharma, A.; Maysinger, D.; Kakkar, A., *Chem. Commun.* **2011**, *47*, 9572-9587.
- 22. Kolb, H. C.; Finn, M. G.; Sharpless, K. B., *Angew. Chem., Int. Ed.* **2001**, 40, 2004-2021.
- 23. Franc, G.; Kakkar, A. K., Chem. Soc. Rev. 2010, 39, 1536-1544.
- 24. Lallana, E.; Sousa-Herves, A.; Fernandez-Trillo, F.; Riguera, R.; Fernandez-Megia, E., *Pharm. Res.* **2011**, 1-34.
- 25. Khanna, K.; Varshney, S.; Kakkar, A., *Macromolecules* **2010**, *43*, 5688-5698.
- 26. Hourani, R.; Jain, M.; Maysinger, D.; Kakkar, A., *Chem.–Eur. J.* **2010**, *16*, 6164-6168.
- 27. Gao, H.; Matyjaszewski, K., J. Am. Chem. Soc. **2007**, 129, 6633-6639.
- 28. Hansen, C. M., J. Paint Technol. 1967, 39, 104-17.
- 29. Mahmud, A.; Patel, S.; Molavi, O.; Choi, P.; Samuel, J.; Lavasanifar, A., *Biomacromolecules* **2009**, *10*, 471-478.
- 30. Yan, J.; Ye, Z.; Chen, M.; Liu, Z.; Xiao, Y.; Zhang, Y.; Zhou, Y.; Tan, W.; Lang, M., *Biomacromolecules* **2011**, *12*, 2562-2572.
- 31. Danquah, M.; Fujiwara, T.; Mahato, R. I., *Biomaterials* **2010**, *31*, 2358-2370.
- 32. Hourani, R.; Sharma, A.; Kakkar, A., *Tetrahedron Lett.* **2010**, *51*, 3792-3795.
- 33. Kim, B.-S.; Park, S. W.; Hammond, P. T., ACS Nano **2008**, 2, 386-392.
- 34. Wei, X.; Gong, C.; Gou, M.; Fu, S.; Guo, Q.; Shi, S.; Luo, F.; Guo, G.; Qiu, L.; Qian, Z., *Int. J. Pharm.* **2009**, *381*, 1-18.

- 35. Murphy, M. P.; Smith, R. A. J., *Adv. Drug Delivery Rev.* **2000**, *41*, 235-250.
- 36. Richter, A.; Olbrich, C.; Krause, M.; Kissel, T., *Int. J. Pharm.* **2010**, *389*, 244-253.
- 37. Lin, J.; Zhu, J.; Chen, T.; Lin, S.; Cai, C.; Zhang, L.; Zhuang, Y.; Wang, X.-S., *Biomaterials* **2009**, *30*, 108-117.
- 38. Boddapati, S. V.; Tongcharoensirikul, P.; Hanson, R. N.; D'Souza, G. G. M.; Torchilin, V. P.; Weissig, V., *J. Liposome Res.* **2005**, *15*, 49-58.
- 39. Liu, L.; Li, C. X.; Li, X. C.; Yuan, Z.; An, Y. L.; He, B. L., *J. Appl. Polym. Sci.* **2001**, *80*, 1976-1982.
- 40. Nederberg, F.; Appel, E.; Tan, J. P. K.; Kim, S. H.; Fukushima, K.; Sly, J.; Miller, R. D.; Waymouth, R. M.; Yang, Y. Y.; Hedrick, J. L., *Biomacromolecules* **2009**, *10*, 1460-1468.
- 41. Stojkovic, M.; Westesen, K.; Zakhartchenko, V.; Stojkovic, P.; Boxhammer, K.; Wolf, E., *Biol. Reprod.* **1999**, *61*, 541-547.
- 42. Ankola, D. D.; Viswanad, B.; Bhardwaj, V.; Ramarao, P.; Kumar, M. N. V. R., *Eur. J. Pharm. Biopharm.* **2007**, *67*, 361-369.
- 43. Kwon, S. S.; Nam, Y. S.; Lee, J. S.; Ku, B. S.; Han, S. H.; Lee, J. Y.; Chang, I. S., *Colloids Surf.*, A **2002**, *210*, 95-104.
- 44. Amorim, C. d. M.; Couto, A. G.; Netz, D. J. A.; de Freitas, R. A.; Bresolin, T. M. B., *Nanomed. Nanotech. Biol. Med.* **2010**, *6*, 745-752.
- 45. Dwan'Isa, J. P. L.; Rouxhet, L.; Preat, V.; Brewster, M. E.; Arien, A., *Pharmazie* **2007**, *62*, 499-504.
- 46. Patel, S. K.; Lavasanifar, A.; Choi, P., *Biomacromolecules* **2009**, *10*, 2584-2591.
- 47. Liu, J.; Xiao, Y.; Allen, C., J. Pharm. Sci. **2004**, 93, 132-143.
- 48. Zhang, W.; Li, Y.; Liu, L.; Sun, Q.; Shuai, X.; Zhu, W.; Chen, Y., *Biomacromolecules* **2010**, *11*, 1331-1338.
- 49. Swarnakar, N. K.; Jain, A. K.; Singh, R. P.; Godugu, C.; Das, M.; Jain, S., *Biomaterials* **2011**, *32*, 6860-6874.

- 50. Hsu, C.-H.; Cui, Z.; Mumper, R. J.; Jay, M., *AAPS PharmSciTech* **2003**, *4*, 269-280.
- 51. Xu, Y.; Zhang, Y.; Fan, Z.; Li, S., *J. Polym. Sci., Part B: Polym. Phys.* **2010**, *48*, 286-293.
- 52. Gref, R.; Minamitake, Y.; Peracchia, M. T.; Trubetskoy, V.; Torchilin, V.; Langer, R., *Science* **1994**, *263*, 1600-1603.
- 53. Jeong, Y.-I.; Cheon, J.-B.; Kim, S.-H.; Nah, J.-W.; Lee, Y.-M.; Sung, Y.-K.; Akaike, T.; Cho, C.-S., *J. Controlled Release* **1998**, *51*, 169-178.
- 54. Yang, X.; Zhu, B.; Dong, T.; Pan, P.; Shuai, X.; Inoue, Y., *Macromol. Biosci.* **2008**, *8*, 1116-1125.
- 55. Francis, M. F.; Lavoie, L.; Winnik, F. M.; Leroux, J.-C., *Eur. J. Pharm. Biopharm.* **2003**, *56*, 337-346.
- 56. Nagarajan, R.; Ganesh, K., *Macromolecules* **1989**, 22, 4312-4325.
- 57. Bule, M. V.; Singhal, R. S.; Kennedy, J. F., *Carbohydr. Polym.* **2010**, 82, 1290-1296.
- 58. McCarthy, S.; Somayajulu, M.; Sikorska, M.; Borowy-Borowski, H.; Pandey, S., *Toxicol. Appl. Pharmacol.* **2004**, *201*, 21-31.

Chapter 5

Design and Evaluation of Multifunctional Inherently Fluorescent Dendrimers for Theranostics

In the previous chapters, we have reported design and synthesis of multifunctional dendrimers, where the imaging dye, drug, and solubilising agents were attached to the periphery of dendrimers. It is highly desirable to limit the introduction of entities while maximizing the number of therapeutic agents to enhance the efficacy of nanocarriers. In addition, it is becoming increasingly important to design trackable nanocarriers to visualize their passage and accumulation at the target site. In this chapter, we report the design and synthesis of dendrimer backbones with inherent imaging capabilities. We demonstrate that

such macromolecules simplify the design, and maximize the therapeutic ability of multifunctional dendrimers. This chapter reports a simple and novel synthetic methodology for the construction of inherently fluorescent dendrimers. The dendrimers are designed to have hydroxyl groups on the surface, which can be used to attach a diverse variety of pharmaceutical agents through ester linkages. We have demonstrated the attachment of α -lipoic acid at the periphery of these trackable dendrimers as a model drug. Detailed synthetic strategies and biological results are discussed.

Reproduced in part with permission from:

Sharma A., Mejia D., Maysinger D., and Kakkar A., Manuscript in preparation for *Chemistry and Biology*, **2013.**

Unpublished work copyright, 2013.

5.1 Introduction

In the past few decades, the continuous improvements in the fields of nanoscience and nano-technology have brought a great revolution in conventional medicine and healthcare system (Khandare, et al., 2012; Zhang, et al., 2013). The efforts are being made to develop new formulations of nanomedicine to obtain better pharmacological effects. Various nanomaterials have been developed as carriers for the delivery of drugs, proteins, siRNA and genes (Alabi, et al., 2012; Arima, et al., 2012; Nakase, et al., 2011). Multifunctional nanocarriers that can combine delivery of therapeutics with diagnostic imaging capabilities are the emerging area of research in nanomedicine. This includes the development of nanocarriers which can simultaneously monitor the disease along with the treatment, an approach which is termed as 'theranostics' (Svenson, 2013).

Among various formulations which are currently under investigation, dendrimers have gained high interest of scientific community in the field of biomedicine, due to their unique surface topology (Khandare, et al., 2012; Soliman, et al., 2011). Dendrimers are hyperbranched and monodisperse macromolecules with defined composition and molecular architecture (Hawker and Frechet, 1990; Hourani and Kakkar, 2010; Tomalia and Fréchet, 2002). These star burst molecules have been considered as outstanding candidates in the field of biomedicine and there are several ways through which these can be modified for biological applications. The drugs can either be encapsulated or covalently conjugated in the dendrimers, and at the same time the imaging moieties can be incorporated for tracking of these pharmaceutical agents (Kaminskas, et al., 2012; Parveen, et al., 2012). Our group has previously reported several multifunctional dendrimers based nanocarriers in which the therapeutic agents and imaging dyes have been covalently linked to the periphery of the dendrimers (Hourani, et al., 2010; Sharma, et al., 2011; Sharma, et al., 2011).

Nanomedicine is advancing and the design of trackable therapeutics for theranostic applications has now become an emerging field of research (Mura and Couvreur, 2012; Nyström and Wooley, 2011; Prabhu and Patravale, 2012). Towards this goal, we are reporting dendrimers based inherently

fluorescent nanocarriers for the delivery of active pharmaceutical agents. The presence of imaging agent as the core of the dendrimer backbone provides an opportunity to append high loads of drug molecules at the periphery. In addition, imaging capability as being the inherent part of dendrimer structure gives additional space on the periphery to attach any other functional units including targeting ligands or solubilising polymers. We have used 2',4',5',7'tetraiodofluorescein (TIF) as a model dye in our study, as it is easily commercially available and contains hydroxyl functional group which can be modified to perform a variety of chemical reactions while retaining its properties. We have used this dye as the core of the dendrimers to which acetylene functional groups are appended. With this core as a starting point, we have developed a simple and convenient methodology to construct trackable dendrimers using a combination of highly efficient Cu (I) catalyzed azide alkyne click reaction (CuAAC) (Franc and Kakkar, 2010; Kolb, et al., 2001) and Steglich esterification (Neises and Steglich, 1978). This strategy allows facile construction of inherently fluorescent dendrimers with functional surface groups, which can be further utilized to covalently link any desired variety of active pharmaceutical agents. We have chosen to use α -lipoic acid (α -LA) as the model drug linked to the periphery of the dendrimers. Lipoic acid is an endogenous cofactor for many enzymes involved in mitochondrial respiration and it helps maintain redox homeostasis by scavenging reactive nitrogen and oxygen species and reducing antioxidant species in cells such as glutathione (Rochette, et al., 2013).

In order to explore the *in-vitro* properties of our constructs, biological experiments were carried out on peripheral and central nervous system macrophages, namely J774A.1 macrophages and N9 microglia. Microglia are the immune cells of the CNS and the first line responders to insult, playing a central role in maintaining brain homeostasis (Nimmerjahn, et al., 2005). Conversely, depending on the extent of their activation, microglia can exist in state that is deleterious to the brain. As such, these cells are key players in the health and wellness of the brain and are the targets for our multifunctional nanocarriers.

5.2 Results and discussion

5.2.1 Synthesis

The synthesis of tagable dendrimers was initiated around a fluorescent core based on imaging dye tetraiodofluorescein. Tetraiodofluorescein was used as a model dye, as it is easily available, and can be conveniently modified. To develop the dendrimer starting from this core, several different building blocks were first constructed. Diacetylenbenzyl bromide (4) was synthesized using our previously published procedure (Hourani, et al., 2010). The acetylene arms of 4 were then utilized to perform click reactions with 6-azidohexanoic acid to synthesize compound 5 with two carboxylic acid functions and a bromo focal point. The benzyl bromide in 5 was then converted to benzyl azide via azidation reaction to afford compound 6 which can participate in CuAAC click reaction (Scheme 5.1). The purpose of synthesizing this building block is to introduce two carboxylic acid groups to the dye to modify it to serve as a core with multiple arms (Scheme 5.2). Another click reaction using 2-azido ethanol was performed on 4 to construct building block 7 with 2 hydroxyl functions and a bromo focal point. It was subsequently converted to azide via an azidation reaction using sodium azide to give compound 8 (Scheme 5.1). This di-hydroxy building block 8 was later used to introduce hydroxyl functions at the periphery of trackable dendrimer.

Scheme 5.1. Synthesis of building blocks with carboxylic acid or hydroxyl functional groups.

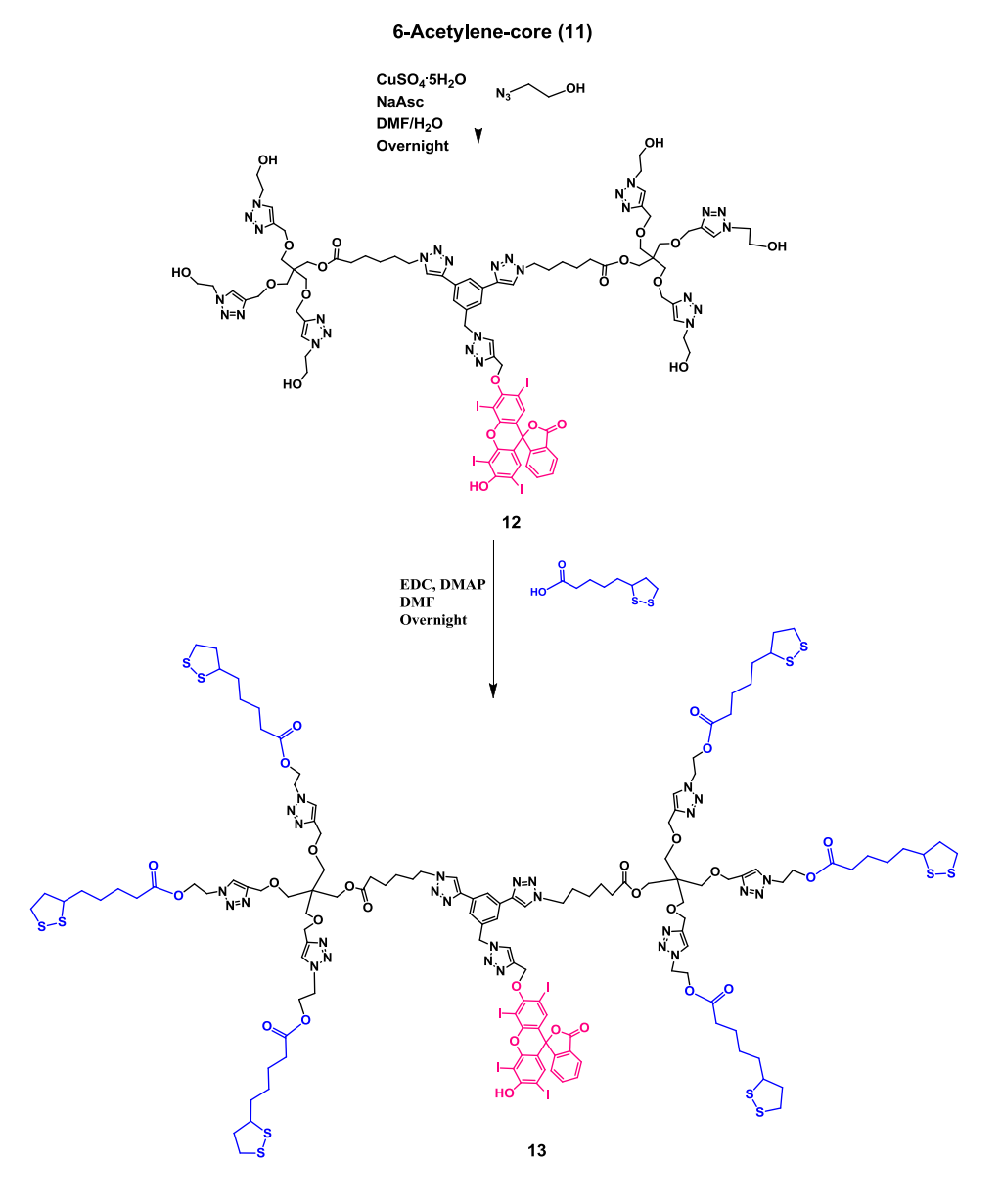
The synthesis of fluorescent core was achieved starting from imaging dye tetraiodofluorescein and modifying its hydroxyl group by performing a reaction with propargyl bromide to get monoparopargylated tetraiodofluorescein 9 (Scheme 5.2). It is important to perform only mono-propargylation of tetraiodofluorescein to retain its fluorescent properties, as dipropargylated derivative involving propargylations at both hydroxyl and carboxylic acid positions is non-fluorescent. Monopropargyl derivative 9 was subsequently reacted with building block 6 with two acid groups and an azido focal point via azide alkyne click reaction to achieve compound 10. The acid groups of

compound 10 were further used to perform Steglich esterification with tripropargylated pentaerythritol derivative to get a fluorescent core molecule 11 with six propargyl functions (Scheme 5.2).

Scheme 5.2. Synthesis of fluorescent core with six propargyl functions.

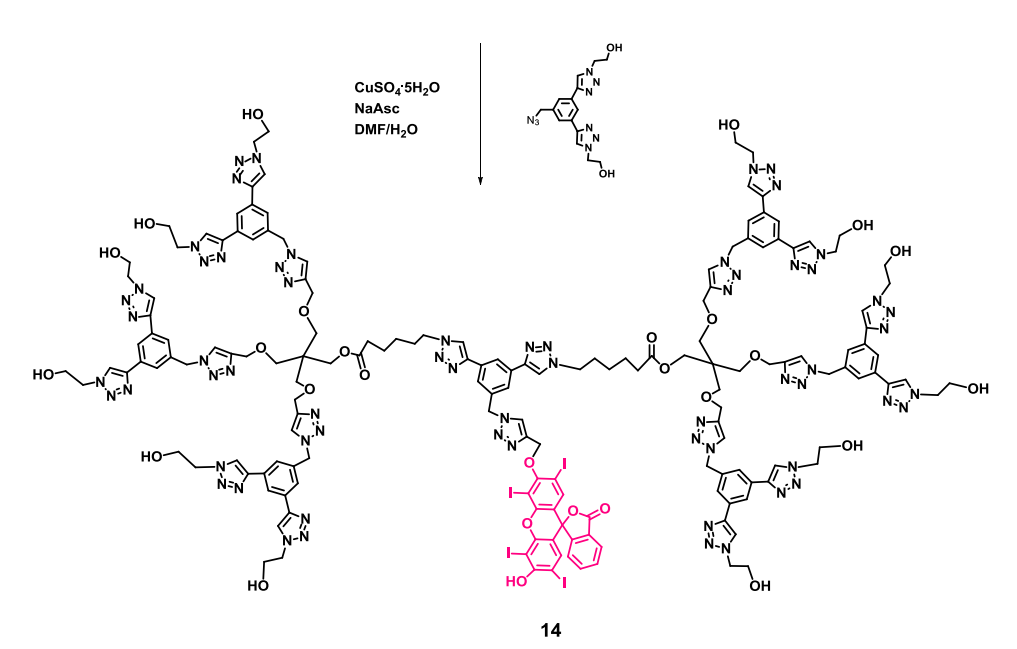
The acetylene arms of fluorescent core 11 were used to perform click reaction with 2-azido ethanol to get fluorescent dendrimer 12 with six hydroxyl groups at the periphery (Scheme 5.3). The reaction was monitored by the appearance of triazole protons at 7.98 ppm in ¹H NMR This synthesis was further elaborated to get a fluorescent dendrimer with 12 hydroxyl groups at the periphery. In order to construct dendrimer with 12 hydroxyl groups (14, Scheme 5.4), the fluorescent core 11 was reacted with building block 8 with two hydroxyl groups and an azido focal point via click reaction. Again the appearance of

triazole protons at 8.55 ppm confirmed the product formation. These trackable dendrimer backbones with multiple hydroxyl groups on the periphery can be utilized to append any desired therapeutic agents through Steglich esterification reaction. To demonstrate this, we used dendrimer 12 with six hydroxyl functions to covalently link six molecules of α -lipoic acid to obtain dendrimer 13 (Scheme 5.3). The disappearance of hydroxyl protons and appearance of new proton peaks for lipoic acid clearly indicated the formation of the product.



Scheme 5.3. Synthesis of trackable dendrimer **12** with 6 hydroxyl functional groups and **13** with 6 drug molecules.

6-Acetylene core 11



Scheme 5.4. Synthesis of trackable dendrimer **14** with 12 hydroxyl functional functions.

In order to examine the dendritic effect, we also constructed the linear counterparts of hydroxyl terminated as well as lipoic acid terminated dendrimer. Monopropargylated tetraiodofluorescein was reacted with 2-azido ethanol via click reaction to obtain compound **15** which was further reacted with α-lipoic acid through Steglich esterification reaction to afford compound **16** (Scheme **5.6**). All the building blocks and dendrimers were characterized by ¹H, ¹³C NMR and mass spectra analysis. The absorption and emission spectra of intermediates and dendrimers are shown in Figure **5.1**. Tetraiodofluorescein absorbs around 530 nm and emits at 540. The monopropargylated derivative showed absorption around 540 nm, and emission at 560. All other fluorescent intermediates and dendrimers (Figure **5.1**) showed similar shifts around 10 nm in absorption and 20 nm in emission as compared to tetraiodofluorescein.

Scheme 5.5. Synthesis of linear compounds 15 and 16.

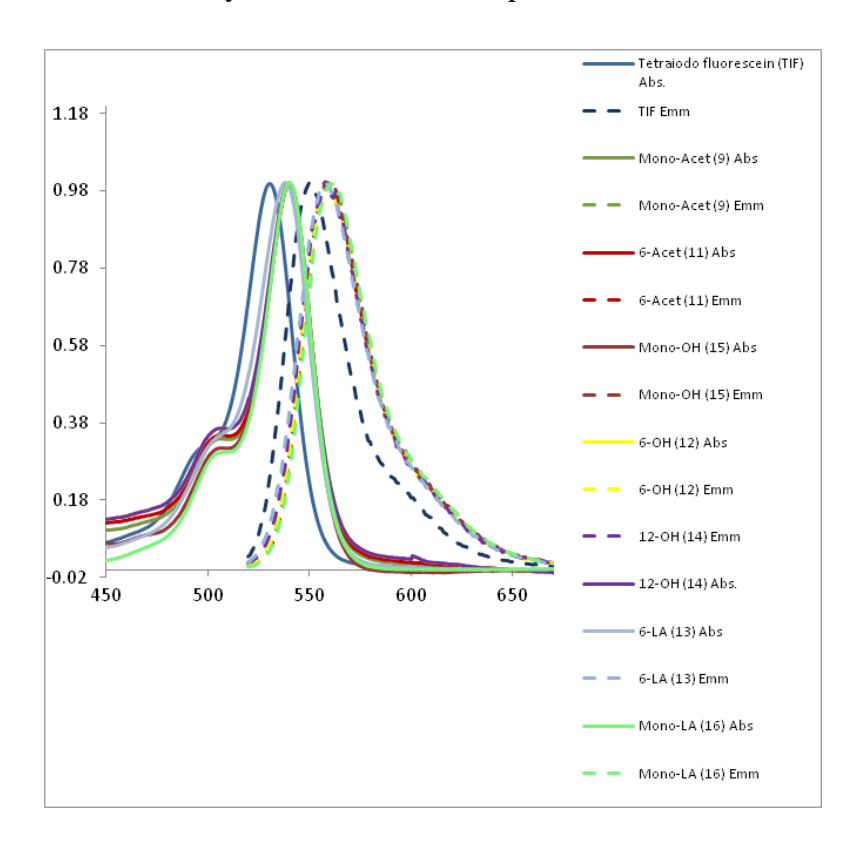


Figure 5.1 Absorption and emission spectra of intermediates, fluorescent dendrimers and linear counterparts.

5.2.2 Biological studies

The first aim of our biological studies was to demonstrate the safety of the dendrimer constructs. To this end, the mitochondrial activity of N9 microglia was assessed using an MTT assay after 6 and 24 hours of treatment with 6-OH dendrimer (**Figure 5.2A**). No significant change in the metabolic activity was observed. Similarly, macrophages were treated with dendrimers (6-OH, 12-OH, 6-Ac) for 24 hours (**Figure 5.2B**). Dendrimer treatment up to 1 µM in concentration had no significant effect on the mitochondrial activity of J774.2 macrophages. Representative brightfield images of N9 microglia under conditions used for fluorescent experiments (90 min, 0-1 µM) were acquired using a 20X objective (**Figure 5.2C**). No visible changes in microglial morphology can be seen as compared to untreated control cells.

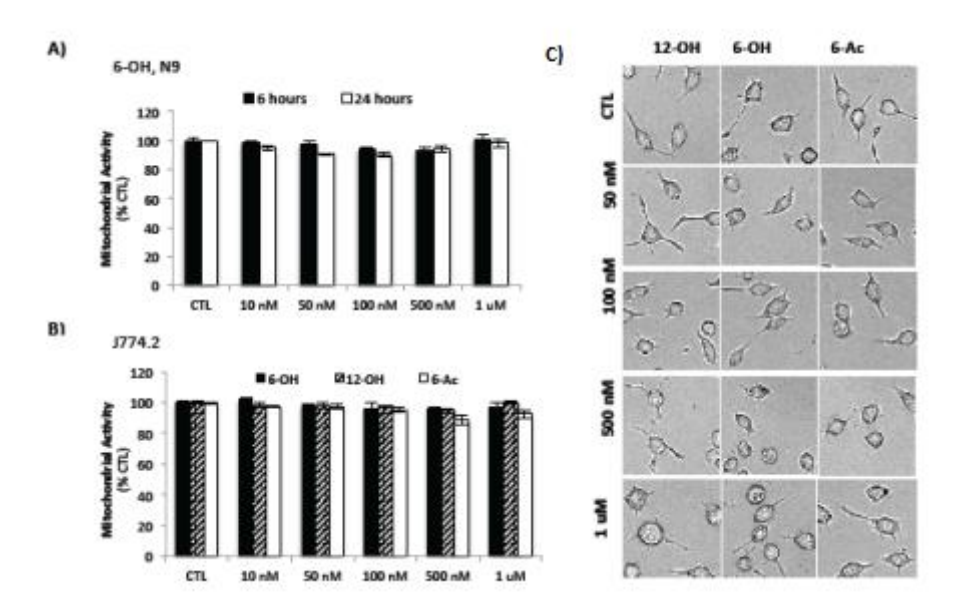


Figure 5.2 Fluorescent dendrimers do not affect N9 or J774.2 cell viability. Microglia and macrophages were assayed for cell viability as measured by the extent of mitochondrial activity with an MTT assay. N9 microglia were treated with 6-OH dendrimer for 6 and 24 hours **B**). At treatment end-time point, MTT was added to cells and formazan crystal formation was measured using a spectrophotometer at 595 nM. Data is represented as mean \pm standard deviation (n=3). Representative brightfield images were acquired for microglia treated for 90 minutes with fluorescent dendrimers **C**).

Having assessed the cytotoxicity of dendrimers in cell culture, we next wanted to investigate the uptake dynamics and fluorescence of dendrimers, linear counterparts and the tetraiodofluorescein (TIF) dye. Fluorescence was assessed by treating cells with dye, linear counterparts, or dendrimers for 90 minutes, followed by a wash and measurement at ex 544/ em 590. N9 microglia were first treated with TIF, dye-mono-acetylene and dye-mono-OH. These were detectable and significantly different from control at concentrations as low as 500 nM (**Figure 5.3A**). Dendrimer fluorescence intensity fell within the range of dye, and linear counterparts, indicating that the constructs are detectable and comparable to regular dyes in cell systems (**Figure 5.3B**).

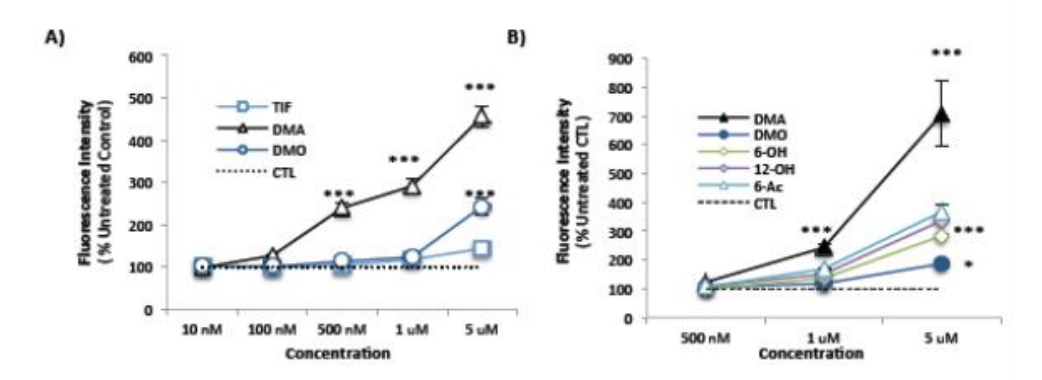


Figure 5.3 Fluorescent intensity of dyes and dendrimers taken up by N9 microglia. Microglia were treated with fluorescent dyes $(10nM-5\mu M)$ or dendrimers $(500nM-5\mu M)$ for 90 minutes. At treatment end-time point, cells were washed and fluorescence intensity was measured. All data are presented as group means \pm SEM. Values are indicated by * (p < 0.05), ** (p < 0.01) and *** (p < 0.001).

Time course experiments demonstrate that dye and linear counterparts are taken up within minutes of treatment, plateauing in fluorescence intensity within 40-60 minutes (**Figure 5.4A**) However, images show that dye and linear counterparts are taken up in a dose dependent manner but remain diffused within microglia, staining in a non-selective fashion (**Figure 5.4B**). In contrast,

dendrimers with incorporated dyes show a punctate distribution within N9 cells after 90 minutes of treatment and are comparable in fluorescence to the free dye. (**Figure 5.5A**). To confirm dendrimer internalization, z-stacks were acquired using confocal microscopy. A representative image of 12-OH dendrimer internalization is shown (**Figure 5.5B**).

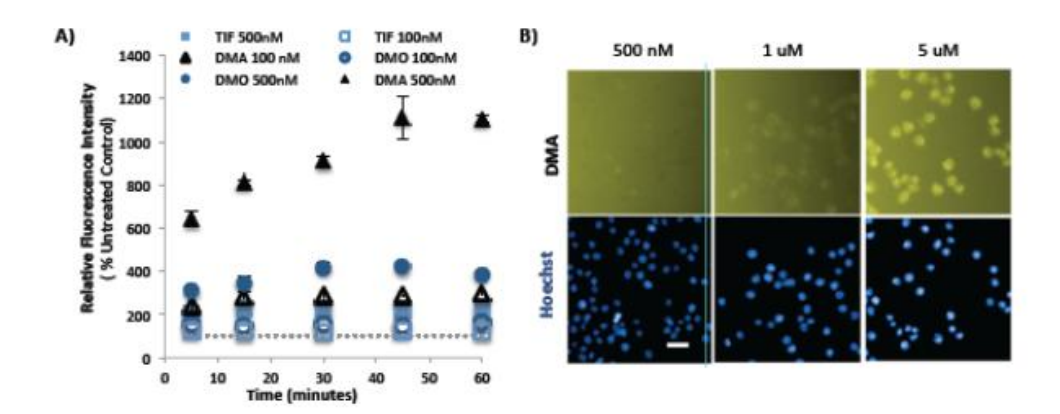


Figure 5.4 Fluorescent dyes are taken up by N9 microglia rapidly and non-specifically. N9 microglia were treated with dyes (100 or 500 nM) for indicated time and fluorescence intensity was measured (A). Representative images of microglia treated with dyes (500 nM - 5 μ M, 90 min) and hoechst (10 μ M, 10 min) are shown (**B**).

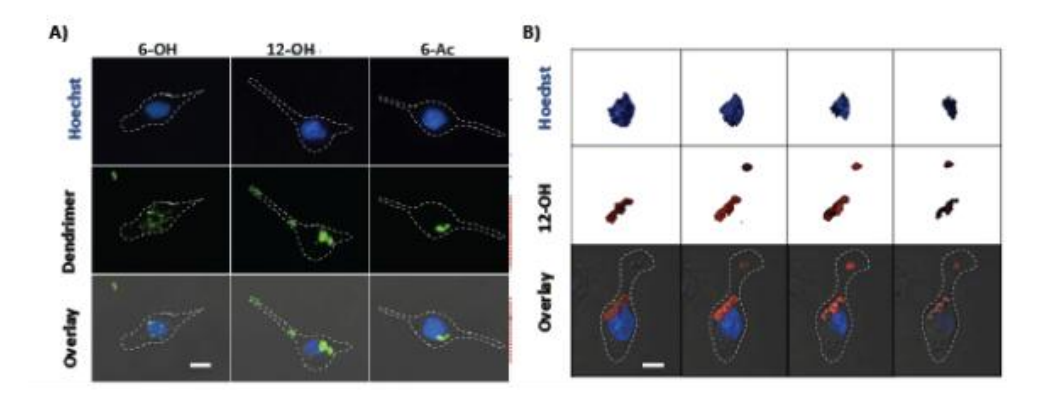


Figure 5.5 Dendrimers are taken up by N9 microglia and show a punctate distribution within the cells. Representative images of microglia treated with dendrimers (1 μ M, 90 min) are shown (A). Cells were fixed and nuclei stained with Hoechst (10 μ M, 10 min). Confocal images of treated microglia were acquired to confirm dendrimer internalization (B).

5.3 Conclusions:

We have demonstrated a convenient methodology to design and construct inherently fluorescent dendrimer backbones. The hydroxyl groups on the periphery of these dendrimers can be used to attach a variety of active pharmaceutical agents. The biological results show that the dendrimers are trackable, have comparable fluorescence intensities to commercially available dye such as TIF, are non-toxic, and are internalized quickly by microglia (within minutes). These results suggest possible uses of these inherently fluorescent dendrimers for drug delivery purposes and imaging in live cells, and possibly as novel theranostic devices.

5.4 Experimental

5.4.1 Materials and methods

Tetraiodofluorescein was purchased from TCI (Tokyo Chemical Industry Co., Ltd. and used as received. Copper (II) sulfate pentahydrate (CuSO₄.5H₂O) (>98.0%), sodium ascorbate (NaAsc) (crystalline) (98%), 6-bromohexanoic acid tetrabutylammonium fluoride (Bu_4NF) (1.0 M in tetrabromomethane (CBr₄) (99%), K₂CO₃, CuI, Bis(triphenylphosphine)palladium dichloride [PdCl₂(PPh₃)₂], triphenylphosphine (TPP), 2-bromo-ethanol (98%), αlipoic acid (>99%), 1-[3-(dimethylamino)propyl]-3-ethylcarbodiimidemethiodide (EDC), 4(dimethylamino)pyridine (DMAP) (99%), and sodium azide (NaN₃) (>99.5%) were purchased from Sigma-Aldrich Canada, and used as received. (Trimethylsilyl)acetylene was purchased from Oakwood Products, Inc., and 3,5dibromobenzyl alcohol was purchased from Alfa Aeser, and used as received. All other solvents were used as received in their anhydrous forms. NMR spectra were recorded on a 200 MHz, 400MHz or 500MHz (as specified) spectrometer at ambient temperatures. The chemical shifts in ppm are reported relative to tetramethylsilane as an internal standard for ¹H and ¹³C{ ¹H} NMR spectra. The high resolution and high accuracy mass spectra (ESI-MS) were obtained using an Exactive Orbitrap spectrometer from ThermoFisher Scientific, and MALDI-TOF spectra on Autoflex III Mass Spectrometer (Bruker) using α-Cyano-4hydroxycinnamic acid (HCCA) as the matrix as specified. Absorption spectra were recorded with Jasco V-670 spectrophotometer and the fluorescence was recorded on Cary Eclipse fluorimeter in methanol.

5.4.2 Synthesis:

The following compounds were synthesized by adaptation of the previously published procedures: 3, 5-diethynylbenzyl bromide (4) (Hourani, et al., 2010), 2-azido ethanol (Yu, et al., 2013), 6-azido hexanoic acid (Parrish and Emrick, 2006), and tripropargylated pentaerythritol (Schunack, et al., 2012).

Synthesis of compound 5: Compound 4 (200 mg, 0.913 mmol) and 6-azidohexanoic acid (430 mg, 2.739 mmol) were dissolved in 3 mL of tetrahydrofuran (THF), followed by the addition of sodium ascorbate (36.1 mg, 0.182 mmol). An aqueous solution (1 mL) of CuSO₄.5H₂O (22.1 mg, 0.091 mmol) was added dropwise to the solution. The reaction mixture was left to stir overnight at room temperature. THF was then evaporated, water (10 mL) was added, and the solution was extracted with DCM (3x20 mL). The organic layer was washed with ethylenediaminetetraacetate (EDTA) solution and brine (3x50 mL). It was dried over MgSO₄, and the solvent was evaporated. The residue was washed several times with ether to afford the product as white solid (405 mg, 83%). ¹H NMR (400 MHz, DMSO): δ (ppm) 1.24-1.30 (m, 4H, -CH₂), 1.49-1.56 (m, 4H, -CH₂), 1.83-1.91 (m, 4H, -CH₂), 2.19 (t, 4H, -CH₂), 4.40 (t, 4H, -CH₂), 4.79 (s, 2H, -CH₂Br), 7.87 (s, 2H, ArH), 8.24 (s, 1H, ArH), 8.68 (s, 2H, triazoleH), and 11.99 (s, 2H, -COOH). ¹³C{¹H} NMR (125 MHz, DMSO): δ (ppm) 24.34, 25.86, 29.75, 33.86, 34.54, 49.92, 122.06, 122.20, 125.63, 132.37, 139.93, and 146.03. ESI-MS: m/z (-) Theoretical 531.14 [(M-H)], found 531.13 [(M-H)].

Synthesis of compound 6: To a solution of compound **5** (1.05 g, 1.969 mmol) in N,N-dimethyl formamide (DMF), NaN₃ (320 mg, 4.921 mmol) was added. The reaction mixture was left to stir at room temperature for overnight. The solution was diluted with water and extracted with DCM (3x20 mL). The organic phase was washed with brine (3x70 mL). It was dried over MgSO₄ and followed by removal of the solvent. The residue was washed with ether and the product was obtained as a white solid (915 mg, 94%). ¹H NMR (400 MHz, DMSO): δ (ppm) 1.22-1.30 (m, 4H, -CH₂), 1.49-1.56 (m, 4H, -CH₂), 1.83-1.91 (m, 4H, -CH₂), 2.19

(t, 4H, -CH₂), 4.40 (t, 4H, -CH₂), 4.57 (s, 2H, -CH₂N₃), 7.79 (s, 2H, ArH), 8.28 (s, 1H, ArH), 8.69 (s, 2H, triazoleH), and 12.02 (s, 2H, -COOH). 13 C{ 1 H} NMR (125 MHz, DMSO): 24.37, 25.87, 29.77, 33.91, 36.21, 49.92, 53.93, 121.88, 122.19, 124.64, 132.38, 137.64, 146.16, and 174.78. ESI-MS: m/z (-) Theoretical 494.23[(M-H)⁻], found 494.22 [(M-H)⁻].

Synthesis of compound 7: Compound **4** (300 mg, 1.369 mmol) and 2-azido-ethanol (262 mg, 3.013 mmol) were dissolved in 3 mL of tetrahydrofuran (THF), followed by the addition of sodium ascorbate (54.2 mg, 0.273 mmol). An aqueous solution (1 mL) of CuSO₄.5H₂O (34.1 mg, 0.136 mmol) was added dropwise to the solution. The reaction mixture was left to stir overnight at room temperature. THF was then evaporated, water (10 mL) was added, and the solution was extracted with DCM (3x20 mL). The organic layer was washed with EDTA solution and brine (3x50 mL). It was dried over MgSO₄, and the solvent was evaporated. The residue was washed several times with ether to afford the product as white solid (420 mg, 78%). ¹H NMR (200 MHz, DMSO): δ (ppm) 3.83 (q, 4H, -CH₂), 4.45 (t, 4H, -CH₂), 4.80 (s, 2H, -CH₂Br), 5.09 (t, 2H, -OH), 7.89 (s, 2H, ArH), 8.26 (s, 1H, ArH), and 8.63 (s, 2H, triazoleH). ¹³C{ ¹H} NMR (125 MHz, DMSO): 34.58, 46.39, 52.97, 60.23, 122.01, 122.78, 125.08, 125.54, 132.41, 139.93, and 145.90. ESI-MS: m/z (+) Theoretical 393.06 [(M+H)⁺], found 393.06 [(M+H)⁺].

Synthesis of compound 8: To a solution of compound **7** (500 mg, 1.272 mmol) in N,N-dimethyl formamide (DMF), NaN₃ (206.7 mg, 3.180 mmol) was added. The reaction mixture was left to stir at room temperature for overnight. The solution was diluted with water and extracted with DCM (3x20 mL). The organic phase was washed with brine (3x70 mL). It was dried over MgSO₄ and followed by removal of the solvent. The residue was washed with ether to afford the product as a white solid (390 mg, 86%). ¹H NMR (400 MHz, DMSO): δ (ppm) 3.83 (q, 4H, -CH₂), 4.45 (t, 4H, -CH₂), 4.57 (s, 2H, -CH₂N₃), 5.10 (t, 2H, -OH), 7.82 (s, 2H, ArH), 8.31 (s, 1H, ArH), and 8.64 (s, 2H, triazoleH). ¹³C{¹H} NMR (125 MHz, DMSO): 13.93, 23.50, 52.96, 53.92, 60.24, 121.83, 122.78, 124.57,

132.42, 137.60, and 146.01. ESI-MS: m/z (+) Theoretical 356.15 [(M+H)⁺], found 356.15 [(M+H)⁺].

Synthesis of compound 9: To a stirring solution of tetraiodofluorescein (500 mg, 0.598 mmoles) in DMF (2mL) was added K₂CO₃ (450 mg) followed by the addition of propargyl bromide; 80% in toluene (0.2 mL). The reaction mixture was stirred at room temperature for overnight. On completion, the reaction mixture was washed with ether to remove DMF. The residue was then precipitated using ice and cold water, and filtered to afford a red solid (420 mg, 80%). ¹H NMR (300 MHz, CD₃OD): δ (ppm) 2.61 (t, 1H, AcetyleneH), 4.60 (d, 2H, -OCH₂), 7.42 (s, 2H, ArH), 7.46 (dd, 1H, ArH), 7.80-7.86 (m, 2H, ArH), and 8.27 (dd, 1H, ArH). ¹³C{¹H} NMR (125 MHz, DMSO): 31.22, 36.24, 53.16, 76.26, 78.00, 78.18, 96.64, 111.68, 129.55, 130.54, 131.06, 131.27, 133.75, 134.41, 136.72, and 148.67. ESI-MS: m/z (-) Theoretical 872.67 [(M-H)⁻], found 872.66 [(M-H)⁻].

Synthesis of compound 10: Compound 9 (176.8 mg, 0.202 mmol) and compound 6 (100 mg, 0.202 mmol) were dissolved in 3 mL of DMF, followed by the addition of sodium ascorbate (4 mg, 0.020 mmol). An aqueous solution (1 mL) of CuSO₄.5H₂O (2.5 mg, 0. 010 mmol) was added dropwise to the solution. The reaction mixture was left to stir overnight at room temperature. On completion, the reaction mixture was washed with ether to remove DMF. The residue was then precipitated using ice and cold water, and filtered to afford a red solid (200, 72%). %). ¹H NMR (400 MHz, DMSO): δ (ppm) 1.22-1.30 (m, 4H, -CH₂), 1.49-1.56 (m, 4H, -CH₂), 1.83-1.91 (m, 4H, -CH₂), 2.17-2.22 (m, 4H, -CH₂), 4.39 (t, 4H, -CH₂), 5.09 (s, 2H, -CH₂), 5.62 (s, 2H, -CH₂), 7.15 (s, 2H, ArH), 7.45 (d, 1H, ArH), 7.73 (s, 2H, ArH), 7.77-7.86 (m, 2H, ArH), 7.89 (s, 1H, ArH), 8.12 (d, 1H, ArH), 8.27 (s, 1H, triazoleH), 8.66 (s, 2H, triazoleH), and 11.97 (brs, 2H, -COOH). ¹³C{¹H} NMR (125 MHz, DMSO): 14.42, 15.61, 22.50, 24.58, 25.99, 29.8, 31.40, 49.93, 53.16, 53.60, 58.70, 65.35, 65.63, 78.00, 78.18, 111.96, 121.97, 122.31, 124.68, 129.53, 130.01, 130.47, 131.01, 131.19, 132.13, 132.46, 133.48, 133.74, 134.14, 134.42, 136.74, 137.53, 146.04, and 148.55. ESI-MS: m/z (-) Theoretical 1368.90 [(M-H)], found 1367.89 [(M-H)].

Synthesis of compound 11: To a strirring solution of compound 10 (100 mg, 0.073 mmol), tripropargylated penta erythritol (55 mg, 0.219 mmoles), and DMAP (13.3 mg. 0.109 mmoles) in DMF (3 mL), was added EDC (42 mg, 0.219 mmoles), and the solution was stirred at room temperature for 12h. On completion, the reaction mixture was washed with ether to remove DMF. The residue was then precipitated using ice and cold water, and filtered to afford a red solid. The solid was washed several times with diethyl ether to remove impurities and yield compound **11** (110, 83%). ¹H NMR (400 MHz, DMSO): δ (ppm) 1.24-1.30 (m, 4H, -CH₂), 1.55-1.58 (m, 4H, -CH₂), 1.84-1.89 (m, 4H, -CH₂), 2.28-2.31 (m, 4H, -CH₂), 3.39 (s, 12H, -CH₂), 3.94 (s, 4H, -COOCH₂), 4.08 (s, 12H, -CH₂), 4.39 (t, 4H, -CH₂), 5.09 (s, 2H, -CH₂), 5.61 (s, 2H, -CH₂), 7.12 (s, 2H, ArH), 7.44-7.46 (m, 1H, ArH), 7.73 (s, 2H, ArH), 7.81-7.86 (m, 2H, ArH), 8.10-8.12 (m, 2H, ArH), 8.28 (s, 1H, triazoleH), and 8.66 (s, 2H, triazoleH). ¹³C{¹H} NMR (125) MHz, DMSO): 24.27, 25.82, 29.74, 31.40, 33.75, 43.85, 49.91, 53.61, 58.56, 63.18, 68.82, 77.70, 80.57, 110.00, 121.97, 122.28, 124.71, 130.03, 130.45, 131.01, 131.21, 132.45, 133.47, 134.13, 136.79, 137.51, 145.99, 157.52, 165.10, and 172.94. ESI-MS: m/z (-) Theoretical 1832.12 [(M-H)], found 1832.11 [(M- $H)^{-}$].

Synthesis of compound 12: Compound **11** (105 mg, 0.057 mmol) and 2-azido-ethanol (49.8 mg, 0.572 mmol) were dissolved in 3 mL of DMF, followed by the addition of sodium ascorbate (6.8 mg, 0.034 mmol). An aqueous solution (1 mL) of CuSO₄.5H₂O (4.3 mg, 0.017 mmol) was added dropwise to the solution. The reaction mixture was left to stir overnight at room temperature. On completion, the reaction mixture was washed with diethyl ether to remove DMF. The residue was then precipitated using ice and cold water, and filtered to afford a red solid. The solid was washed several times with EDTA solution and diethyl ether to remove impurities to yield compound **12** (98, 73%). ¹H NMR (400 MHz, DMSO): δ (ppm) 1.22-1.30 (m, 4H, -CH₂), 1.49-1.54 (m, 4H, -CH₂), 1.83-1.91 (m, 4H, -CH₂), 2.17-2.20 (m, 4H, -CH₂), 3.36 (s, 12H, -CH₂), 3.74 (q, 12H, -CH₂OH), 3.91 (s, 4H, -COOCH₂), 4.34 (t, 12H, -CH₂), 4.35-4.41 (m, 4H, -CH₂), 4.42 (s, 12H, -CH₂), 4.99 (t, 6H, -OH), 5.09 (s, 2H, -CH₂), 5.61 (s, 2H, -CH₂), 7.15 (s, 2H, ArH),

Synthesis of compound 13: To a strirring solution of compound 12 (100 mg, 0.042 mmol), α-lipoic acid (70.05 mg, 0.339 mmoles), and DMAP (18.1 mg. 0.148 mmoles) in DMF (3 mL), was added EDC (56.9 mg, 0.297 mmoles), and the solution was stirred at room temperature for 12h. On completion, the reaction mixture was diluted with water and extracted with DCM (3X10mL). The combined organic extracts were washed with water and brine. The organic layer was dried over sodium sulfate and concentrated. The residue was washed with diethylether and methanol to remove impurities and to afford compound 13 as red solid (95mg, 65%). %). ¹H NMR (500 MHz, DMSO): δ (ppm) 1.19-1.27 (m, 16H, -CH2), 1.38-1.60 (m, 28H, -CH2), 1.75-1.90 (m, 6H, -SCHCH₂ and 4H, -CH₂)), 2.18-2.23 (m, 12H, -CH₂COO- and 4H, -CH₂), 2.30-2.38 (m, 6H, -SCHCH₂-), 3.02-3.16 (m, 12H, -SSCH₂), 3.35 (s, 12 H, -CH₂), 3.49-3.53 (m, 6H, -SCH), 3.91 (s, 4H, -COOCH₂), 4.36-4.40 (t, 16H, -CH₂), 4.43 (s, 12H, -CH₂), 4.57 (t, 12H, -CH₂), 5.08 (s, 2H, -CH₂), 5.60 (s, 2H, -CH₂), 7.13 (s, 2H, ArH), 7.43 (d, 1H, ArH), 7.72 (s, 3H, ArH), 7.74-7.83 (m, 2H, ArH), 8.04 (s, 6H, triazoleH), 8.10 (d, 1H, ArH), 8.29 (s, 1H, triazoleH), and 8.65 (s, 2H, triazoleH).). ¹³C{¹H} NMR (125 MHz, DMSO): 24.23, 24.46, 25.84, 28.41, 29.77, 33.51, 33.66, 34.41, 38.52, 44.36, 48.94, 49.91, 56.43, 58.67, 62.58, 63.11, 64.61, 68.93, 111.81, 121.93, 122.27, 124.58, 130.04, 130.45, 131.01, 131.18, 132.46, 133.45, 134.12, 136.79, 137.48, 137.98, 144.48, 146.00, 148.63, 157.64, 165.11, and 172.82.

Synthesis of compound 14: Compound **11** (40 mg, 0.021 mmol) and compound **8** (54.2 mg, 0.152 mmol) were dissolved in 2 mL of DMF, followed by the addition of sodium ascorbate (2.6 mg, 0.013 mmol). An aqueous solution (1 mL) of CuSO₄.5H₂O (1.6 mg, 0.006 mmol) was added dropwise to the solution. The

reaction mixture was left to stir overnight at room temperature. On completion, the reaction mixture was washed with diethyl ether to remove DMF. The residue was then precipitated using ice and cold water, and filtered to afford a red solid. The solid was washed several times with EDTA solution and diethyl ether to remove impurities to yield compound 14 (55 mg, 64%). ¹H NMR (400 MHz, DMSO): δ (ppm) 1.08-1.21 (m, 4H, -CH₂), 1.30-1.60 (m, 4H, -CH₂), 1.70-1.90 (m, 4H, -CH₂), 2.08-2.16 (m, 4H, -CH₂), 3.36 (s, 12H, -CH₂), 3.78-3.84 (m, 24H, -CH₂), 3.88 (s, 4H, -COOCH₂), 4.30-4.33 (m, 4H, -CH₂), 4.20-4.45 (m, 24H+12H, -CH₂), 5.08 (t, 12H, -OH + s, 2H, -CH₂), 5.59 (s, 2H, -CH₂), 5.63 (s, 12H, -CH₂), 7.10 (s, 2H, ArH), 7.43 (d, 1H, ArH), 7.68-7.76 (m, 3H, ArH), 7.76 (s, 12H, ArH), 7.67-7.81 (m, 2H, ArH), 8.08-8.11 (m, 1H, ArH), 8.15 (s, 6H, ArH), 8.23 (s, 6H, triazoleH), 8.29 (s, 1H, triazoleH), 8.55 (s, 12H, triazoleH) and 8.62 (s, 2H, triazoleH).). ¹³C{¹H} NMR (125 MHz, DMSO): 13.93, 23.50, 24.10. 25.78, 29.73, 33.52, 44.33, 49.88, 52.93, 53.14, 60.23, 64.54, 69.00, 76.23, 96.55, 111.69, 121.99, 122.73, 124.37, 124.49, 132.45, 136.76, 137.85, 144.74, 145.89, 157.65, 172.03, and 172.90. MALDI: m/z Theoretical 3989.14 [(M+Na)⁺], found $3989.27 [(M+Na)^{+}].$

Synthesis of compound 15: Compound **9** (200 mg, 0.228 mmol) and 2-azido-ethanol (23.8 mg, 0.274 mmol) were dissolved in 3 mL of DMF, followed by the addition of sodium ascorbate (4.5 mg, 0.022 mmol). An aqueous solution (1 ml) of CuSO₄.5H₂O (2.8 mg, 0.011 mmol) was added dropwise to the solution. The reaction mixture was left to stir overnight at room temperature. On completion, the reaction mixture was washed with diethyl ether to remove DMF. The residue was then precipitated using ice and cold water, and filtered to afford a red solid. The solid was washed several times with EDTA solution and diethyl ether to remove impurities to yield compound **15** (160 mg, 73%). ¹H NMR (500 MHz, DMSO): δ (ppm) 3.70 (q, 2H, -CH₂OH), 4.32 (t, 2H, -CH₂), 4.94 (t, 1H, -OH), 5.09 (s, 2H, -OCH₂), 7.14 (s, 2H, ArH), 7.45 (d, 1H, ArH), 7.71 (s, 1H, triazoleH), 7.74 (t, 1H, ArH), 7.83 (t, 1H, ArH), and 8.12 (d, 1H, ArH). ¹³C{¹H} NMR (125 MHz, DMSO): 52.97, 58.71, 60.16, 88.74, 112.04, 125.47, 127.84, 129.96,

130.45, 131.00, 131.18, 13.53, 134.24, 136.69, 157.57, 165.09, and 169.18. ESI-MS: m/z (-) Theoretical 959.71 [(M-H)⁻], found 959.70 [(M-H)⁻].

Synthesis of compound 16: To a strirring solution of compound 15 (40 mg, 0.0421 mmol), α-lipoic acid 10.3 mg, 0.049 mmoles), and DMAP (5.1 mg, 0.041 mmoles) in DMF (3 mL), was added EDC (9.6 mg, 0.049 mmoles), and the solution was stirred at room temperature for 12h. On completion, the reaction mixture was diluted with water and extracted with DCM (3X10mL). The combined organic extracts were washed with water and brine. The organic layer was dried over sodium sulfate and concentrated. The residue was washed with diethylether and methanol to remove impurities and to afford compound 16 as red solid (32mg, 67%). ¹H NMR (500 MHz, DMSO): δ (ppm) 1.20-1.25 (m, 2H, -CH2), 1.38-1.45 (m, 2H, -CH2), 1.52-1.57 (m, 2H, -CH2), 1.75-1.78 (m, 1H, -SCHCH₂), 2.20 (t, 2H, -CH₂COO-), 2.30-2.34 (m, 1H, -SCHCH₂-), 3.02-3.16 (m, 2H, -SSCH₂), 3.49-3.53 (m, 1H, -SCH) 4.32 (t, 2H, -CH₂), 4.54 (t, 2H, -CH₂), 5.11 (s, 2H, -OCH₂), 7.13 (s, 2H, ArH), 7.45 (d, 1H, ArH), 7.73 (s, 1H, triazoleH), 7.74-7.77 (m, 1H, ArH), 7.83 (t, 1H, ArH), and 8.11 (d, 1H, ArH). ¹³C{¹H} NMR (125 MHz, DMSO): 24.49, 28.41, 33.59, 34.39, 34.58, 38.52, 49.28, 56.43,56.58, 58.67, 62.47, 110.00, 111.99, 125.29, 130.00, 130.45, 130.96, 131.23, 133.53, 134.24, and 136.75. ESI-MS: m/z (-) Theoretical 1147.75 [(M-H)⁻], found $1147.73 [(M-H)^{-}].$

5.4.3 Cell culture

Murine N9 microglia cells (Mouse embryonic brain primary cultures, ATCC Castagnoli, Italy) were cultured in Iscove's Modified Dulbecco's Medium (IMDM, Gibco #12440-053) supplemented with 5% (v/v) fetal bovine serum (FBS, Gibco #26140-079) and 1% (v/v) Pen-Strep (Gibco #15140-122). Cells were seeded 24h prior to treatment. Treatment was performed in 1% serum-containing media for indicated amounts of time. Cell growth and treatment were performed at 37°C with 5% CO and >95% relative humidity. Murine macrophages were cultured in Dulbecco's Modified Eagle Medium (DMEM, Gibco #11995-073) containing 1% (v/v) Pen-Strep (Gibco #15140-122) in 10% (v/v) fetal bovine serum (FBS, Gibco #26140-079) media solution.

5.4.4 Measurement of mitochondrial metabolic activity and cell viability

MTT ASSAY N9 microglia cells were seeded in 24-well cell culture plate (Sarstedt) at a density of $2 \cdot 10^5$ cells/well in a final volume of 500 µl. Macrophages were seeded at a density of $1.75 \cdot 10^5$ cells/well. In both cases, cells were treated as indicated and at time-end point 50 µl of 3-(4,5-Dimethylthiazol-2yl)-2,5-diphenyltetrazolium bromide (MTT) solution in PBS (5 mg/ml) was added to the cells and incubated at 37°C with 5% CO and >95% relative humidity for 30-35 min. 500 µl of dimethyl sulfoxide (DMSO) was added to lyse the cells and dissolve the formazan crystals. Aliquots of 100 µl were collected from each well and transferred in triplicate to a 96 well plate (Sarstedt). The absorbance was measured at 595 nm using a Benchmark microplate reader (Bio-Rad, ON, Canada). CELL COUNTING N9 microglia cells were seeded at 3.0 · 10⁵ cells/well in 6-well cell culture plate (Sarstedt). Following treatment cell supernatant was collected and centrifuged at 4°C for 10 minutes. Similarly, adherent cells were washed, collected and centrifuged. Cell pellets were resuspended in PBS and stained with trypan blue. A live/dead cell count was performed using a brightfield microscope.

5.4.5 Spectrofluorometric measurements

To acquire fluorescence measurements for dyes and dendrimers, N9 cells were seeded in a 96 well black plate (Sarstedt) at a density of 15 000 cells/well and incubated for 24 hours at 37°C. Phenol-free media was used for treatment with dyes or dendrimers. Cells were incubated for 90 minutes, or as stated and washed with PBS after treatment end-time. Cells were measured immediately using a BMG spectrofluorometer (ex 544 / em 590).

5.4.6 Confocal microscopy

Cells were grown on rat-tail collagen treated cover slips at a seeding density of 20 000 cells/well and incubated for 24 hours at 37°C. Cells were treated for 90 minutes with dyes or dendrimers. At treatment end-time point, cells were washed with PBS and fixed with 4% PFA (parafomaldehyde). They were then stained with 10 µM Hoechst 33342 (Life Technologies Inc.) for 10 min at room temperature and washed at least once with PBS. The cells were imaged on

microscope slides using a Leica DMI4000B inverted fluorescence microscope at 63×. Pictures were captured with the Leica DFC350FX digital camera through a UV filter (ex 350/ em 461 nm) and Cy3 filter (ex 543 / em 593) and analyzed using the Leica Application Suite software for image acquisition. To acquire z-stack images, a Zeiss microscope was used with a DAPI filter and Cy3 filter. Images were processed using ImageJ and Microsoft Office tools.

5.4.7 Measurement of nitric oxide release

NO release was assessed by measuring nitrite concentration (NO_2^-) using Griess reagent. N9 microglia cells were seeded in 24-well cell culture plate (Sarstedt) at a density of $2 \cdot 10^5$ in a final volume of 500 µl. Lipopolysaccharides (LPS) from E. Coli (L2880) were solubilized in DPBS to 1mg/ml and used to activate microglia at an effective concentration of 100 ng/ml. At treatment end-time, 50 µl supernatant aliquots were collected in triplicate into a 96 well plate (Sarstedt)IGN. A standard curve (0-100 µM) was generated using sodium nitrite in serum-free cell media. Griess reagent (1% sulfanilamide, 0.1% *N*-[1-naphthyl]-ethyleneamine dihydrochloride, 5% phosphoric acid) (Sigma, G-4410) was added to samples and standards and incubated at room temperature for 15 min. Absorbance was measured at 540 nm using a microplate reader (ASYS[©] UVM 340).

5.4.8 Data and Statistical analysis

Data was graphed and tabulated using Microsoft Excel[®]. Values in bar graphs are collected from triplicate samples from at least two independent experiments unless otherwise indicated. All data are presented as group means \pm SEM. Student's t-test was used to analyze significant differences between two group means. In all statistical tests, values are indicated by * (p <0.05), ** (p<0.01) and *** (p<0.0).

5.5 References

Alabi, C., Vegas, A., and Anderson, D. (2012). Attacking the genome: emerging siRNA nanocarriers from concept to clinic. Curr. Opin. Pharmacol. 12, 427-433.

Arima, H., Motoyama, K., and Higashi, T. (2012). Polyamidoamine Dendrimer Conjugates with Cyclodextrins as Novel Carriers for DNA, shRNA and siRNA. Pharmaceutics 4, 130-148.

Franc, G., and Kakkar, A.K. (2010). "Click" methodologies: efficient, simple and greener routes to design dendrimers. Chem. Soc. Rev. 39, 1536-1544.

Hawker, C.J., and Frechet, J.M.J. (1990). Preparation of polymers with controlled molecular architecture. A new convergent approach to dendritic macromolecules. J. Am. Chem. Soc. 112, 7638-7647.

Hourani, R., Jain, M., Maysinger, D., and Kakkar, A. (2010). Multi-tasking with Single Platform Dendrimers for Targeting Sub-Cellular Microenvironments. Chemistry – A European Journal 16, 6164-6168.

Hourani, R., and Kakkar, A. (2010). Advances in the Elegance of Chemistry in Designing Dendrimers. Macromol. Rapid Commun. 31, 947-974.

Hourani, R., Sharma, A., and Kakkar, A. (2010). Designing dendritic frameworks using versatile building blocks suitable for CuI-catalyzed alkyne azide 'click' chemistry. Tetrahedron Lett. 51, 3792-3795.

Kaminskas, L.M., McLeod, V.M., Porter, C.J.H., and Boyd, B.J. (2012). Association of Chemotherapeutic Drugs with Dendrimer Nanocarriers: An Assessment of the Merits of Covalent Conjugation Compared to Noncovalent Encapsulation. Molecular Pharmaceutics 9, 355-373.

Khandare, J., Calderon, M., Dagia, N.M., and Haag, R. (2012). Multifunctional dendritic polymers in nanomedicine: opportunities and challenges. Chem. Soc. Rev. 41, 2824-2848.

Kolb, H.C., Finn, M.G., and Sharpless, K.B. (2001). Click Chemistry: Diverse Chemical Function from a Few Good Reactions. Angew. Chem. Int. Ed. 40, 2004-2021.

Mura, S., and Couvreur, P. (2012). Nanotheranostics for personalized medicine. Advanced Drug Delivery Reviews 64, 1394-1416.

Nakase, I., Akita, H., Kogure, K., Gräslund, A., Langel, Ü., Harashima, H., and Futaki, S. (2011). Efficient Intracellular Delivery of Nucleic Acid Pharmaceuticals Using Cell-Penetrating Peptides. Acc. Chem. Res. 45, 1132-1139.

Neises, B., and Steglich, W. (1978). Simple Method for the Esterification of Carboxylic Acids. Angewandte Chemie International Edition in English 17, 522-524.

Nimmerjahn, A., Kirchhoff, F., and Helmchen, F. (2005). Resting Microglial Cells Are Highly Dynamic Surveillants of Brain Parenchyma in Vivo. Science 308, 1314-1318.

Nyström, A.M., and Wooley, K.L. (2011). The Importance of Chemistry in Creating Well-Defined Nanoscopic Embedded Therapeutics: Devices Capable of the Dual Functions of Imaging and Therapy. Acc. Chem. Res. 44, 969-978.

Parrish, B., and Emrick, T. (2006). Soluble Camptothecin Derivatives Prepared by Click Cycloaddition Chemistry on Functional Aliphatic Polyesters. Bioconjugate Chem. 18, 263-267.

Parveen, S., Misra, R., and Sahoo, S.K. (2012). Nanoparticles: a boon to drug delivery, therapeutics, diagnostics and imaging. Nanomedicine: Nanotechnology, Biology and Medicine 8, 147-166.

Prabhu, P., and Patravale, V. (2012). The Upcoming Field of Theranostic Nanomedicine: An Overview. Journal of Biomedical Nanotechnology 8, 859-882.

Rochette, L., Ghibu, S., Richard, C., Zeller, M., Cottin, Y., and Vergely, C. (2013). Direct and indirect antioxidant properties of α-lipoic acid and therapeutic potential. Molecular Nutrition & Food Research 57, 114-125.

Schunack, M., Gragert, M., Döhler, D., Michael, P., and Binder, W.H. (2012). Low-Temperature Cu(I)-Catalyzed "Click" Reactions for Self-Healing Polymers. Macromol. Chem. Phys. 213, 205-214.

Sharma, A., Khatchadourian, A., Khanna, K., Sharma, R., Kakkar, A., and Maysinger, D. (2011). Multivalent niacin nanoconjugates for delivery to cytoplasmic lipid droplets. Biomaterials 32, 1419-1429.

Sharma, A., Neibert, K., Sharma, R., Hourani, R., Maysinger, D., and Kakkar, A. (2011). Facile Construction of Multifunctional Nanocarriers Using Sequential Click Chemistry for Applications in Biology. Macromolecules 44, 521-529.

Soliman, G.M., Sharma, A., Maysinger, D., and Kakkar, A. (2011). Dendrimers and miktoarm polymers based multivalent nanocarriers for efficient and targeted drug delivery. Chem. Commun. 47, 9572-9587.

Svenson, S. (2013). Theranostics: Are We There Yet? Molecular Pharmaceutics 10, 848-856.

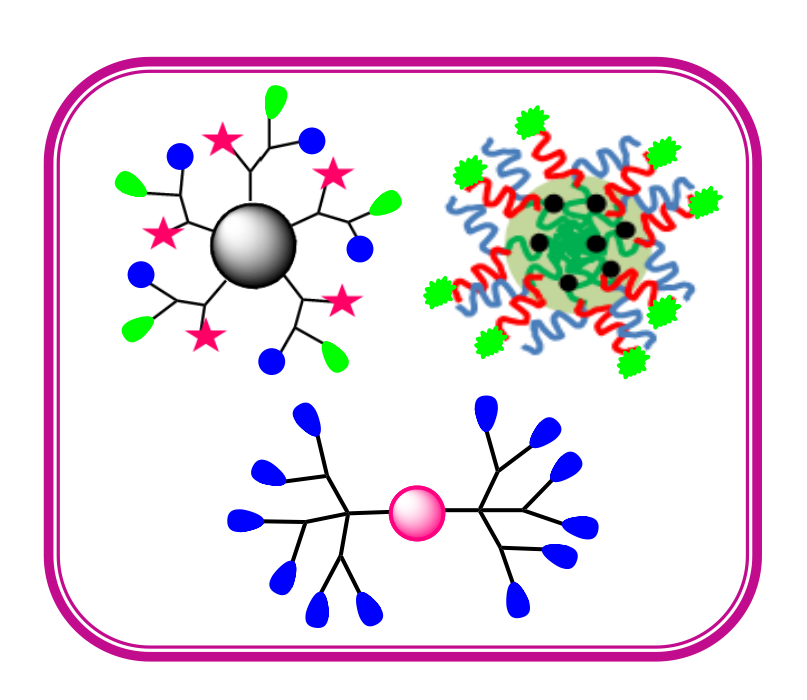
Tomalia, D.A., and Fréchet, J.M.J. (2002). Discovery of dendrimers and dendritic polymers: A brief historical perspective*. J. Polym. Sci., Part A: Polym. Chem. 40, 2719-2728.

Yu, S.S., Lau, C.M., Barham, W.J., Onishko, H.M., Nelson, C.E., Li, H., Smith, C.A., Yull, F.E., Duvall, C.L., and Giorgio, T.D. (2013). Macrophage-Specific RNA Interference Targeting via "Click", Mannosylated Polymeric Micelles. Molecular Pharmaceutics 10, 975-987.

Zhang, Y., Chan, H.F., and Leong, K.W. (2013). Advanced materials and processing for drug delivery: The past and the future. Advanced Drug Delivery Reviews 65, 104-120.

Chapter 6

Conclusions, Contributions to Original Knowledge, and Suggestions for Future Work



6.1 Conclusions and Contributions to Original Knowledge

Nanocarriers based on hyperbranched and branched macromolecules such as dendrimers and miktoarm polymers continue to draw attention of scientific community, due to their potential for a variety of applications, including drug delivery. Tremendous success has been achieved in the synthesis and characterization of these macromolecules, and the focus of research now is to design and develop new synthetic methodologies towards multitasking nanocarriers which are able to direct therapeutic agents to desired intracellular locations.

This thesis has first provided a detailed summary of the recent developments in the field of targeted drug delivery using macromolecular nanocarriers based on dendrimers and miktoarm polymers. It has then demonstrated the design and development of multifunctional macromolecules using simple and highly versatile synthetic strategies. These methodologies allow the exploration of efficient drug delivery, by covalent linking of drugs in dendrimers and physical entrapment in the hydrophobic core of miktoarm polymer micelles. The synthetic methodology reported in this thesis is versatile enough, and can be used to develop a wide variety of tunable multifunctional nanomaterials to target drugs and bioactive molecules to various cellular organelles. For example, we developed a niacin conjugated nano-delivery system based on bi-functional dendrimers to deliver the drug to intracellular lipid droplets (LDs). LDs are one of the relatively new cellular organelle being explored for subcellular targeting by nanostructures. This approach can open new doors in nanomedicine for the treatment of diseases caused due to excessive accumulation of triglycerides, e.g. atherosclerosis and obesity.

The versatility of our chemistry was further expanded to bi-functional and tri-functional nanocarriers based on dendrimers, using a combination of click reactions in sequence with esterification. Multiple functions were covalently incorporated into a single dendrimer scaffold using molecular building blocks with orthogonal functionalities. We used this methodology to synthesize two bifunctional dendrimers, one with a combination of a model therapeutic agent (α -

lipoic acid) and a stealth agent (PEG), other with a comination of an imaging dye (BODIPY) and PEG. We also constructed a trifunctional dendrimer where we introduced all the three functions, *i.e.* therapeutics, imaging and stealth in one dendrimer. The biological studies have shown that these nanocarriers are noncytotoxic and can reduce H₂O₂-induced oxidative stress in PC12 cells. This is an exciting discovery as using this strategy we can construct dendrimers with any combination of multiple functionalities for biological applications. The synthetic methodology developed in this thesis is highly versatile and can be applied to design and construct other multifunctional macromolecules for a diverse range of applications.

We have demonstrated that the drug molecules can be efficiently physically encapsulated into miktoarm polymer micelles which can be directed towards a specific organelle. We developed an easy and efficient way to construct multifunctional nanocarriers based on ABC type miktoarm polymers using click chemistry in combination with ring-opening polymerization. Our results have demonstrated that these miktoarm polymers can be used to form micelles in an aqueous medium, and extraordinarily large quantities of CoQ10 can be loaded into these micelles. Our studies showed that these carriers did indeed reach mitochondria, and thus can be used as a suitable means of drug delivery to this organelle. These results can be easily extended to the construction of nanocarriers for other targeted nano-delivery sytems, and can incorporate different pharmacological agents.

We have also demonstrated the synthesis of fluorescent dendrimers with inherent imaging capabilities. The presence of imaging agent as the integral part of nanocarrier structure provides opportunities to track the passage of these nanocarriers. It also offers the ability to introduce large amount of therapeutical agents alone or in combination with solubilising polymers or targeting ligands.

6.2 Suggestions for future work

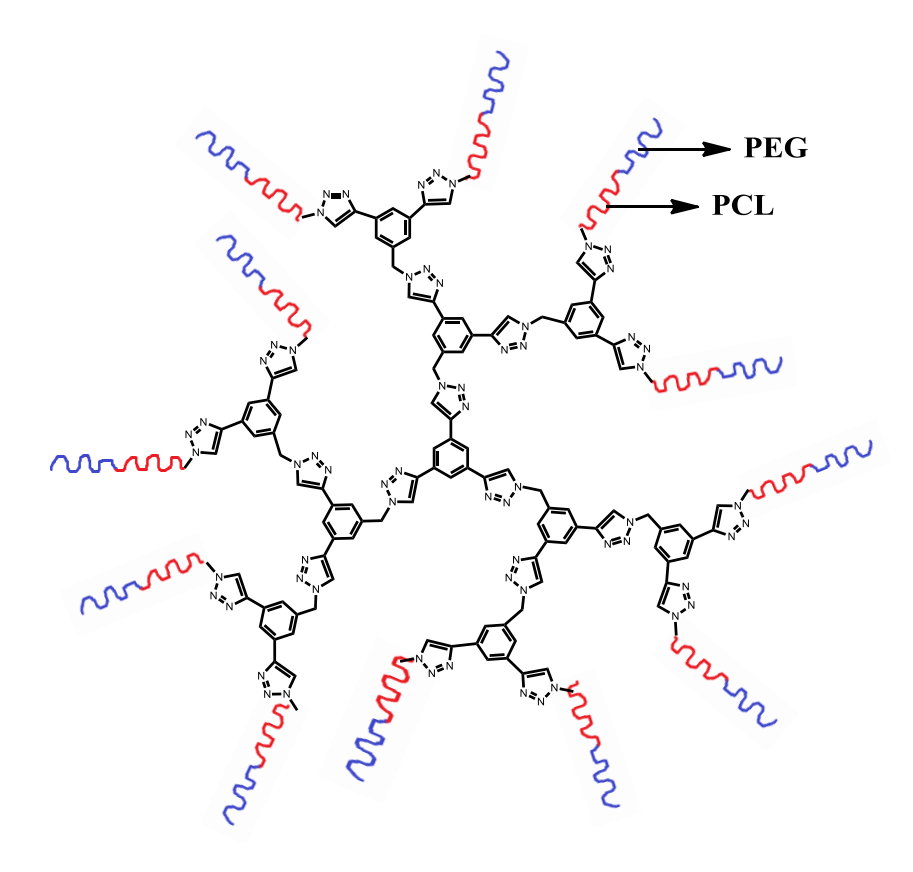


Figure 6.1. Amphiphilic dendritic polymer

6.2.1. Designing amphiphilic dendritic polymers using Click chemistry

We have designed and evaluated dendrimers and miktoarm polymers based nanocarriers separately for drug delivery. It will be interesting to combine these two platforms to construct dendritic polymers and evaluate their potential as nanocarriers for the delivery of therapeutic molecules. Amphiphilic dendritic polymers composed of poly(ethyleglycol) (PEG) and poly(caprolactone) (PCL) can be constructed based on acetylene terminated dendrimer backbones described in the beginning of chapter 2. A library of linear block copolymers constituting different lengths of PEG and PCL can be synthesized by performing ring-opening polymerization of \(\varepsilon\)-caprolactum on terminal hydroxyl group of monomethoxy poly(ethyleneglycol). The terminal hydroxyl group of PEG-PCL linear block copolymer can be transformed to an azide focal point to participate in click reaction on acetylene terminated dendrimers. The self assembly of these

amphiphilic dendritic polymers can be studied to understand the type of unique architectures these can produce. The hydrophobic core of these self assembled structures can be utilized for physical entrapment of hydrophobic drugs.

6.2.2. Designing tetrafunctional dendrimer: Combining Therapeutics, Imaging, Stealth and Targeting

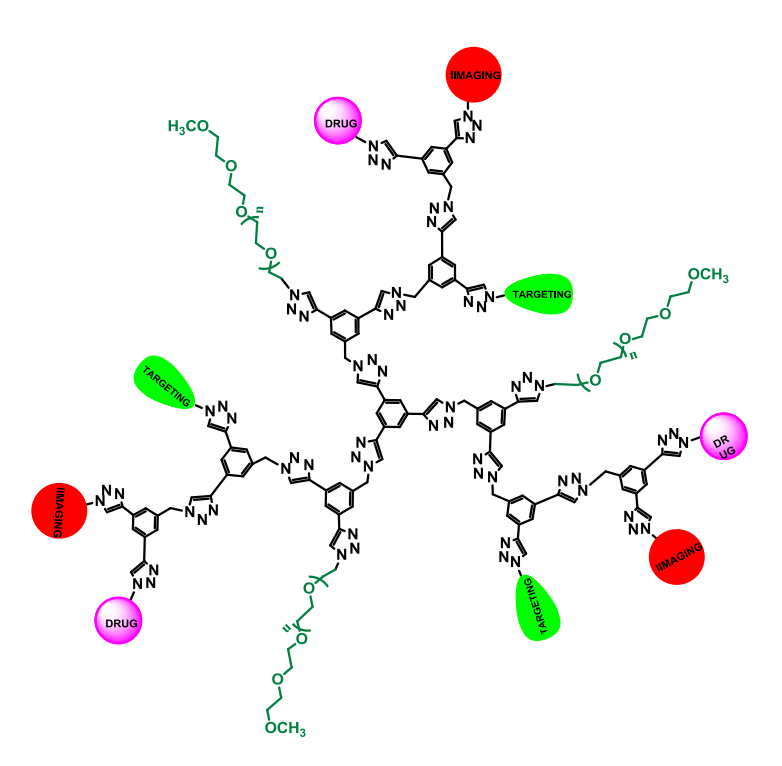


Figure 6.2. Tetrafunctional dendrimer with a combinition of therapeutics, imaging, stealth and targeting agents.

We have demonstrated simple and efficient synthetic mathodologies to construct bi- and tri-functional dendrimers. As the dendrimer backbones described in this thesis are not cytotoxic, the synthetic methodology presented here can be extended further to incorporate four different functionalities in single dendrimer scaffold developing a tetra-functional nanocarrier. The single nanocarrier can be designed to accommodate drug molecules, targeting ligand, imaging agent and solubilising polymers. Combination of all these functions in a single nanocarrier can provide aqueous solubility as well as enhance the efficacy of drugs by bringing them to specific site of action in the body. These dendrimers can also be

utilized to develop carriers for combination therapy by putting two different drugs with synergistic effects along with targeting and tracking agents for enhanced therapeutic effect. This sytem will allow a variety of combinations of drug molecules and targeting moieties, and thus can be utilized to target a wide variety of cellular organelles for treatment of various diseases.

6.2.3. Designing multifunctional trackable dendrimers for theranostic applications.

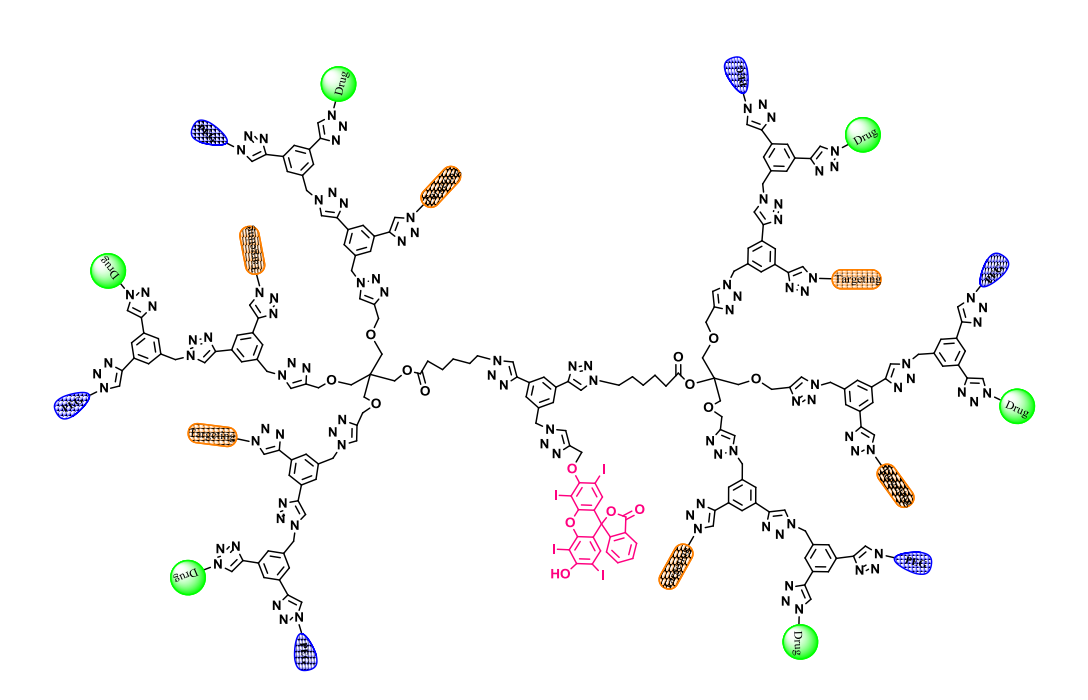


Figure 6.3. Multifunctional trakable dendrimer

The trackable dendrimer backbones described in chapter 5 can be further extended using orthogonal building blocks described in this thesis to incorporate multiple functionalities on the periphery. The combination of functionalities on the periphery can be varied in terms of targeting agent, tracking ligand or solubilising molecules, based on the requirement and need. The synthetic methodology described in this thesis can be easily used to develop these trackable nanocarriers. As the imaging is inherent part of dendrimer structure the periphery

can be utilized and extended to incorporate any desired combination of active pharmaceutical agents with other functional moieties. These multifunctional inherently fluorescent dendrimers can be used as potential candidates to deliver drugs to their targeted intracellular locations.

Appendix 1

Designing dendritic frameworks using versatile building blocks suitable for Cu^I-catalyzed alkyne azide 'click' chemistry

Reproduced in part with permission from Hourani, R.; Sharma, A.; and Kakkar, A. *Tetrahedron Letters* **2010**, 51, 3792-3795.

Copyright, 2010, Elsevier

ELSEVIER

Contents lists available at ScienceDirect

Tetrahedron Letters

journal homepage: www.elsevier.com/locate/tetlet



Designing dendritic frameworks using versatile building blocks suitable for Cu^I-catalyzed alkyne azide 'click' chemistry

Rami Hourani, Anjali Sharma, Ashok Kakkar*

Department of Chemistry, McGill University, 801 Sherbrooke St. West, Montreal, Qc, Canada H3A 2K6

ARTICLE INFO

Article history:
Received 21 April 2010
Revised 11 May 2010
Accepted 13 May 2010
Available online 21 May 2010

ABSTRACT

Synthesis of molecular building blocks that incorporate azide and alkyne-terminated functionalities suitable for Cu^L-catalyzed cycloaddition between alkynes and azides is reported. Their utility in constructing dendritic frameworks with 4, 6, or 12 peripheral acetylene groups using either the convergent or divergent methodology, and their functionalization with desirable end groups are demonstrated.

© 2010 Elsevier Ltd. All rights reserved.

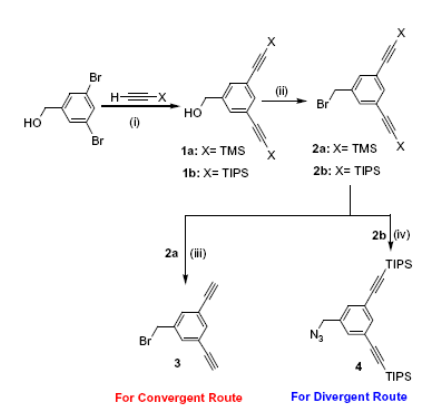
Dendrimers constitute key components in the quest to build smart nanodevices for applications in a diverse range of areas including biology and medicine.1 The synthesis of these monodisperse macromolecules has attracted the imagination of scientists, and it has already generated a large library with varied backbones.2 A major contribution to this increasing interest in dendrimer synthesis has been made by one of the highly efficient 'click' reactions that involves Cul-catalyzed coupling of an alkyne with an azide (CuAAC).3 The versatility of this methodology lies in the design of appropriate alkyne and azide-terminated molecular units which can then be 'clicked' together under a variety of mild reaction conditions. We report herein the synthesis of highly versatile AB2 (A: N3; and B: C=CH) building blocks that can be used to perform CuAAC 'click' chemistry to construct dendrimers using either the divergent or the convergent synthetic methodology. We demonstrate that the scope and utility of this 'greener' approach to the synthesis of dendrimers can be easily elaborated by designing such building blocks. We used these molecular units to construct dendritic frameworks which contain 4, 6, or 12 peripheral alkynes using 'click' chemistry. The potential of surface active acetylene groups in these dendrimers is demonstrated by coupling functional molecules of interest4 such as a fluorescent dye (BODIPY PM 605) and positively charged amine centers leading to water-soluble dendrimers.

For the dendrimer synthesis using CuAAC 'click' chemistry, we envisioned a molecular unit that will incorporate a primary azide and two protected acetylenes which could be made active at the desired stage. The synthetic elaboration was begun using 3,5-dibromobenzyl alcohol, and to which trimethylsilylacetylene (1a) or triisopropylsilylacetylene (1b) was linked through bromo position using Sonogashira coupling (Scheme 1). It was subsequently followed by bromination of the benzylalcohol group (2a and 2b). The building blocks 2a and 2b provide versatile platforms to con-

0040-4039/\$ - see front matter @ 2010 Elsevier Ltd. All rights reserved. doi:10.1016/j.tetlet.2010.05.061

struct dendrimers using either (i) the convergent methodology, ^{2f} in which dendrons are built separately, and then as a final step their focal point is activated and used to anchor the dendron onto the appropriate core or (ii) the divergent methodology, ^{2h} insideout approach that employs an iterative build-up starting from the core molecule.

For the convergent construction of dendrimers, the protective (TMS) groups of **2a** were removed using a mild deprotection process with K₂CO₃. The two acetylene arms in **3** are now available for performing CuAAC click reaction, while the bromo-benzyl consti-



Scheme 1. Synthesis of building blocks for convergent and divergent routes to dendritic frameworks. Reagents and conditions: (i) PdCl₂(PPh₃)₂/Cul (cat.), NE₂H, reflux, overnight, 1a: 89%, 1b: 90%; (ii) CBr₄/TPP, THF 2 h, 2a: 72%, 2b: 87%; (iii) K₂CO₃, H₂O/acetone, overnight, 3: 89%; (iv) NaN₃, DMF, room temperature (rt), 2 h, 4: 96%,

^{*} Corresponding author. Tel.: +514 398 6912; fax: +514 398 3797. E-mail address: ashok.kakkar@mcgill.ca (A. Kakkar).

Scheme 2. Model reaction. Reagents and conditions: (i) CuSO₄·SH₂O/sodium ascorbate, DMF/H₂O/THF, rt, overnight; (ii) Bu₄NF, THF, **5a**: 92%, **5b**: 89%.

tutes a focal point that can be activated later by converting it to an azide for coupling to core molecules of interest.

For the divergent synthesis, we converted the bromide arm of 2b to an azide (4) by a simple azidation reaction using NaN₃ in DMF. Compound 4 is used in performing CuAAC click reaction with acetylene-terminated core molecules such as 1,4-diethynylbenzene (DEB) with two acetylene arms and 1,3,5-triethynylbenzene (TEB) with three acetylenes, using the divergent methodology, as will be demonstrated below. Interestingly, azidation of 2a, and its subsequent use in divergent synthesis with CuAAC click reaction, in the presence of the more labile TMS protective groups, did not proceed very well, and yielded a mixture of products. We believe that it was mainly due to a premature deprotection of the TMS groups in situ under the CuAAC reaction conditions. This was confirmed by the appearance of the acetylene protons in its ¹H NMR. Thus, the TMS-protected acetylenes are not ideal silent partners in CuAAC 'click' chemistry.

As a model reaction, compound 4 was first reacted with a divalent core (DEB) using the 'click' reaction with copper sulfate pentahydrate (CuSO₄·5H₂O) and sodium ascorbate (Scheme 2) to give a four-arm structure with protected acetylene groups (5a). The removal of TIPS groups was then achieved using Bu₄NF (5b). It should be noted that in this general procedure the sequence of adding the reactants and solvents is highly crucial to ensure a complete reaction. All reactants, except CuSO₄·5H₂O, were dissolved in a minimal amount of DMF, followed by the addition of CuSO₄·5H₂O as an aqueous solution, and then finally THF was added to the mixture. Varying the solvent mixture or the order of addition led to incomplete reactions and lower yields. Thus, we followed the general procedure described above throughout the work reported here for building dendritic frame-

Br
$$\frac{(i)}{4}$$
 $\frac{N-N}{N}$ $\frac{6a}{(iii)}$ $\frac{N-N}{N}$ $\frac{N-N}{N}$

Scheme 3. Reagents and conditions: (i) CuSO₄·5H₂O/sodium ascorbate, DMF/H₂O/THF, rt, overnight, 6a: 97%; (ii) Bu₄NF, THF, 6b: 72%; (iii) NaN₃, DMF, rt, 2 h, 7: 89%.

works, with only slight variation of temperature and the time of reaction

For the convergent synthesis of dendrimers, dendrons using building blocks 3 and 4 were prepared (Scheme 3). The CuAAC click reaction was carried out using a similar procedure as described above for the construction of 5a, and it yielded a second generation dendron with four TIPS-protected arms (6a). The TIPS protective groups can be easily removed to give free acetylene arms (6b), made available for further click reaction, to build higher generation dendrons. Alternatively, the bromine focal point of dendron 6a can be activated by converting it to an azide, which could be covalently linked to a core molecule while keeping the acetylene peripheries protected. It is important to mention here that the deprotection of 6a with Bu₄NF gave lower yield than expected. This was due to the fact that Bu₄NF deprotection is also accompanied by the substitution of Br with F at the focal point, as confirmed by 1H NMR, and mass spectroscopies. The fluoro-substituted core does not yield to subsequent azidation.

The synthesis of the first generation dendrimer with six TIPS-protected acetylenic arms (8a) was achieved using the divergent methodology (Scheme 4), in which the trivalent core TEB was reacted with compound 4. Subsequent removal of the protective groups using Bu₄NF yields the first generation dendrimer with six free acetylenes (8b) available for functionalization with any azide-terminated molecule of interest. To demonstrate this possibility, and the feasibility of building higher dendrimer generations, 8b was reacted with compound 4 to give the second generation dendrimer with 12 TIPS-protected acetylene arms (9a) as shown in Scheme 4. The reaction was performed using the general procedure described in the synthesis of 5a, however it was left to proceed for 48 h instead of overnight to ensure complete reaction of compound 4 with all the available six acetylene arms of the first generation dendrimer (8b).

We believe that the increasing polarity of the system with an increase in generation number, and steric crowding at the periphery, slows down the reaction, and thus requires longer time for completion.

Alternatively, the TIPS-protected second generation dendrimer (9a) can also be synthesized using the convergent methodology by reacting the previously prepared dendron 7 with the trivalent TEB core (Scheme 4). The reaction conditions were similar to those employed in the divergent methodology, however, heating at 40 °C was necessary for complete substitution. The TIPS protective groups of the second generation dendrimer, from both convergent and divergent routes, were then removed using Bu₄NF to give the second generation dendrimer with 12 acetylene peripheral groups (9b).

It is worth mentioning that in all the 'click' reactions reported here, we used slight excess of azide-terminated molecules to ensure completion to almost quantitative yields (>90%). The removal of excess azide-terminated compound was found to be very easy via flash column chromatography, due to a clear difference in polarity and solubility, as more polar triazole ring-containing products are formed. The lower polarity of the starting materials facilitated their removal using low polarity solvent mixtures, except in the case of the protected second generation dendrimer 9a, in which the presence of 12 triisopropylsilyl groups enhanced its solubility to a great extent, and it could be flushed down a short column with hexanes, while the excess of the starting material stayed on the column. The synthetic elaboration of the dendrimers was monitored by TLC, ¹H and ¹³C{¹H} NMR spectroscopy. The latter were found to be diagnostic since there is a clear shift in the 1H and ¹³C(¹H) NMR signals as the triazole rings were formed. Interestingly, all compounds reported here were found to be soluble in most organic solvents with the exception of 5b and 9b, in which upon removal of the protective TIPS groups the compounds were

Scheme 4. Convergent and divergent syntheses of dendritic frameworks. Reagents and conditions: (i) CuSO₄·5H₂O/sodium ascorbate, DMF/H₂O/THF, rt, overnight, 8a: 96%; (ii) Bu₄NF, THF, 8b: 95%; (iii) and (iv) CuSO₄·5H₂O/sodium ascorbate, DMF/H₂O/THF, rt, 48 h; 9a: 90%, 9b: 89%.

found to be soluble only in DMF and DMSO. This is intriguing, and we are currently investigating the relationship between the number of triazole rings and free acetylene groups in the structure, on the solubility of these dendrimers.

The potential of these dendrtic frameworks in coupling desired functional groups at the periphery was successfully demonstrated by performing the 'click' reaction with two different azide-terminated molecules. For example, dendrimer 8b containing six terminal acetylene groups was reacted with azide-functionalized BODIPY dye (pyrromethene 605) in the presence of copper sulfate pentahydrate (CuSO₄·5H₂O) and sodium ascorbate (Scheme 5). It led to the formation of dendrimer 10 with six covalently linked imaging dye molecules. In a similar manner, dendrimer 8b was coupled with azide-functionalized t-BOC-protected amine to form dendrimer 11a.

The deprotection of six periphery situated t-BOC-protected amines in 11a using trifluoroacetic acid (TFA) gave a water-soluble dendrimer 11b containing six terminal NH $_3$ + groups. These reactions were easily monitored using FT-IR spectroscopy, as the acetylene peak at 2104 cm $^{-1}$ in 8b disappeared upon peripheral coupling (10 and 11a).

In summary, we have demonstrated that by designing appropriate building blocks for highly efficient CuAAC click reaction, one could tailor the synthesis to create a small series of dendritic frameworks with different valencies for further functionalization. Recent reports in the literature have suggested that it is easier and more practical to build the dendritic frameworks, and then introduce suitable surface functionalities as the final step.^{2b,5} The free acetylene groups at the periphery of compounds 5b, 8b, and 9b provide this opportunity, and can be used to couple a diverse range of azide-ter-

$$8b \xrightarrow{N-N} N = 0$$

$$N = N$$

$$N$$

Scheme 5. Reagents and conditions: (i) CuSO₄·5H₂O/sodium ascorbate, DMF/H₂O/THF, rt, 48 h, 11a BOC-NH-CH₂-CH₂-: 82%, 11b NH₃+-CH₂-CH₂-: 86%.

minated molecules of interest including fluorescent dyes and charged centers leading to water-soluble dendrimers.

Acknowledgments

We would like to thank NSERC (Canada) and Center for Self-Assembled Chemical Structures (FQRNT, Qc Canada) for financial assistance, and for a post-graduate fellowship to R.H.

Supplementary data

Supplementary data (detailed synthetic and characterization data for all the compounds) associated with this article can be found, in the online version, at doi:10.1016/j.tetlet.2010.05.061.

References and notes

(a) Gillies, E. R.; Dy, E.; Fréchet, J. M. J.; Szoka, F. C. Mol. Pharm. 2004, 2, 129; (b) Islam, M.; Majons, I. J.; Baker, J. R., Jr. J. Chromatogr. B. Analyt. Technol. Biomed. Life Sci. 2005, 21, 822; (c) Svenson, S.; Tomalia, D. A. Adv. Drug Delivery Rev. 2005, 57, 2106; (d) Langereis, S.; Dirksen, A.; Hackeng, T. M.; van Genderena, M. H. P.; Mcijer, E. W. New J. Chem. 2007, 31, 1152; (e) Hourani, R.; Kakkar, A. Macromol. Rapid Commun. 2010. doi:10.1002/marc.200900712.

- (a) Joralemon, M. J.; O'Reilly, R. K.; Matson, J. B.; Nugent, A. K.; Hawker, C. J.; Wooley, K. L. Macromolecules 2005, 38, 5436; (b) Grayson, S. M.; Fréchet, J. M. J. Chem. Rev. 2001, 101, 3819; (c) Gosage, R. A.; van de Kuil, L. A.; van Koten, G. Acc. Chem. Res. 1998, 31, 423; (d) Majoral, J.-P.; Caminade, A.-M. Chem. Rev. 1998, 31, 423; (d) Majoral, J.-P.; Caminade, A.-M. Chem. Rev. 1999, 99, 1689; (f) Hawker, C. J.; Fréchet, J. M. J. J. Am. Chem. Soc. 1990, 112, 7638–7647; (g) Newkome, G. R.; Yao, Z.; Baker, G. R.; Gupta, V. K. J., Org. Chem. 1985, 50, 2003–2004; (h) Tomalia, D. A.; Baker, H.; Dewald, J.; Hall, M.; Kallos, G.; Martin, S.; Rock, J.; Ryder, J.; Smith, P. Polym. J. 1985, 17, 117.
 (a) Kolb, H. C.; Finn, M. G.; Sharpless, K. B. Argew. Ghem., Int. Ed. 2001, 40, 2004; (b) Wu, P.; Hawker, C. J.; Scheel, A.; Vott, B.; Pyun, J.; Fréchet, J. M.; Sharpless, K. B.; Pokin, V. V.; Feldman, P.; Nugent, A. K. Argew. Chem., Int. Ed. 2001, 40, 3094; (e) Antoni, P.; Nyström, D.; Hawker, C. J.; Hult, A.; Malkoch, M. Chem. Commun. 2008, 5267; (e) Carlmark, A.; Hawker, C. J.; Hult, A.; Malkoch, M. Chem. Soc. Rev. 2009, 38, 352; (f) Antoni, P.; Hed, Y.; Nordberg, A.; Nyström, D.; von Holst, H.; Hult, A.; Malkoch, M. Argew. Chem., Int. Ed. 2009, 48, 2126; (g) Fabbritzzi, P.; Cicchi, S.; Brandi, A.; Sperotto, E.; van Koten, G. Eur., J. Org. Ghem. 2009, 5423; (h) Franc, G.; Kakkar, A. Chem. Soc. Rev. 2010, 39, 1536.
 (a) Wu, P.; Malkoch, M.; Hunt, J. N.; Vestberg, R.; Kaltgrad, E.; Finn, M. G.; Fokin, V. V.; Sharpless, K. B.; Hawker, C. J. Chem. Commun. 2005, 5775; (b) Gopin, A.; Bener, S.; Attali, B.; Shabat, D. Biocongigate Chem. 2006, 17, 1432; (c) Parrish, B.; Emrick, T. Bioconjugate Chem. 2007, 18, 263; (d) Ornelas, C.; Ruiz Aranzaes, J.; Cloutet, E.; Alves, S.; Astruc, D. Angew. Chem., Int. Ed. 2007, 46, 872; (e) Kolb, H. C.; Sharpless, K. B. DDT 2003, 8, 1128.
 (a) Goodwin, A. P.; Lam., S. S.; Fréchet, J. M. J., Am. Chem. Soc. 2007, 129, 6994; (b) Gillies, E.; F

Appendix 2

Supporting Information - Chapter 2: Multivalent Niacin Nanoconjugates for Delivery to Cytoplasmic Lipid Droplets

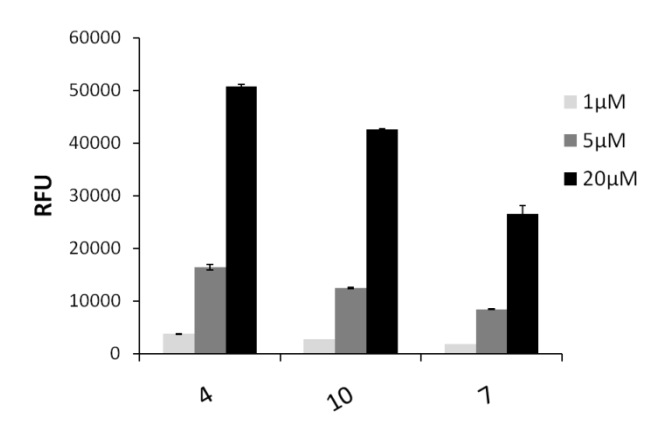


Figure S2.1. Spectrofluorometric measurements of relative fluorescence intensity of each carrier (**4**, **10**, **7**) were performed in dimethyl sulfoxide at the indicated concentrations. Fluorescence intensity, expressed in relative fluorescence units (RFU), was measured by using a 544/590 nm (excitation/emission) setup.

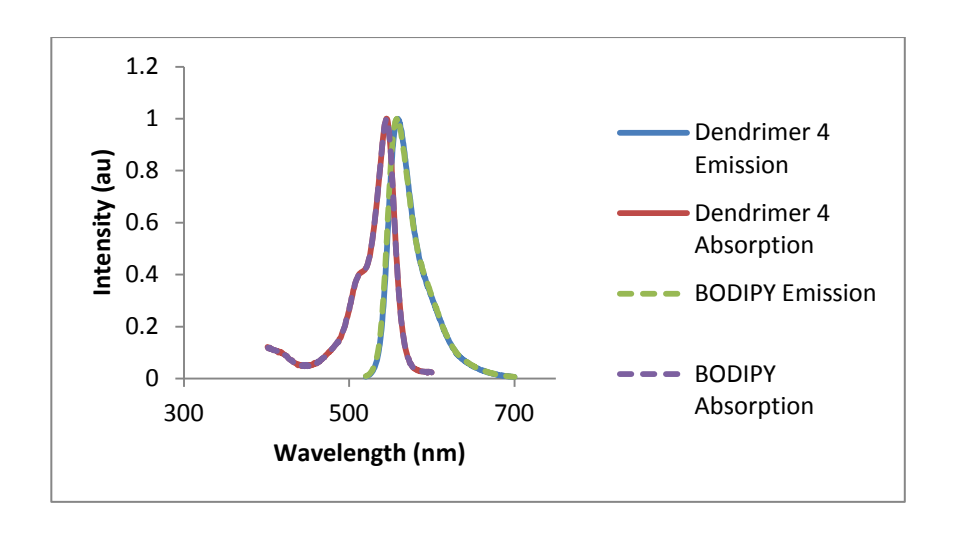
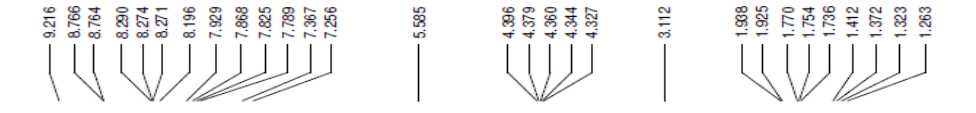


Figure S2.2 The absorption and emission spectra of the commercial red BODIPY dye and dendrimer 4. A typical λ max (absorption) at 545 nm, and λ max (emission) at 559 nm was observed in p-dioxane. Similar results were obtained with all other dye containing compounds: The linear compound 7 and the trifunctional miktoarm compound 10.



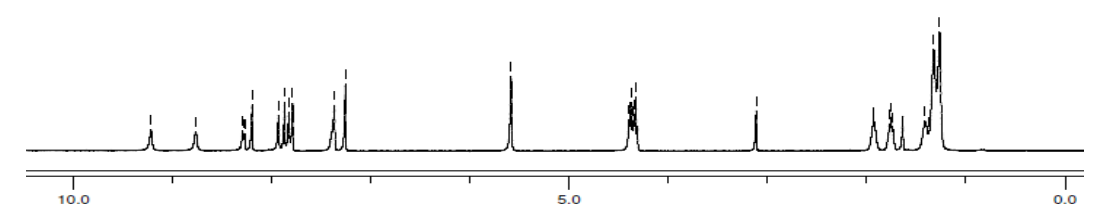


Figure S2.3a. ¹H NMR (400 MHz, CDCl₃) spectrum of compound **3**.

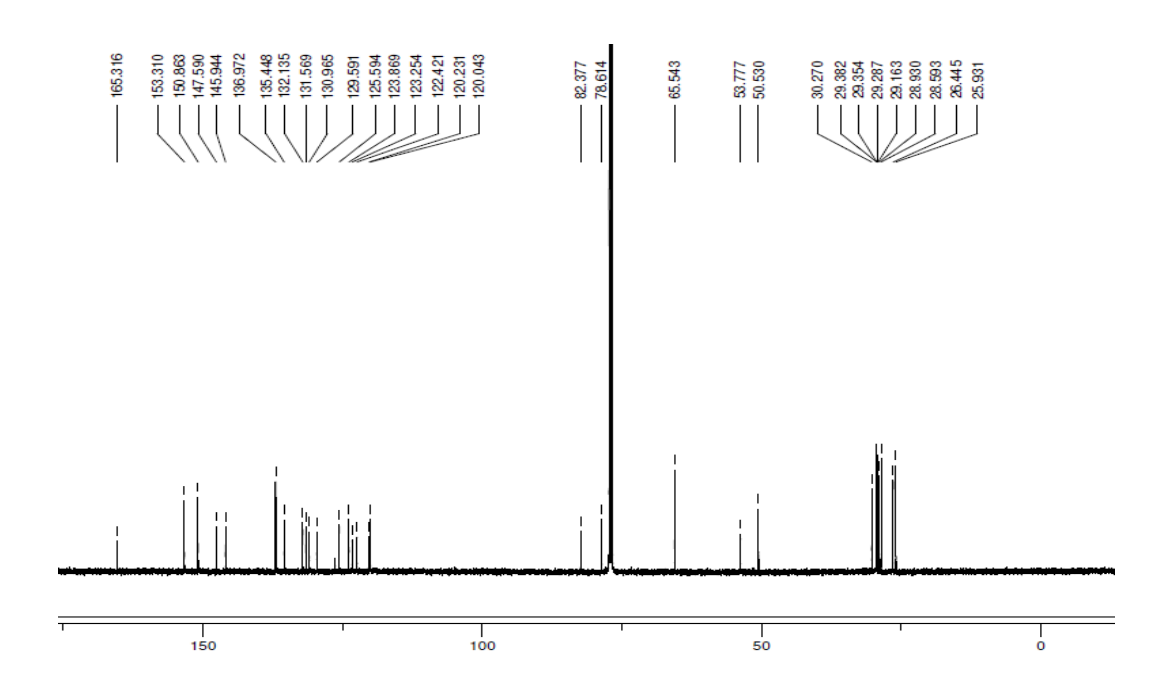


Figure S2.3b. ¹³C{¹H} NMR (125 MHz, CDCl₃) spectrum of compound 3.

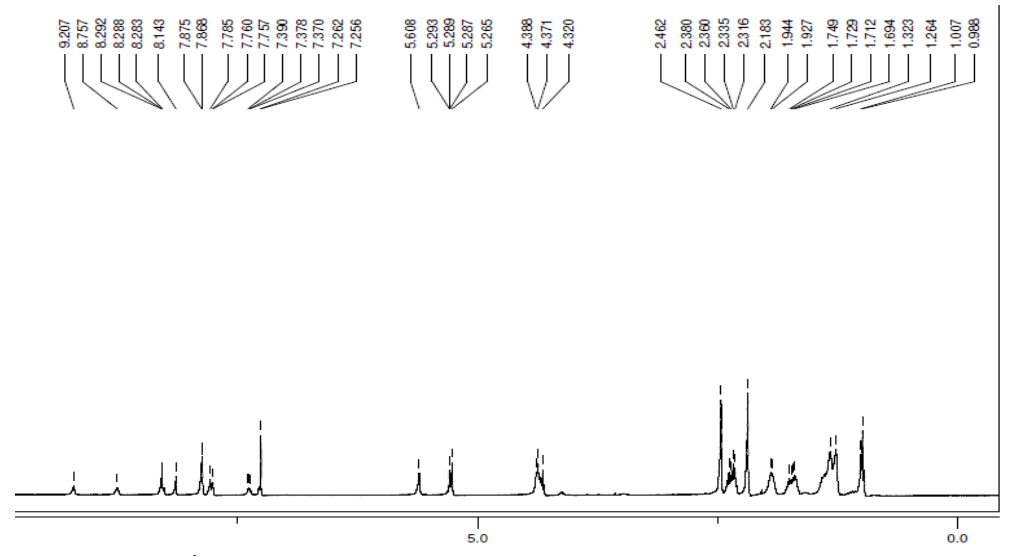


Figure S2.4a. 1 H NMR (400 MHz, CDCl₃) spectrum of compound 4.

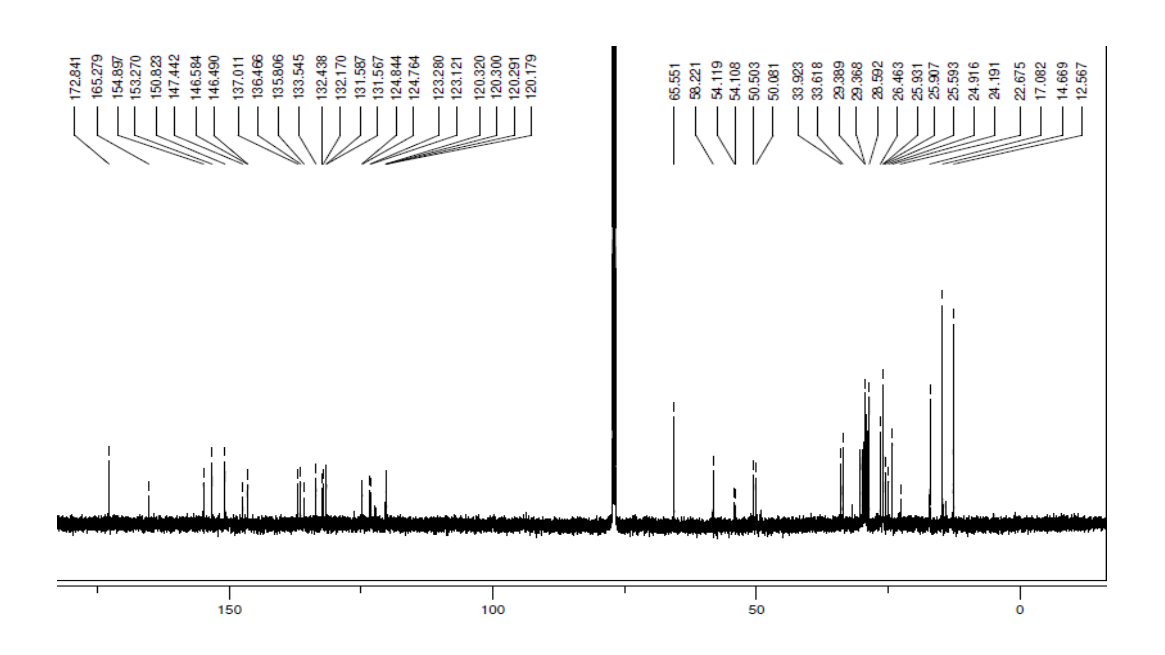


Figure S2.4b. ¹³C{¹H} NMR (125 MHz, CDCl₃) spectrum of compound **4**.

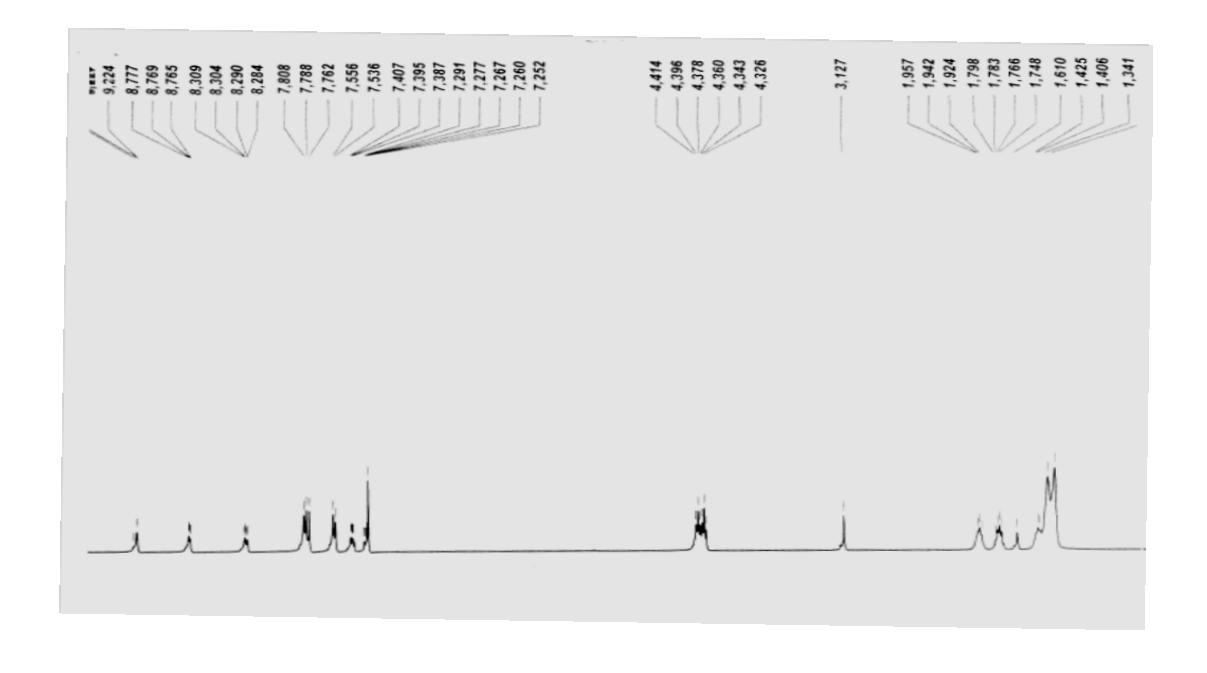


Figure S2.5a. ¹H NMR (400 MHz, CDCl₃) spectrum of compound **6**.

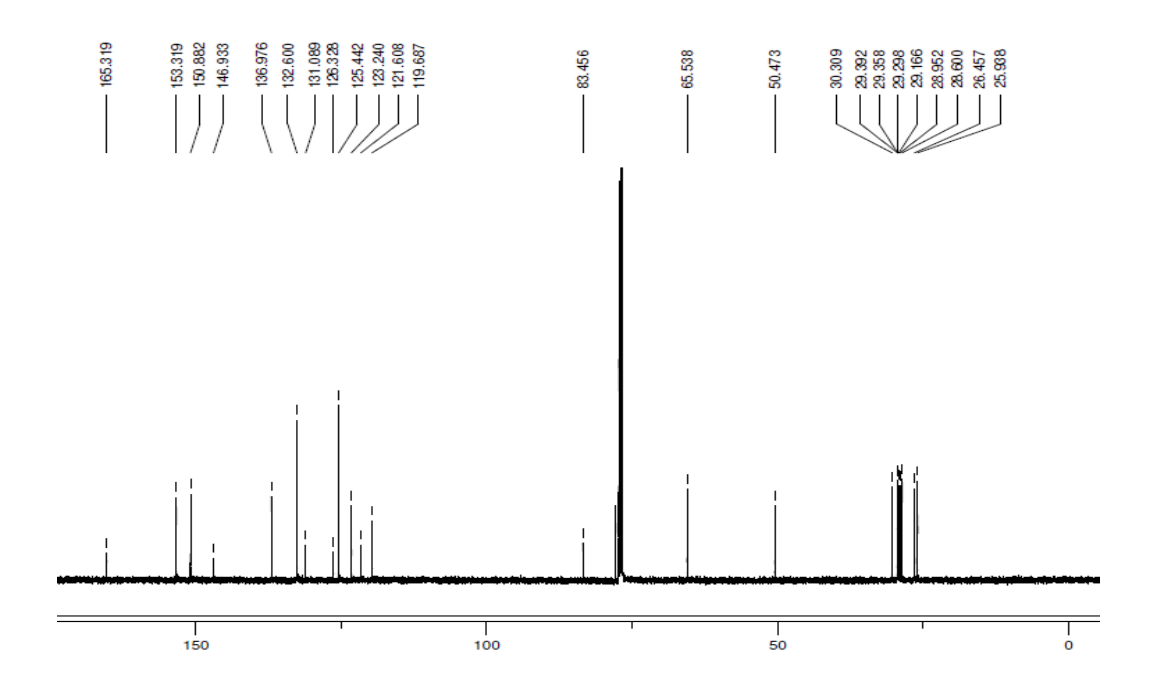


Figure S2.5b. ¹³C{¹H} NMR (125 MHz, CDCl₃) spectrum of compound 6.

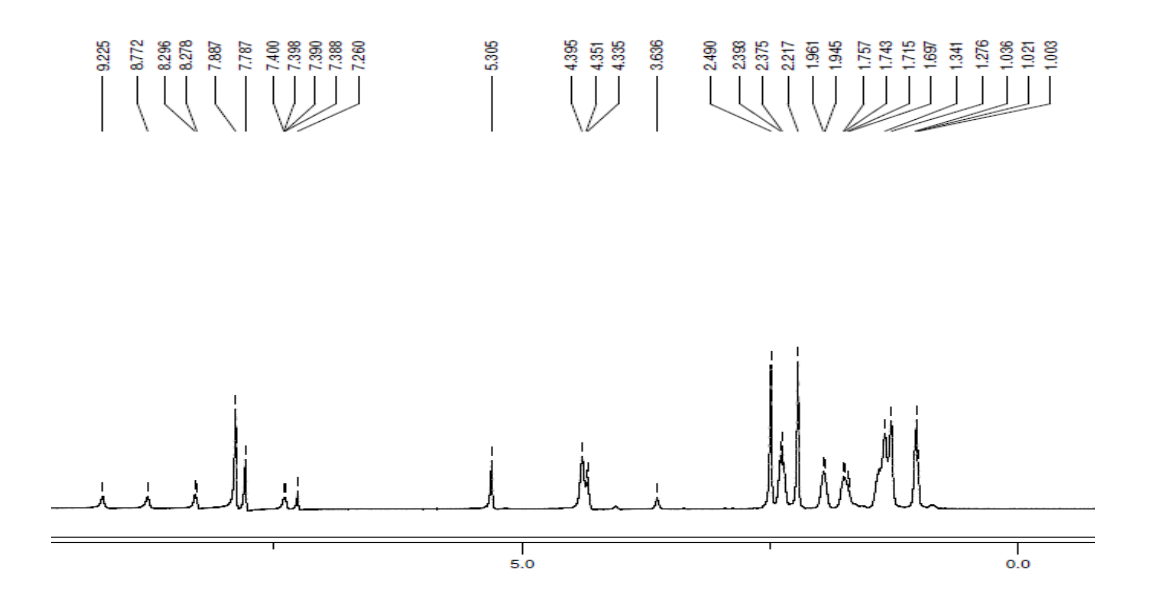


Figure S2.6a. ¹H NMR (400 MHz, CDCl₃) spectrum of compound **7**.

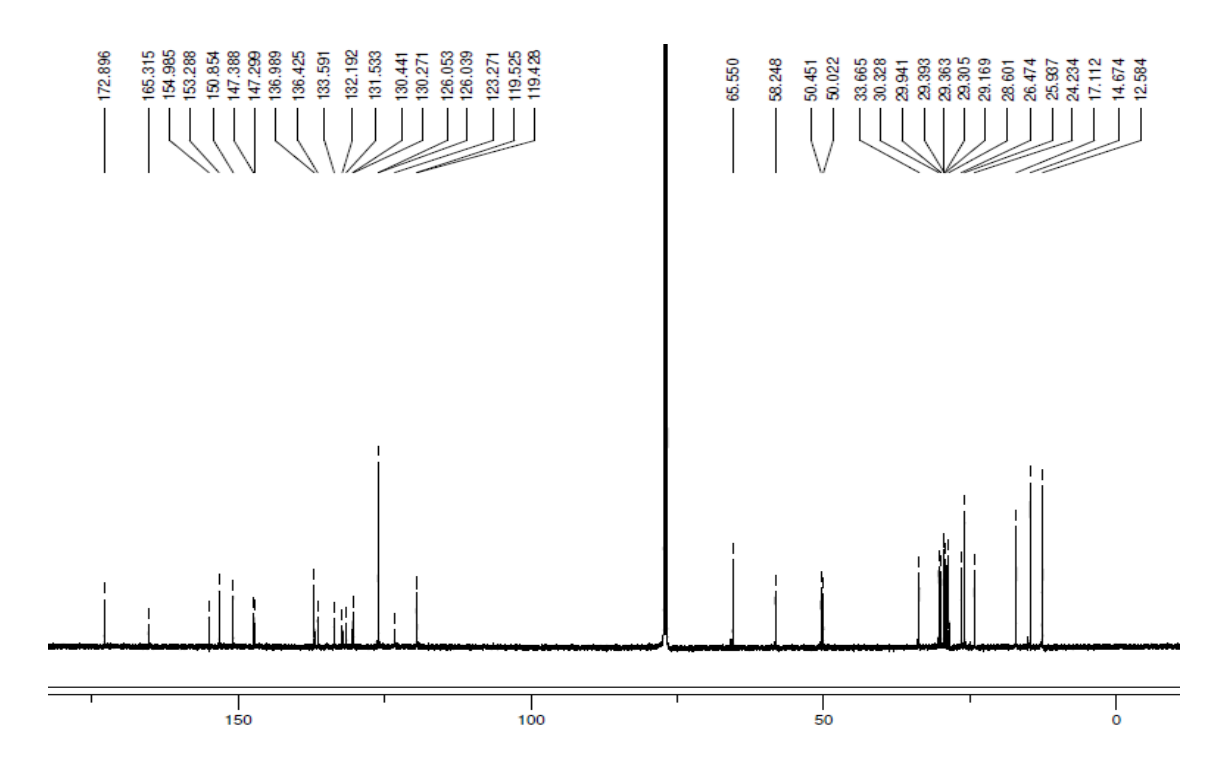


Figure S2.6b. ¹³C{¹H} NMR (125 MHz, CDCl₃) spectrum of compound 7.

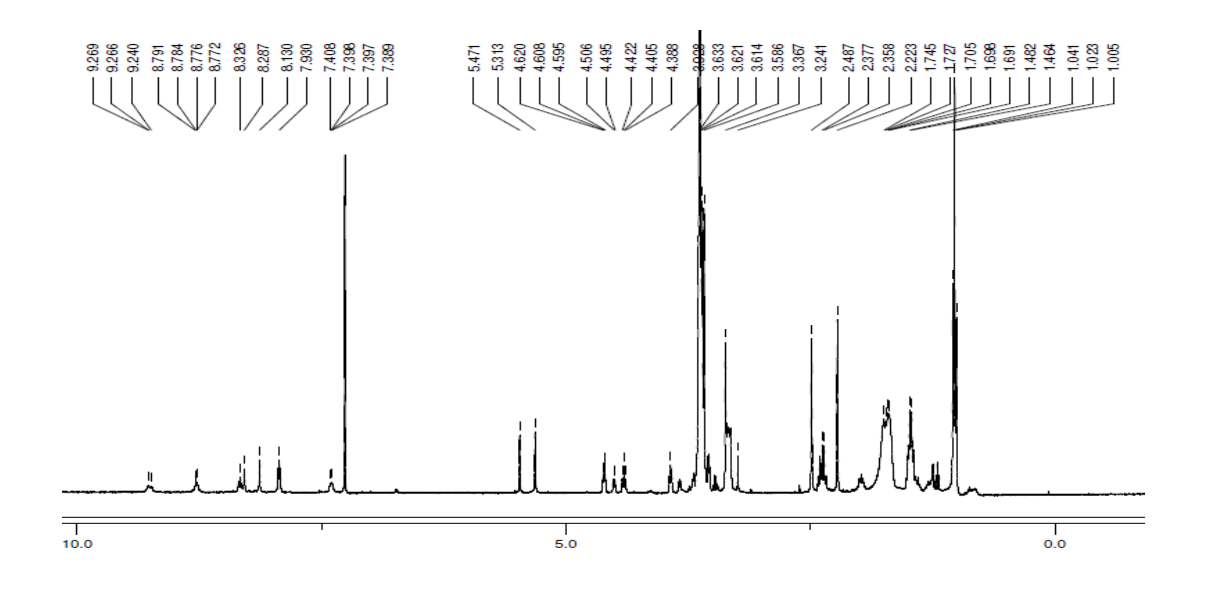


Figure S2.7a. ¹H NMR (400 MHz, CDCl₃) spectrum of compound **10**.

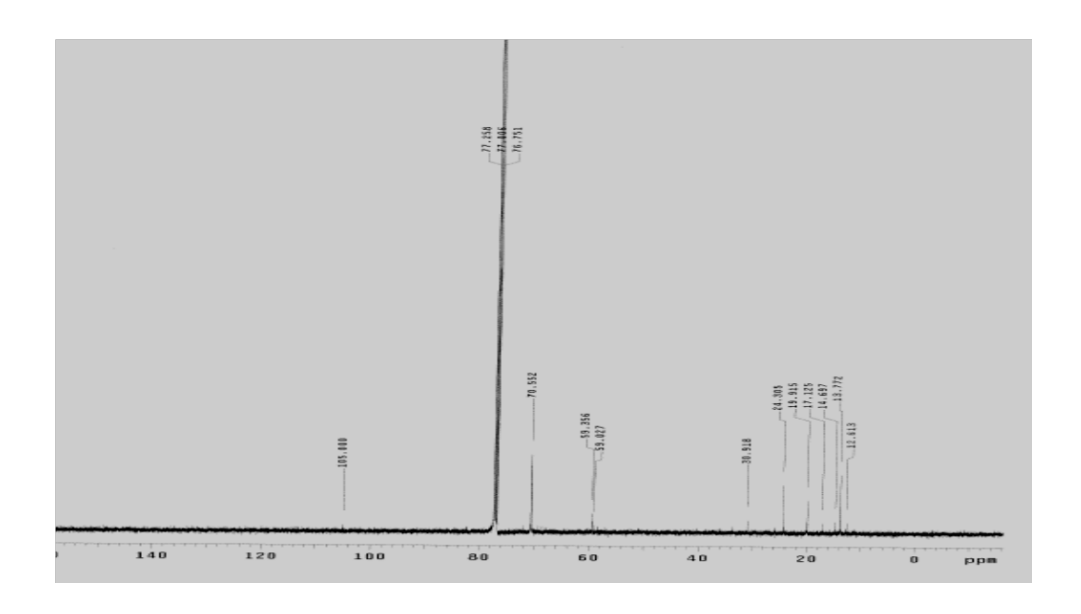


Figure S2.7b. $^{13}C\{^{1}H\}$ NMR (125 MHz, CDCl₃) spectrum of compound **10**.

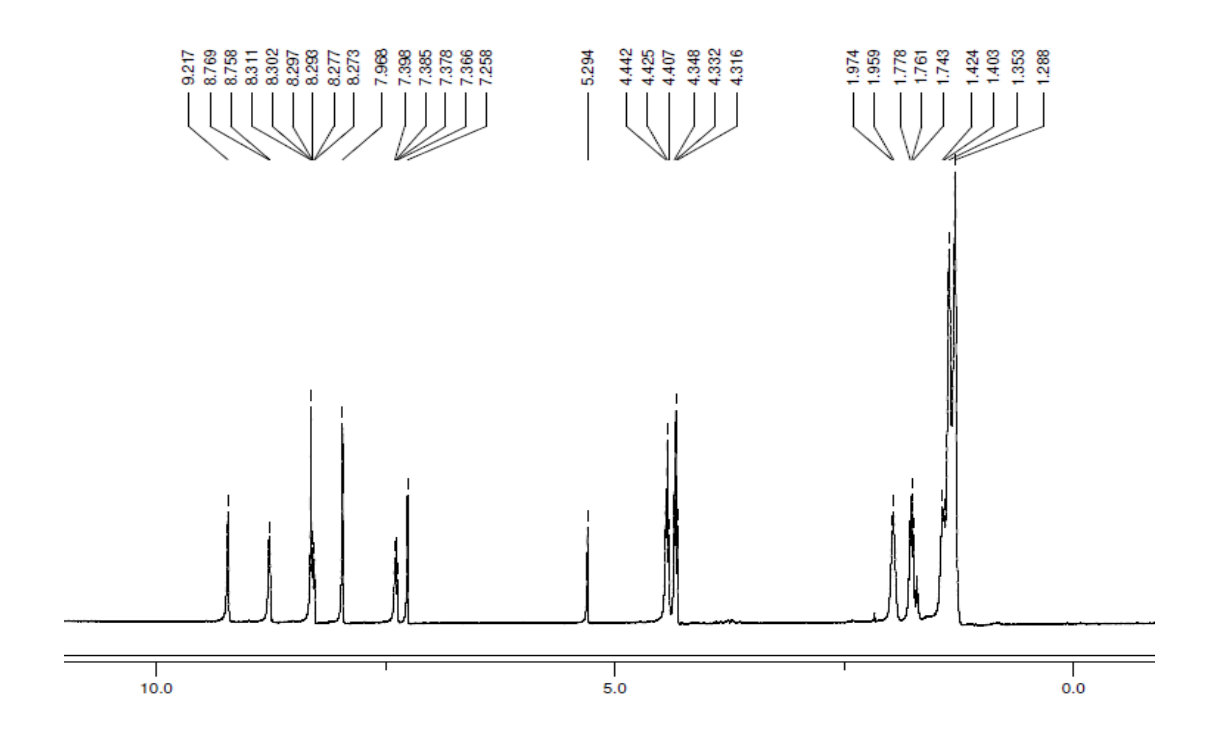


Figure S2.8a. ¹H NMR (400 MHz, CDCl₃) spectrum of compound 12.

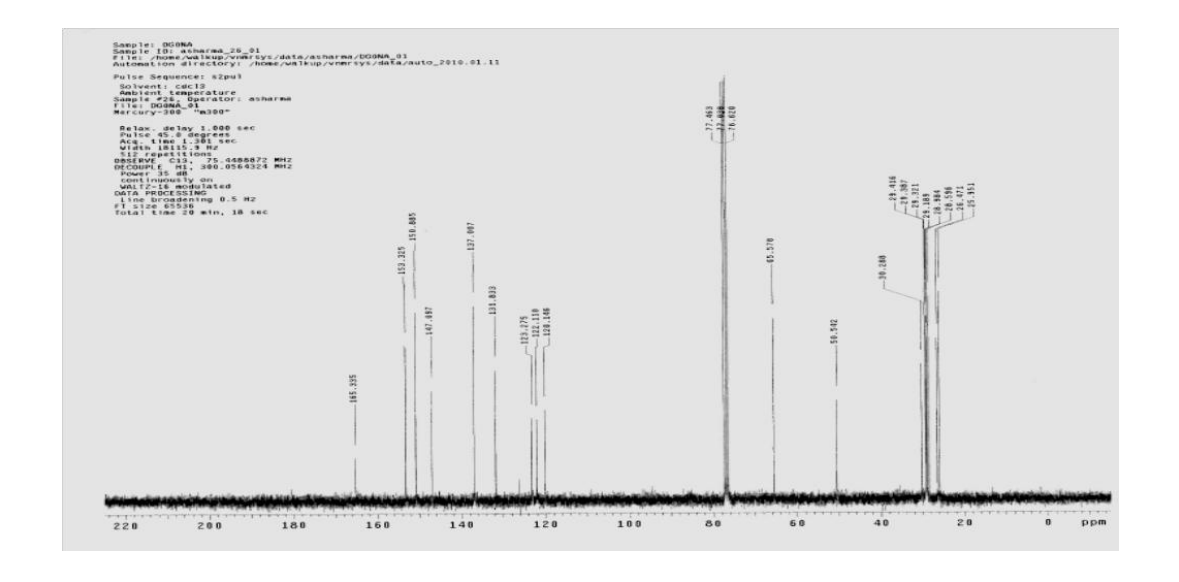


Figure S2.8b. ¹³C{¹H} NMR (75 MHz, CDCl₃) spectrum of compound 12.

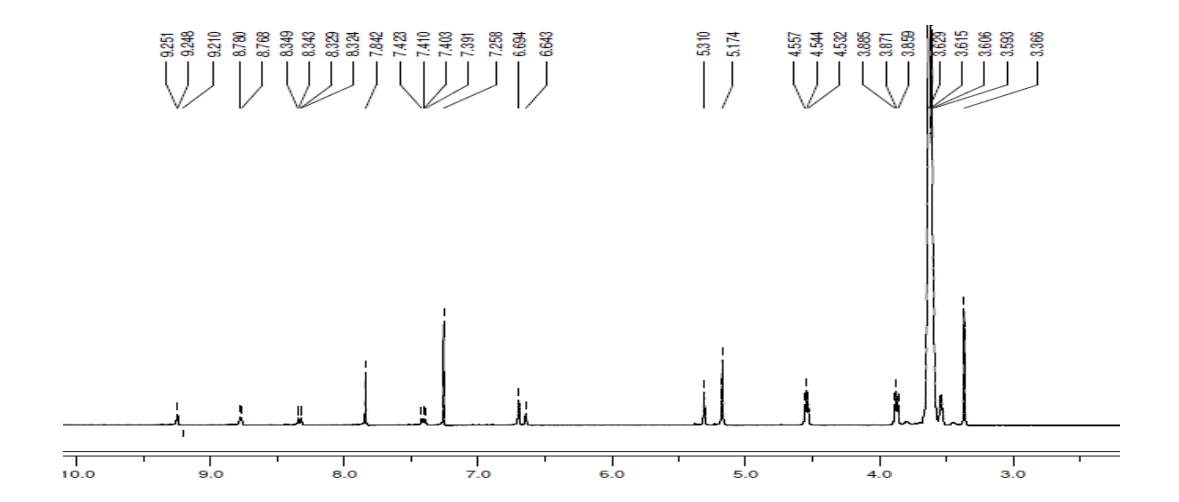


Figure S2.9a. ¹H NMR (400 MHz, CDCl₃) spectrum of compound **15**.

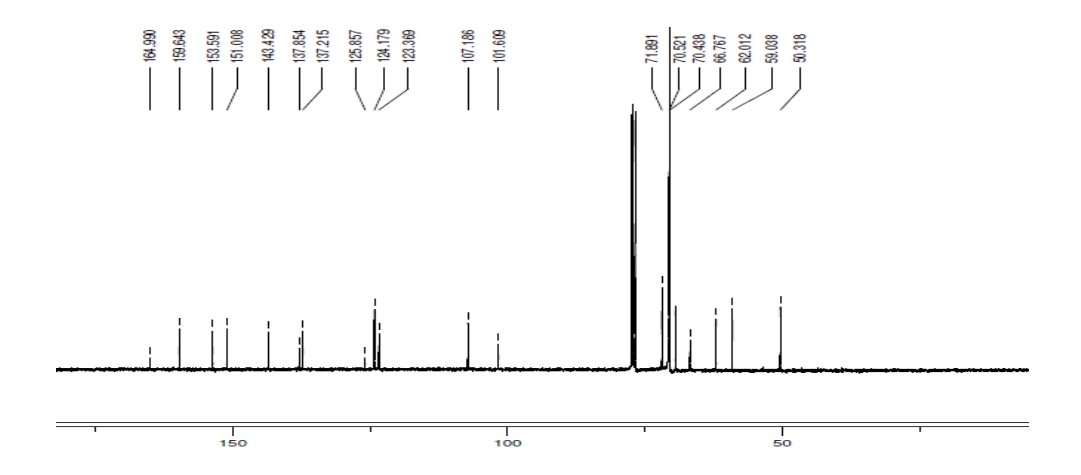
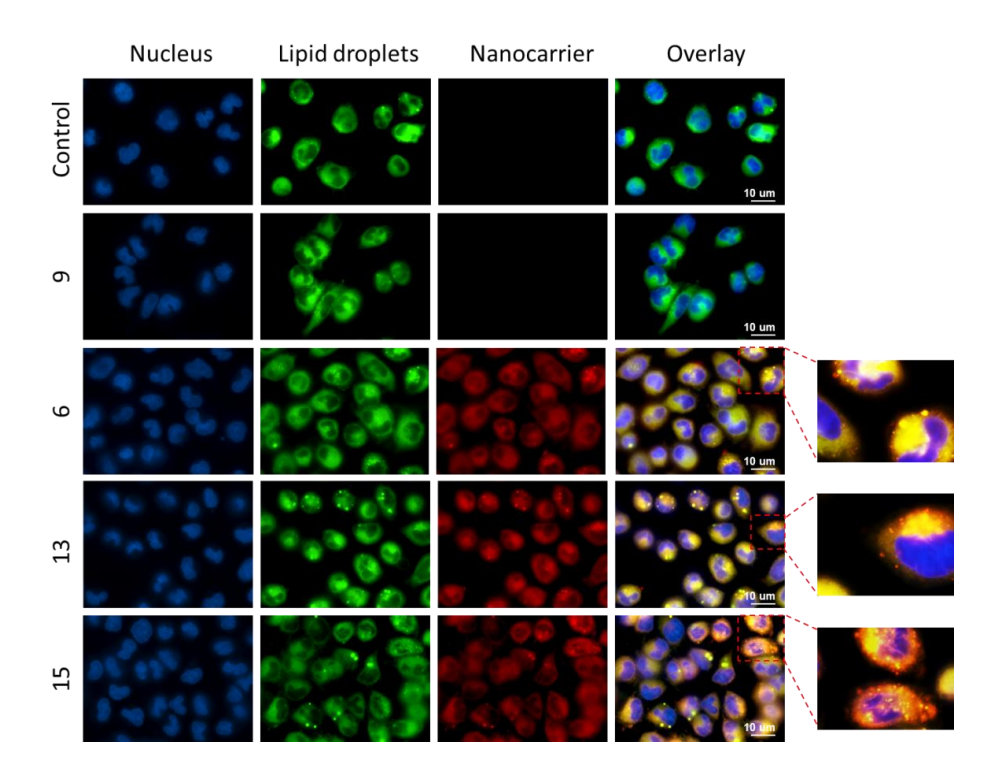


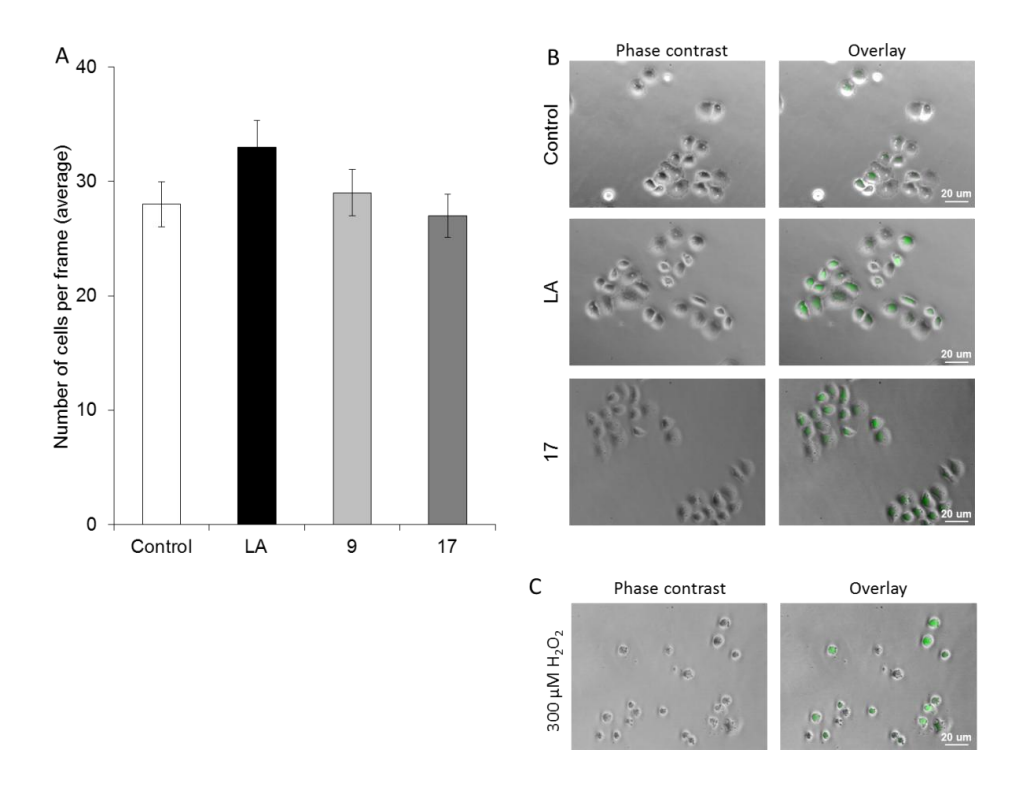
Figure S2.9b. ¹³C{¹H} NMR (100 MHz, CDCl₃) spectrum of compound 15.

Appendix 3

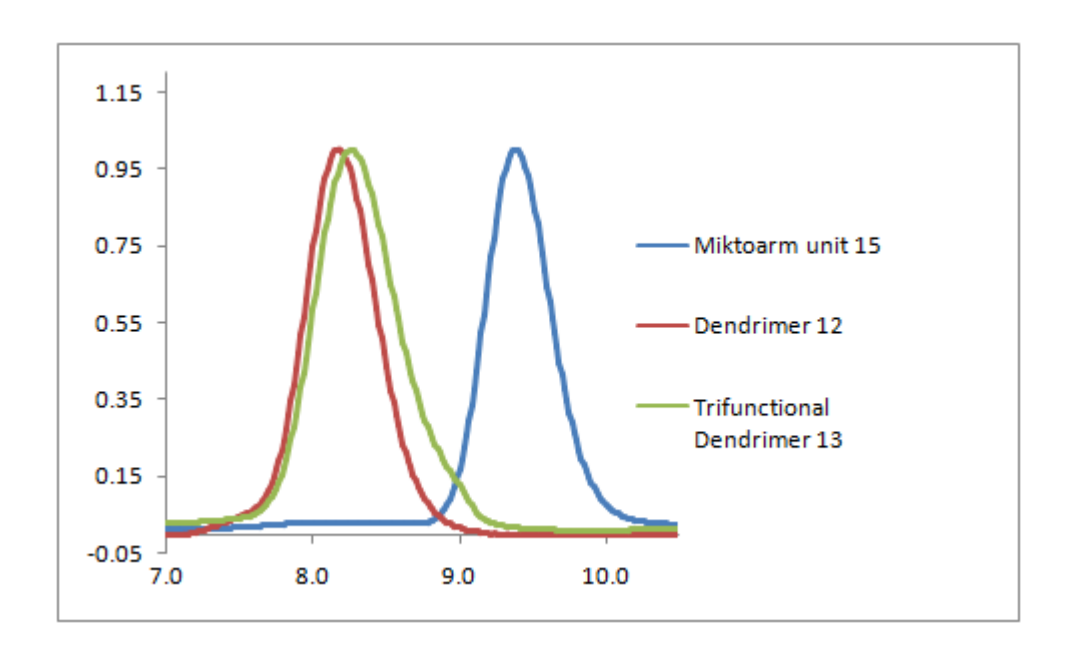
Supporting Information – Chapter 3: Facile Construction of Multifunctional Nanocarriers Using Sequential Click Chemistry for Applications in Biology



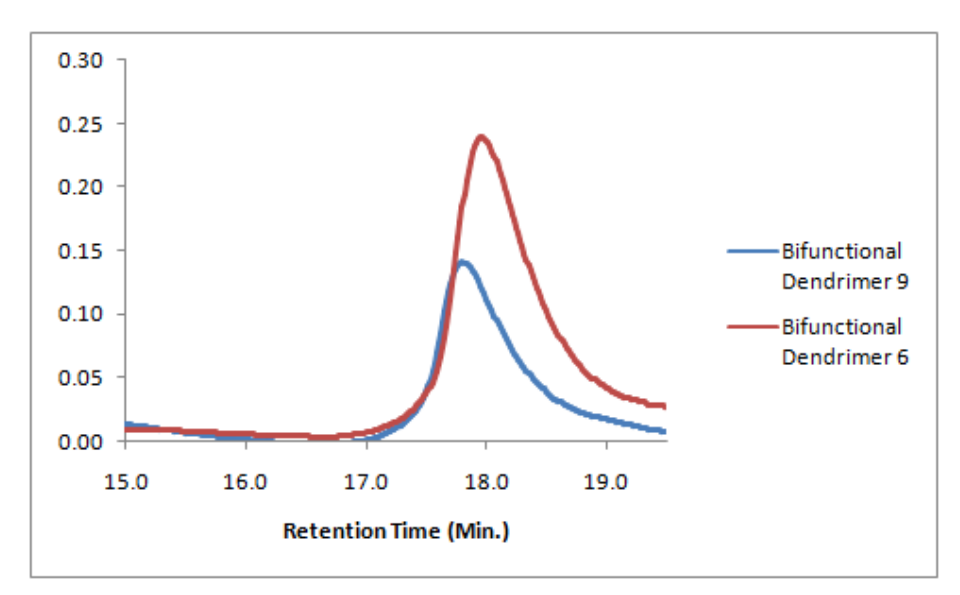
Supplemental Figure 3.1 – Assessment of cellular uptake of bodipy and/or lipoic acid conjugated dendrimer and miktoarm nanocarriers. Cellular uptake of nanocarriers and colocalization with lipid droplets is shown in representative fluorescent micrographs. PC12 cells were treated for 30 minutes with 6 (BP-PEG-Dendrimer), 13 (BP-LA-PEG-Dendrimer) and 15 (BP-LA-PEG-Miktoarm) in equimolar concentrations with respect to BP (1 μ M). Cells were treated with 9 (LA-PEG-Dendrimer) as a control. The nucleus was labeled with Hoechst 33258 (10 μ M; 10 mins) and is visible in blue. Lipid droplets were labeled with BODIPY 493/503 (20 μ M; 10 mins) and are visible in green. BODIPY conjugated nanocarriers are visible in red. Pictures were selected from three independent experiments of triplicates. Scale bars represent 10 um.



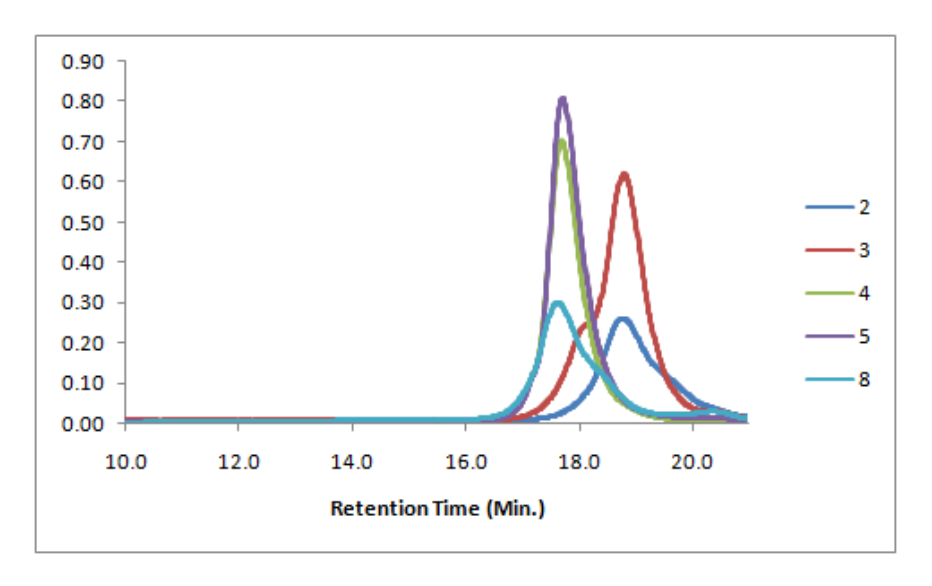
Supplemental Figure 3.2 - Assessment of cellular viability. PC12 cells were treated for 24 hours with equimolar concentrations of various dendrimer and miktoarm nanocarriers with respect to \Box -lipoic acid (200 μ M). Cellular viability was measured A) by cell counting and B-C) by assessing changes in cell morphology. Data are presented as means \pm SEM of three individual experiments of triplicates. Representative phase contrast and fluorescent overlay images of mCBi labeled cells were selected from three independent experiments of triplicates. Scale bars represent 20 uM.



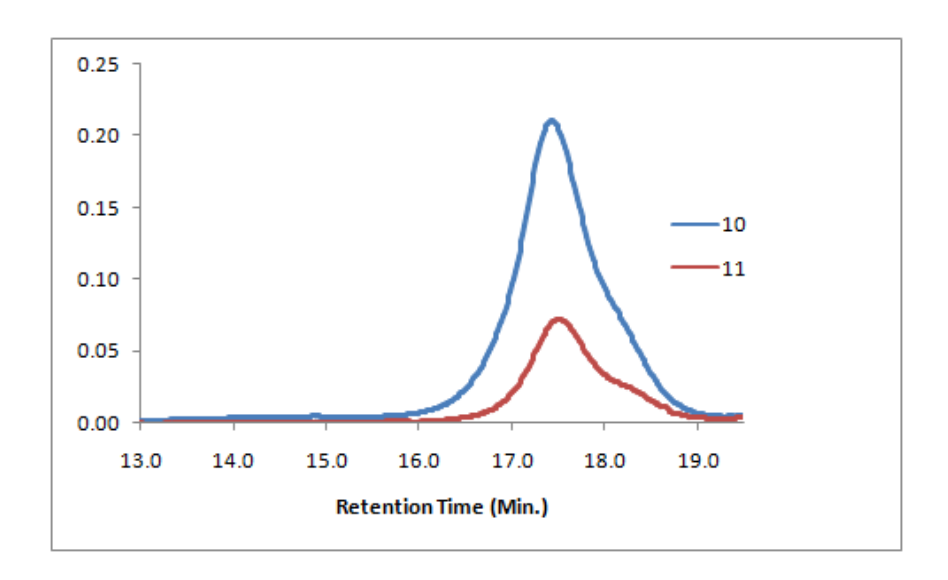
Supplemental Figure 3.3 GPC analyses of a) miktoarm carrier **15**; b) dendrimer **12**; and c) trifunctional dendrimer **13**.



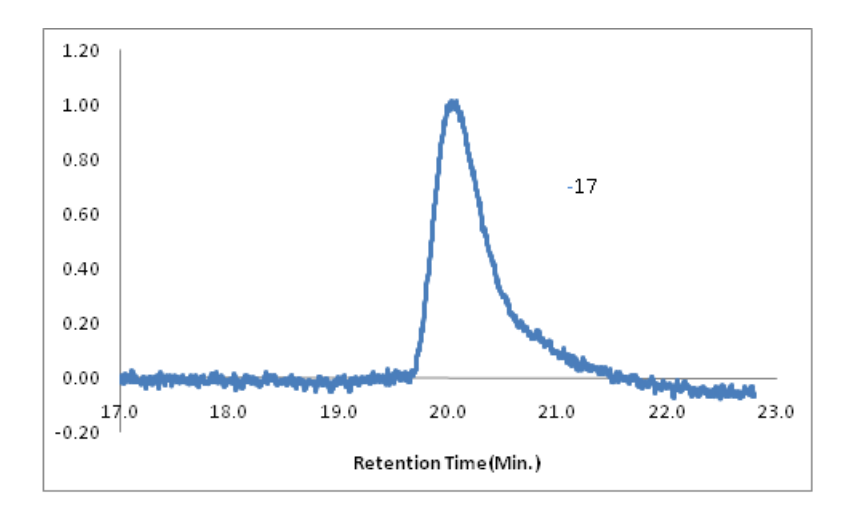
Supplemental Figure 3.4 GPC analyses of bifunctional dendrimers: a) **6** with PEG and BODIPY; b) **9** with PEG and α -lipoic acid.



Supplemental Figure 3.5 GPC analyses of compounds 2, 3, 4, 5 and 8.



Supplemental Figure 3.6 GPC analyses of compounds 10 and 11

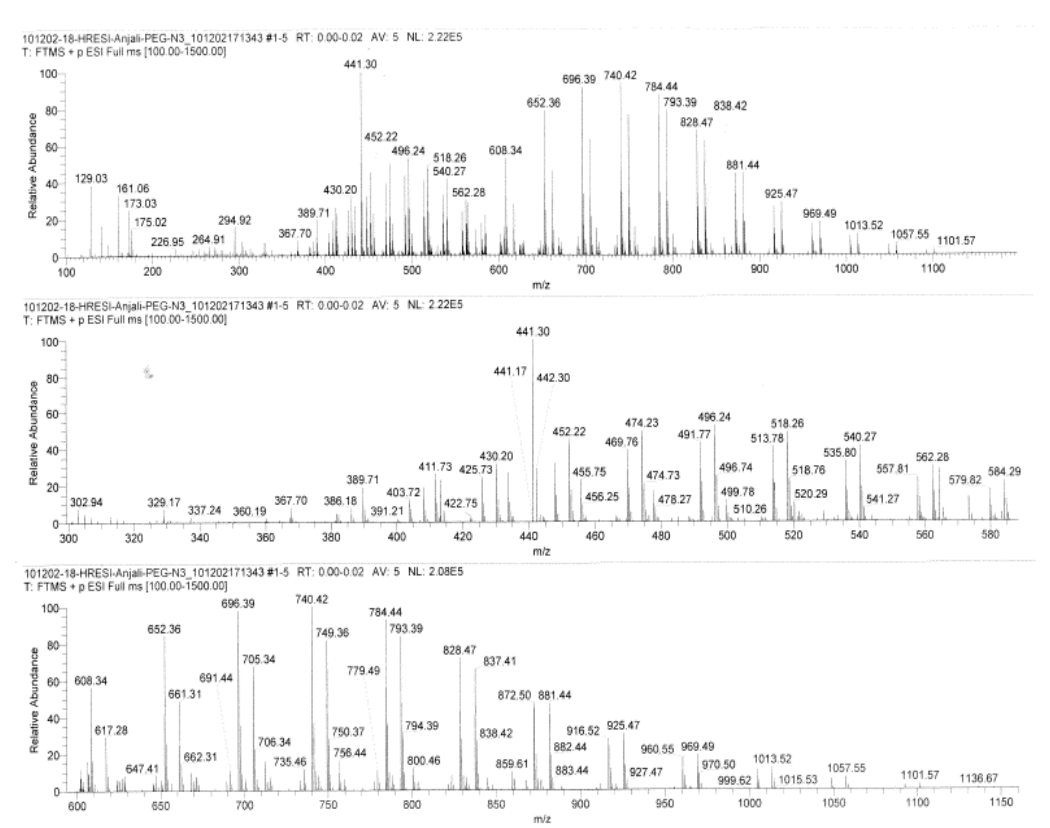


Supplemental Figure 3.7 GPC analysis of miktoarm 17

Mass Spectra:

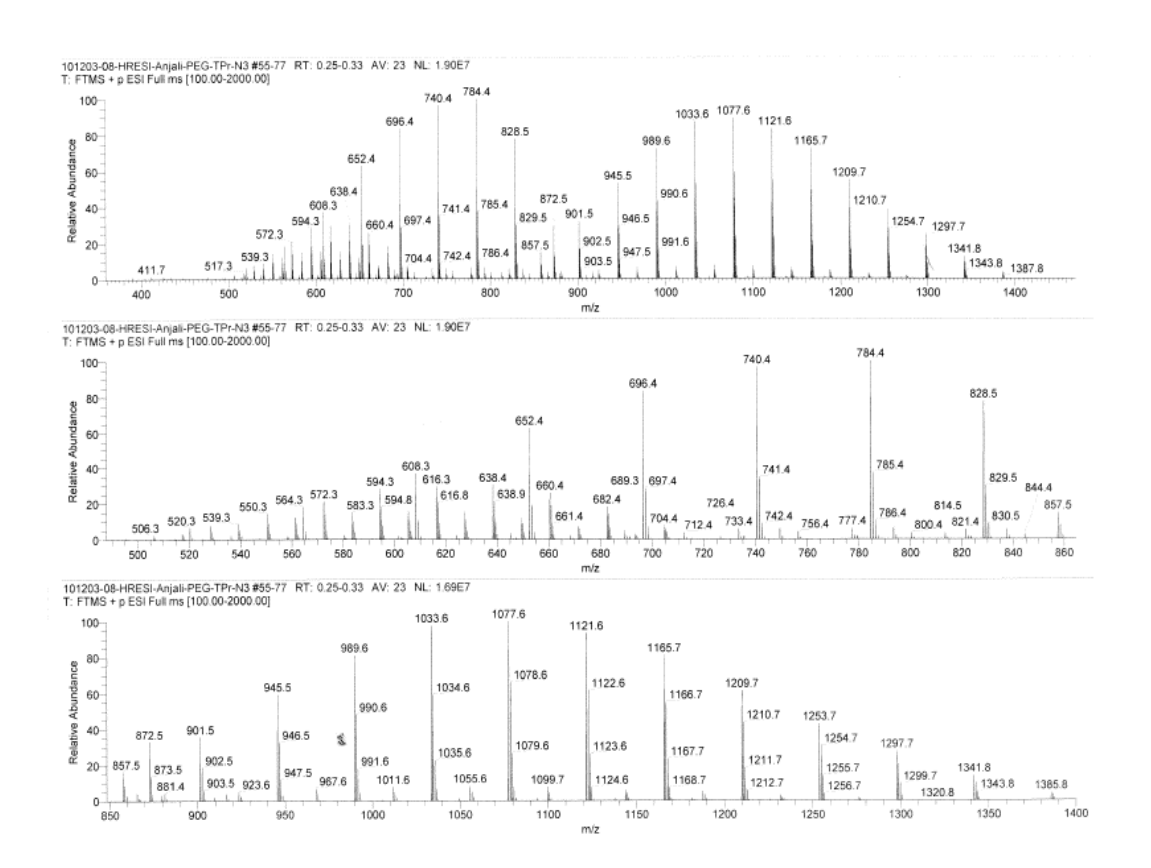
Materials and methods: Mass spectra were recorded on Thermo Scientific Orbitrap mass analyzer (ES) and Kratos MS25 (EI) mass spectrometers, and MALDI-TOF spectra on Autoflex III Mass Spectrometer (Bruker) using LiBr-dithranol as the matrix for compound $\bf 9$ and α -Cyano-4-hydroxycinnamic acid as the matrix for compound $\bf 6$.

Supplemental Figure 3.8 ES-MS of polyethyleneglycol-azide, PEG-N₃:



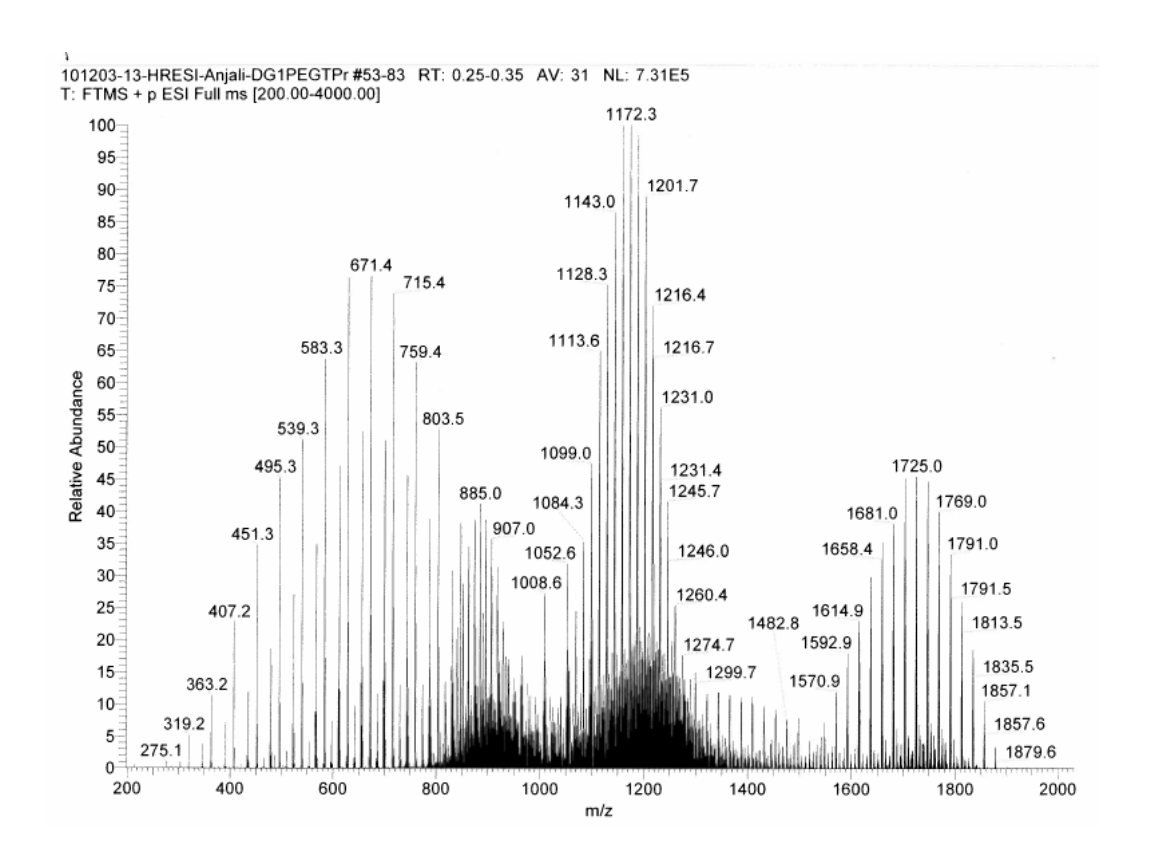
Supplemental Figure 3.8 The expected mass for PEG-N₃ is 775. The mass spectrum above shows a range of masses which differ by 44 units (fragment corresponding to –CH₂CH₂O-). This characteristic fragmentation pattern of PEG is commonly observed (Franska, M. *et al.*, *Eur. J. Mass Spectrum*, **2003**, 9, 165-173; Chen, R. *et al.*, *J. Am. Soc. Mass Spect.* **2002**, *13*, 888-897; Hittle, L.R. *et al.*, *Anal. Chem.* **1994**, *66*, 2302-2312). The higher masses than the expected mass of 775 are associated with the polydispersity of PEG.

Supplemental Figure 3.9 ES-MS of **Compound 3**:



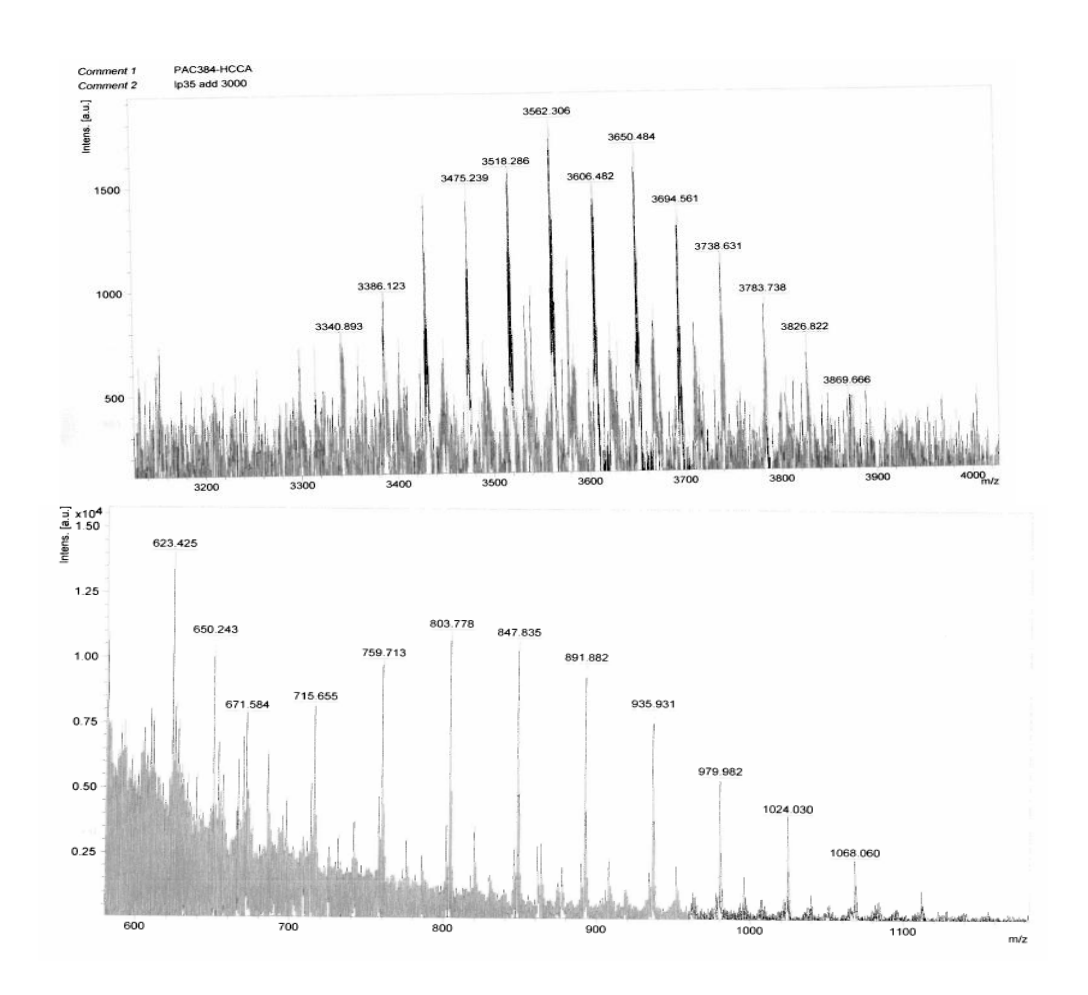
Supplemental Figure 3.9 The expected mass of compound **3** is 1123 g/mol. The mass spectrum showed a range of masses which differ by 44 units (fragment corresponding to $-CH_2CH_2O$ -), and correspond to the fragmentation pattern of PEG (see **Supplementary Figure 3.8** above). In addition, we observed the doubly charged species which showed a similar fragmentation pattern (44 units, fragment corresponding to $-CH_2CH_2O$ -).

Supplemental Figure 3.10 ES-MS of **Compound 4**:



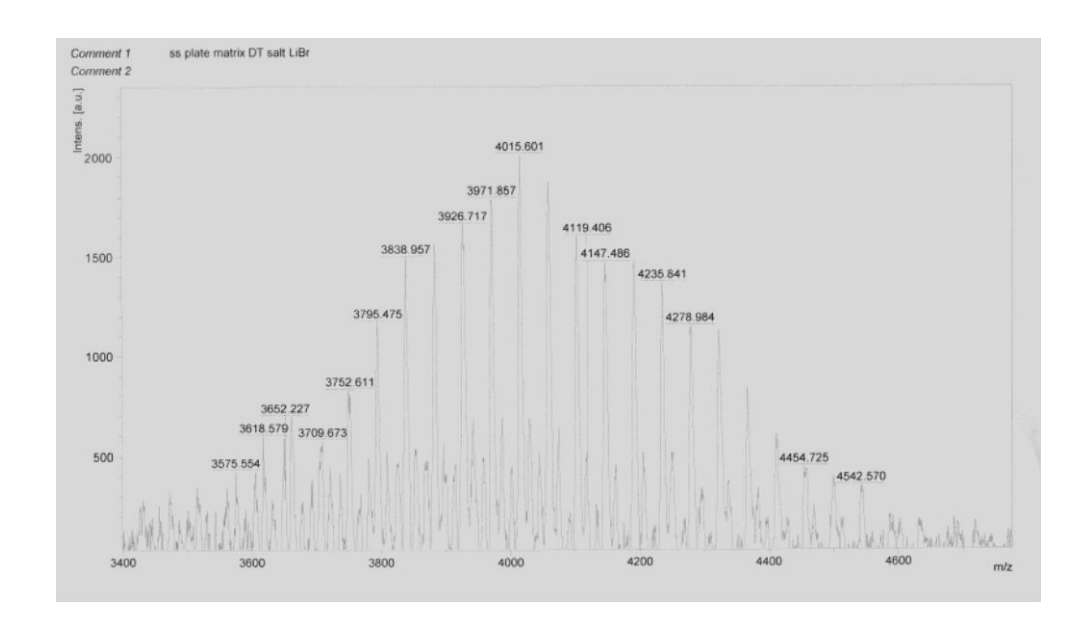
Supplemental Figure 3.10. The expected mass of compound **4** containing three PEG chains and three protected acetylenes is 3519. The above spectrum shows doubly charged (M/2), triply charged (M/3) and quaternary charged (M/4) species. The fragmentation pattern again is similar to that shown above with a difference of 44 units corresponding to –CH₂CH₂O- from PEG.

Supplemental Figure 3.11. MALDI-TOF MS of **Compound 6**:



Supplemental Figure 3.11. The expected mass of compound **6** containing three PEG arms and three BODIPY dye molecules is 4438. The above spectrum shows a mass range which indicates the cleavage of one PEG chain from the molecule under the conditions of mass determination, and the fragmentation pattern which resembles that of PEG, with fragments of a difference of 44 units.

Supplemental Figure 3.12 MALDI-TOF MS of **Compound 9**:



Supplemental Figure 3.12 The expected mass of compound **9** with three PEG chains and three α -lipoic acid molecules is 4223. We observed a range of masses in this region with fragments which differ by 44 units (corresponding to – CH₂CH₂O- of PEG). The observed higher masses are associated with polydispersity of PEG.

Appendix 4

Supporting Information – Chapter 4: Design and Evaluation of Multi-functional Nanocarriers for Selective Delivery of Coenzyme Q10 to Mitochondria

1. Synthesis of a series of targeted and non-targeted PEG-PCL miktoarm polymers:

PEG2-PCL3.5-Br: A solution of compound **6** (50mg, 0.02mmoles) in dry toluene (2 ml) was placed in a flame-dried two neck round bottom flask fitted with a condenser. The solution was degassed by evacuation, and distilled ε -caprolactone (0.07mL, 0.67mmoles) was added under nitrogen with a syringe through the rubber septum. A nitrogen purged solution of Sn(II) 2-ethylhexanoate (catalytic) in toluene (1 mL) was then added to the reaction flask, and the mixture was refluxed for 24 h. The reaction mixture was then cooled to room temperature, and the solvent was removed under vacuum. The product was dissolved in dichloromethane and precipitated in cold methanol. The polymer was filtered and washed with diethylether to yield a white powder. GPC: Mn = 5992, Polydispersity Index (PDI) =1.2.

PEG2-PCL3.8-Br: Compound **6** (50mg, 0.02mmoles) and ε -caprolactone (0.08mL, 0.74mmoles) were reacted together using the above mentioned procedure for ring opening polymerization. GPC: Mn = 6252, PDI =1.3.

PEG2-PCL4.4-Br: Compound **6** (50mg, 0.02mmoles) and ε -caprolactone (0.10mL, 0.88mmoles) were reacted together using the above mentioned procedure for ring opening polymerization. GPC: Mn = 6911, PDI =1.3.

PEG2-PCL5.5-Br: Compound **6** (50mg, 0.02mmoles) and ε -caprolactone (0.12mL, 1.10mmoles) were reacted together using the above mentioned procedure for ring opening polymerization. GPC: Mn = 7932, PDI =1.4.

PEG2-PCL7.0-Br: Compound **6** (50mg, 0.02mmoles) and ε -caprolactone (0.15mL, 1.37mmoles) were reacted together using the above mentioned procedure for ring opening polymerization. GPC: Mn = 9574, PDI =1.3.

PEG2-PCL7.8-Br: Compound **6** (50mg, 0.02mmoles) and ε -caprolactone (0.18mL, 1.58mmoles) were reacted together using the above mentioned procedure for ring opening polymerization. GPC: Mn = 10247, PDI =1.2.

PEG2-PCL3.5-TPP⁺**Br**⁻: A solution of PEG2K_PCL3500_Br (100mg, 0.02mmoles) and triphenyl phosphine (TPP) (8.8mg, 0.03mmoles) in acetonitrile (ACN) was refluxed for 48 h. The solvent was then evaporated and the residue was washed several times with hexanes and diethylether to remove excess of TPP. The white solid was then dried under vacuum. GPC: Mn = 6022, PDI =1.3.

PEG2-PCL3.8-TPP⁺**Br**⁻: PEG2K_PCL3800_Br (100mg, 0.02mmoles) and TPP (8.4mg, 0.03mmoles) were reacted together using a similar procedure as mentioned above to afford the product as white solid. GPC: Mn = 6284, PDI =1.4.

PEG2-PCL4.4-TPP⁺**Br**⁻: PEG2K_PCL4400_Br (100mg, 0.01mmoles) and TPP (7.6mg, 0.03mmoles) were reacted together using a similar procedure as mentioned above to afford the product as white solid. GPC: Mn = 7353, PDI =1.3.

PEG2-PCL5.5-TPP⁺**Br**⁻: PEG2K_PCL5500_Br (100mg, 0.02mmoles) and TPP (6.6mg, 0.03mmoles) were reacted together using a similar procedure as mentioned above to afford the product as white solid. GPC: Mn = 8374, PDI =1.4.

PEG2-PCL7.0-TPP⁺**Br**⁻: PEG2K_PCL7000_Br (100mg, 0.01mmoles) and TPP (5.5mg, 0.02mmoles) were reacted together using a similar procedure as mentioned above to afford the product as white solid. GPC: Mn = 11140, PDI =1.6.

PEG2-PCL7.8-TPP⁺**Br**⁻: PEG2K_PCL7800_Br (100mg, 0.01mmoles) and TPP (5.1mg, 0.02mmoles) were reacted together using a similar procedure as mentioned above to afford the product as white solid. GPC: Mn = 12072, PDI =1.6.

2. Supplementary Tables and Figures

Table 4.1. Calculated solubility parameters and Flory-Huggins interaction parameters for PCL, nimodipine and coenzyme Q10

Drug/Polymer	Total solubility parameter (J/cm ³) ^{1/2} a	χ_{sm}^{b}
PCL	20.59	-
Nimodipine	26.10	4.57
Coenzyme Q10	18.14	2.54

^a: Solubility parameters estimated by the Hansen theory of solubility group contribution method (GCM) using Molecular Modeling Pro software

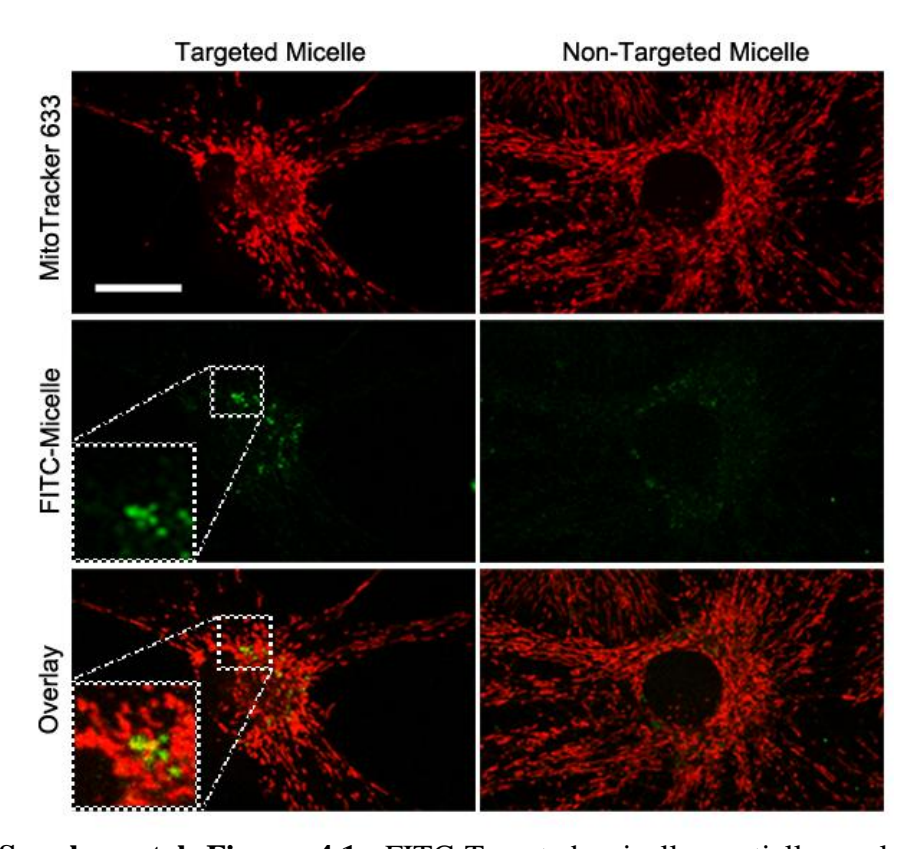
$$\chi_{\rm sm} = \frac{(\delta_{\rm s} - \delta_{\rm m})^2 V_{\rm s}}{RT} \tag{1}$$

 δ_s and δ_m are solubility parameters for the drug and the micellar core, respectively; V_s is the molar volume of drug, R is the universal gas constant, and T is the Kelvin temperature.

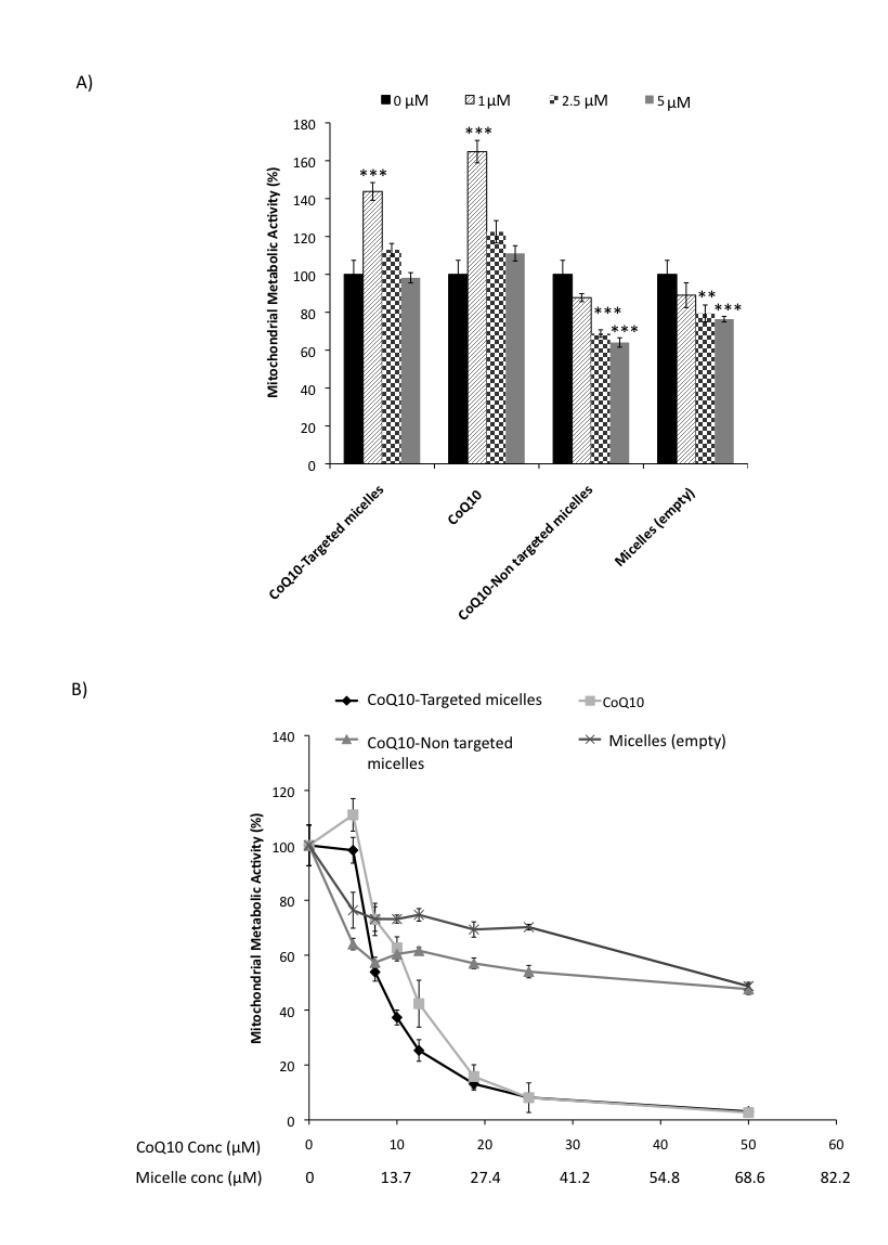
^b: Flory-Huggins interaction parameters between PCL and different drugs calculated using equation 1

Table 4.2. Zero and first order kinetics for the degradation of CoQ10 under UV irradiation

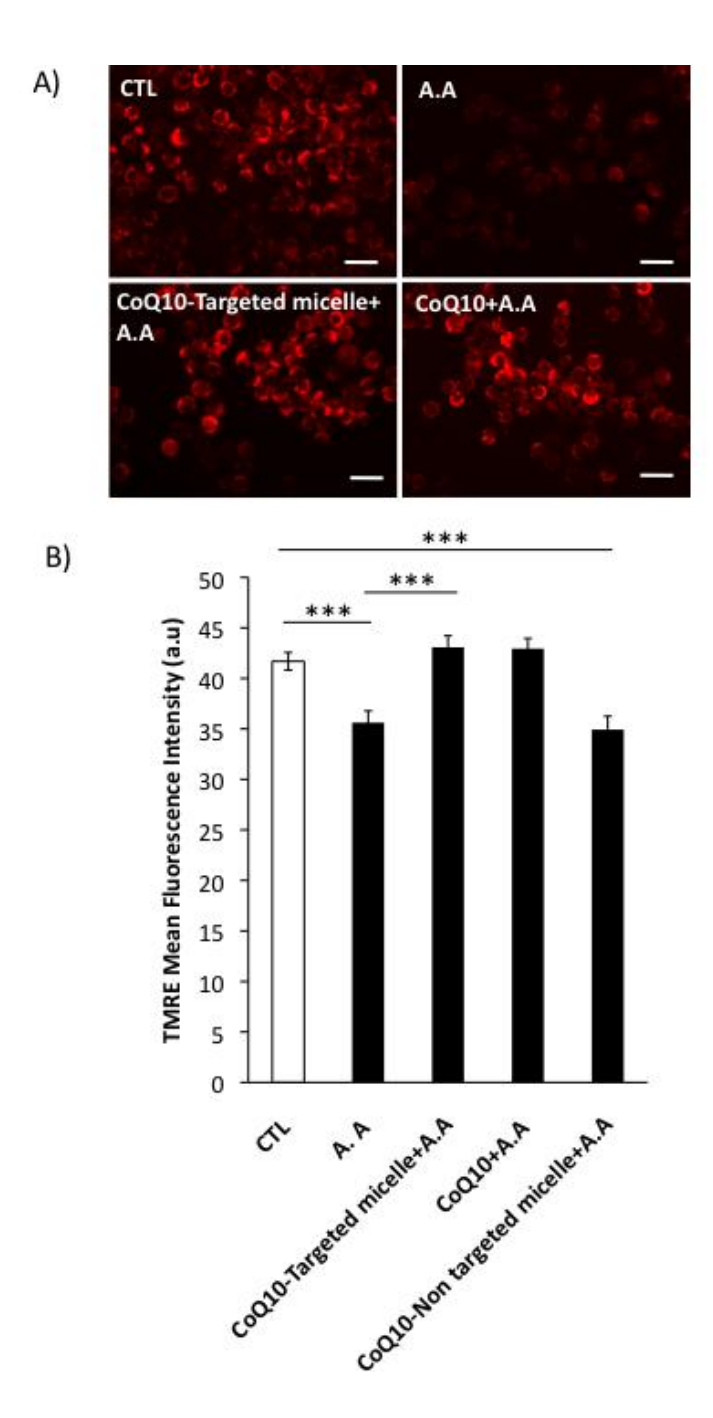
Sample	R^{2a}		K^{b}	$T_{0.5}^{\ \ c}$
	Zero order	First order	(min ⁻¹)	(min)
CoQ10 solution (0.50 mg/mL)	0.976	0.966	0.10	6.85
CoQ10 micelles (0.10 mg/mL)	0.971	0.991	0.06	11.66
CoQ10 micelles (0.25 mg/mL)	0.966	0.998	0.04	19.05
CoQ10 micelles (0.50 mg/mL)	0.958	0.996	0.03	25.74
CoQ10 micelles (0.75 mg/mL)	0.981	0.998	0.01	56.67



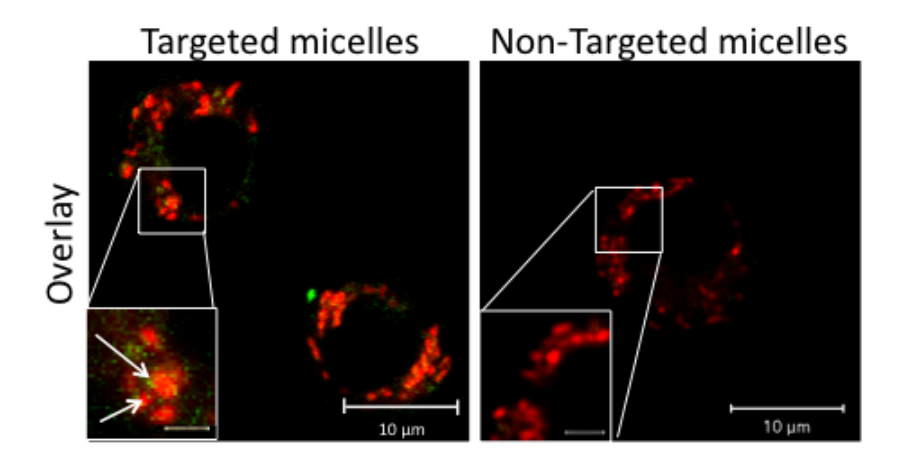
Supplemental Figure 4.1. FITC-Targeted micelle partially co-localize with mitochondria. Confocal micrographs of primary hippocampal neurons and glia cells treated with FITC-PEG2-PCL3.8-TPPBr (Targeted Micelle, 1 μ M, 3 h, green fluorescence) or FITC-PEG2-PCL3.8-Br (Non-Targeted Micelle, 1 μ M, 3 h, green fluorescence) and Mitotracker 633 (100 nM, 3 min, deep red fluorescence). FITC-Targeted micelle partially co-localize with mitochondria as shown in overlay image (inset, yellow), which was not found in cell cultures treated with FITC-Non targeted micelles (bottom, right panel). Each image represents a Z-stack consisting of 6-8 confocal sections taken at an interval of 0.3 μ m. Images were acquired using HeNe (633 nm) and Argon (488 nm) excitation lasers for detection of deep red and green fluorescence, respectively. Scale bar (20 μ m) is representative for all images.



Supplemental Figure 4.2. Mitochondrial metabolic activity measured by MTT assay. Microglia cells treated with CoQ10, CoQ10/PEG2-PCL3.8-TPPBr (CoQ10-Targeted micelles), CoQ10/PEG2-PCL3.8-Br (CoQ10-Non targeted micelles) and PEG2-PCL3.8-TPPBr (empty micelles for 24 h (panels A and B). Mitochondrial metabolic activity (%) is expressed relative to controls (untreated cells that were set to 100%, n=9). The data are presented as mean ±SEM obtained from at least three independent experiments performed in triplicates. Statistically significant differences are indicated by p** <0.01, p*** <0.001.



Supplemental Figure 4.3. Microglia cells were treated with CoQ10/PEG2-PCL3.8-TPPBr (CoQ10-Targeted micelle), CoQ10, or CoQ10/PEG2-PCL3.8-Br (CoQ10-Non targeted micelle) (5 μ M with respect to CoQ10, 24 h). (A) Fluorescent micrographs showing mitochondrial membrane potential using TMRE (200 nM, 30 min) following antimycin A exposure (A.A, 1 μ M, 24 h). Scale bar =20 μ m. (B) Semiquantification of TMRE mean fluorescence intensity (arbitrary units) was performed using Image J software from cells treated as in A (n=16). The data are presented as mean \pm SEM obtained from at least three independent experiments performed in triplicates. Statistically significant differences are indicated by p*** <0.001.



Supplemental Figure 4.4. Targeted micelles with non covalently bound FITC (green) partially co-localize with mitochondria (red). Confocal micrographs of microglia cells treated with targeted Micelle or Non-Targeted Micelles is shown. Each image represents a Z-stack consisting of 12 confocal sections taken at an interval of $0.6 \, \mu m$. Scale bar ($10 \, \mu m$).

4. Detailed caption for Fig. 4.6 from Chapter 4. Production of reactive oxygen species (ROS). (A) Fluorescent micrographs showing reactive oxygen species generation following H_2O_2 exposure (2 mM, 3 h) using DCFH-DA, a fluorescent probe sensitive to ROS radicals. Scale bar= 20 μ m. (B) Spectrofluorometric detection and quantification of DCF fluorescence intensity (arbitrary units) was expressed relative to untreated controls (CTL=1, white bar) (n=8). (C) Fluorescent micrographs showing superoxide anion (O_2 -) generation following PQ exposure (10 μ M, 24 h) using dihydroethidium (DHE), a fluorescent probe sensitive to superoxide radicals. Scale bar=20 μ m. (D) Spectrofluorometric detection and quantification of ethidium fluorescence intensity (arbitrary units) was expressed relative to untreated controls (CTL=1, white bar) (n=8). The data are presented as mean \pm SEM obtained from at least three independent experiments performed in triplicates. Statistically significant differences are indicated by p** <0.01, p*** <0.001.